NOTICE

The quality of this microform is heavily dependent upon the quality of the original thesis submitted for microfilming. Every effort has been made to ensure the highest quality of reproduction possible.

If pages are missing, contact the university which granted the degree.

Some pages may have indistinct print especially if the original pages were typed with a poor typewriter ribbon or if the university sent us an inferior photocopy.

Reproduction in full or in part of this microform is governed by the Canadian Copyright Act, R.S.C. 1970, c. C-30, and subsequent amendments.

AVIS

La qualité de cette microforme dépend grandement de la qualité de la thèse soumise au microfilmage. Nous avons tout fait pour assurer une qualité supérieure de reproduction.

S'il manque des pages, veuillez communiquer avec l'université qui a conféré le grade.

La qualité d'impression de certaines pages peut laisser à désirer, surtout si les pages originales ont été dactylographiées à l'aide d'un ruban usé ou si l'université nous a fait parvenir une photocopie de qualité inférieure.

La reproduction, même partielle, de cette microforme est soumise à la Loi canadienne sur le droit d'auteur, SRC 1970, c. C-30, et ses amendements subséquents.

Canada

THE CONTROL OF CAVITY PRESSURE THROUGHOUT THE INJECTION MOLDING CYCLE

by

Furong Gao

A thesis submitted to the Faculty of Graduate Studies
and Research in partial fulfilment of the
requirements for the degree of
Doctor of Philosophy

Department of Chemical Engineering
McGill University
Montréal, Québec, Canada

October, 1993

ISBN 0-315-94622-9

ABSTRACT

The injection molding process, due to its versatility, cost effectiveness, and ability to produce intricate shapes to tight specifications, is widely used in plastics processing. Mold cavity pressure plays an important role in determining the quality of the molded articles. The dynamic behaviour and control of cavity pressure were studied in this research project. The work deals with all phases of the process: filling, packing, and cooling.

A real-time data acquisition and computer control system has been developed to assist the implementation of advanced control techniques for injection molding machine operation. Modularity and extensibility were emphasised in its development.

The dynamics of cavity pressure during filling were investigated and found to be both non-linear and time-varying in relation to the hydraulic servo-valve opening which is the manipulated variable. A self-tuning control system was designed and tested for a wide range of conditions.

The transition of the filling-to-packing was found to be best detected by the derivative of the cavity pressure. The dynamics of cavity pressure during packing were studied and modelled similarly as for filling. The self-tuning technique was successfully extended into the packing phase.

Cavity pressure is essentially independent of the hydraulic servo-valve opening once the cavity gate freezes and the process enters the cooling phase. A cooling system was designed to provide quick manipulation of coolant temperature. Controlled pressure cooling time (CPCT) was proposed to represent the behaviour of cavity pressure during

the cooling phase. Its dynamics in relation to coolant temperature were found to be best described as a first order system. A control system for CPCT was designed and successfully tested.

RESUME

Etant donnée sa grande diversité, sa rentabilité et sa capacité à produire des formes complexes sous des exigences très précises, le procédé de moulage par injection est appliqué à grande échelle pour la fabrication de plastiques. La pression de cavité dans le moule joue un rôle important dans la détermination de la qualité des articles moulés. Le comportement dynamique et le contrôle de la pression de cavité ont été étudiés dans ce projet de recherche. Ce travail analyse toutes les phases du procédé: le remplissage, le compactage et le refroidissement.

Un système de contrôle par ordinateur avec acquisition de données en temps réel a été développé pour l'application à des techniques de contrôle avancées lors de l'opération de machines effectuant le moulage par injection. L'emphase de cette étude a été donnée sur la modalité et l'extensibilité.

L'étude de la dynamique de la pression de cavité lors du remplissage a permis de trouver une relation non-linéaire et variable dans le temps selon l'ouverture du cerveau-valve, laquelle est la variable manipulée. Le design d'un système de contrôle interne a été conçu et testé pour une large gamme de conditions.

La dérivée de la pression de cavité s'est avérée la meilleure méthode pour détecter le passage du remplissage au compactage. La dynamique de la pression de cavité lors du compactage a été étudiée et définie de façon similaire au remplissage. Le système de contôle interne a été étendu à la phase de compactage avec succès.

La pression de cavité est essentiellement indépendante de l'ouverture hydraulique du cerveau-valve une fois que le procédé entre dans la phase de

refroidissement. Le design d'un système de refroidissement a été conçu de manière à obtenir la manipulation rapide de la température de refroidissement. Le temps de refroidissement à pression contrôlée (CPCT) a été proposé pour représenter le comportement de la pression de cavité lors de la phase de refroidissement. La meilleure description de sa dynamique, en relation avec la température de refroidissement, est un système de premier ordre. Le design d'un système de contrôle pour le CPCT a été conçu et testé avec succès.

ACKNOWLEDGMENTS

Throughout this project, I have received a great amount of assistance, motivation, and scientific input from many people. I wish to convey my deep appreciation to them all, in particular to:

Professor W. Ian Patterson and Professor Musa R. Kamal, my research directors, for their patience, fruitful discussions, advice, and great interest throughout the course of this study. I would also like to thank them for their critical review of the thesis which instilled some measure of clarity and completeness in this work.

Professor O.M. Fulier, for his philosophical and helpful advice. His introduction to the QNX real-time operating system was necessary for this work.

Mr. A. Krish and the staff of the machine and electronics workshops for their assistance in constructing and modifying the experimental equipment. My thanks extend to Mr. L. Cusmich, Mr. J. Dumont, and Mr. W. Greenland for their help in maintaining the research facilities and instrumentation.

Mr. H. Fusser, my colleague, for his cooperation in the development of the real-time computer control and data acquisition system, and for the computer-user interface he developed for the system.

Mr. J. Campanelli, Mr. M. Samara, Dr. T. Papathanasiou, Dr. E. Chu, Mr. Y. Sasaki, Mr. M. Weber, Mr. B. Nelson, Dr. T. Broadhead and the whole polymer group on the 5th floor, for their valuable discussions and comments throughout the project. Special thanks to Mr. F. Koran for translating the abstract into French.

Dr. B. Huang, Dr. D. Jiao, and Mr. K. Lin, for their useful discussions and

comments on computer programming, instrumentation, and other scientific information.

The financial support from McGill University, the National Science and Engineering Research Council of Canada, and the Government of Quebec is also greatly appreciated.

Finally, I would like to express my deep gratitude to my wife, my mother, and my family for their love, support, encouragement, and understanding.

TABLE OF CONTENTS

LIST OF FIGURES

LIST OF TABLES

Chapter 1

INTRODUCTION AND LITERATURE REVIEW

1.1 Introduction

Plastics continue to have expanding applications in a variety of important sectors such as transportation, packaging, construction, appliances, electronics, and medicine. One of the most widely used plastics-forming processes is injection molding due to its versatility, cost effectiveness, and ability to produce intricate shapes to demanding specifications.

Injection molding is accomplished in an injection molding machine which has three basic components: the injection, clamping and hydraulic units. The injection unit melts the polymeric material by means of heaters, and injects it under pressure into a mold cavity which is held by the clamping unit. The molten polymer is then cooled and solidified in the shape and dimensions of the mold cavity. The hydraulic unit serves as a manipulator for the other two units. Figure 1.1 shows a basic injection molding machine together with important process and machine variables.

The injection molding process is cyclic. Each cycle is divided into three phases (stages): filling, packing and holding, and cooling as depicted by the cavity pressure versus time profile shown in Figure 1.2.

During the filling stage, cavity pressure rises slowly as the molten, non-Newtonian, polymeric material flows into the cavity. Among a number of variables, injection rate (sometimes also called ram velocity, or screw velocity) plays an important role in determining the rate of cavity filling, and the occurrence of molding

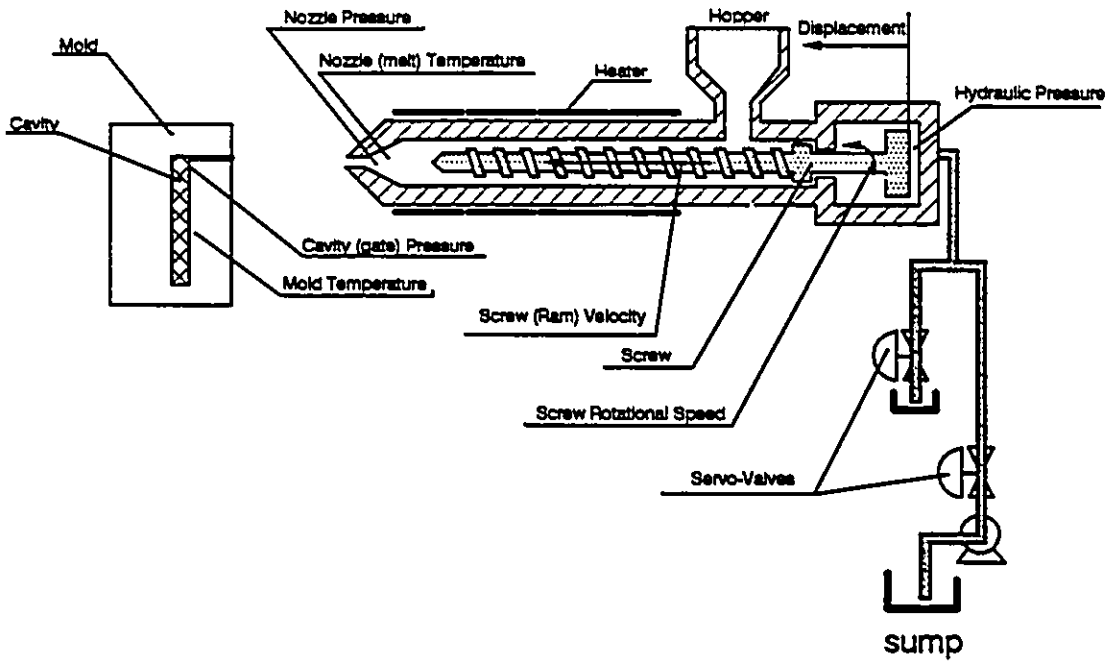

Figure 1.1 Injection molding machine: basic components and major variables

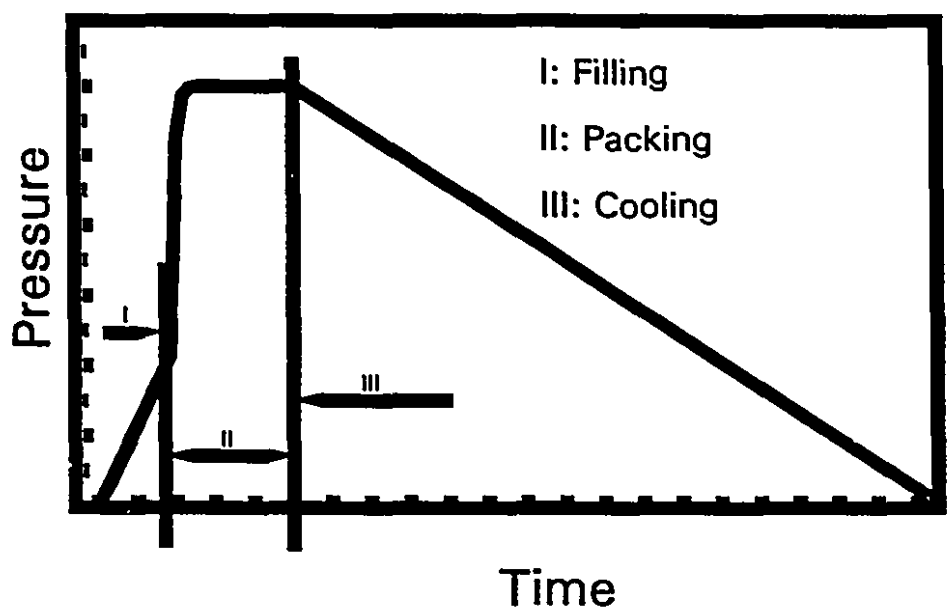

Figure 1.2 Cavity pressure profile during the injection molding cycle

defects such as short-shots or jetting. It is a complex function of back pressure, screw speed, displacement, melt temperature, and nozzle pressure. Back pressure (hydraulic pressure) is directly associated with the opening of the servo-valve in the hydraulic system. Cavity pressure during filling is also a function of the degree of fill.

When the mold is filled, the cavity pressure rises rapidly and the injection speed reduces to near zero as the packing commences. The purpose of packing is to force additional material into the cavity to compensate for the shrinkage accompanying cooling and solidification. Packing is critical for producing a molded part with good mechanical properties, dimensional stability, and surface characteristics. However, over-packing can lead to mold flash. Cavity packing pressure, a good indicator of the degree of packing, is an important process parameter which should be controlled. Cavity pressure is determined by nozzle pressure, cavity geometry, and the melt and mold temperatures.

Cooling continues after the packing stage finishes. Ideally there should be no polymer flow into or out of the mold cavity during this phase. Cavity pressure, polymer temperature and mold temperature decrease due to the removal of thermal energy by coolant circulation inside the mold cooling channels.

In injection molding, consistency and repeatability from cycle to cycle are important objectives of process control. The injection molding process is a complex process in which material, machine, and process variables interact with each other to produce the final molded article. Figure 1.3 illustrates the relationship among these variables.

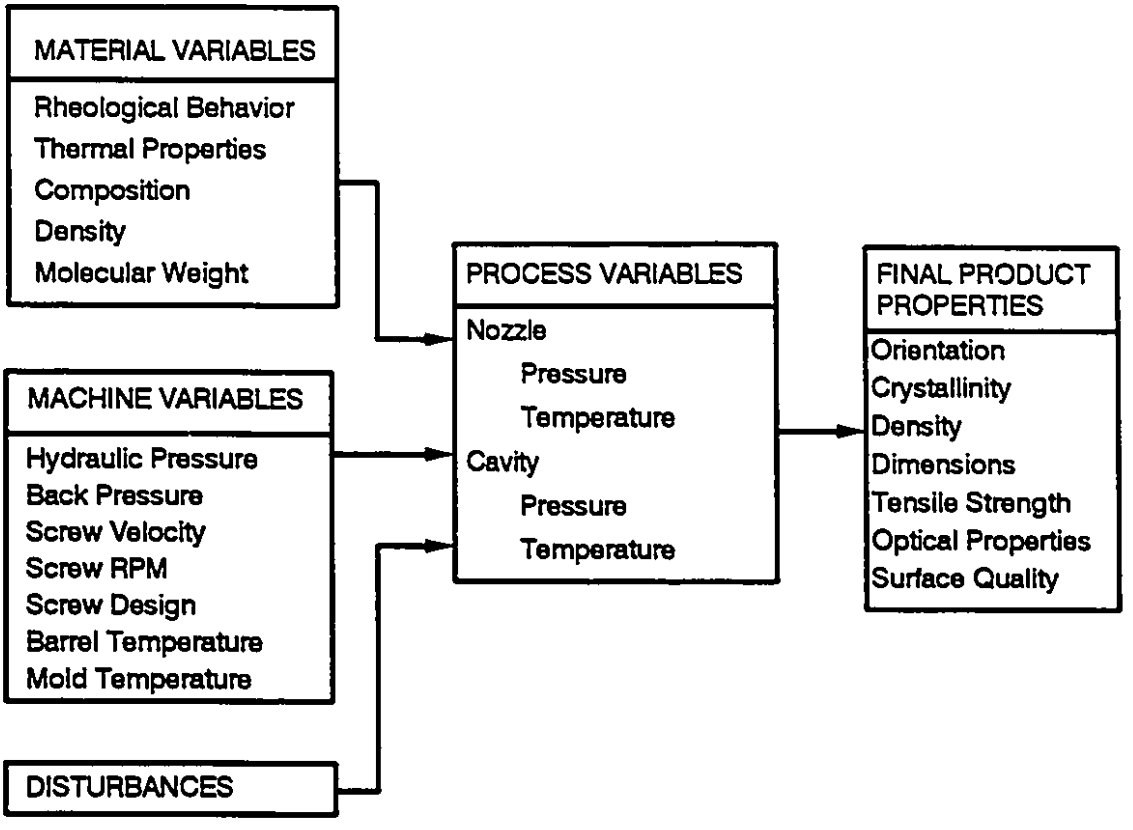

Figure 1.3 Injection molding relationship

Considerable research efforts both at McGill and elsewhere have attempted to obtain an understanding of the interactions between the above variables of the injection molding process. Some of the research employs first principles to construct a mathematical model, while other work is mainly experimental. Both the theoretical and experimental results have emphasised the importance of repeatability of some crucial machine and process variables, such as mold temperature, melt temperature, nozzle pressure, cavity pressure and ram velocity. Control of at least some of these variables is essential for achieving reliable product quality. Abu Fara [1] has carried out a comprehensive review of the major research in the areas of simulation, control and experimental analysis of the injection molding process. The following sections update his review to incorporate some recent advances in these areas.

The thesis is divided into seven chapters. This chapter is an introduction to the injection molding process and a literature review on the related areas with emphasis on dynamics and control. Chapter 2 states the research objectives of the project. Chapter 3 presents the design and implementation of a data acquisition and computer control system. Chapter 4 gives a review of system identification and control algorithms. Chapter 5 studies the injection dynamic modelling and self-tuning control of cavity pressure for the filling and packing stages. Chapter 6 describes cavity pressure dynamics and controller design for the cooling stage. Chapter 7 summarizes the conclusions, outlines the contributions of this work, and offers some recommendations for future work.

1.2 Studies of the Correlation of Product Properties with Process Conditions

Over the past two decades, researchers have been investigating the correlation between the operating conditions in injection molding and the final product quality.

Criens, Händler and Moslé [2] studied the influences of the injection molding conditions on the strength of thermoplastics. They observed that the pressure drop in the sprue was a function of melt and mold temperatures. The influence of mold temperature was small in comparison with that of melt temperature. The same was true for the effect on the tensile strength. The degree of orientation was found to depend only on cavity pressure; therefore, it appeared to be independent of melt temperature, mold temperature, and filling speed which cause the pressure difference. The tensile strength increased as the pressure drop in the sprue increased.

Chiu and Hsieh [3] investigated the correlation between the residual stress of ABS Terpolymers and the injection molding conditions. The layer-removal method and microscopic measurement techniques were used to evaluate the stresses in these molded articles. The relationships between residual stress and processing parameters such as injection pressure, holding pressure, holding time, injection time, injection rate, and mold temperature were examined. Experimental results indicated that, at high injection rates (>10g/s), the residual stresses were compressive in the surface layer and tensile in the interior; however, at low injection rates (<10g/s), the residual stresses were tensile in the surface layer and compressive in the interior. The results also indicated that higher injection rates causes lower residual stresses. Also, compressive residual stresses increased in proportion to the increase of holding

pressure. The residual stress could be decreased by a higher mold temperature. A longer holding time produced higher compressive residual stresses and lower tensile residual stresses.

Some injection molding machines start by controlling injection velocity during filling and then transfer to pressure control when packing commences. Fritch [4] found that the proper detection of the velocity-to-pressure transition had a strong effect on the orientation-sensitive properties and the consistency.

Chao and Maul [5] carried out experimental studies of the effects of injection velocity on jetting, warpage, and flashing. The following conclusions were drawn: 1) reducing the melt flow speed does not avoid the jetting problem; 2) a constant melt flow and variable flow speed have the same effect on the warpage of the molded part of uniform thickness; 3) it is necessary to reduce the injection speed to avoid flash when the injection cavity is nearly filled.

Studies by Cox and Mentzer [6] showed that the effect of filling time on the properties of filled polymer articles was very significant. Differences were also observed in the peak tensile stress, flexural strength and surface properties.

Greener [7] observed that the effect of pressure was to cause a densification in the molded part. This densification was also found to be a function of the cooling rate.

Thomas and McCaffery [8] developed a model to predict shrinkage and distortion based on simulations of filling, packing and cooling, and suggested that a pragmatic approach to predict shrinkage was to develop a hybrid theoretical and

experimental relationship.

Mathew, Nunn and Orroth [9] reported that a low mold temperature resulted in a low degree of crystallinity, and required a long cycle time to achieve dimensionally stable parts free from warpage and distortion. Melt temperature, mold temperature, residence time in the barrel and moisture level in the material had a significant influence on the final properties of the parts molded from crystallizing polyethylene terephthalate (CPET).

Patel and Nunn [10] studied the effect of the process conditions (maximum cavity shear rate during filling, mold temperature, packing pressure, cooling time) on injection molded poly(phenylene sulfide) articles. Two different commercial grades of 40% glass filled poly(phenylene sulfide), A40 and B40, were used. Physical properties and percent crystallinity of the injection molded material A40 were enhanced by higher mold temperature (280 °F or greater), whereas minimum possible cooling time (just enough to avoid warpage during demolding), slow filling rate (just sufficient to fill the cavity), and low packing pressures (sufficient to avoid back flow) were found to be ideal. For Material B40, higher mold temperature (280 °F or greater), high cooling time, higher filling rate, and low packing pressure were required to obtain maximum crystallinity and flexural modulus. Opposite conditions for A40 and B40 were required to obtain maximum tensile strength and flexural strength.

Boldizar, Kubát, and Rigdahl [11] reported that appearance of high modulus structures in HDPE was associated with a high degree of orientation encountered in

high degree of orientation encountered in high pressure injection molding. It was found to be necessary to use high pressures to obtain these structures.

Nelissen, Nies and Lemstra [12] reported that, during compression or injection molding of the system polystyrene/poly(2,6-dimethyl-1,4-phenylene ether), phase separation was induced. This phase behaviour, detected by differential scanning calorimetry and transmission electron microscopy, was rationalized in terms of the influence exerted by pressure on the location of the phase boundary.

Pierick and Noller [13] investigated the effects of the process conditions (cavity pressure, hold pressure, injection speed, melt temperature, and mold temperature) on shrinkage, and found that cavity pressure was the parameter most directly related to shrinkage.

Hastenberg, Wildervanck and Leenen [14] found that the stress distributions along the flow path were influenced by the varying pressure histories from the entrance to the end of the mold cavity. The various features of the stress profiles were explained by the influence of the pressure decay rate in the injection-molding process.

Matsuoka, Takabatake, Koiwai, Inoue, and Yamamoto [15] discussed an integrated simulation system to predict warpage of injection molded parts. The warpage was predicted from the temperature difference between upper and lower surfaces, temperature distribution and flow induced shear stress, and shrinkage.

In addition to the above experimental and empirical studies, researchers have employed computer simulations to understand the interactions between process

conditions and product quality parameters in a more fundamental approach.

1.3 Simulation of Injection Molding

Computer simulation of injection molding started almost two decades ago with one-dimensional models. With the development of computers and computational methods, computer simulation has become fairly sophisticated. There exist several commercial products such as MOLDFLOW and CFLOW to predict the temperature, pressure, flowrate and the distribution of some properties in the product [16, 17].

Kamal, Chu, Lafleur and Ryan [18] outlined the features of a comprehensive computer simulation of the filling stage of an injection molding process to obtain predictions regarding temperature, pressure, velocity, stress and structure of the melt front region. The simulation incorporated a visco-elastic rheological equation and took non-isothermal crystallization kinetics into consideration.

Wang, Hieber and Wang [19] used a control-volume approach to simulate the pressure field, melt front advancement, and temperature field for the mold filling stage of the injection molding of three dimensional thin parts.

Gogos, Huang and Schmidt [20] dealt with the simulation of the filling of a cavity utilizing the Marker-and-Cell numerical technique. The cavity was treated as two parallel plates. The flow was assumed to be isothermal and incompressible with a rheological power law model. The results of the simulation were found to be in qualitative agreement with experimental results using tracer particles.

Goyal, Chu and Kamal [21] later developed a comprehensive two-dimensional

mathematical model for filling a disc-shaped cavity. The model took into account the effects of visco-elasticity, non-isothermality, fountain flow and slip of the flow front. A variable slip boundary condition was used to avoid discontinuity in the flow structure. The results of the simulations were obtained using the White-Metzner (visco-elastic) and generalized power-law (inelastic) constitutive equations.

Huilier, Lenfant, Terrisse and Deterre [22] presented a model of the packing stage in injection molding of thermoplastics. It calculates the time evolution of the pressure and temperature fields and stress variations in a simple geometry.

Nguyen, and Kamal [23] studied two-dimensional packing, assuming that the process was isothermal because the pressure build-up during this phase occurs in a very short time. The polymer melt was assumed to behave like a Maxwell fluid with a Power-law viscosity and a constant relaxation time. The density was assumed to follow the Spencer-Gilmore [118] relation.

Titomanlio and Piccarolo [24] established a function relating the mass entering the mold during the packing-holding stage as a function of holding time. The model was tested with nylon (NY66) resin.

Turng, Wang and Wang [25] proposed a methodology for analyzing the flow of two different polymer melts injected sequentially into a three-dimensional thin cavity using co-injection molding.

Papathanasiou and Kamal [26] presented a model for the filling stage of injection of visco elastic thermoplastics into cavities of complex shapes. The model considered two-dimensional melt flow, with converging and diverging flow regions

induced by the complex boundary shape and by the presence of an obstacle. The model was non-isothermal with the melt losing heat to the mold walls as it travelled into the cavity. It used a visco-elastic (White-Metzner) model, and the properties of the material varied with temperature, shear rate, and pressure. Boundary-fitted curvilinear coordinates were used in the mapping of the flow field into a time invariant rectangle, which permitted the use of the finite difference method. The numerical results revealed geometry-induced asymmetries in the flow and thermal fields, as well as the effect of various process parameters on the pressure and temperature profiles in cavity. The model could deal with a cavity of variable thickness, thus allowing for a treatment of cavity thickness as a process parameter in the simulations. Kamal and Papathanasiou [27] compared the model simulation results with experimental data, showing that the theoretical pressure predictions were in fairly good agreement with experiments with the maximum deviations occurring towards the end of filling.

Chu, Kamal, and Goyal [28] presented a detailed two-dimensional mathematical model to describe all three stages of the injection molding cycle in a simple rectangular cavity. The predictions of velocities, pressures, temperatures, and shear stresses were compatible with experimental results.

Chiang, Hieber and Wang [29] proposed a unified simulation of filling and post-filling stages in injection molding. The model involved a hybrid finite-element/finite-difference numerical solution of the generalized Hele-Shaw flow of a compressible viscous fluid under non-isothermal conditions. The shear viscosity of

the polymeric material was represented by a Cross model [119] of the shear-rate dependence and a WLF-type [120] functional form for the temperature and pressure dependence, whereas the specific volume was modeled in terms of a double-domain Tait [121] equation. Complex thin parts of variable thickness were modelled and described by flat, triangular finite elements. In a second part paper [30], the cavity pressure prediction was compared favourably with the experimental results.

Simulation of the injection molding process is desirable because it would provide comprehensive relationships between some major process variables, properties, and process conditions, without carrying out expensive and time-consuming tests. Simulation results can assist mold and machine designers in choosing a proper design based on quantitative information, rather than relying on costly trial and error. Irrespective of the degree of accuracy of the simulation and machine design, there will always exist machine noise, vibration, wear-out and raw material variability which cause the quality inconsistency of the final molded part. Process control is the commonly accepted technology in industry to assure that the process and machine variables remain close to the desired operating conditions, consequently maintaining product quality.

The above review suggests that both quality analysis and computer simulation indicate that mold temperature, melt temperature, injection velocity, hydraulic pressure, nozzle pressure and cavity pressure have significant influences on the final product. Closed-loop control of the above variables has become increasingly common in order to minimize variability of product quality. The following gives a review of

recent significant work on the control of these variables.

1.4 Mold Temperature Control

A comprehensive review of mold temperature control has been presented earlier by Gao [31].

Patterson, Kamal and Gao [31 - 33] installed a number of fast response thermocouples both at the mold surface and inside the mold metal of a simple fan-gated injection cavity to measure mold surface temperatures and mold metal temperatures. The temperature distributions in both space and time were obtained. Due to the variability of mold temperature in both time and space, it would be very difficult to develop a control strategy to control temperature distribution at all points and times. Therefore, an alternative strategy based on representative thermal parameters is desirable. A number of alternative parameters were considered: mold surface cycle averaged temperature, mold surface peak temperature, mold partial cooling time, mold metal cycle averaged temperature, and mold metal peak temperature. The dynamic models suitable for control were obtained for the above parameters. They were all found to be best fitted with a first order plus delay model. The performance of Dahlin and PID controllers was compared with Dahlin control found to be slightly better.

Rinderle [34] proposed to use heat pipes to construct a mold such that its temperature could be controlled. The construction of such a mold appears expensive, and the strength of the mold is questionable.

Kim et al [35 - 37] presented a concept of low thermal inertia molding (LTIM). The mold surface temperature is kept at the same temperature as the incoming molten polymer; therefore, filling can be done isothermally. Upon the completion of filling, the surface temperature of the mold is lowered to cool the part. They claim that the quality of the part is improved due to the reduction of flow-induced molecular orientation, and that the injection hydraulic pressure can be reduced greatly. In order to make the overall injection cycle time to be the same as that obtained with the conventional mold, they proposed to use high conductivity materials and/or thermoelectric modules for the mold. No application of this technique to injection molding has been reported. In any case, the technique suffers from the following shortcomings: (i) the heating-up process may take a long time, (ii) the mold strength is limited, (iii) the mold has to be specially designed.

1.5 Melt Temperature Control

Gomes [38] and later Ruscitti [42] conducted extensive reviews of the dynamics of melt temperature. These findings will not be repeated here.

Kamal, Patterson and Gomes [39 - 41] installed a thermocouple in the injection screw tip to measure the melt temperature. Step change and PRBS tests were carried out to determine the dynamics of melt temperature as well as front and rear barrel zone temperatures. The models of front and rear zone heater temperatures were found to be essentially first order plus delay, while that of the melt temperature was found to be best described as second order plus delay. The

interaction between the front and rear zones was negligible. The melt temperature was strongly affected by the front zone barrel temperature. PID control and other classical control techniques were applied to control the melt temperature, and satisfactory results were obtained. Later, Ruscitti [42] installed four heater zones in the same barrel. He also installed a number of thermocouples at various positions in the nozzle to determine the spatial distribution of melt temperature. A Vanzetti infrared temperature transducer was also installed to compare it with the thermocouples. He found that the thermocouples provided more accurate melt temperature measurement because the Vanzetti appeared to indicate the averaged temperature of a small volume of the melt in front of its probe. A time-proportional algorithm was employed to control barrel heater power and melt temperatures. The long control interval was found to cause ripple fluctuations in the barrel temperatures [42].

1.6 Closed-Loop Control of Hydraulic, Nozzle and Cavity Pressures

An early study of pressure dynamics was carried out by Kamal, Patterson and Abu Fara [43, 44]. Dynamic models useful for control purposes were obtained for both nozzle and hydraulic pressures. The dynamic model for hydraulic pressure during filling was found to be best described by a first order plus dead-time model together with an underdamped second order model, as given by Equation (1.1):

$$P_H = G(1-e^{-(t-D)/\tau)}) + \frac{G_1}{(1-\xi^2)^{1/2}} e^{-\xi t/\tau_1} \sin((1-\xi)^{1/2}\frac{t}{\tau_1}) \qquad (1.1)$$

where G, G_1 = process gains

τ, τ_1 = process time constants

ξ = damping factor

D = process time delay

The nozzle pressure was found to be best modelled as a second order over-damped process as shown below:

$$P_N = G\left[1 - \frac{\tau_1\tau_2}{\tau_1-\tau_2}\left(\frac{1}{\tau_2}e^{-t/\tau_1} - \frac{1}{\tau_1}e^{-t/\tau_2}\right)\right] \qquad (1.2)$$

where P_N = nozzle pressure during filling

G = process gain

τ_1, τ_2 = time constants

They concluded that for pressure control of injection molding, it is preferable to use nozzle pressure rather than hydraulic pressure.

Kamal, Patterson, Conley and Abu Fara [45, 46] later carried out a more detailed study to understand the dynamics of pressure variation at different points in the injection molding system. Both step changes and a pseudo-random binary sequence (PRBS) were employed to obtain the dynamics for both nozzle and cavity pressures. The cavity pressure was found to be best modelled as a first-order plus delay with an added ramp component to allow for the steady increase of cavity pressure:

$$P_c(t)=k_1 t+k_2(1-e^{-(t-D)/\tau}) \qquad (1.3)$$

where $P_c(t)$ = cavity pressure

k_1 = ramp slope

k_2 = process gain

τ = process time constant

D = time delay

An experiment was carried out with proportional and integral (PI) feedback control. The cavity pressure followed the set-point closely in the early stages of filling; then it became increasingly oscillatory. This was attributed to the non-linearity of the process. Table 1.1 gives the process parameters associated with the servo-valve openings. A gain scheduling control strategy, in which the controller gain was reduced throughout the injection stage, improved the control response. They did not give an explicit expression to describe the pattern of gain reduction or the nature and causes of the non-linear dynamics during the filling.

Chiu, Wei and Shih [47], based on Equation (1.3) of Kamal et al [46], designed a PI controller and an adaptive model following controller (AMFC) for cavity pressure during filling. They compared the performance of these two types of controllers, and found that the control response of AMFC was better in terms of set-point tracking. However, only simple set-point profile, fixed operating conditions and simple cavity geometries were used in the test. The results under different process conditions were not projected. Furthermore, process dynamics were not reported due to the inherent nature of AMFC.

Table 1.1 Values of parameters for cavity gate pressure model during filling [46]

Change in Valve Opening (%)	Ramp Slope k_1 (psi/s %)	Process Gain k_2(psi/%)	Time Constant τ(s)	Time Delay D(s)
15-35	12.06	3.84	0.116	0.011
20-40	13.25	4.41	0.091	0.012
30-50	16.82	1.76	0.110	0.010
35-15	9.01	2.91	0.178	0.040
40-20	9.89	2.32	0.134	0.070
50-30	11.85	0.75	0.098	0.040

Costin, Okonski and Ulicy [48], based on the model structure of Equation (1.1) proposed by Kamal et al [43], developed a hydraulic pressure control system for injection filling. They used screw displacement increments instead of time to determine the sampling instants. A self-tuning regulator (STR) and PI control systems were programmed to control the hydraulic pressure for both HDPE and ABS. In both cases, the self-tuning controller was found to perform better than PI. However, both STR and PI exhibited some significant errors. They suggested that if the nozzle pressure was used instead of hydraulic pressure, the results might improve. However, no experiment was performed to verify this claim. Furthermore, using the screw displacement increments as the sampling period prevents extending the filling control strategies into the packing phase.

Agrawal, Pandelidis, and Pecht [49] gave a comprehensive review on injection molding process control. They categorized the injection molding variables into all-phase control, phase-dependent control, and cycle-to-cycle control. All-phase control includes variables that must be controlled all times. The control of variables triggered by a transition to a specific phase is said to be phase-dependent control. In cycle-to-cycle control, previous data are used to predict future trends and to take appropriate corrective actions.

Based on the dynamic models in Equations (1.2) and (1.3) obtained by Kamal et al [45, 46], Srinivasan, Srinivasan and Maul [50, 52] proposed a learning control for cavity or nozzle pressure during injection mold filling. Learning control can be applied to a process which is subject to periodic inputs. For this reason, it is sometimes also referred to as repetitive control [51]. The resulting controller utilizes an error signal from the preceding injection cycle to improve the effectiveness of control in the current injection molding cycle. For this reason, learning control is classified as cycle-to-cycle control. The simulation results showed an improvement in terms of error reduction from cycle to cycle. However, there was no experimental verification of the simulation results. since the control is based on a cycle-to-cycle basis, there is no improvement possible within an injection cycle.

Malloy, Chen and Orroth [53] studied injection holding pressure transition techniques. The importance of the transition was stressed in this investigation in terms of part weight consistency. The problems associated with the time based transition were well explained. Five different transition techniques based on time,

position, cavity pressure, nozzle melt pressure and hydraulic injection pressure were evaluated experimentally. Significant differences in molded part weight repeatability were observed among the different techniques. The transition detection based on position or cavity pressure was found to be the most effective; with the latter offering other advantages, such as providing information on the melt condition inside the cavity over the course of the molding cycle. Pressure transfers based on peak nozzle melt and peak hydraulic injection pressures were also shown to perform well when melt viscosity was constant. Injection-to-packing pressure transition based upon fixed injection time was found to be the least repeatable.

Haber and Kamal [54, 55] studied the cavity pressure fluctuation from cycle to cycle. The use of a servo-valve in the hydraulic system of the injection molding machine, coupled with a microprocessor to control the servo-valve opening, was shown to reduce the peak pressure variations. The manipulation was based on a cycle to cycle basis, rather than within cycle control.

Abu Fara, Patterson and Kamal[1, 56, 57] developed a closed-loop cavity pressure control system for the packing phase. The dynamic model was found to be a first order plus delay as expressed in the following equation:

$$P_c(t) = k(1-e^{-(t-D)/\tau}) \qquad (1.4)$$

Where $P_c(t)$ = the cavity pressure during packing

k = the process gain

τ = the process time constant

D = the process delay

Table 1.2 Model parameter values of cavity pressure during packing [57]

Change in Valve Opening (%) & Pressure at which it occurred	Process Gain k, Mpa/%	Time Constant τ (s)	Time Delay D (s)
30 % @ 2000psi	0.439	0.179	0.010
50 % @ 2000psi	0.290	0.209	0.011
40 % @ 2000psi	0.341	0.187	0.007
40 % @ 3000psi	0.275	0.451	0.005

The process dynamics exhibited strong non-linearity, because the process gain, time-constant, and delay were found to vary with both the valve opening and the cavity pressure itself. The parameters of the model obtained under different experimental conditions are given in Table 1.2. A classical PI controller was designed, implemented and tested experimentally. Reasonably good experimental results were obtained. The switch from filling to packing was found to be best based on the rate of change of the cavity pressure. However, the control responses seemed to be strongly related to the packing profile. The best result was obtained with a packing profile fitting a 4th order polynomial of pressure variation with time.

Smud, Harper and Leffew [58] demonstrated the control of cavity pressure during the packing phase by manipulating the clamp pressure (or clamp force), instead of the most common approach using one or more hydraulic servo-valves to drive additional material into the injection cavity. The dynamic model was found to

be related to the sign of the error. The models for both the positive and negative errors were found to fit with first order plus delay models. The controlled cavity pressure followed the set-point profile reasonably well. However, using the mold separation (or clamping force) as the manipulated variable inherently causes variation of the molded part thickness, i.e. the molded part thickness would not be the same as the set value, unless there is no mold separation.

No published results can be found, to the best knowledge of the author, regarding the modelling and control of cavity pressure during the cooling phase.

1.7 Closed-Loop Control of Ram Velocity

Abu Fara [59] reported that ram velocity had a fast response (less than 0.01 second) to the supply servo-valve opening in the hydraulic system. He assumed that it had a linear relationship with the servo-valve opening:

$$c_t = G \cdot M_t \qquad (1.5)$$

where c_t is the controlled variable, ram velocity at the sampling time t,

M_t is the manipulated variable, the percentage change in the valve opening at time t, and

G is the process gain.

On the other hand, Wang et al [60] reported that a 4th order dynamic relation

existed between ram velocity and the servo-valve opening as follows:

$$G(s) = \frac{c(s)}{M(s)} = \frac{2.144\times10^{11}}{(s+125)(s+1138)[(s+383)^2+1123^2]} \qquad (1.6)$$

where M is the manipulated variable, voltage to the servo-valve, and

c is the controlled variable, the ram velocity during injection filling.

Both of the above models for ram velocity were assumed to be linear time-invariant, neglecting the effect of the increasing cavity pressure during filling on the ram velocity during injection.

Pandelidis and Agrawal [61], based on Equation (1.6), proposed a self-tuning control with a deadbeat design for the ram velocity control. The simulation results demonstrated that the controller response followed a varying velocity profile closely. However, no experimental verification of the controller was provided.

Pandelidis and Agrawal [62] later, again limiting themselves to the control algorithm itself, citing the above two ram velocity models developed by Abu Fara [59] and Wang et al [60], and chose the latter for their simulation study. They proposed that the ram velocity follow the fixed trajectory shown in Figure 1.4, based on the following reasoning:

(i) high ram velocity during filling of less critical volumes such as runners, results in minimum heat loss and shorter injection time;

(ii) slower ram speed when the melt reaches the gates eliminates jetting;

(iii) velocity adjusted so as to maintain constant flow front velocity prevents inconsistencies in flow pattern that can cause non-uniform surface orientation

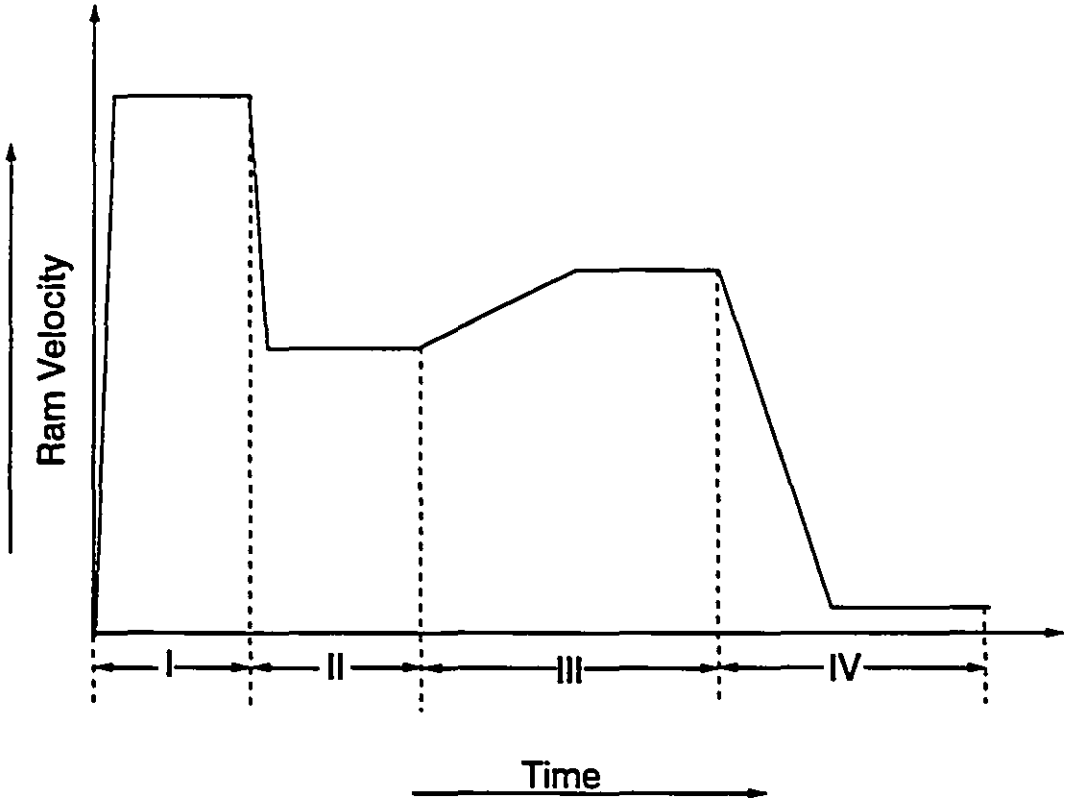

Figure 1.4 Ram velocity profile suggested by Agrawal [62]

resulting in warping of the moulded part;

(iv) significant reduction of the ram velocity just prior to the moment of complete cavity filling prevents over-packing and/or flashing.

They proposed that the objective of the optimal anticipatory control of ram velocity was to minimize the deviation of the actual speed profile from a desired pre-specified reference. They defined their objective function as:

$$J = \frac{1}{2}\{e^T(k_f)Se(k_f)\} + \sum_{k=0}^{k_f-1}\{e^T(k)Q(k)e(k) + u^T(k)R(k)u(k)\} \qquad (1.7)$$

where e(k) is the tracking error at kth sample

u(k) is the manipulated variable

k_f is a finite final time

S is a positive semi-definite weighting matrix for final time (assumed zero in their case)

Q is a positive semi-definite weighting matrix of the states

R is the weight matrix of the controlling variable, which should be positive.

Their simulation results indicated that the optimal anticipatory control (with proper weight matrices Q and R, producing the smallest objective function J) was slightly better than a PID controller. However, they did not test their results experimentally and the non-linearity and time-varying characteristics of ram velocity during filling were ignored.

1.8 Selection of the Controlled Variable

The machine hydraulic pressure, nozzle pressure, cavity pressure, screw displacement, and ram velocity all share the same manipulator: the hydraulic servo-valve. The change of servo-valve opening introduces a change in hydraulic pressure first. The hydraulic pressure changes then propagate to the nozzle pressure. The ram velocity is driven by the hydraulic pressure and counter-driven by the nozzle pressure. The pressure buildup in the nozzle drives the molten resin into the injection mold cavity. The cavity pressure increases gradually with the accumulation of the polymer during filling and rises abruptly when the cavity is completely filled. All of the above five variables are either directly or indirectly related to the servo-valve opening. A block diagram of the relationships (in the Laplace form) is shown in Figure 1.5. Detailed information on these relationship functions can be obtained by mathematical modelling as shown in Chapter 5. The system has multiple outputs but only one input. At any time, only one of the five variables can be closed-loop controlled. It is important to point out that the control of any one of the five variables implies that the other four variables are also being controlled without explicit set-point profiles, because they are interrelated.

Among the three pressures, the cavity pressure is the best choice as the controlled variable, if the injection cavity allows the installation of a pressure transducer. The cavity pressure is the clearest indicator of the status of the material in the cavity. The status of material is mainly determined by its pressure and temperature. Various studies [6, 7, 13, 14] have indicated that cavity pressure has the

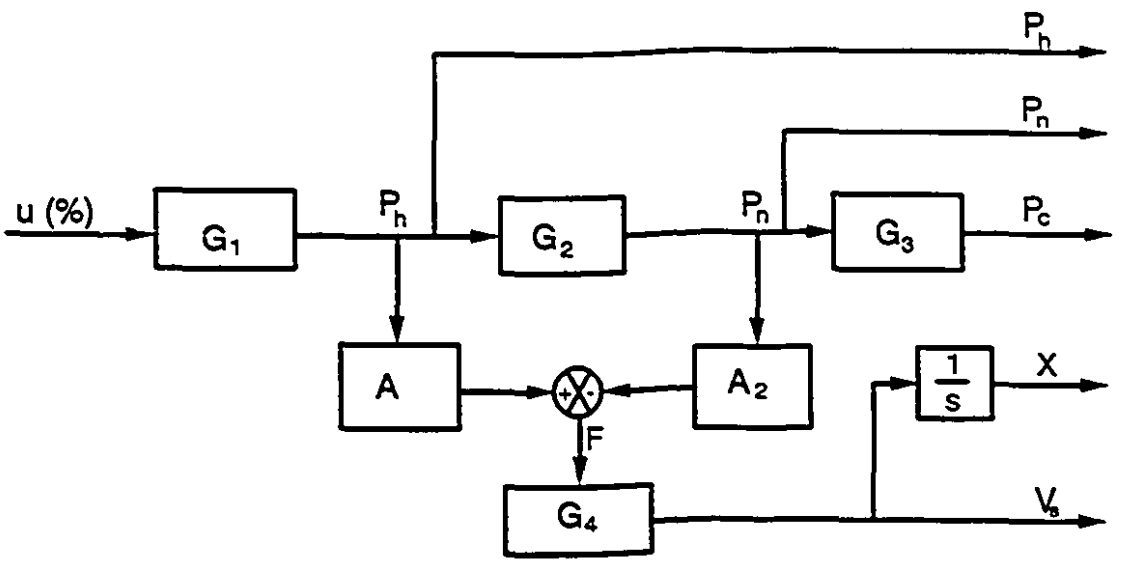

$$G_1(s) = \frac{P_h(s)}{u(s)} \qquad G_3(s) = \frac{P_c(s)}{P_n(s)}$$

$$G_2(s) = \frac{P_n(s)}{P_h(s)} \qquad G_4(s) = \frac{V_s(s)}{F(s)}$$

A_2 = effective area of the screw,
P_h = hydraulic cylinder back pressure,
P_n = nozzle pressure,
P_c = cavity pressure,
V_s = screw velocity, and
u = servo-valve opening (%),
X = screw displacement,
A = cross-sectional area of cylinder,
F = effective force on the screw,
$F = P_h \cdot A - P_n \cdot A_2$.

Figure 1.5 Relationship between hydraulic pressure, nozzle pressure, cavity pressure, ram velocity, screw displacement and servo-valve opening

most direct effect on the microstructure and product quality.

Although ram velocity is often used as the controlled variable during filling, it is actually a machine variable. Back-flow leakage, temperature changes, and compression of the melt in the nozzle all cause a deviation of polymer flow entering the cavity to differ from that calculated simply from the screw (ram) displacement. It is also very difficult to control ram velocity when the injection cavity is close to being completely filled because the rapid cavity pressure increase causes rapid changes in the machine characteristics. Furthermore, it is not possible to use ram velocity as the controlled variable after the injection cavity is filled. The screw velocity is nearly zero during the packing phase and only pressure can be used to indicate the degree of material compression.

In view of the above arguments, cavity pressure is judged to be the best candidate as the controlled variable for both the filling and packing phases. If it is not possible to install a pressure transducer in the cavity, the choice would be nozzle pressure.

The process non-linearity during the filling and packing phases (see Tables 1.1 and 1.2) causes problems in the implementation of classical closed-loop control. The cavity pressure controllers [43 - 46, 50 - 51, 54 - 57] reviewed were mostly based on a linear time invariant model even though the non-linearity was found to be significant. In most cases, the designed classical controller has to be operated close to the conditions under which model parameters were obtained, otherwise the controller performance deteriorates. Furthermore, the time-invariant and linear

models could only be used with the same machine and test cavity. Changes require the controller to be retuned. However, an injection molding machine is usually employed in conjunction with many different cavities. Retuning the controller for each new cavity or material or condition requires a very tedious and expensive effort. It is therefore highly desirable to have a cavity pressure control system capable of yielding good performance for a wide range of conditions including different cavities.

Adaptive control, suitable for a wide range of conditions and time-varying and/or nonlinear processes, is growing in importance [63 - 82, 85 - 95], with continuous development of computer technologies and computational algorithms. A number of applications have been reported [76 - 82]; some are even applications to polymer processing [80, 81]. It was therefore decided to implement a self-tuning regulator (STR) for cavity pressure control in this work.

STR control requires substantial computational power, which was not available on the old injection molding machine installed in the McGill polymer laboratories. The decision to design a real-time computer control and data acquisition system, with some level of intelligence to replace the existing obsolete system, was made.

Chapter 2

RESEARCH OBJECTIVES

The objectives of this research project may be stated as follows:

(1) to develop and implement a real-time computer control and data acquisition system for the injection molding process,

(2) to develop a cavity pressure control system to operate over a wide range of conditions throughout the complete injection cycle. This objective is divided into the following subobjectives,

   (a) to investigate the evolution of cavity pressure dynamics during the filling phase,

   (b) to design and test a self-tuning controller for cavity pressure during filling,

   (c) to determine the appropriate method to detect the filling-to-packing transition,

   (d) to investigate the evolution of cavity pressure dynamics in the packing phase,

   (e) to design a cavity pressure controller for the packing phase,

   (f) to investigate cavity pressure dynamics in the cooling phase, and

   (g) to implement a cavity pressure control system for the cooling phase.

Chapter 3

THE INSTRUMENTATION, DATA ACQUISITION AND COMPUTER CONTROL SYSTEM

3.1. Introduction

Process automation has reached a high degree of application in the plastics processing industries. Modern injection molding operations can be almost totally automated to the extent that one operator can supervise the operation of many machines. Machine set-ups, once determined, can be loaded automatically when a job is changed. Injection profiles, barrel temperatures and other variables are thus less subject to operator errors, since the operator no longer has responsibility for entering them into the injection molding machine control system. Nevertheless, the determination of the temperatures, injection velocity profile and other variable values to produce acceptable parts at an economic rate is still largely a trial and error process.

Although commercially available control systems of considerable power, complexity and completeness are commonly installed on modern molding machines, these systems are generally unsuitable for research purposes. As part of our ongoing research on injection molding, the ability to change and develop control algorithms was sought. In particular, the capability to employ different algorithms in different phases of the injection molding cycle (for example, filling versus packing) was desired. No commercially available injection molding machine control system could be found to provide the degree of flexibility of operation that was needed. It was

therefore decided to develop a custom system that would satisfy the above needs.

The knowledge and experience gained in previous modifications of the injection molding machine led to the choice of a micro-computer (PC type) as a base for the control system. Modern programming practice dictates a modular construction of programs. This allows for easy modifications and extension to the computer-based control system. It was also determined that it was desirable to have a hierarchical structure for the control system, since different users require different operational levels of machine use. Although the primary objective was the investigation of control strategies and algorithms, the injection molding machine (IMM) would also be used for the "production" of samples for various testing purposes. It was decided to provide three levels of sophistication of operation. These levels are summarized below.

LEVEL	DESCRIPTION
1. (production)	System set-up by default to predetermined machine settings
2. (molding research)	Explicit configuration of the machine settings by the operator
3. (control research)	Explicit configuration of machine settings and the control system

3.2 System Design Characteristics

A number of other capabilities of the system were deemed to be essential.

The overall objectives were to be introduced via software (programming), rather than hardware, in order to preserve as much flexibility as possible for future studies and for unforeseen modifications to the IMM. The desirable characteristics can be summarized as:

(i) a hierarchical structure to accommodate different operational levels,

(ii) an emphasis on software, as opposed to hardware, realisation of functions,

(iii) the utilization of a real-time operating system to accomplish characteristic (ii) above,

(iv) the presentation of user-configurable parameters appropriate to each operating level, and

(v) the presentation of the IMM status during a molding cycle.

Satisfying the characteristics within the constraints of limited resources (computer size and configuration, budget and program development time) presented an interesting problem.

3.3 Required Tasks

A number of tasks had to be completed to achieve the objectives:

(i) The basic tools: a computer, suitable data acquisition boards with analog and digital input-output and a real-time operating system had to be chosen.

(ii) Transducers for various machine variables had to be installed and appropriate signal conditioning performed. Because of previous work,

a number of sensors were already in place on the injection molding machine[1, 31 - 33, 38, 42, 57].

(iii) A computer interface to the injection molding machine had to be developed and tested.

(iv) A suite of programs had to be developed to monitor and control, in real-time, the injection molding machine operation and measure and regulate variables such as barrel temperatures, mold coolant temperature, and cavity pressure.

(v) A "user friendly" interface, suitable for both novice and expert users, and with intelligence to reject invalid or unreasonable user inputs, was necessary.

3.4 Operating System

3.4.1 Operating System Selection

The development of the data acquisition and control programs was key to the success of the project. A multi-tasking operating system was judged necessary. This allowed individual tasks to be associated with particular program modules. The modular programming approach permits easy modification and expansion. It has to operate in real time, since it has to deal with machine requests in a time - critical manner. For example, it has to stop screw movement when the screw forward limit switch is activated. A number of real-time operating systems (PDOS from Eyring, iMAX from Intel, and QNX from QNX Software Systems Ltd.) were examined and

the QNX operating system was chosen. A partial list of the advantages of QNX follows [105 - 113]:

(i) QNX is a real-time, multitasking, POSIX compliant operating system running on IBM PC compatible computers. POSIX is the acronym for portable operating system information exchange.

(ii) QNX has a large suite of user utilities and an industry leading optimizing C compiler (WATCOM C).

(iii) The QNX structure is in a micro-kernel, modular form. Thus it is easy to add, remove or modify a control process (task) without modifying the programs for other tasks.

(iv) QNX has a rich set of inter-process communication functions.

(v) The QNX operating system is stable. Since its introduction in the early 1980's, a number of process control systems for various industries have been successfully developed with it.

(vi) QNX is peer to peer network transparent, which makes it easy to add a second computer to the system, should the original computer not have enough computation power, due to future expansion.

3.4.2 Brief Introduction to QNX OS

QNX consists of a small kernel (less then 8 k bytes) in charge of a group of cooperating processes. The kernel is dedicated to only two essential functions: message passing and scheduling. All other services are handled via system processes.

A typical QNX configuration has the following four system processes: process manager, filesystem manager, device manager, and network manager.

The process manager and kernel provide essential operating system services. QNX supports three process creation primitives: fork(), exec(), and spawn(). Each process is assigned a priority by the programmer. The priorities assigned to processes range from 0 (the lowest) to 31 (the highest).

Three scheduling methods are available with QNX: first in first out (FIFO), round-robin, and adaptive. Each process may run using any one of these scheduling methods. They are effective on a per-process basis, and apply only when two or more processes are of the same priority.

QNX supports three essential types of inter-process communication (IPC): messages, proxies, and signals.

Message passing is the fundamental form of IPC in QNX. It provides synchronous communication between cooperating processes where the process sending the message requires proof of receipt and possibly a reply to the message.

Proxies are a special form of message. They are especially suited for event notification where the sending process doesn't need to interact with the recipient.

Signals are a traditional form of IPC. They are used to support asynchronous inter-process communication.

In QNX, time management is based on a system timer maintained by the operating system. A process can create timers, arm them with a time interval, and remove timers. A QNX function, mktimer(), allows the user to specify one of the

following event-reporting mechanisms:

sleep until completion: the process sleeps from the time it issues the timer arming call until the interval expires.

notify with proxy: a proxy will be used to notify the process that the time interval has expired.

notify with signal: a user-specified signal will be delivered to the process when the time interval expires.

Interrupt handlers service the computer's hardware interrupt system by reacting to hardware interrupts and manage the low-level transfer of the data between the computer and external devices. Interrupt handlers are physically packaged as part of a standard QNX process, but they always run asynchronously to the process with which they are associated.

QNX allows processes to share portions of memory. This is an effective way to communicate and share dynamic information among processes.

3.5. System Description

The hardware and software aspects of the real-time computer control system of the injection molding machine are described below.

3.5.1 Control System Hardware and Components

3.5.1.1 Computer and Data Acquisition Board

An ALR (Micro-Channel bus) computer was chosen to host the data

acquisition and control system. This machine, running at 33 MHz with an i80486DX CPU, has nine megaby'es of memory, and a 240 megabyte IDE hard disk. Two data acquisition boards from Analog Devices (RTI220) were selected for their large input/output capability [96, 97]. Each data acquisition board has a maximum of 64 inputs and 16 outputs. The boards can generate an interrupt to the computer when an analog-to-digital conversion is completed. Two data acquisition boards were installed to have one board for rapidly varying signals (such as pressure) and the other board for slowly changing signals (such as barrel temperature). A digital input/output board, also from Analog Devices, (RTI217), which has 32 input/output lines, was selected for digital signal interface [98]. The addresses and interrupt numbers occupied by these three boards are listed as in Table 3.1.

The real-time computer control system was developed for a 60 ton Danson Metalmec 2 1/3 oz, reciprocating screw injection molding machine. Major machine specifications are given in Table 3.2. The hydraulic system and injection barrel had previously been modified [1]. A number of sensors and instruments had been installed to measure important machine and process parameters such as cavity pressures, nozzle pressure [1], mold temperature and heat flux at various points in the mold [31, 32] as well as barrel and melt temperatures [42]. Two hydraulic servo-valves had been incorporated into the hydraulic system to control cavity or nozzle pressure. In the present work, two control valves were incorporated into the cooling system to control coolant flowrate and temperature, and consequently the mold temperature. Also, an improved heater control system was developed to control

Table 3.1 The addresses and interrupt numbers of the data acquisition boards and digital I/O board

Computer Slot	Descriptions	
1	Name	RTI-217 DIO Board
	Base Address	Base-1: 2000H
	Interrupt Number	11
2	Name	RTI-220 A/D Board (fast)
	Base Address	Base-2: 6000H
	Interrupt Number	10
	ADC Coding	Offset Binary
3	Name	RTI-220 A/D Board (slow)
	Base Address	Base-3: 7000H
	Interrupt Number	7
	ADC Coding	Offset Binary

barrel temperatures.

A simplified computer-injection molding machine interface is shown in Figure 3.1. The directions of the arrows indicate the signal and flow directions. T, P, H and F enclosed in small circles represent the thermocouple, pressure transducer, heat flux sensor, and flow meter, respectively. Dotted lines represent a shielded wire housing through which a number of signal cables pass. Detailed information regarding the major components of the control system is given in the following sections.

Table 3.2 Major machine specifications

Machine Model	Danson Metalmec 60-SR
Capacity	2 1/3 oz (66.1 g)
Screw Diameter	1.375 in
Screw L/D Ratio	15/1
Screw RPM	40-150
Clamping Force	60 Ton (US)
Hydraulic Pump	Sperry-Vickers Vane Pump
Pump Capacity	8 US gpm flow at 2000 PSI Pressure
Electric Motor	20 hp, 3 phase, 60 Hz

3.5.1.2 Injection Barrel and Screw Instrumentations

The instrumentation of the barrel and screw is shown in Figure 3.2. All the thermocouples installed are type E from NANMAC. One thermocouple, installed in each barrel heater zone, measures its temperature. A thermocouple is installed with its tip flush with the injection screw tip to measure the melt temperature. The last thermocouple is installed with its tip immersed into the melt. A Vanzetti infrared sensor [99] is also installed to measure the molten resin temperature. The detailed geometric location of the thermocouples and the Vanzetti can be found in reference [42]. An MTS Temposonics [100] linear displacement (LDT) and velocity (LVT) transducer (Model 011012070208, S/N: 21468-02-010N) was attached to the injection

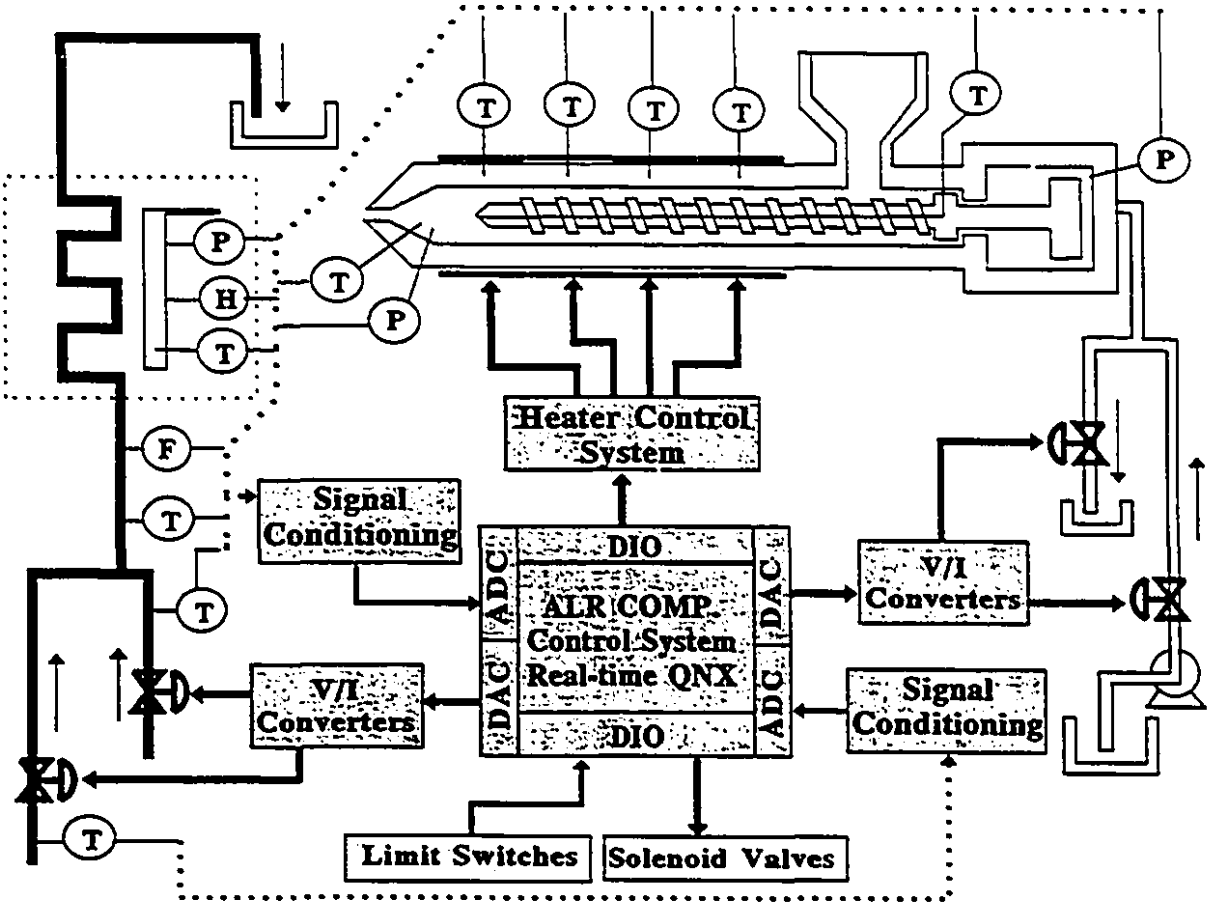

Figure 3.1 Computer interface for the McGill injection molding machine (DIO = digital input / output, V/I = voltage to current converter, ALR = a micro-channel computer)

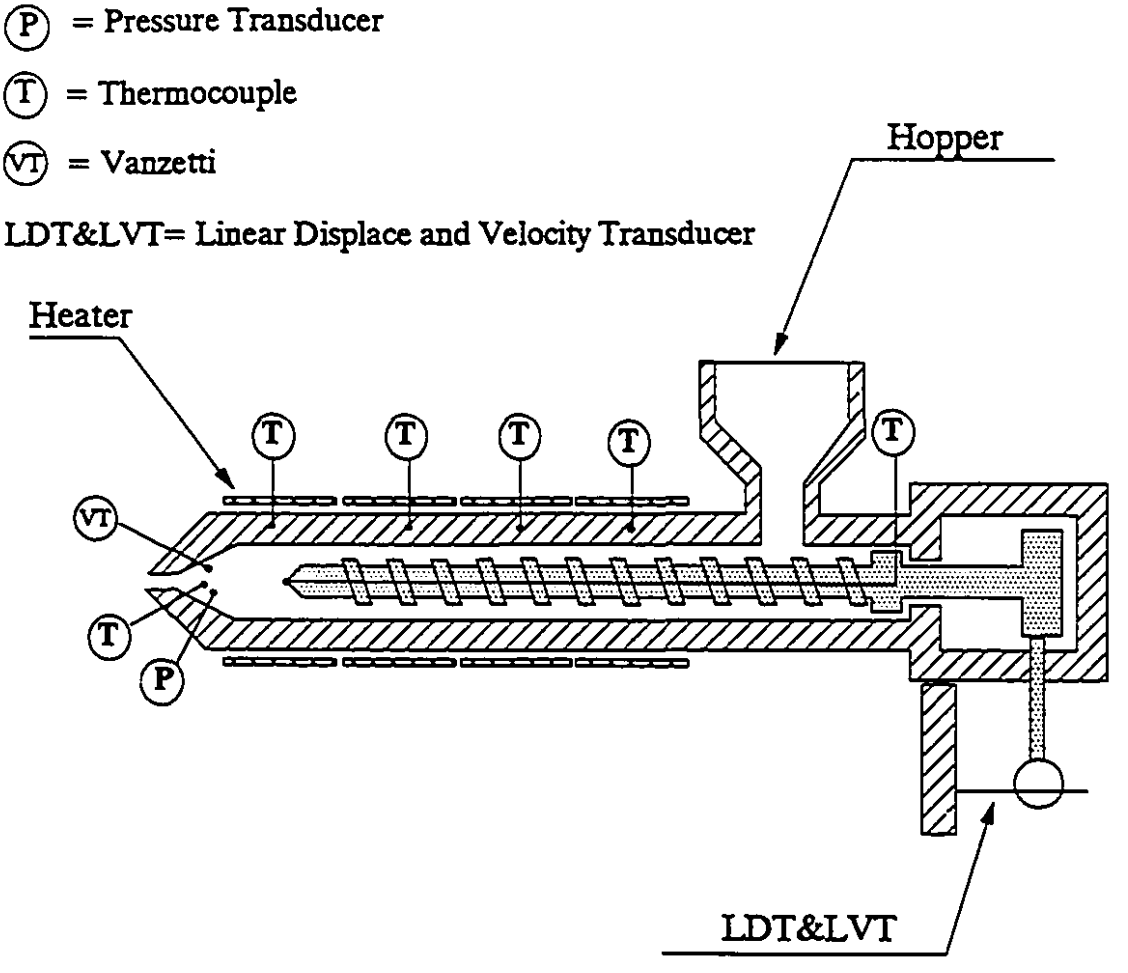

Figure 3.2 Instrumented barrel and screw of the injection molding machine

screw to measure the screw displacement and velocity. The Temposonics transducer obtains the velocity measurement by electronically differentiating the displacement signal. Both LDT and LVT signal outputs are in the range of 0-10 volts. The screw displacement has the following relationship with the sensor output:

$$X=3.05v+4.27 \tag{3.1}$$

where X is the screw displacement, unit: cm, and

v is the LDT output, unit: Volts.

and the velocity has the following relationship equation:

$$V_s = 2.03 \cdot vi \tag{3.2}$$

where V_s is the screw velocity, unit: cm/s, and

vi is the LVT output, unit: Volts.

3.5.1.3 Injection Cavity

Two Dynisco pressure transducers (PT425A-3M), three NANMAC type E thermocouples, and three custom-made thermocouples were installed on the fixed plate of the injection molding machine with their tips flush to the cavity surface [1, 31]. Figure 3.3 gives the sensor locations and cavity geometries. The thickness of the fan-gated cavity is 3.18mm (⅛ inch). The custom-made thermocouples have their hot junction 1 mm away from the cavity surface [31]. The NANMAC and the custom-made thermocouples were installed to be geometrically symmetric around the mold center axis. Therefore, it was assumed that they measured the temperature at the

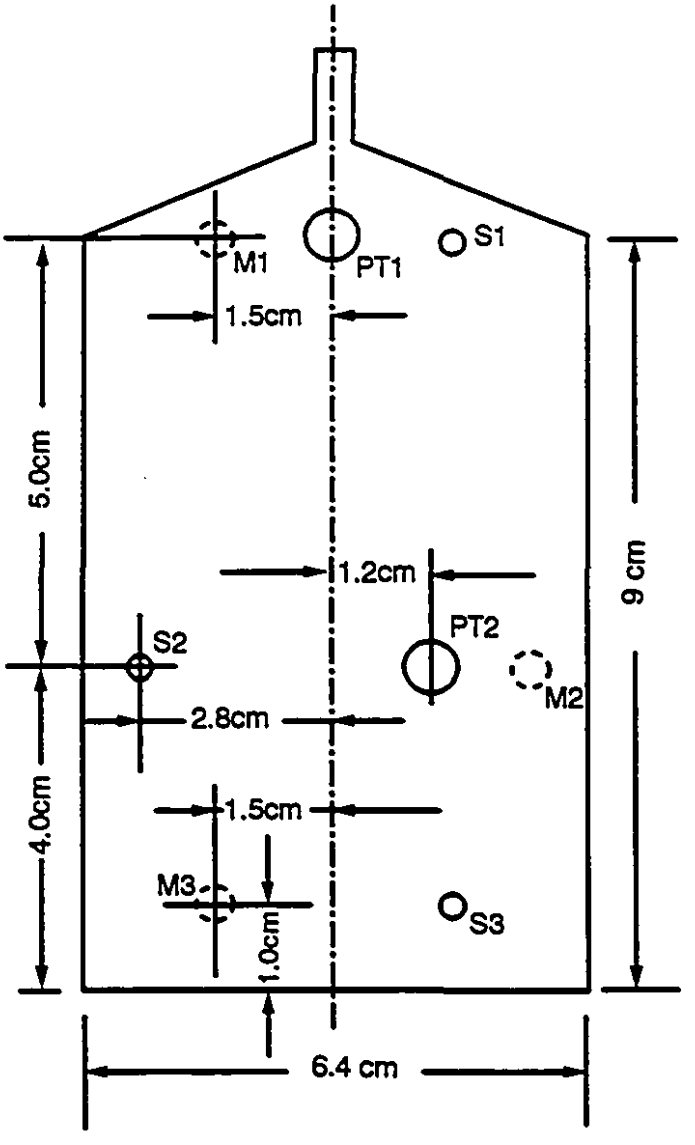

Figure 3.3 Fan-gated cavity and sensor locations (fixed platen)

same location in the cavity, but at different distances from the surface [31 - 33].

Three heat flux sensors (RDF Co. Micro-Foil™ part no. 20455-2) were installed to be flush with the cavity surface at the moveable plate of the machine, as shown in Figure 3.4 [31].

3.5.1.4 Cooling System.

The cooling system design, computer interface, instrumentation and dynamic characteristics are all presented in Chapter 5.

3.5.1.5 Hydraulic Servo System

The hydraulic system was modified to have two hydraulic servo-valves (Moog AO-76-103). A simplified schematic of the hydraulic system is illustrated in Figure 3.5. Either of the two servo-valves can be used as the supply or relief servo-valve depending on the configuration of the nine manual valves incorporated in the hydraulic circuit. The possible operations are listed in Table 3.3. Case 3 was selected to control the cavity pressure throughout this investigation. sv1 is used as the supply servo-valve (Ssv) to provide the hydraulic source to the injection cylinder, while sv2 is the relief servo-valve (Rsv) used to divert the hydraulic oil from the injection cylinder to the sump. Both servo-valves are driven by 0-10 mA dc current. Zero mA current corresponds to a completely shut servo-valve (0% open), while 10 mA corresponds to a completely open servo-valve (100% open). Both of the servo-valves are linear, i.e. their openings are linearly proportional to the supplied current. The

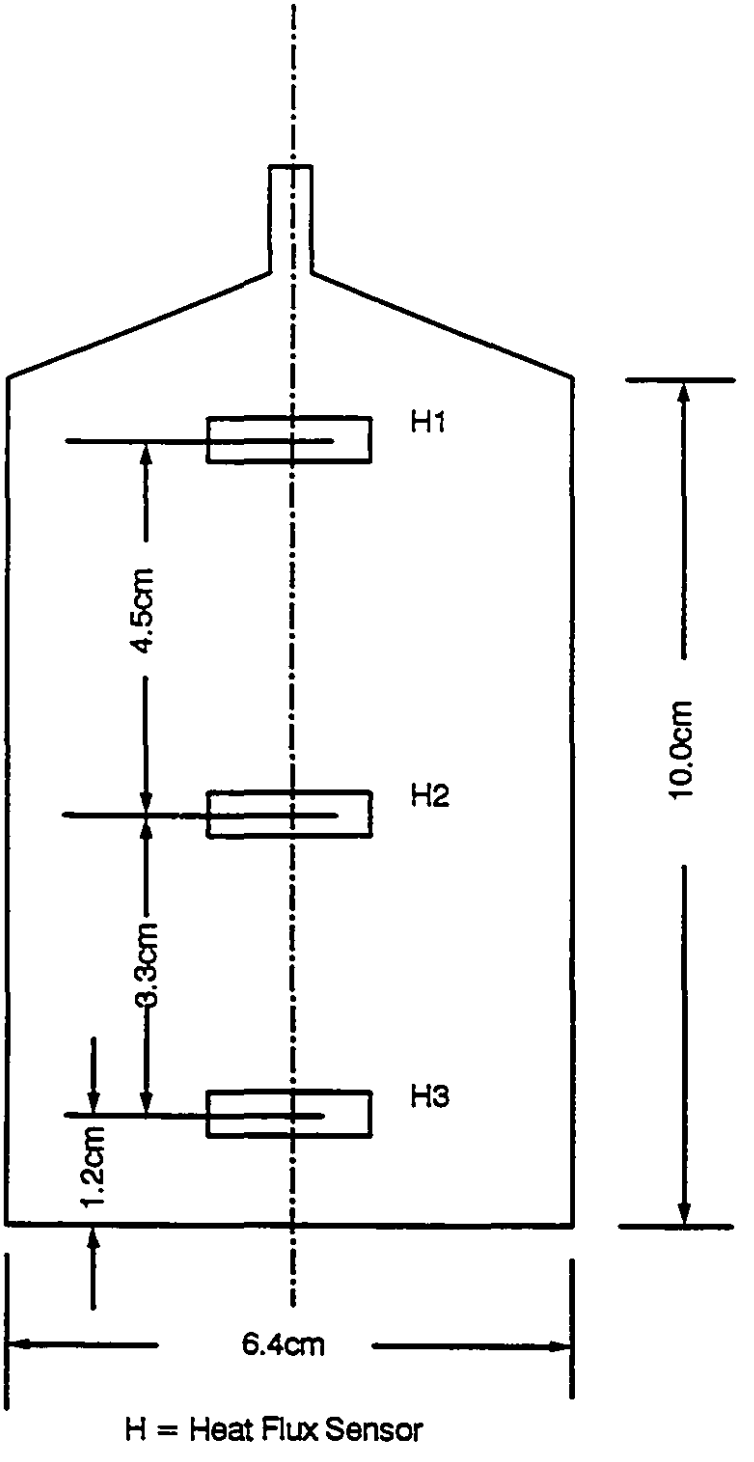

Figure 3.4 Fan-gated cavity and sensor locations (movable platen)

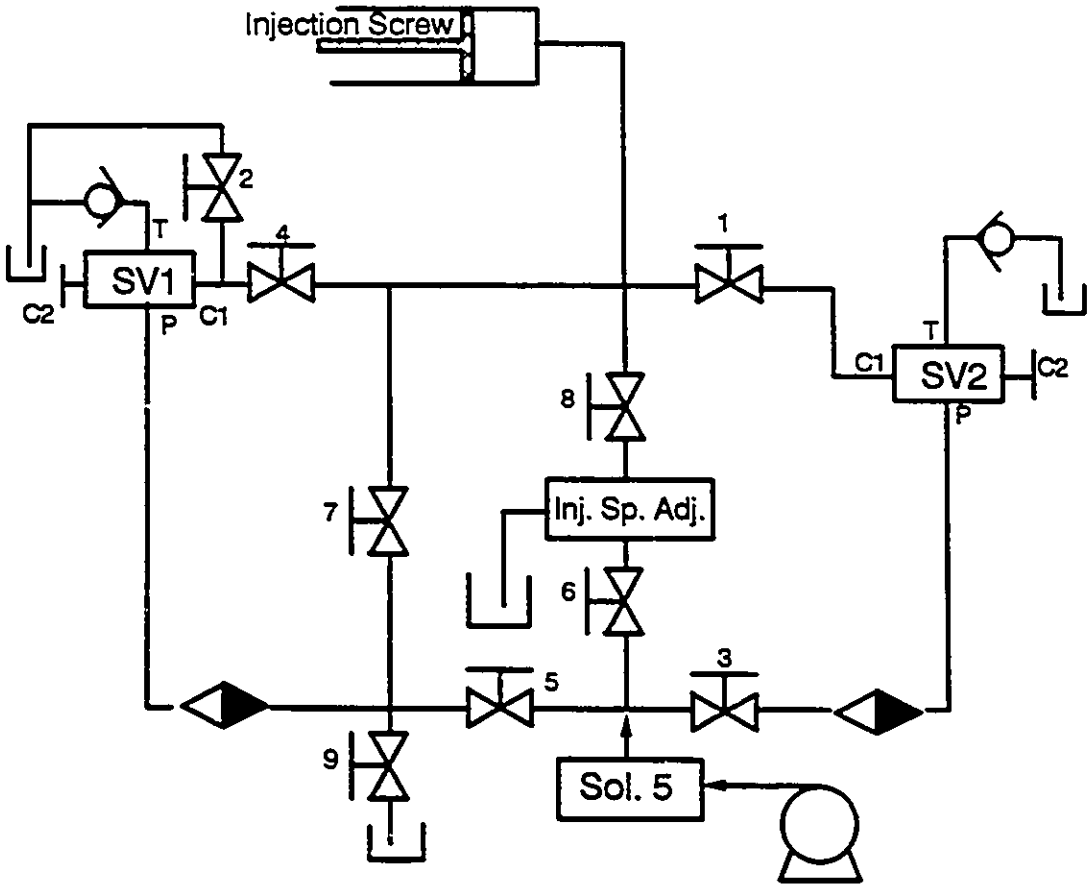

Figure 3.5 Modified hydraulic system of the McGill injection molding machine (Inj. Sp. Adj. = injection speed adjusting valve)

Table 3.3 Hydraulic manual valve positions and functions

Function		Manual Valve Position	
		Position	Valves
1	sv2 as the supply Valve.	Open	1, 3
		Closed	2, 4, 5, 6, 7, 8, 9
2	sv1 as the supply Valve.	Open	5, 4
		Closed	1, 2, 3, 6, 7, 8, 9
3	sv2 as the supply valve, sv1 as the relief valve.	Open	1, 3, 4
		Closed	2, 5, 6, 7, 8, 9
4	sv1 as the supply valve, sv2 as the relief valve.	Open	1, 4, 5
		Closed	2, 3, 6, 7, 8
5	No servo-valve is used. (Original machine configuration)	Open	6, 8
		Closed	1, 2, 3, 4, 5, 7, 9

control of these two servo-valves is achieved through digital-to-analog converter (DAC) outputs of RTI220. Output of the DAC has 0-5 V dc, which is further converted to the required 0-10 mA dc current through a home-built voltage-to-current converter (V/I). The V/I schematic is shown in Appendix A.

3.5.1.6 Limit Switches

There are nine limit switches installed on the injection molding machine. They

guarantee the machine integrity by preventing machine parts from travelling beyond their set limits. The electrical signals were found to "bounce" when the switches closed or opened. A de-bouncing circuit was developed to remedy this problem. The de-bouncing circuit is shown in appendix B. The heart of this circuit is an integrated circuit (IC) chip MC14490 from Motorola. Its working principle can be found in reference [101]. The de-bounced limit switch signals are connected to digital port 0 of RTI-217 as the inputs to the computer control system. The status changes of the limit switches produce an interrupt to the computer. Table 3.4 gives the limit switch functions, as well as their normal positions and connections to the port 0. An open position produces a logic one (5 V dc) to the associated bit of port 0 of RTI217.

3.5.1.7 Solenoid Valves

There are nine solenoid valves connected to the injection molding machine. They have open and shut positions, and they are used to direct the machine's hydraulic fluid. All injection molding machine movements are achieved through the combination of these valves. The output of port 3 of RTI-217 is used to manipulate the operation of these valves through optically isolated solid state relays. The connections to the solenoid valves and their functions are given in Table 3.5. A logic one to a bit of port 3 of RTI217 opens the solenoid valve connected to that bit.

3.5.1.8 Heater Control System

Previously, four zero-crossing relays were used to control barrel temperatures.

Table 3.4 Limit switch functions, positions, and connections

(NC = Normally Closed, NO = Normally Open)

	Function	Position	BITS
LS1	Mold Safety Cover	NC	0
LS2	Mold Open	NC	1
LS3	Pressure Switch (up) / Mold Closed	NO	2
LS4	Carriage Forward	NC	3
LS5	Screw Back	NC	4
LS6	Screw Forward	NC	5
LS7	Carriage Back	NO	6
LS8	Pressure Switch (Down)	NO	7
LS9	Same as LS3	NC	

An integral ac cycle time proportional control method was employed to determine the heater on and off times. The advantage of this realization is hardware simplicity. However, it suffers a limitation of a long sampling period, when a high resolution (≥12 bit) is employed, it causes a ripple effect in the barrel temperatures. A new heater control system was developed which eliminates this effect. The temperature sampling period may be as small as one half of an ac cycle (1/120 second). The electronic circuit and its description are given in Appendix C.

The system divides each half ac cycle into 4095 equal time intervals. The total number of power-on intervals to the heaters can be programmed by the output of

Table 3.5 Solenoid valve functions and their connections

Valve	FUNCTION	BIT
S1	Disconnected	
S2	Mold Close	0
S3	Carriage Backward	1
S4	Switch to High Pressure	2
S5	Screw Forward	3
S6	Switch to Low Pressure	4
S7	Screw Forward	5
S8	Mold Open	6
S9	Carriage Forward	7

port 1 of RTI-217 board. This technique is commonly called phase control.

Ruscitti [42] developed a barrel temperature dynamic model in relation to the percentage of power to the heater. With the heater control system developed above, the conducting ac cycle fraction is not linearly related to the power to the heater. Figure 3.6 gives a pictorial representation of the electrical voltage signal and the percentage of power to the heater, where x is the percentage of power on. The total power delivered by x - fraction is:

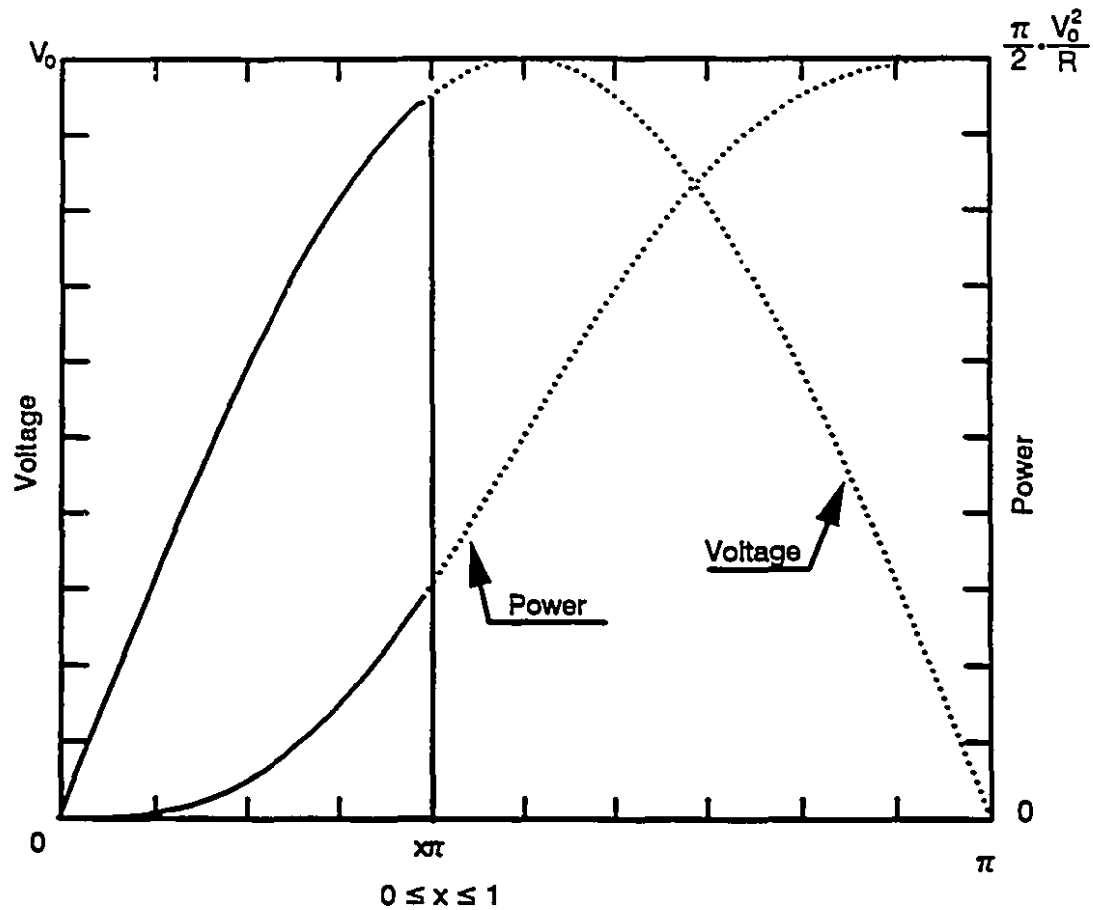

Figure 3.6 Representation of electric voltage and percentage of power to a barrel heater.

$$P(x)=\int_0^{\pi x}\frac{V_0^2}{R}\sin^2(t)dt=\frac{V_0^2}{R}\left[\frac{\pi}{2}x-\frac{1}{4}\sin(2\pi x)\right] \tag{3.3}$$

where R is the heater resistance, and

V_0 is the peak voltage of the power supply.

When x equals 1, the power is on throughout the half cycle. The total power is:

$$P(1)=\frac{\pi}{2}\cdot\frac{V_0^2}{R} \tag{3.4}$$

The fraction of power (y) and the fraction of conducting half ac cycle (x) has the following relationship:

$$y=\frac{p(x)}{p(1)}=x-\frac{1}{2\pi}\sin(2\pi x) \tag{3.5}$$

The relationship indicated in Equation (3.3) is non-linear. The fraction (x) of conducting half ac cycle is linearly related to the value output from the computer port.

3.5.1.9 Pressure Transducers and Their Calibration

The pressure transducers used in this research are all from Dynisco Inc. They were calibrated before being installed in their respective locations. A first order polynomial fit was found to be adequate to describe the relationship between the sensor output and the pressure. The calibration equations, installed locations and the models and serial numbers are all listed in Table 3.6. The output of a pressure

transducer is proportional to its excitation voltage; therefore, the calibration equations in Table 3.6 are based on the millivolts output divided by their respective excitation voltages.

3.5.1.10 Signal Conditioning

The analog inputs of the data acquisition cards were configured to accept 0 to +5Vdc signals. The low level signals from the thermocouples and pressure transducers were amplified before being connected to the RTI220 boards. The non-

Table 3.6 Dynisco pressure transducer calibrations and their installed locations

Sensor	Sensor Location and Calibration Equation	
PT435A-3M S/N:226385	Location	Cavity (gate)
	Equation	P=914.4*(mv/V)-211.4 (psi)
PT435A-3M S/N:290264	Location	Cavity (middle)
	Equation	P=908.1*(mv/V)-180.5 (psi)
PT435A-10M S/N:160039	Location	Nozzle
	Equation	P=3010.9*(mv/V)+22.9 (psi)
PT435-3M S/N:226386	Location	Servo-Valve
	Equation	P=915.6*(mv/V)-158.5 (psi)
PT432A-1M S/N:10423	Location	Injection Cylinder
	Equation	P=326.6*(mv/V)-275.2 (psi)

linear millivolt signals from the thermocouples are linearized, cold-junction compensated and amplified by an integrated circuit (AD594) from Analog Devices. The AD594 produces a high level voltage output of 10mv/°C [104]. The electronic circuit is shown in Appendix D. The differential millivolt output signals from the pressure transducers are amplified (gain = 100) by instrumentation amplifiers AD624 [104], also from Analog Devices, before being applied to the data acquisition input. A schematic of this arrangement is presented in Appendix E. The excitation voltages for all the pressure transducers were set to be 10 Volts. The amplified pressure signals also pass through a first order low-pass filter (cut-off frequency about 250 Hz) before the connection to the data acquisition input panel.

The hardware configuration of the computer control system is illustrated in Figure 3.7, along with some selected major process variables. A list of inputs and outputs is given in Table 3.7.

3.5.2 Software

The proper design of data acquisition and computer control systems increases productivity and reduces operating and set-up errors. Simplicity and flexibility are the design principles. The goal is to make it simple for production use, yet convenient for users examining different control strategies in a research context. Many considerations enter into the design and implementation of the system.

After many rounds of discussion with professionals in the computer, control and plastics processing areas, a design structure emerged, and a control system was

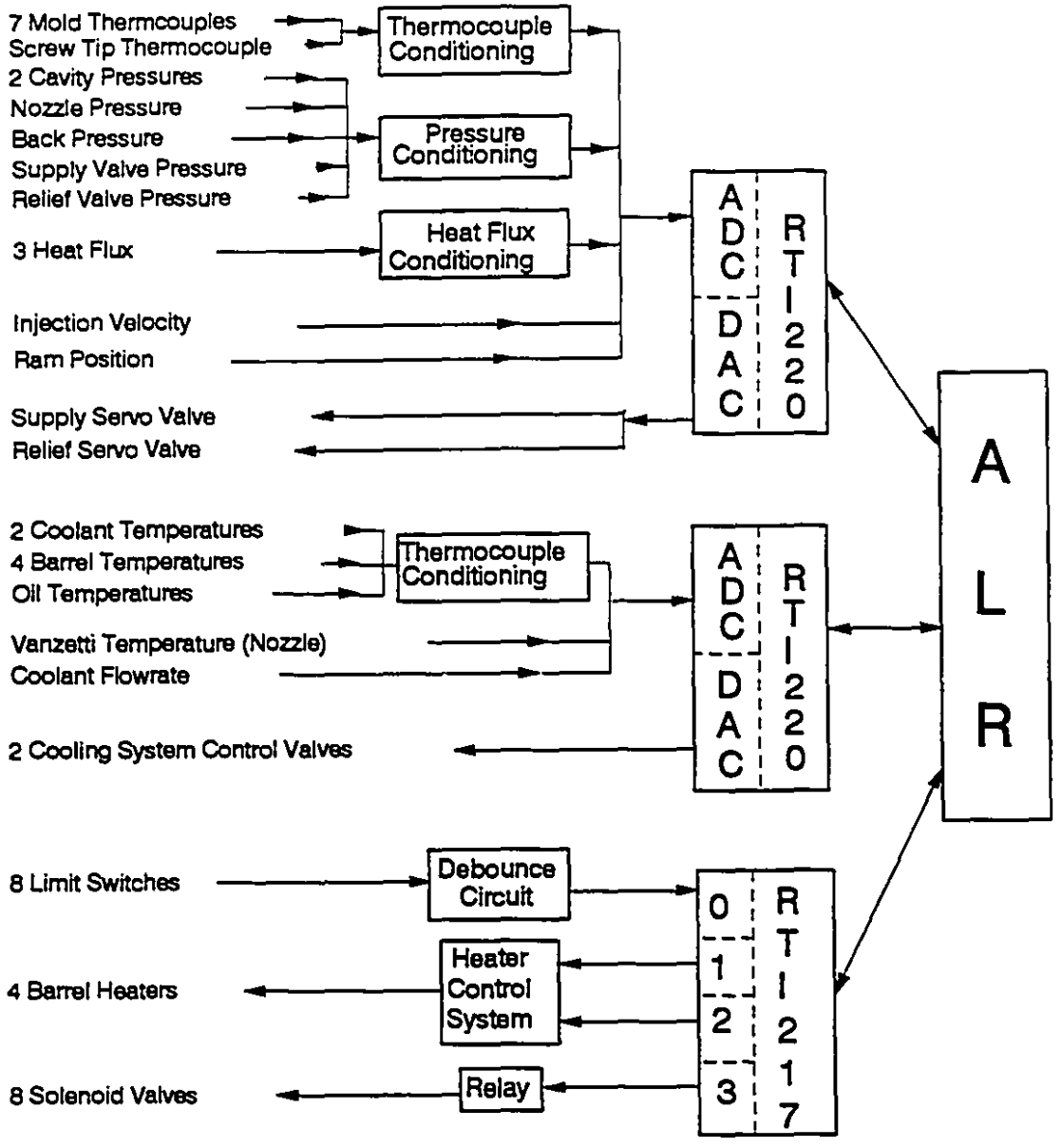

Figure 3.7 Computer interface to injection molding process and machine variables (ALR is the micro-channel computer)

Table 3.7 A list of analog and digital inputs and outputs

Analog Inputs:	**Analog Outputs**
Temperatures	2 Servo-valves
7 Mold Cavity Temperatures	Relief servo-valve
Surface temp. near the gate	Supply servo-valve
Surface Temp. in the middle	2 Control Valves
Surface temp. at bottom	Control valve (hot water side)
Metal temp. near the gate	Control valve (cold water side)
Metal temp. in the middle	
Metal temp. at the bottom	**Digital Inputs**
Metal temp. on the center	8 Limit Switches (LS)
Screw Tip Temperature	Mold safety cover LS
Nozzle Melt Temperature	Screw back LS
Oil Temp. in Injection Cylinder	Screw forward LS
Nozzle Vanzetti Temperature	Barrel back LS
4 Barrel Temperature	Barrel forward LS
Barrel heater temp. zone 1	Mold open LS
Barrel heater temp. zone 2	Mold close LS
Barrel heater temp. zone 3	Pressure change LS
Barrel heater temp. zone 4	
3 Coolant Temperatures	**Digital Outputs**
Coolant hot water temp.	8 Solenoid Valves
Coolant cold water temp.	Mold open solenoid valve
Coolant mixed water temp.	Mold close solenoid valve
6 Pressures	Screw forward solenoid valve
Cavity pressure near the gate	Screw retreat solenoid valve
Cavity pressure in the middle	Barrel forward solenoid valve
Nozzle pressure	Barrel retreat solenoid valve
Cylinder back pressure	Pressure step up solenoid valve
Supply servo-valve pressure	Pressure step down solenoid valve
Relief servo-valve pressure	Heater Control System (14 lines)
3 Heater Flux at Cavity Surface	8 Data lines
Heat flux near the gate	6 Control lines
Heat flux in the middle	
Heat flux at the bottom	
Injection Velocity of Piston	
Injection Displacement	
Coolant Flowrate	

developed using WATCOM C running under the QNX 4.1 operating system. Figure 3.8 is a functional description of the real-time computer control system developed for the McGill injection molding machine. Ellipses represent individual tasks which run concurrently. Rectangles indicate messages (information) that tasks use for communication, with arrows showing the direction of information flow. The tasks and their relationships are described below.

User Interface and Display:

This task distributes all the necessary information to various tasks from user input through the keyboard or mouse. This information is also saved in a small database. The user can load and modify the information from the database, and save it back to the database. The interface has sufficient intelligence to reject unreasonable or invalid values. A major function of this task is to display relevant process information so that the user can monitor and adjust the process. To make the system modular, the actual user interface program *IMM* (text in italics represents program (process) name) creates three sub-processes: *barreltemp*, *statdip2*, and *variable*. Program *barreltemp* is responsible for the information display regarding barrel heaters; *statdip2* is responsible for the machine status display such as injection cycle information; program *variable* is responsible for the distribution of all the relative information to other tasks. The information exchanged among different programs (processes) can be found in the actual programs.

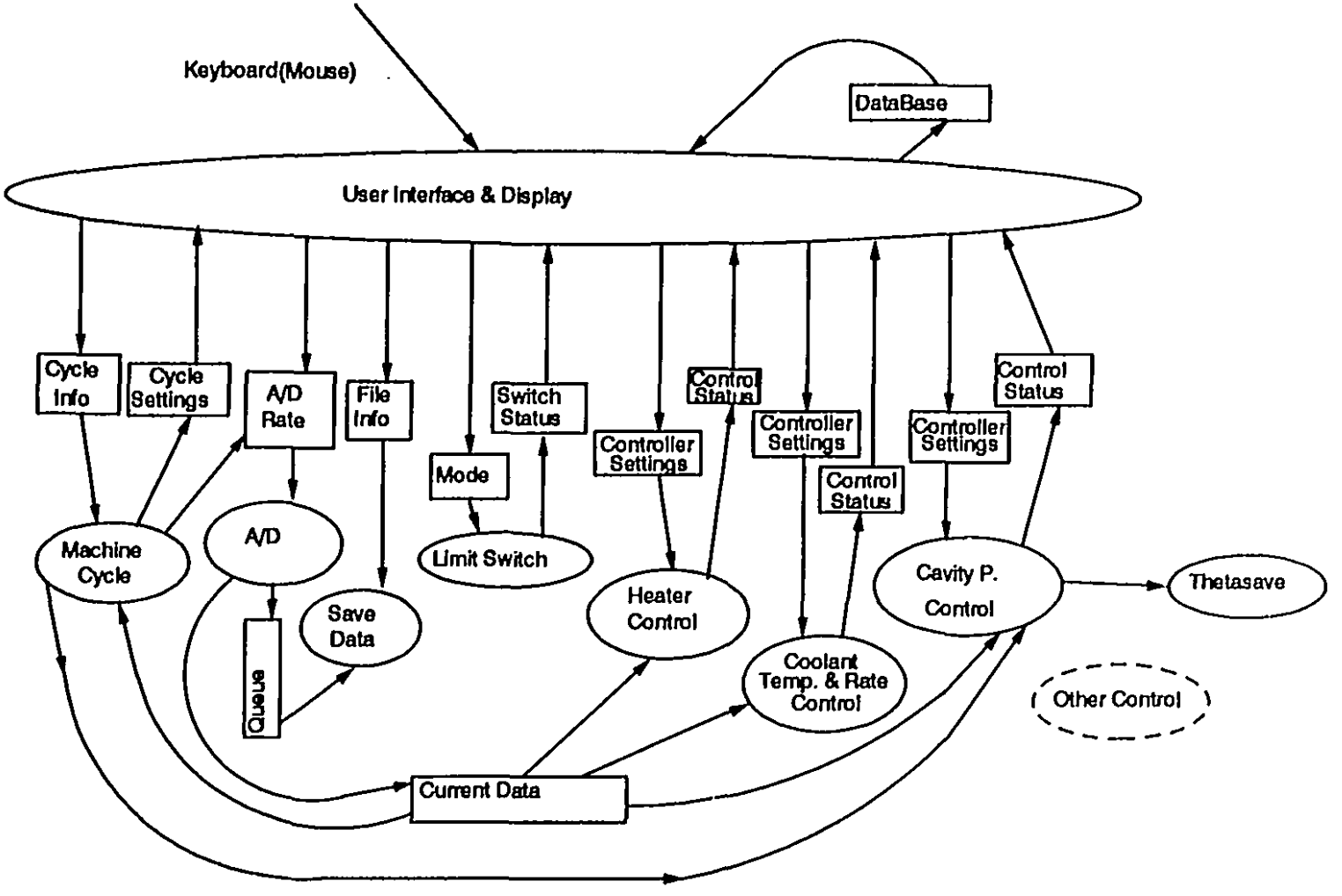

Figure 3.8 Relationship between major tasks of the designed data acquisition and computer control system

Machine Cycle:

This task is responsible for all the cyclic movement of the injection machine based on its current status and the information provided by the user. The cyclic information received is the injection, packing, cooling and recycling times. The current status provided to the user interface includes the current stage of the machine operation and its fraction of completion. The task also adjusts the data acquisition rate according to the different injection molding phases, and provides cyclic information to all phase-related control tasks. The purpose of different phase related sampling rates is to avoid an excessive amount of data without missing any essential process data. The machine cyclic movement is made possible by manipulating the solenoid valves. A program called *cycle* is the actual implementation of the above. The information exchange is implemented using shared memory.

Analog-to-Digital Conversion (A/D):

This task performs all the data collection based on the A/D rate specified by the user interface task and the machine cycle task. It updates the data to the most recent values which other tasks can access. Based on the information from the user interface, it determines whether to staff the data queue. The queue is a circular buffer which can temporarily save the data in memory which is then saved to the disk later when cpu is relatively free. This has been realized by two modular programs: *fadc* is responsible for the fast changing data while *sadc* collects the slowly changing

data. Two circular queues for fast and slow changing data are maintained by two additional modular programs *fadcbufw* and *sadcbufw*, respectively.

Save Data:

This saves all the data in the queues onto hard disk using the file information specified by the user interface and display task. The file information consists primarily of the filenames and their locations. In actual implementation, two programs, *fadcsave* and *sadcsave*, save the data from the queues maintained by *fadcbufw* and *sadcbufw*, respectively. The file information is exchanged by message passing.

Limit Switch:

This task is loaded into memory but suspended, it becomes active when the computer receives a hardware interrupt caused by a limit switch status change. Based on information from the user interface and display task, it activates different solenoid valves for machine movement and provides limit switch information for the display task. Then, it cedes the cpu to other tasks and waits for the next interrupt. Three modes of operation: manual, semi-automatic, and automatic determine the different responses to the limit switch changes. The limit switches have two positions: activated or not. The actual program name for this task is *RTI217*.

Heater Control:

This is a low priority task that only becomes active when control interval time is up. The controller settings include controller types such as PID, Dahlin and user defined, and the values of their parameters. The control status provided provides to the users are controller output and error. It uses the set-point values provided by the user interface and the current temperature measurement to calculate the controller output to the heaters. It then updates the information for the display task, and suspends itself until the next control interval time. The non-linear relationship between percentage of power and percentage of power-on shown in Equation (3.5) was pre-calculated and loaded into a look-up table to save time. The controller algorithm, set-point and control interval can be set independently for each of the four barrel heaters by the user. The program *heater* accomplishes the above functions. The QNX timer functions were used to set the control time interval.

Coolant Temperature & Flowrate Control:

This task, like the heater control task, becomes active when the control interval time is up. Based on the controller settings from the user interface and on current data, the task adjusts the control valves in the cooling system and updates the coolant temperature and flow rate for the display, then it suspends itself until the next control interval time has elapsed. The program *moldtemp.control* is the actual implementation of this task.

Cavity Pressure Control:

This task operates at a high priority. It starts to work when it receives an injection start signal from the machine cycle task. It determines the output to both supply and relief valves to force the cavity pressure to follow the set-point profile. In the meantime, it updates the display information. An adaptive control system has been implemented for the cavity pressure control. It estimates process dynamic model parameters concurrently, and passes them to the program *theatsave* to be saved onto the hard disk. The program *pcontrol.adaptive* is the implementation of this task. Details on the cavity pressure and control are discussed in Chapter 5.

Other:

This is a pseudo-task. It is presented to demonstrate that additional tasks can be easily incorporated without modifying the other program modules. For example, this pseudo-task can be nozzle pressure or injection velocity control.

Figure 3.9 is a snapshot of the program family tree of the data acquisition and control system. The "——" represents a "father" and "son" relationship. *IMM* is the original process which creates three sub-processes: *statdip2*, *barreltemp*, and *variable*. Process *variable* further creates a number of sub-processes. The programs *IMM*, *barreltemp*, and *statdip2* have been developed by Fusser and details are given in reference [117]. All the other programs shown in Figure 3.9 were developed by the author.

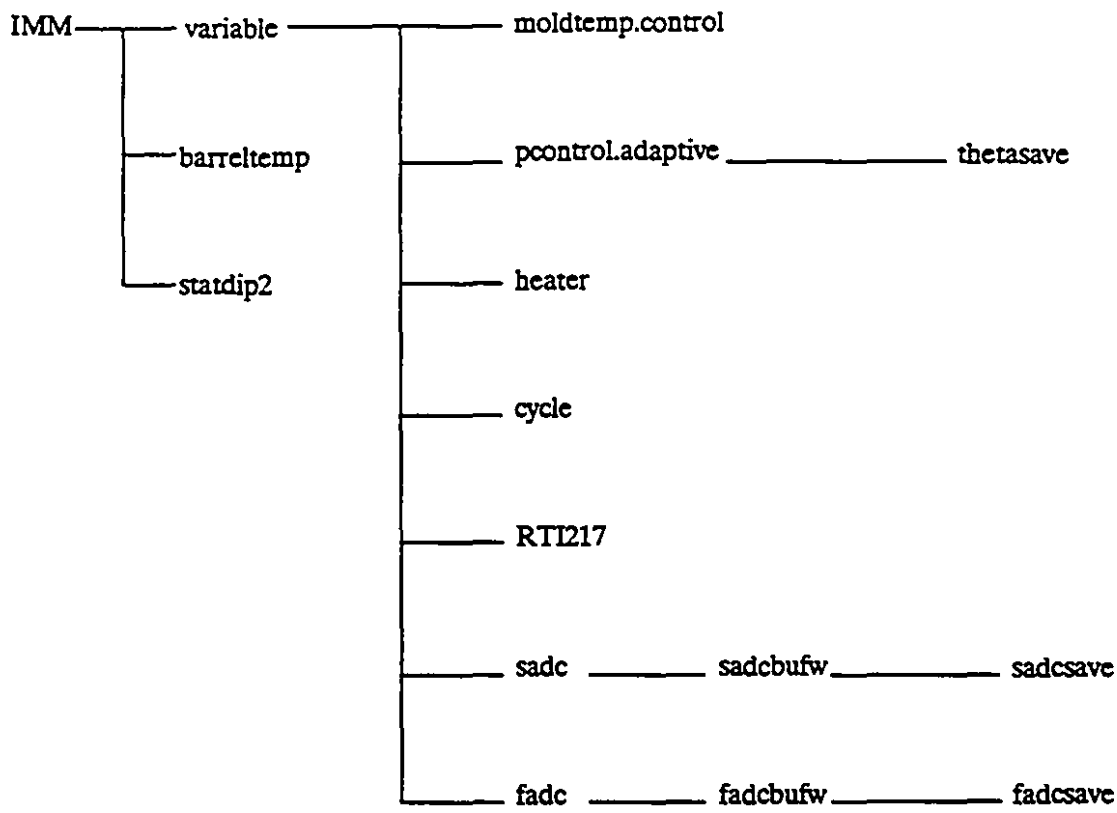

Figure 3.9 Injection molding data acquisition and control system program tree

3.6. Summary

A real-time computer control and data acquisition system has been developed for the McGill injection molding machine. It has the following characteristics:

1) A control task can be easily added, removed or modified, with little modification to program *variable* (see Figure 3.9).
2) The total number of analog input channels can be up to of 128 (limited by hardware).
3) The total number of output channels can be up to 32 (limited by hardware).
4) The data sampling rate can be chosen to relate to various injection phases. It is possible to sample quickly during the injection and packing phases and slower in the cooling phase to avoid excessive data.
5) The injection-to-packing phase transition can be determined by not only timer setting, but also from key variables such as the nozzle or cavity pressures.
6) Multiple control loops and data acquisition have been achieved with a single computer.
7) The system exhibits some "intelligence", in that it rejects improper inputs and suggests what reasonable inputs should be.

3.7. Conclusions

The real-time computer control and data acquisition system using the QNX operating system is user friendly and flexible for both production and research purposes. Error checking has been incorporated into the user interface to prevent

machine damage caused by erroneous inputs. Three levels of operation have been provided: production, data collection, and process control levels. A mode to acquire production statistics has not been implemented but could be added due to the extensible nature of the system and the emphasis placed on modular programming throughout the project.

Chapter 4

REVIEW ON SYSTEM IDENTIFICATION AND CONTROL SYSTEM DESIGN

An effective control system is largely dependent on the understanding of process dynamics. There are two ways to determine process dynamics: mathematical modelling and system identification. The first approach develops process dynamics from the fundamental mass, energy, and momentum balances. This approach leads to a good understanding of the process and allows the implementation of a control based on inferential methods. However, the effort needed to develop such a model is usually enormous. Furthermore, many required parameters are unknown and have to be obtained from experimental measurements. On the other hand, system identification produces the dynamic models from collected input and output data of the process. The model is generally valid only for the conditions where the system identification takes place, unless the process is linear and time-invariant (LTI).

4.1 System Identification

System identification methods can be classified into classical non-parametric and modern parametric types. They can also be divided into off-line and on-line (recursive) methods. The principles of modelling and the practical issues involved has been reported by many researchers [64 - 75, 85 - 91]. The following sections describe briefly the essential aspects of different approaches to process modelling.

4.1.1 Non-Parametric Methods

Classical system identification approaches, such as step test, frequency response, fast Fourier transform, correlation, and spectral analysis methods, are non-parametric. These methods lead to process characterization in the form of impulse or step response plots, or in the form of frequency response plots such as Bode or Nyquist diagrams. They are useful to examine the stability of classical feedback control systems [85, 93, 94]. They were not used in this work.

4.1.2 Parametric Models

For a linear time-invariant (LTI) single-input-single-output (SISO) system, the input and output model can be written as follows:

$$y(t) = G(q)u(t)+v(t) \tag{4.1}$$

where q is the shift operator: $y(t-1) = q^{-1}y(t)$,

t is the time,

u(t) is the system input,

y(t) is the system output,

v(t) is the system noise, and

G(q) is the system transfer function (dynamic model).

The disturbance v(t) (or the system noise) can be described as filtered white noise:

$$V(t) = H(q)e(t) \tag{4.2}$$

where e(t) is white noise, and

H(q) is the noise transfer function (noise model).

Therefore, Equation (4.1) can be rewritten as:

$$y(t) = G(q)u(t)+H(q)e(t) \tag{4.3}$$

The transfer function (G) and noise transfer function (H) are usually parameterized as rational functions in the delay operator q^{-1} or z-transform form.

A commonly used parametric model is the ARX (auto-regressive, or the least squares) model that corresponds to:

$$G(q) = q^{-nk}\frac{B(q)}{A(q)} \tag{4.4}$$

$$H(q) = \frac{1}{A(q)} \tag{4.5}$$

Therefore Equation (4.3) becomes:

$$A(q)y(t) = B(q)u(t-nk)+e(t) \tag{4.6}$$

where A(q) and B(q) are the polynomials in the delay operator q^{-1},

$A(q)=1+a_1q^{-1}+\cdots+a_{na}q^{-na}$,

$B(q)=b_1q^{-1}+\cdots+b_{nb}q^{-nb}$,

na and nb are the order of polynomials A(q) and B(q), and

nk is the order of the system delay.

The disadvantage of the simple ARX model is the lack of adequate freedom

in describing the properties of disturbance. Flexibility can be added by describing the equation error (disturbance) as a moving average of white noise. This leads to the auto-regressive moving average model (ARMAX), or the Maximum Likelihood model. It is expressed as:

$$A(q)y(t) = B(q)u(t-nk)+C(q)e(t) \tag{4.7}$$

where A(q), B(q), y(t), u(t), e(t), na, nb, and nk are described earlier,

$C(q)=1+c_1q^{-1}+\cdots+c_{nc}q^{-nc}$, and

nc is the order of polynomial C(q).

Both the ARX and ARMAX models are special cases of a general parametric model structure:

$$A(q)y(t) = \frac{B(q)}{F(q)}u(t-nk) + \frac{C(q)}{D(q)}e(t) \tag{4.8}$$

where A(q), B(q), C(q), na, nb, nc, and nk are previously described,

$D(q)=1+d_1q^{-1}+\cdots+d_{nd}q^{-nd}$,

$F(q)=1+f_1q^{-1}+\cdots+f_{nf}q^{-nf}$, and

nd and nf are the orders of polynomials D(q) and F(q), respectively.

With C(q)=1, D(q), and F(q)=1, Equation (4.8) becomes ARX model Equation (4.6). And, with D(q)=1, and F(q)=1, Equation (4.8) becomes ARMAX model Equation (4.7).

The third special case with C(q)=1, D(q)=1, and A(q)=1 results in the output

error (OE) model:

$$y(t)=\frac{B(q)}{F(q)}u(t-nk)+e(t) \tag{4.9}$$

Equation (4.9) indicates that the relationship between the input and undisturbed output is a linear difference relation, and the disturbances consist of white noise.

With A(q)=1, Equation (4.27) becomes the Box-Jenkins (BJ) model:

$$y(t) = \frac{B(q)}{F(q)}u(t-nk)+\frac{C(q)}{D(q)}e(t) \tag{4.10}$$

The BJ model gives the transfer functions G and H independently as rational functions.

4.1.3 Obtaining an LTI Model

The output of a physical process is measured, while the input is usually a simple signal like a step change, sine wave or impulse. Because an impulse is physically difficult and sine wave test requires a large number of experiments with different frequencies, the impulse and sine wave test methods are rarely used. The step test input signal is easy to produce and is used widely. The pseudo-random binary signal (PRBS), which consists of a series of positive and negative step changes of different durations, is a widely accepted test signal. The advantage of the PRBS is that it has a rich and predetermined frequency spectrum, but the testing duration of a PRBS is much longer than the step test [87, 92].

All the parameters of the above mentioned models (ARX, ARMAX, OE and

BJ) can be obtained with the System Identification Toolbox [84, 85] running under MATLAB [83], once the input and output data are available. The general procedure of linear parametric model identification is illustrated in Figure 4.1.

The steps to determine the dynamic models are as follows. Firstly, a graphical examination of the input and output determines the approximate orders of the models (i.e. na and nb of ARX and ARMAX). Secondly, begin with the smallest feasible value of delay (nk) to calculate the model parameters with na and nb. Increase nk until an acceptable final prediction error (FPE) is obtained. The FPE is a measure of the variance of the model error [85, 86]. Thirdly, na and nb are varied to search for an improvement of the model, if there is no satisfactory improvement, the simplest model (i.e the lowest na and nb) is chosen. Fourthly, to determine the ARMAX models, with the na, nb, and nk from ARX model and nc = 0, increase nc until a minimum FPE is obtained. Finally, perform a residual analysis (RESID) to check the validation of the model. Similar approaches are taken to determine the model structure for OE and BJ model. If the FPEs of the best fitted ARX, ARMAX, OE, BJ models are close, the simplest model is then chosen.

4.1.4 Conversion between Continuous and Discontinuous Models

Although most chemical processes are physically of high order, they can often be modelled satisfactorily as a first order plus delay process (i.e. ARX[1 1 nk]). The

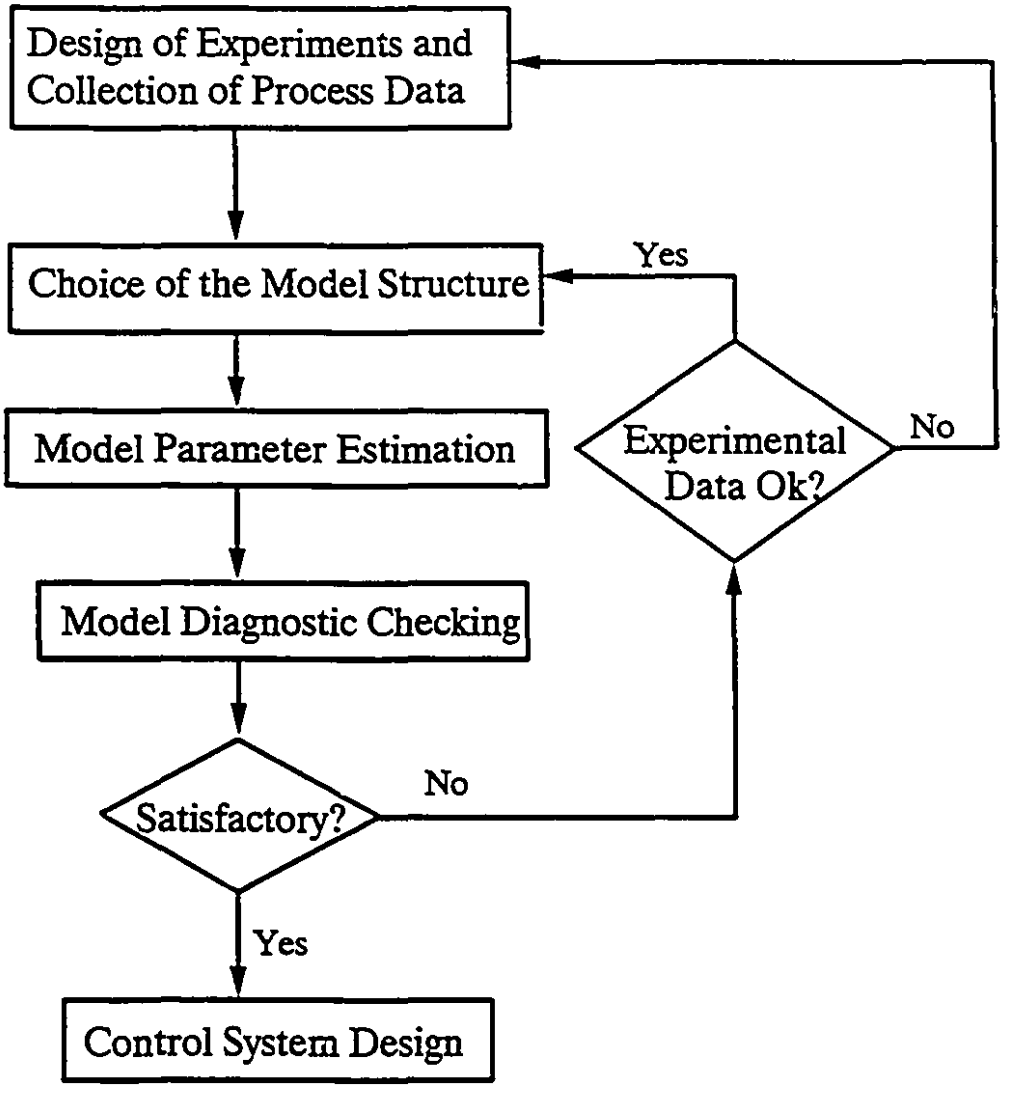

Figure 4.1 A general procedure for an off-line system identification

model can be expressed as:

$$y(k+1) = a_1 y(k) + b_1 u(k-nk) + e(k) \tag{4.11}$$

The Laplace transforms are commonly used to describe continuous process models. A first order plus delay continuous process model is expressed as:

$$y(s) = \frac{k_p}{\tau s+1} \cdot \epsilon^{-t_d s} \cdot u(s) \tag{4.12}$$

Where k_p is the process gain,

τ is the process time constant,

t_d is the process time delay,

y(s) is the output in Laplace transform, and

u(s) is the input in Laplace transform.

The continuous first order plus delay and discrete first order plus delay models can be easily converted to each other by the following equations [93, 94].

$$a_1 = \frac{\tau - T}{\tau} \tag{4.13}$$

$$b_1 = \frac{T \cdot k_p}{\tau} \tag{4.14}$$

$$nk = \frac{t_d}{T} \tag{4.15}$$

where T = the sampling period.

4.1.5 Recursive System Identification

The System identification methods discussed so far are limited to linear time invariant processes. Recursive system identification, described briefly in this section, can be used for a non-linear and/or time varying process.

Recursive system identification, also called on-line identification, is used on-line with the experimental process. It is the key to adaptive control [87, 91]. There exist different types of recursive system identification techniques. Only the recursive identification with forgetting factor (i.e. recursive least squares, RLS) is used and reviewed in this thesis.

Consider a discrete time transfer function model of a system with an input sequence u(k) and an output sequence y(k) with white noise, e(k). The model can be represented in the form:

$$Ay(k) = Bu(k-nd) + e(k) \tag{4.16}$$

where $A = 1 + a_1 z^{-1} + \ldots + a_{na} z^{-na}$,

na = the order of the polynomial A,

$B = b_1 z^{-1} + \ldots + b_{nb} z^{-nb}$,

nb = the order of the polynomial B, and

nk = the order of the process delay.

The coefficients of polynomials A and B can be estimated from measurements at each sample time, k. It is convenient to rewrite Equation (4.16) in a form which

emphasizes the objects to be estimated and the data available:

$$y(k)=\phi^T(k)\theta(k)+e(k) \tag{4.17}$$

where $\theta(k)$ is a vector of unknown parameters at the kth sample defined as:

$\theta^T = [b_1 \ldots b_{nb} -a_1 -a_2 \ldots -a_{na}]$, and

$\phi^T(k) = [u(k-1-nd) \ldots u(k-1-nb-nd)\ y(k-1) \ldots y(k-na)]$, a measurement vector.

A reasonable way to estimate the process parameter θ is to minimize, by least squares, a loss function defined as follows:

$$J(\theta)=\sum_{k=1}^{N}[y(k)-\phi^T(k)\theta(k)]^2 \tag{4.18}$$

where N is the total number of samples available. One drawback of the loss function as defined in Equation (4.18) is that all data points are given an equal weight. For a time-varying process, it is useful to limit the influence of old data by modifying the loss function as:

$$J(\theta)=\sum_{k=1}^{N}\lambda^{N-k}[y(k)-\phi^T(k)\theta(k)]^2 \tag{4.19}$$

The parameter λ, called a forgetting factor, has a positive value, $0 < \lambda \leq 1$. It gives old data less weight than recent data in an exponential fashion. The older data are said to be forgotten, and smaller values of λ cause quicker forgetting. The estimation of the process parameters of the model can be obtained by solving the following equations iteratively [91, 92]:

$$\theta(k+1)=\theta(k)+K(k)[y(k+1)-\phi^T(k+1)\theta(k)] \tag{4.20}$$

$$K(k+1)=\frac{P(k)\phi(k+1)}{\lambda+\phi^T(k+1)P(k)\phi(k+1)} \tag{4.21}$$

$$P(k+1)=[I-K(k)\phi^T(k+1)]P(k)/\lambda \tag{4.22}$$

where I is a unit matrix of order (na +nb),

P is a covariance matrix of order (na+nb), and

K is a vector of order (na+nb) and can be considered as estimation adjustment gain.

The forgetting factor, λ, can be interpreted as a forgetting "time constant" [87]. It determines the rate of recursive identification following system parameter changes. If the rate of parameter change is large, a small λ should be used. The signal-to-noise ratio has to be large. An input filter is commonly used to boost the ratio. If the speed of parameter changes is small, then a large forgetting factor can be used (λ close to 1), and the signal-to-noise ratio requirements can be relaxed [122]. There is no explicit mathematical expression defining the relationship between the rate of parameter changes and the value of forgetting factor.

Figure 4.2 depicts the procedure of a typical on-line process identification, where the inner loop carries out the recursive identification (Equations (4.20) to

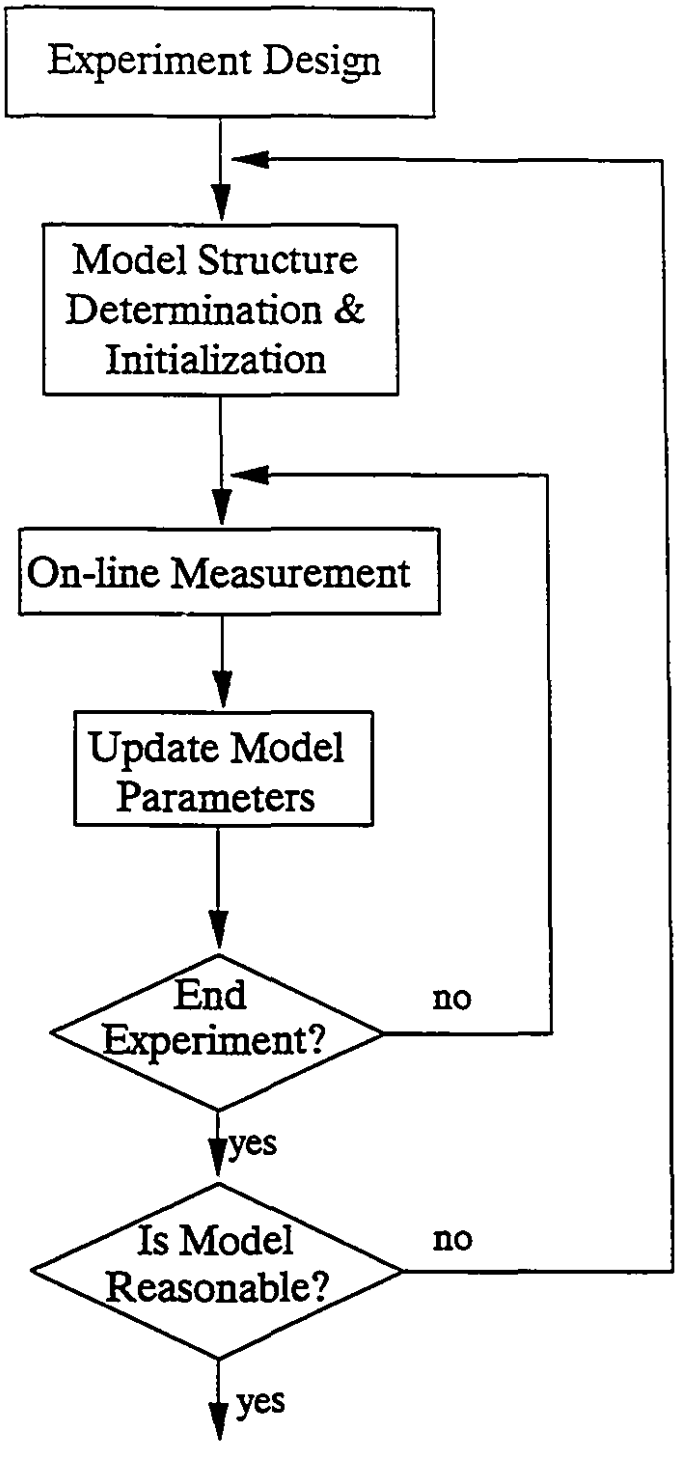

Figure 4.2 A general procedure for an on-line system identification

(4.22)) of the process model. The outer loop is the model structure determination, which is carried out off-line.

4.2 Controller Design

4.2.1 Controller Design Algorithms: LTI Processes

Once the process model is available, the next step is to design a control system for the process. A variety of controller types and methods to determine controller the type and parameters are described in control textbooks and in the literature [86 - 95]. Process dynamics, the requirements of the closed-loop performance, and the designer's personal taste usually dictate the controller structure. The PID controller is, by far, one of most popular controllers. It involves three parameters: controller gain, controller integral time, and controller derivative time. There are different methods to obtain these three parameters. The Dahlin controller and Internal Model Control (IMC) methods have become widely used for chemical process control due to their simplicity (only one parameter to be determined) and to their robustness in handling model mismatch. Reference [31] gives a comparison between PID control with ITAE tuning method and Dahlin control in controlling mold temperature with coolant temperature as the manipulated variable. The results indicated that Dahlin control had better performance. Pole-placement is widely used to design a servo system because it allows the designer to chose where to place the closed-loop poles (which determine the closed-loop response). Dahlin control is a special case of pole-placement design. In this work, Dahlin and IMC controllers are

used in the control of the cooling stage. Pole-placement design is used in conjunction with recursive system identification to control the cavity pressure during the filling sections and packing stages. A brief review of these three types of control design is given in the following. Details can be found in references [80 - 95].

4.2.1.1 Dahlin Control Design

The Dahlin control algorithm specifies that the closed-loop performance of the system should behave similarly to a continuous first-order process plus time delay with respect to the set-point.

$$G_{CL}(s) = \frac{e^{-hs}}{\mu s+1} \tag{4.23}$$

where μ is the desired closed-loop time constant,

h is the time delay of the closed-loop transfer function, and

G_{CL} is the closed-loop transfer function.

The closed-loop time delay (h) is usually selected as $h = t_d = NT$ (T is the sampling period, N is an integer, t_d is the process delay). The time constant (μ) of the closed-loop system determines the speed of response of the closed-loop system.

For a first order plus time-delay process, the discrete-time Dahlin controller is [93, 94]:

$$G_{DC} = \frac{(1-A)}{1-Az^{-1}-(1-A)z^{-N-1}} \frac{1-a_1 z^{-1}}{K(1-a_1)} \tag{4.24}$$

where $A=e^{-T/\mu}$, $a_1 = e^{-T/\tau}$, K is the process gain, and τ is the process time constant.

4.2.1.2 IMC Control

An internal model control (IMC) [94] control block diagram is shown in Figure 4.3B. The IMC controller is determined by first separating the process model, G_p, into two parts such that:

$$G_p = G_p^+ \cdot G_p^- \tag{4.25}$$

where G_p^+ contains the process time delay term, zeros that lie outside the unit circle, and zeros that lie inside the unit circle near (-1,0). G_p^+ has a gain of unity. And, $G_p^- = G_p / G_p^+$. The IMC controller is then, $G_c^*(z)$:

$$G_c^*(z) = \frac{f(z)}{G_p^-(z)} \tag{4.26}$$

where f(z) is generally a low-pass filter chosen to provide control loop robustness and to ensure physical realizability of G_c^* [94]. For a first order system, f(z) is chosen to be the same order:

$$f(z) = \frac{1-\alpha}{1-\alpha z^{-1}} \tag{4.27}$$

The IMC control can be put in the form of the simple feedback controller, G_c, in Figure 4.3A.

$$G_{IMC}(z) = \frac{G_c^*(z)}{1-G_c^*(z)\cdot G_p(z)} \tag{4.28}$$

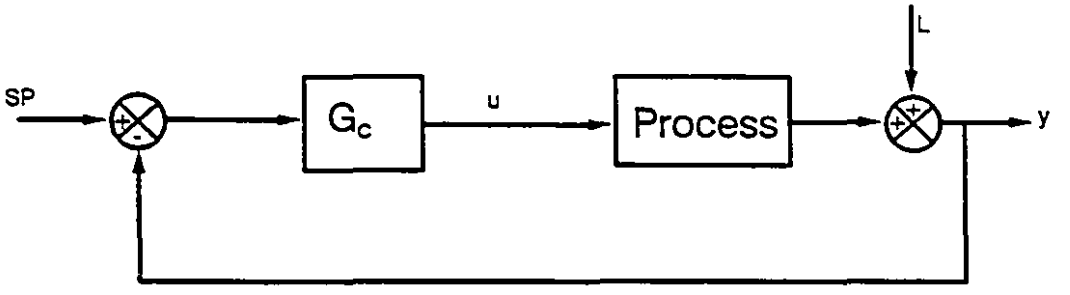

A)

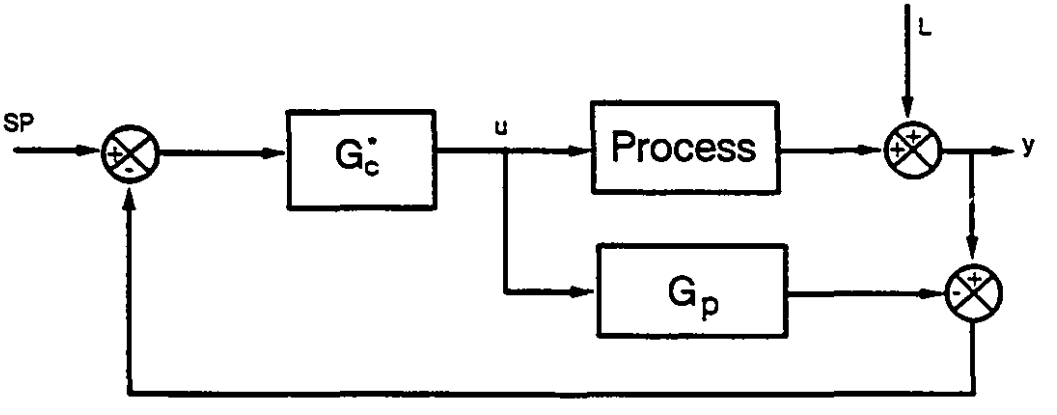

B)

Figure 4.3 Block diagram of a typical feedback control loop (A), and block diagram of an IMC control (B)

For a first order system without delay, the process can be expressed as:

$$G_p(z) = \frac{b_1 z^{-1}}{1-a_1 z^{-1}} \tag{4.29}$$

Therefore, G_p^- of the process is:

$$G_p^-(z) = \frac{b_1}{1-a_1 z^{-1}} \tag{4.30}$$

The IMC controller then is:

$$G_c^*(z) = \frac{1-a_1 z^{-1}}{b_1}\frac{1-\alpha}{1-\alpha z^{-1}} \tag{4.31}$$

Converting the IMC controller into the form of G_c in Equation (4.28) gives:

$$G_{IMC}(z) = \frac{(1-\alpha)(1-a_1 z^{-1})}{b_1 - b_1 z^{-1}} \tag{4.32}$$

For a first order process without delay (Equation 4.29), the Dahlin controller G_{DC}:

$$G_{DC}(z) = \frac{(1-e^{-T/\mu})(1-a_1 z^{-1})}{b_1 - b_1 z^{-1}} \tag{4.33}$$

The Dahlin and IMC controllers are identical when $\alpha = e^{(-T/\mu)}$. Therefore, for a first order system, the only tuning parameter is μ, which determines how well the controlled variable follows set-point changes.

4.2.1.3 Pole-Placement Control Design

This brief description of pole-placement controller design follows that of Astrom [91]. A block diagram of the pole-placement design is shown in Figure 4.4. Polynomials T(z) and R(z) provide a feedforward capability, while polynomials S(z) and R(z) provide the feedback. A(z) and B(z) are the process model as found from the system identification.

Suppose a desired closed loop behaviour (i.e. pulse transfer function, $H_m(z)$) is expressed by Equation (4.34):

$$H_m(z) = \frac{y(z)}{u_c(z)} = \frac{B_m(z)}{A_m(z)} \tag{4.34}$$

$H_m(z)$ is the desired pulse transfer function, and $B_m(z)$ and $A_m(z)$ do not have any common factor. The closed-loop characteristic equation is [91]:

$$AR+BS=B^{+}A_0A_m \tag{4.35}$$

where B^+ are the stable process zeros (i.e. $B=B^+B^-$), B^- are the unstable process zeros and $A_0(z)$ is an observer polynomial. Eliminating the stable poles of the above, the characteristic Equation (4.35) becomes:

$$AR'+B^{-}S=A_0A_m \tag{4.36}$$

where $R=R'/B^+$. For a set-point tracking problem, it is useful to have a high gain at low frequencies in order to have a system that is insensitive to low-frequency

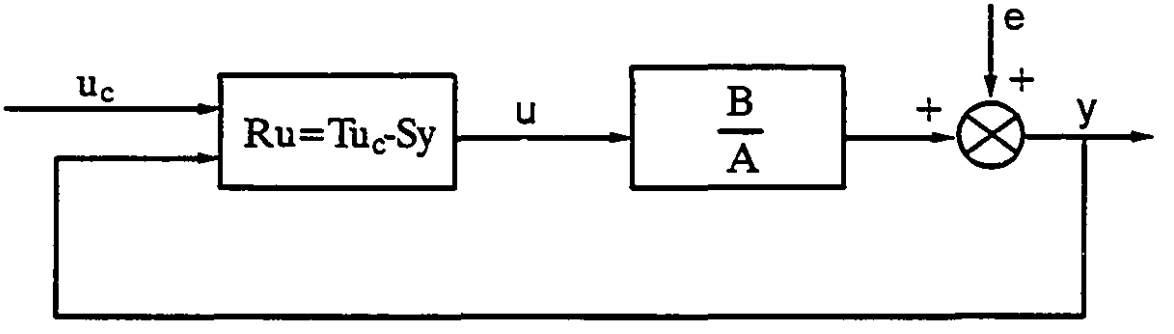

Figure 4.4 Control system design: pole-placement feedback system

modelling errors and low-frequency disturbances. This can be achieved by setting:

$$R^{l}=(z-1)^{l}R_1^{l} \tag{4.37}$$

which introduces an integrating action in the controller. The design Equation (4.36) is thus:

$$A(z-1)^{l}R_1^{l}+B^{-}S=A_0A_m \tag{4.38}$$

In order to ensure the causality of the controller, the following inequality equation has to be satisfied [91]:

$$degA_0 \geq 2degA-degA_m-degB^{+}+l-1 \tag{4.39}$$

Equation (4.38), satisfying Equation (4.39), can be solved by using the Sylvester matrix method [91]. For low order systems, it is also possible to solve the equation directly by equating coefficients of the right and left sides.

4.2.2 Adaptive Control Design

A fixed controller can handle linear time-invariant processes without problems. Recent advances in adaptive control make it possible to control time-varying and/or non-linear processes. There are three principal types of adaptive controllers used today [79 - 81]. A brief review of these systems: gain scheduling, model-reference adaptive system (MRAS), and self-tuning regulator (STR), follows.

4.2.2.1 Gain Scheduling Control

It is sometimes possible to find auxiliary process variables that correlate well

with the changes in process dynamics. It is then possible to eliminate the influences of parameter variations by changing the parameters of the regulator as functions of the auxiliary variables. This technique is called gain scheduling, because the system was originally used to accommodate changes only in process gain. A block diagram of the gain scheduling system is illustrated in Figure 4.5.

Gain scheduling has the advantage that the control parameters can be changed quickly [91]. It suffers from the following drawbacks: (i) it is essentially an open-loop adaptation, because there is no feedback that compensates for an incorrect schedule; (ii) the regulator parameters must be determined for the complete range of operating conditions, and the performance must be checked by extensive simulations [91]; (iii) there must exist an auxiliary measurement that correlates well with the changes in process dynamics.

4.2.2.2 Model-Reference Adaptive Systems (MRAS)

The model-reference adaptive system was originally developed for the servo problem. Figure 4.6 gives its block diagram. The specifications are given in terms of a reference model, which specifies how the process output ideally should respond to the command signal (set-point). The reference model is a part of the control system. The regulator can be thought of as consisting of two loops. The lower loop is an ordinary control loop composed of the process and regulator. The parameters of the regulator are adjusted by the upper loop in such a way that the error, e, between the model output, y_m, and the process output y becomes small. The upper loop in fact

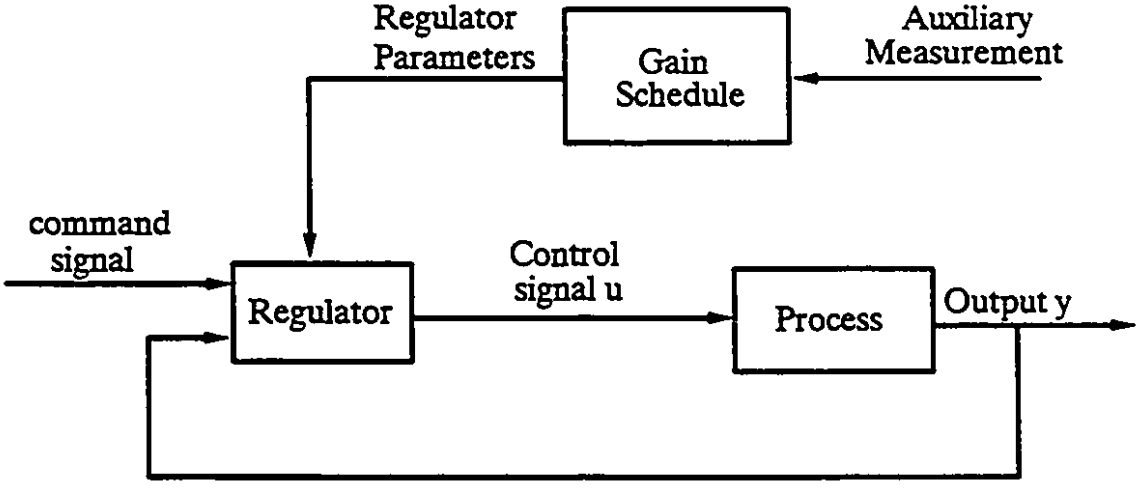

Figure 4.5 Schematic of a gain scheduling control system

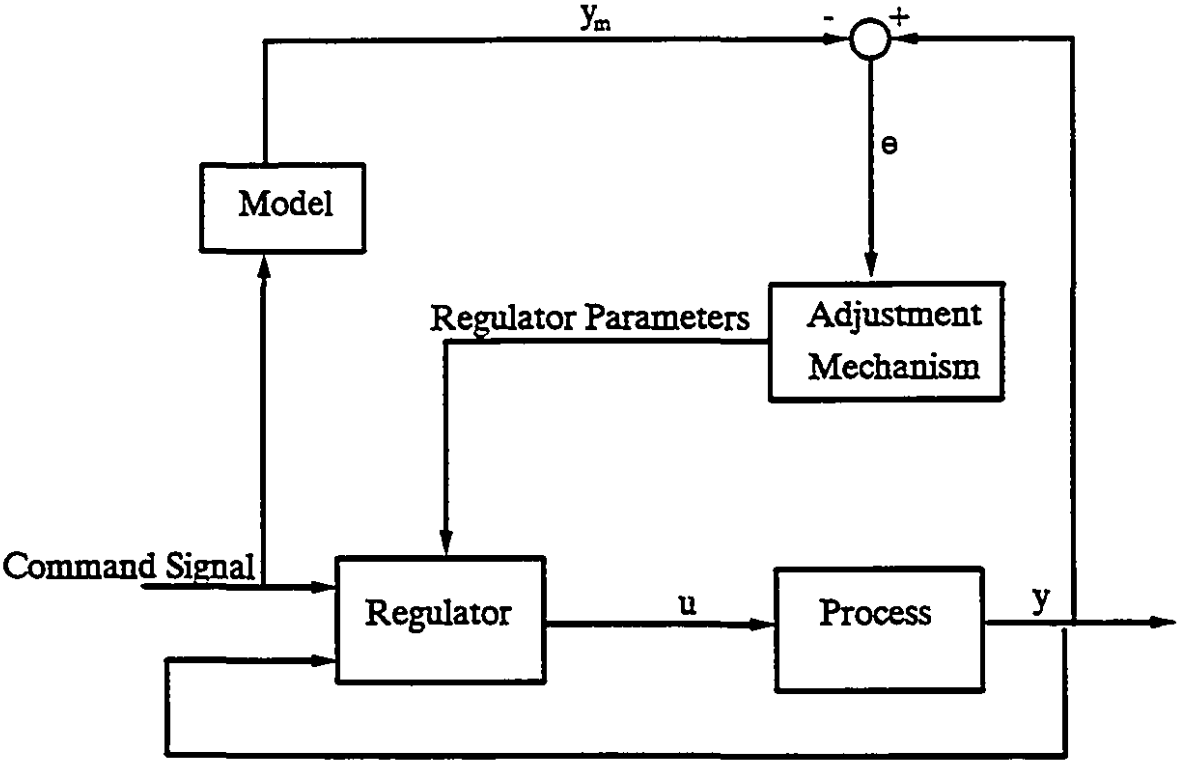

Figure 4.6 Schematic of a model reference adaptive system (MRAS)

is also a regulator loop. The key problem is to determine an adjustment mechanism to bring the error e to zero. This problem is non-trivial [91].

4.2.2.3 Self-Tuning Control

Figure 4.7 is a self-tuning regulator block diagram. It has facilities for tuning its own parameters. Like MRAS, the regulator can be thought of as being composed of two loops. The lower loop consists of the process and an ordinary linear feedback regulator. The parameters of the regulator are adjusted by the upper loop, which is composed of a recursive parameter estimator and a design calculation. The design calculation in Figure 4.7 represents an on-line solution to a control system design problem for a system with known parameters [87, 91].

The self-tuning regulator is very flexible with respect to the design method. Virtually any design technique can be accommodated. Control design techniques like gain and phase margins, pole-placement, minimum-variance control and linear quadratic Gaussian control (LQG) can be used. Different types of on-line parametric model estimation can also be selected.

The self-tuning algorithms can be divided into two major classes: direct and indirect algorithms [87, 91]. In an indirect algorithm, there is an estimation of the process model. The controller parameters are obtained through the design procedure. It is sometimes possible to re-parameterize the process so that it can be expressed in terms of the regulator parameters [87, 91]. The design procedure for an indirect self-tuning control is illustrated in Figure 4.8.

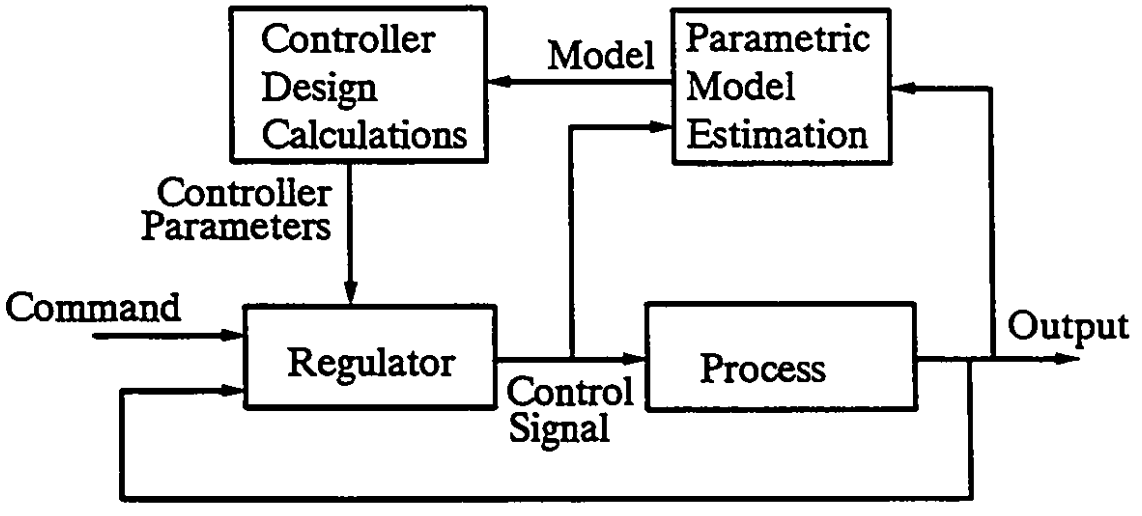

Figure 4.7 Schematic of a self-tuning regulator (STR) control system

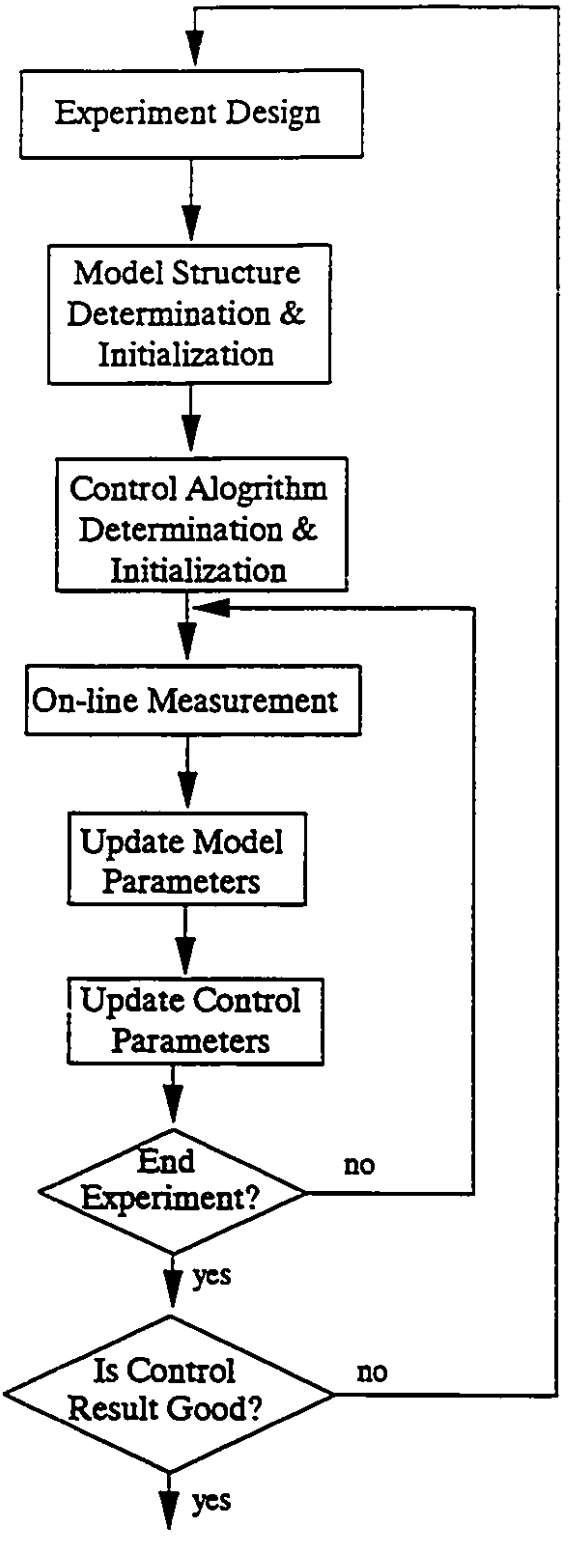

Figure 4.8 An adaptive control system implementation procedure

Chapter 5

CAVITY PRESSURE DYNAMICS AND CLOSED-LOOP SELF-TUNING CONTROL DURING FILLING AND PACKING STAGES.

5.1 Introduction

This chapter starts with a brief summary of simple mathematical models for the injection molding process in section 5.2. This is followed by a description of the experimental set-up and conditions in section 5.3. A preliminary experimental study of injection molding filling and packing stages is presented in section 5.4. Section 5.5 studies the dynamics and control of cavity pressure during the injection filling stage. Section 5.6 discusses the transition detection method of filling-to-packing transition. Wihle the dynamics and control of cavity pressure during the packing stage are presented in section 5.7, and a summary is presented in the final section of this chapter.

5.2 Mathematical Modelling of an Injection Molding Machine

This section does not attempt to develop a precise mathematical modelling of the injection molding machine. Rather, it uses modelling to show the strong non-linearity and time-varying behaviour of the injection molding process and to justify the experimental approach followed in this work.

Figure 5.1 is a schematic representation of an injection molding machine with the major physical variables labelled.

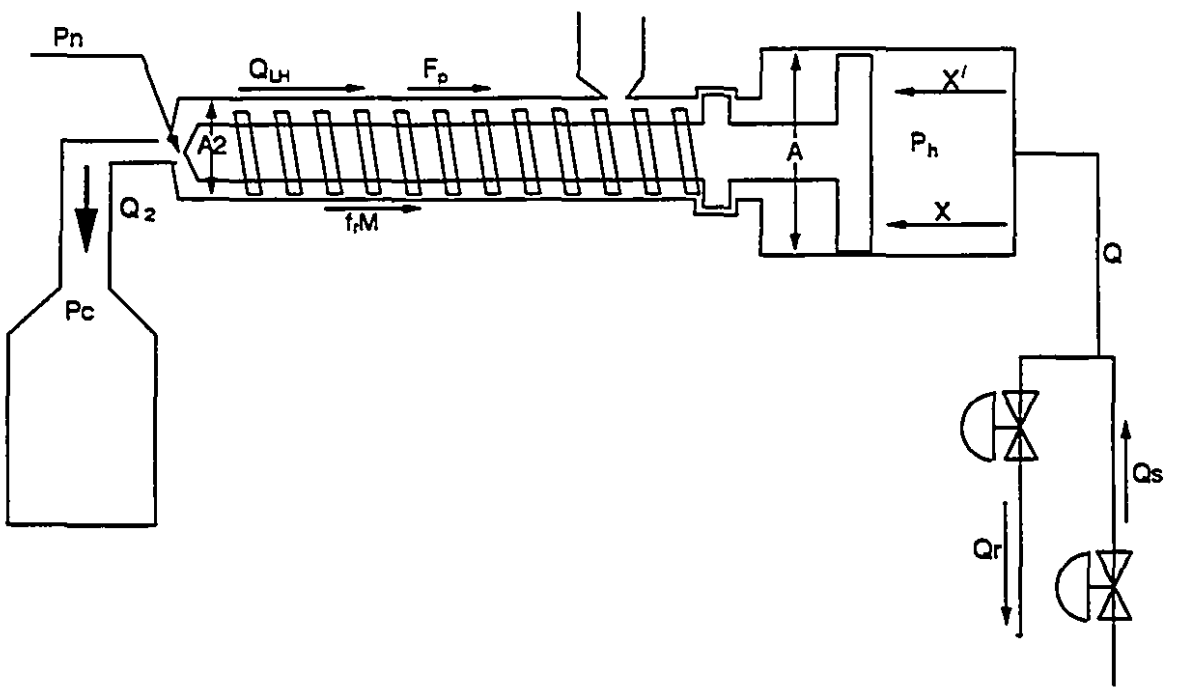

Figure 5.1 Schematic of an injection molding machine

5.2.1 Mass Conservation for Oil in the Injection Cylinder

Assuming that the cylinder body is rigid and applying the principle of mass conservation to the hydraulic oil in the injection cylinder, one obtains:

$$\frac{XA}{K_H}\frac{dP_h}{dt}=Q-Q_{LH}-\frac{dX}{dt}A \tag{5.1}$$

where X is the displacement of the injection piston (assume x=0, when the piston is at the right-most position)

Q is the volume flow rate of hydraulic oil entering the injection cylinder.

Q_{LH} is the leakage of hydraulic oil through the piston to the drain.

P_h is the hydraulic oil pressure inside the injection cylinder, (assume it is uniform inside the injection chamber).

A is the cross-sectional area of the injection piston.

K_H is the hydraulic oil bulk modulus, a function of temperature and pressure. The temperature dependency can be neglected, since the temperature varies within a small (20 to 50 °C) range, while the dependency on pressure has to be considered, because the pressure varies over the range from 0 MPa to 10 MPa.

5.2.2 Barrel Section

The hydraulic oil pressure acting on the piston forces the piston, gear box and screw as well as the melt to move to the left. The mechanical friction between the piston and cylinder shell, gear box and injection machine body resists the movement.

As the screw advances, the molten plastic is forced into the cavity, and builds up pressure. This pressure acts on the screw front to counter the screw movement. In addition, the shearing of the resin between the screw and barrel produces a viscous force to resist the movement. A force balance based on Newton's second law of motion for screw, piston and gear box, can be expressed as:

$$M\frac{d^2X}{d^2t}=P_h A-P_N A_2-f_r M-F_p \tag{5.2}$$

where M is the total mass of the screw, piston, gear box and the molten plastic moving along the screw, (the mass of plastic is small compared to that of screw, piston and gear box, and is therefore neglected).

P_h,A defined earlier,

P_N is the average pressure of molten plastic in the injection nozzle,

A_2 is the effective cross-section area of the injection screw,

f_r is the mechanical friction factor, a constant, and

F_p is the viscosity friction force, which is highly dependent on the temperature of molten plastic as well as the type of plastic.

Considering the injection barrel and screw as rigid bodies, applying the mass conservation law for the melt enclosed in the barrel between the nozzle and injection screw tip, there exists the following relationship:

$$\frac{V}{K_p}\frac{dP_N}{dt} = A_2X'-Q_2-Q_{LP} \tag{5.3}$$

where V is the instantaneous volume of the molten plastic enclosed in the barrel

between the screw tip and nozzle. It can be expressed as $V = V_0 - XA_2$, where V_0 is the molten plastic volume when the injection piston is at the right-most position (i.e. $X = 0$), X and A_2 are as mentioned earlier,

K_p is the bulk modulus of molten plastic, and is a function of the temperature and pressure,

Q_2 is the molten plastic flow rate passing through the injection nozzle,

Q_{LP} is the leakage flow rate of molten plastic, and

P_N, A_2 are previously defined.

5.2.3 Nozzle and Runner System

The following assumptions are made:

1 There is no leakage of molten plastic into the air,

2 The resistance of the nozzle and sprue to the flow of molten plastic is similar to a valve, and the resistance is constant during packing and filling.

Therefore, the flow rate of the molten plastic through the nozzle and sprue is approximated with the following equation:

$$Q_2 = K_N \sqrt{P_N - P_c} \tag{5.4}$$

where K_N is the "valve" constant of the nozzle and sprue,

P_c is the cavity (gate) pressure, and

P_N as defined earlier.

5.2.4 Cavity

During the filling stage, cavity (gate) pressure (P_c) can be approximated by:

$$\frac{dP_c}{dt} = cQ_2 \tag{5.5}$$

where P_c is the cavity (gate) pressure, and

c is a factor for the pressure gradient due to flow, which is dependent on the injection cavity geometry, polymer type, temperature and pressure.

During packing it is assumed that the mold is a rigid body, i.e. the total cavity volume is independent of cavity pressure and temperature, and that the cavity is completely filled with plastic. Apply mass conservation to the plastic in the cavity to obtain the following relationship for cavity (gate) pressure (P_c):

$$\frac{V_c}{K_{PC}}\frac{dP_c}{dt}=Q_2 \tag{5.6}$$

where V_c is the total cavity volume, a constant, and

K_{PC} is the average bulk modulus for molten and solid plastic.

K_{PC} is difficult to estimate, since it not only involves both molten and solidified plastic, but is also dependent on temperature and pressure which are changing. Setting $C = K_{PC}/V_c$, Equation (5.6) is rewritten in the form of Equation (5.5) with c replaced by C.

5.2.5 Hydraulic Pipe Section

Figure 5.2 gives a schematic of the hydraulic pipe system of the injection molding machine.

It is assumed that:

(i) hydraulic oil is incompressible inside the pipe system and the hydraulic volume in the pipe is constant;

(ii) all the stainless steel pipes have the same friction factor f;

(iii) the elevation change in the hydraulic circuit is small, and can be neglected; and

(iv) the hose has a friction factor of f_h.

The equivalent pipe lengths L1, L2, L3, L4, and L5 in Figure 5.2 physically consist of unions, manual valves, tees, crosses, elbows and different length of pipes.

Ls = the equivalent length of the supply servo-valve, and

Lr = the equivalent length of the relief servo-valve

Based on Bernoulli's equation, and the above assumptions, the following equations may be obtained:

$$P_s - P_x = \rho f (L_1 + L_2 + L_3) \frac{V_s^2}{2gD} \tag{5.7}$$

$$P_x - P_h = \rho f_h L_4 \frac{V^2}{2gD} \tag{5.8}$$

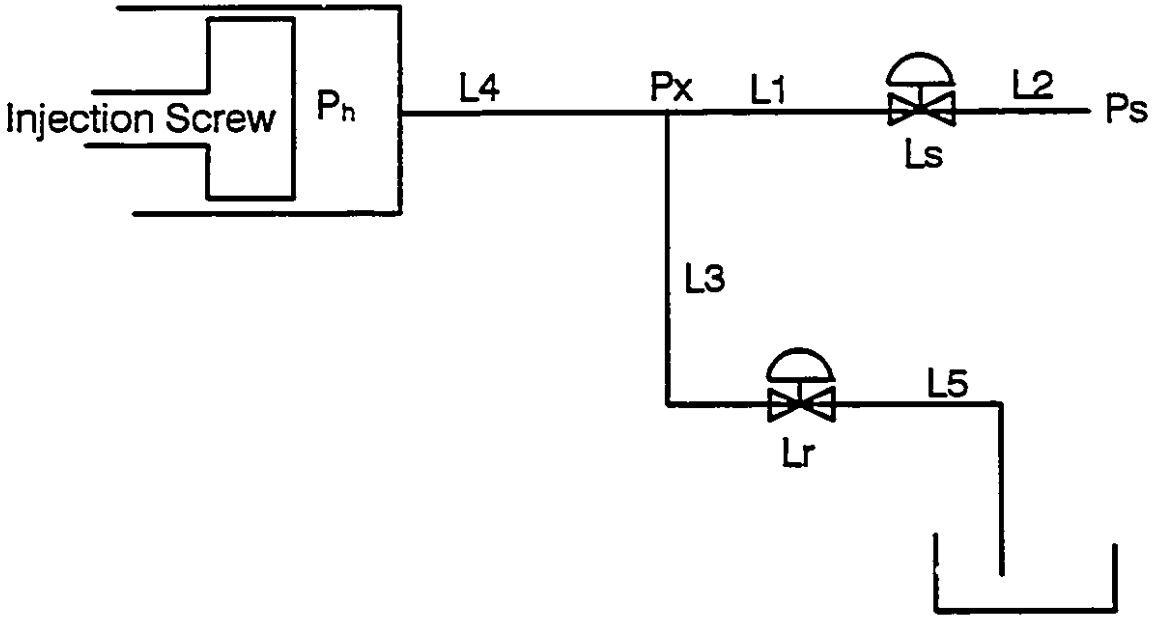

Figure 5.2 Injection molding machine hydraulic schematic

$$P_x = \rho f (L_3 + L_5 + L_r) \frac{V_r^2}{2gD} \tag{5.9}$$

where P_s is the supply hydraulic pressure (measurable),

P_x is the pressure at the interconnection point for the supply and relief pipes (it is an intermediate variable),

ρ is the density of hydraulic oil,

f and f_h are the friction factors for the pipe and hose, respectively,

V_s and V_r are the average oil velocities of the supply and relief servo-valves, respectively, and

V is the oil velocity in the hose.

The relationship between flow rate and velocity is:

$$Q = \pi \left(\frac{D}{2}\right)^2 \cdot V \tag{5.10}$$

where D is the inner diameter of the pipe or hose. Equation (5.10) is valid for Q_s (supply servo-valve flow rate), Q_r (relief servo-valve rate) as well as Q (the oil flow rate entering injection cylinder). Substitution for V_s, V_r, and V in Equations (5.7), (5.8), and (5.9) by using Equation (5.10), yields the following equations:

$$P_s - P_x = \rho f (L_1 + L_2 + L_s) \frac{8Q_s^2}{g\pi^2 D^5} \tag{5.11}$$

$$P_x - P_b = \rho f_h L_4 \frac{8Q^2}{g\pi^2 D^5} \tag{5.12}$$

$$P_x=\rho f(L_3+L5+L_r)\frac{8Q_r^2}{g\pi^2D^5} \tag{5.13}$$

The oil flow rate entering the injection cylinder has the following relationship with the flow through the relief and supply servo-valves:

$$Q=Q_s-Q_r \tag{5.14}$$

Eliminating Q_s, Q_r, and P_x from Equation (5.4), the following equation relating Q to P_s, P_h and the equivalent pipe lengths can be obtained:

$$\begin{aligned} Q=&\left[\left(P_s-P_h-\rho f_h L_4\frac{8Q^2}{g\pi^2D^5}\right)\frac{g\pi^2D^5}{8\rho f(L_1+L_2+L_s)}\right]^{\frac{1}{2}} \\ &-\left[\left(P_h+\rho f_h L_4\frac{8Q^2}{g\pi^2D^5}\right)\frac{g\pi^2D^5}{8\rho f(L_3+L_5+L_r)}\right]^{\frac{1}{2}} \end{aligned} \tag{5.15}$$

For all linear servo-valves, the following equation can be written:

$$Q=C_v i\sqrt{\Delta P} \tag{5.16}$$

where C_v is the servo-valve sizing constant, and

i is the current applied to the servo-valve.

For equivalent pipe length calculation, the following can be written:

$$\Delta P=\rho f L\frac{8Q^2}{g\pi^2D^5} \tag{5.17}$$

Therefore the following equation exists:

$$\frac{1}{(C_v i)^2} = \rho L f \frac{8}{g\pi^2 D^5} \tag{5.18}$$

Equation (5.18) is valid for both the supply and relief servo-valves. Substitution from Equation (5.18) into Equation (5.14) yields:

$$Q = \left[\left(P_s - P_h - \rho f_h L_4 \frac{8Q^2}{g\pi^2 D^5}\right)\frac{1}{\frac{8\rho f(L_1+L_2)}{g\pi^2 D^5} + \frac{1}{(C_{vs} i_s)^2}}\right]^{\frac{1}{2}} - \left[\left(P_h + \rho f_h L_4 \frac{8Q^2}{g\pi^2 D^5}\right)\frac{1}{\frac{8\rho f(L_3+L_5)}{g\pi^2 D^5} + \frac{1}{(C_{vr} i_r)^2}}\right]^{\frac{1}{2}} \tag{5.19}$$

where i_s and i_r represent the electric current applied to the supply and relief servo-valves, respectively.

C_{vs} and C_{vr} are the valve sizing constants for supply and relief servo-valve, respectively, and

all the other parameters are as defined earlier.

5.2.6 Summary of the Injection Molding Mathematical Model

The injection molding process is mathematically described by Equations (5.1), (5.2), (5.3), (5.4), (5.5) and (5.19). Some of the parameters of these six equations can be easily obtained from the machine, screw, and valve design specifications. These parameters include: A (cylinder cross section area), A2 (screw cross section area), M (injection machine mass), C_{vr} (relief valve sizing constant), and C_{vs} (supply valve

sizing constant), and C_{v_s} (supply valve sizing constant). Some of the variables such as effective pipe lengths can be estimated empirically by converting the crosses and tees into their effective lengths. However, variables like K_H, Q_{LH}, f_r, F_p, K_p, Q_{LP}, K_N c, and K_{PC} have to estimated experimentally. Estimating these parameters requires non-trivial work. Furthermore, some of these parameters depend strongly on the machine, cavity, material and operating conditions. This implies that the tedious estimating process has to be repeated whenever the machine, cavity, material or operating conditions change. System identification, determining a process model experimentally, is much more economical in terms of time and effort. On-line recursive identification methods can automatically update model parameters to new operating conditions. Furthermore, the model obtained with system identification can be readily used to design a process control, whereas the mathematical model given by Equations (5.1) to (5.5) and (5.19) has to be linearized. The system identification approach was therefore chosen for this work.

5.3 Experimental

The supply servo-valve was set to have an operating range of 0.5% to 99.5% opening in order to avoid the dead zones of the valve. The relief servo-valve opening was specified by the following relationship to the supply servo-valve:

$$Rsv=(100-Ssv)*0.2+0.4 \tag{5.20}$$

where Ssv is the percent opening of the supply servo-valve, Rsv is the relief servo-valve opening in percent. The maximum opening of the relief servo-valve, as Equation (5.20) indicates, is 20.3%, which prevents excessive hydraulic pressure drops. The minimum opening of 0.5% avoids the dead zone. The servo-valve to computer interface is illustrated in Figure 5.3. The relationship determined by Equation (5.20) for Ssv and Rsv is achieved through computer programming. With this arrangement, the supply and relief servo-valves are controlled by a single controller throughout this investigation.

The pressure transducer installed near the gate in the injection cavity was used to measure the cavity pressure. Information regarding the calibration and location of this pressure transducer and the other sensors is given in Chapter 3.

All the experimental work was carried out using an injection molding grade high density polyethylene resin (Sclair 2907, Dupont Canada). The relevant properties of the resin have been summarized by Abu Fara [1].

The selection of the sampling period is important. A too fast sampling rate will lead to excessive computation power waste and poor control due to susceptibility to noise. A too slow sampling rate will make it impossible to reconstruct the

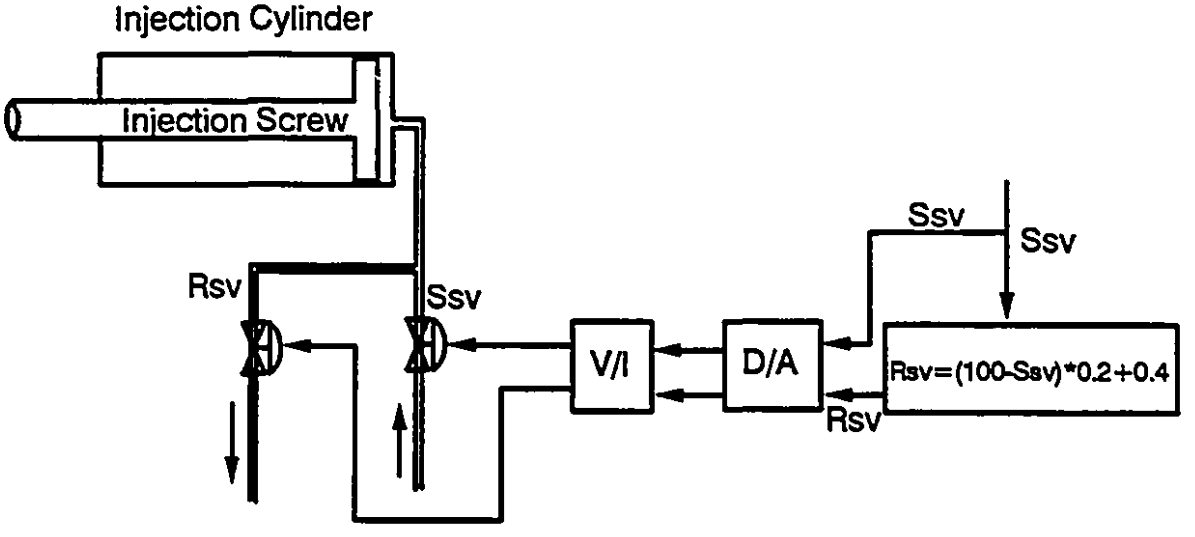

Figure 5.3 Servo-valve interface to computer control system

continuous-time signal, thus leading to difficulties in obtaining good control. Detailed methodologies for selecting a proper sampling interval are given in references [87, 91]. For dynamics and control of the cavity pressure during filling and packing, a sampling period of 20 ms was determined to be sufficient.

The barrel temperature set-points for the four barrel heaters, from the nozzle to the hopper, are 205°C, 195°C, 175°C and 150°C, respectively, unless stated otherwise. Since the pressure transducer is located in the cavity near the gate, it takes some time for the melt to fill the sprue and runner before reaching the sensor. During this period, the supply servo-valve is at the maximum opening to minimize the filling time, and the sensor output is zero. The controller starts to work once it sees a pressure. A threshold of 34.5 kPa (5.0 psi) was used to determine the start of cavity filling. All other relevant conditions are indicated with the experimental results.

5.4 A Preliminary Study of Injection Molding Filling and Packing Stages

Some open-loop experiments were carried out to gain a general understanding of injection molding behaviours and major machine and process variable variations.

Figure 5.4 shows a typical pressure profile measurement for the injection and packing phases for three consecutive cycles without closed-loop pressure control and with constant valve openings. It is obvious that the injection and packing pressure profiles vary from cycle to cycle with consequent variations in the physical properties of the molded parts. This indicates the need for closed-loop cavity pressure control.

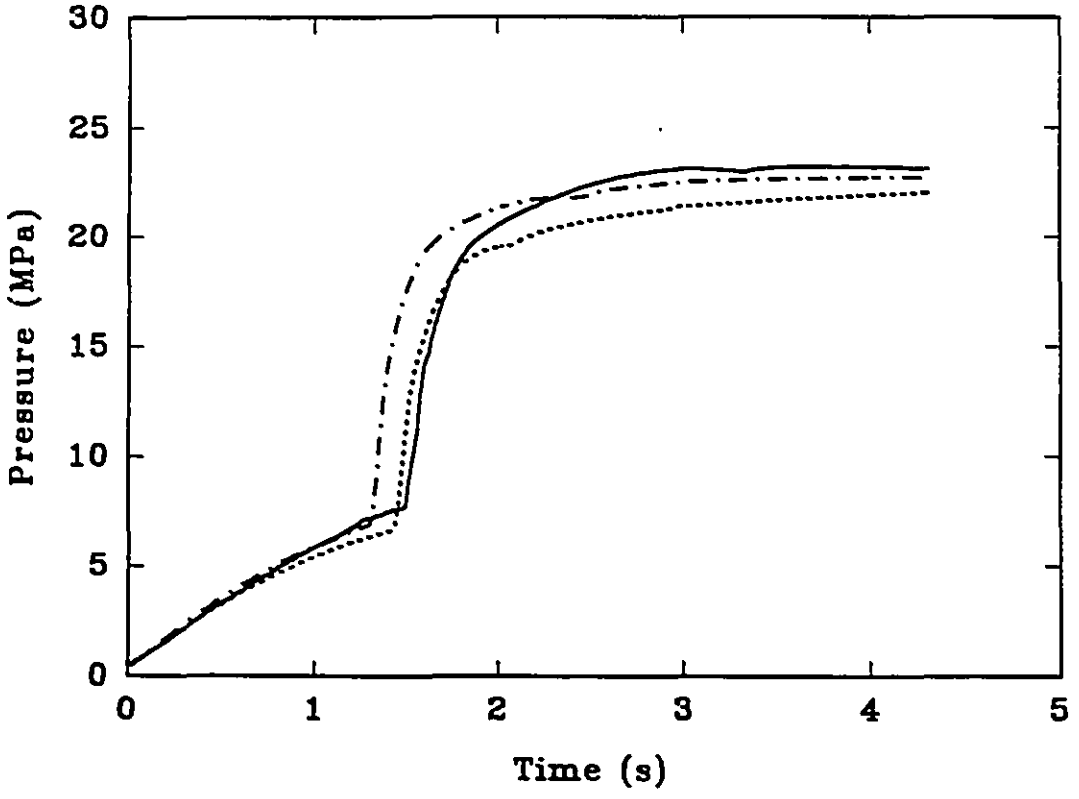

Figure 5.4 Open-loop cavity pressure profiles of three consecutive injection cycles

Figure 5.5 shows typical experimental results for major process and machine variables. Figure 5.5A gives pressure at the nozzle, in the injection cylinder, at the gate and in the middle of the cavity. Figure 5.5B gives both the screw displacement and its velocity. As injection starts, pressure in both the injection cylinder and the nozzle starts to increase gradually, the molten plastic fills the injection sprue, gate, and then the cavity. The cavity pressure near the gate starts to rise gradually. There is no pressure signal from the pressure sensor in the middle of the cavity before the melt reaches it. The resin continues to fill the injection cavity, and the pressures at the gate and in the middle of the cavity increase gradually until the cavity is filled completely. The sudden increase of pressures at about 0.8 s indicates the end of filling and the start of packing. With the continuation of packing, some additional material is forced into the cavity, producing the cavity pressure increase. The screw moves at a high speed at the beginning of filling due to the small flow resistance. The increase of cavity pressure is associated with gradual reduction of screw velocity. At the end of the filling, the sudden increase of the cavity pressure is associated with a decrease in the screw velocity to nearly zero. During the packing stage, the screw moves very slowly to force additional material into the injection cavity.

5.5 Dynamics and Self-Tuning Control of Cavity Pressure during Filling

5.5.1 Dynamics Analysis during Filling Stage

A number of open-loop experiments were conducted to examine the time-varying and non-linear behaviour of the process. Two typical experimental results are

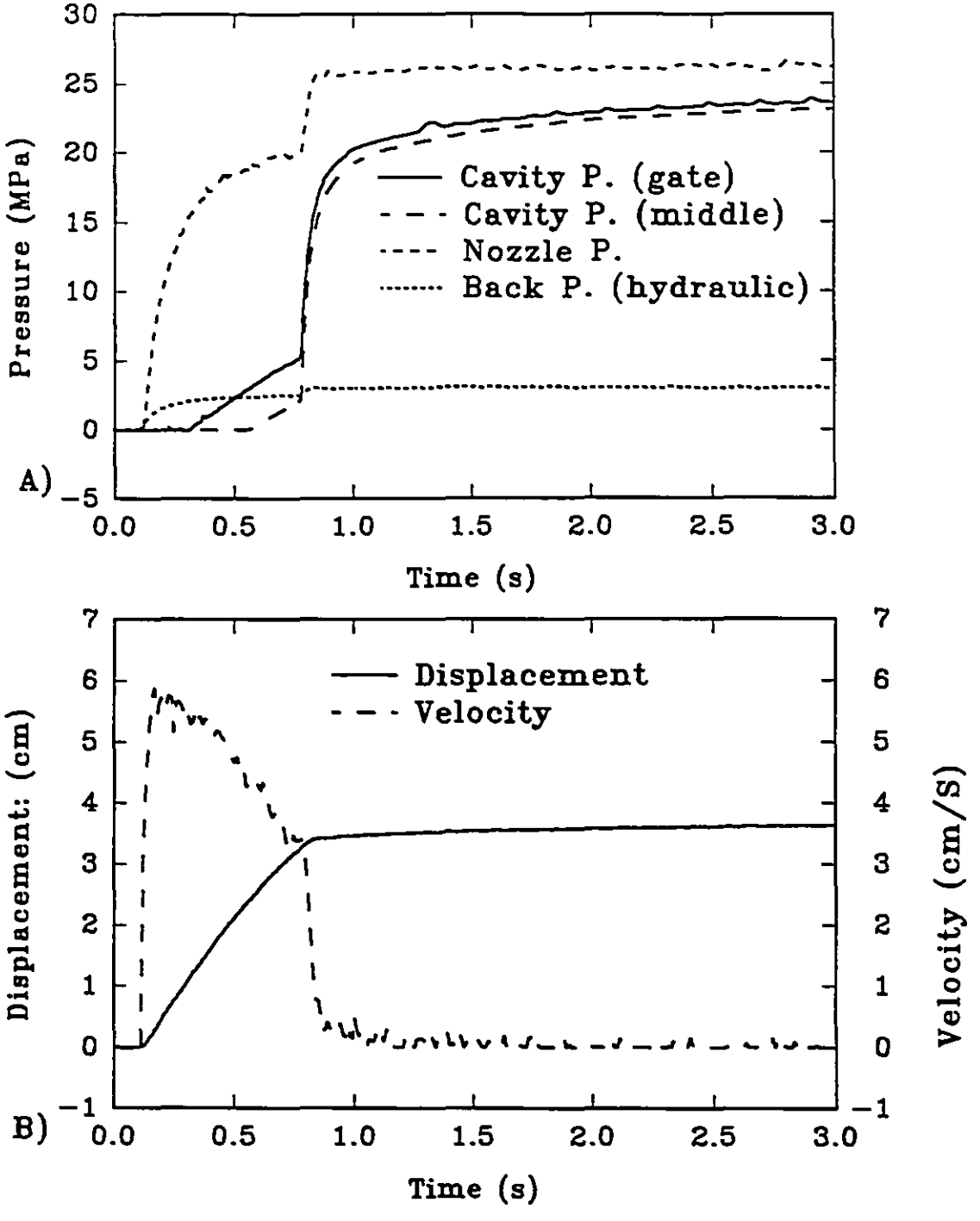

Figure 5.5 Cavity (gate and middle), nozzle and injection cylinder back pressures of a typical injection cycle during filling and packing phases (A), velocity and screw displacement (B)

given here. Figure 5.6A gives the valve opening changes between 20 and 40 %, while Figure 5.6B shows the response of the cavity gate pressure. The cavity pressure increases gradually during the filling of the injection cavity, with the superposition of small pressure ripples caused by the variation of valve opening. The sudden large increase in the cavity pressure at about 2.6s indicates the beginning of packing. The relationship between cavity pressure and valve opening is time-varying; for the same valve opening change, the change of the cavity pressure increases with the degree of fill. Careful examination of Figures 5.6A and 5.6B indicates that there is a delay of one sample period in the response of cavity pressure to the valve opening change. The delay is probably due to the response time of the hydraulic system and the servo-valve.

Examination of the cavity pressure suggests the response can be modelled as a simple integrating process with a time varying gain, in parallel with a first order process with a varying process gain and time constant, in series with a pure delay. A graphic representation of the process is shown in Figure 5.7. The model describing the dynamic relation between the cavity pressure and the valve-opening, in Laplace transform, is:

$$y(s)=\left[\frac{k1(t)}{s}+\frac{k2(t)}{\tau s+1}\right]e^{-t_d s}u(s) \qquad (5.21)$$

where y is the cavity pressure, u is the servo-valve opening, k1(t) is the gain for the integrating process, k2(t) is the gain for the first order process, τ is the process time constant, t_d is the time delay, and s is the Laplace transfer operator. The Laplace

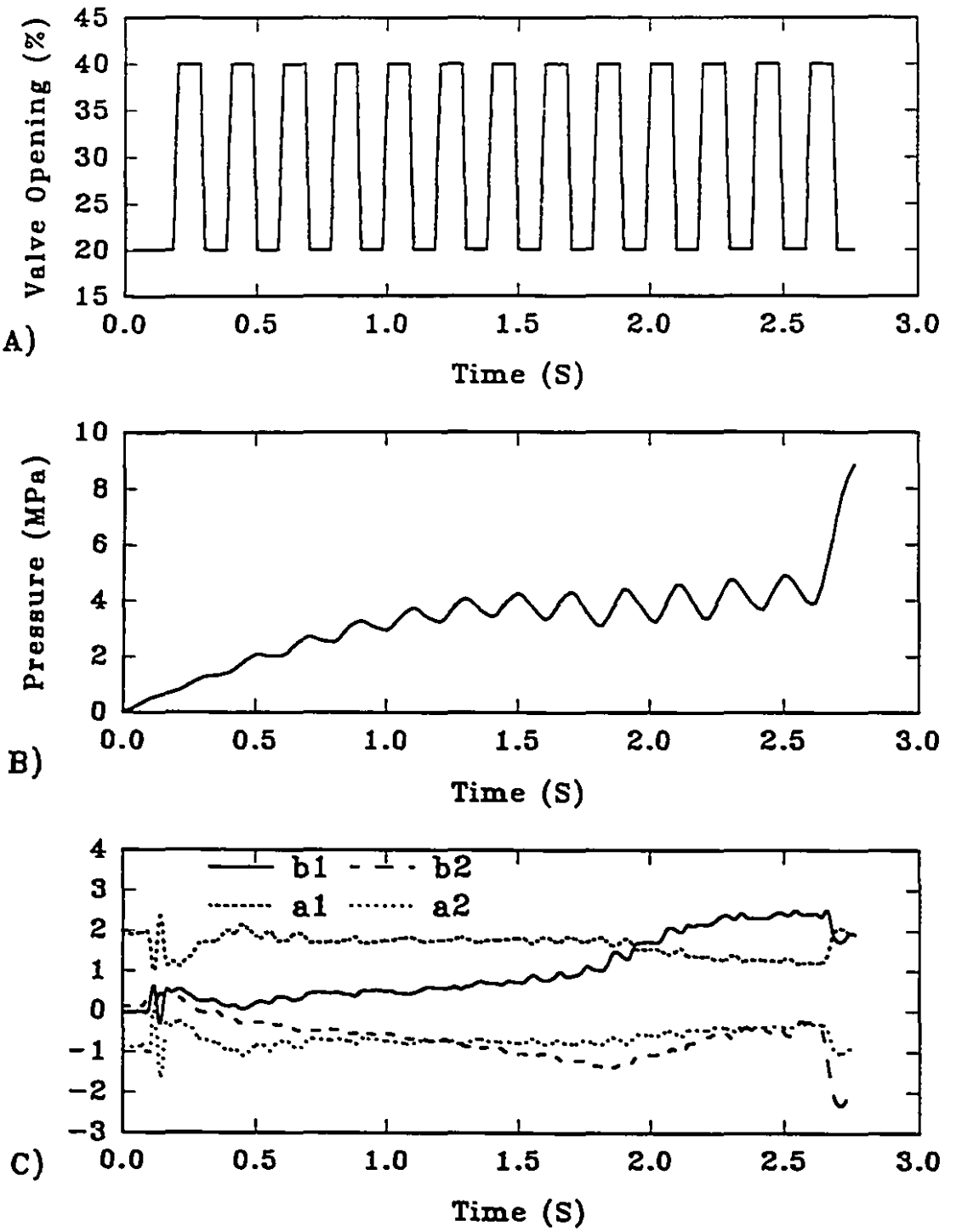

Figure 5.6 Servo-valve opening changes between 20 and 40 % (A), cavity pressure responses (B), and process model parameter variations (C)

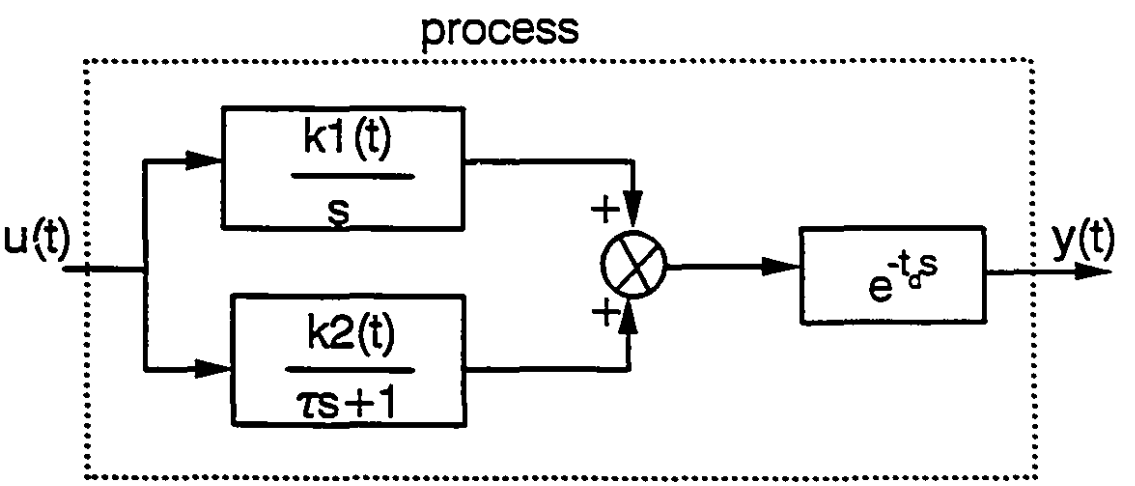

Figure 5.7 Cavity pressure dynamic model structure in Laplace Domain

transfer function can be discretized into Equation (5.22) using the method outlined in reference [94].

$$y(k)=a_1y(k-1)+a_2y(k-2)+b_1u(k-1-nk)+b_2u(k-2-nk) \qquad (5.22)$$

where t_d = nk · T (T=sampling interval), nk is an integer, and

k is the sample number.

It is therefore possible to construct an estimate $\theta=[\ b_1\ b_2\ -a_1\ -a_2]$ using the recursive identification method described in Chapter 4. The choice of λ is important. Too small a value of λ leads to a large variation in the model parameters in response to small disturbances. However, choosing too large a value for λ will make it difficult to detect changes in the model parameters when the process is changing quickly. For most processes, a value between 0.95 and 0.99 is recommended [87 - 91, 122]. As a first estimation, a value of 0.95 was chosen. Figure 5.6C shows the changes in process model parameters with time. It is obvious that all the process parameters change strongly and rapidly with time, confirming the time-varying nature of the process. The sum of a_1 and a_2 is close to 1, indicating that the process has an integral action proposed earlier. The units for parameters b_1 and b_2 are psi/% (1 psi = 6.89 kPa). The large variation in the parameters at the beginning of filling (t < 0.3 s) is due to the limited number of data, while the strong variation at about 2.6 s reflects the beginning of packing. Figure 5.8 gives a comparison of the pressure measurement and the pressure calculated based on the estimated model. The solid line is the cavity pressure measurement, and the dashed line is the predicted pressure. They are in close proximity, indicating that the model is reasonably good.

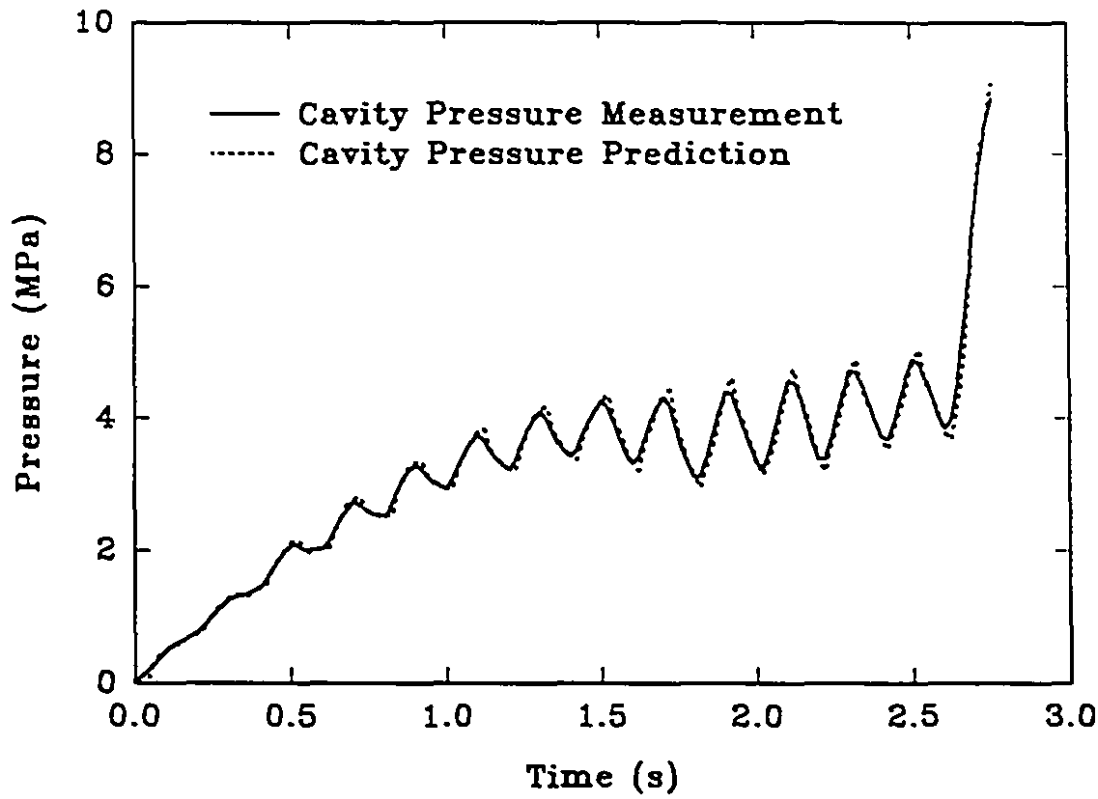

Figure 5.8 Cavity pressure measurement and prediction based on the estimated model

A second experiment was carried out with the valve opening varying between 20 and 80 percent to investigate the non-linear behaviour of the system. Figure 5.9B shows the cavity pressure response to the valve opening changes shown in Figure 5.9A, and the process model parameter changes are shown in Figure 5.9C. Comparison of Figures 5.6 and 5.9 indicates obvious differences between the model parameters. The differences can be considered mainly due to the process non-linearity. The process is thus both non-linear and time-varying. A suitable strategy to control a non-linear and time-varying process, like cavity pressure, is self-tuning control. The time varying and non-linearity have been described and explained by Equations (5.1) - (5.5) and (5.19) in Section 5.1.

5.5.2 Controller Design

Indirect self-tuning control has been chosen for this project, due to its flexibility, and since it gives an explicit process model. The recursive estimation technique used is the forgetting factor method described in the recursive identification section. The control design technique used in this project is based on pole-placement [78], as outlined in Chapter 4.

Equation (5.22) with a delay, $n_{td}=1$, can be expressed in z-transform form:

$$\frac{y(z)}{u(z)}=\frac{b_1z+b_2}{z(z^2+a_1z+a_2)} \qquad (5.23)$$

The parameters a_1, a_2, b_1 and b_2 are all estimated on-line, and there is no guarantee that $|b_2|<|b_1|$ which would represent an unstable zero (a non-minimum phase

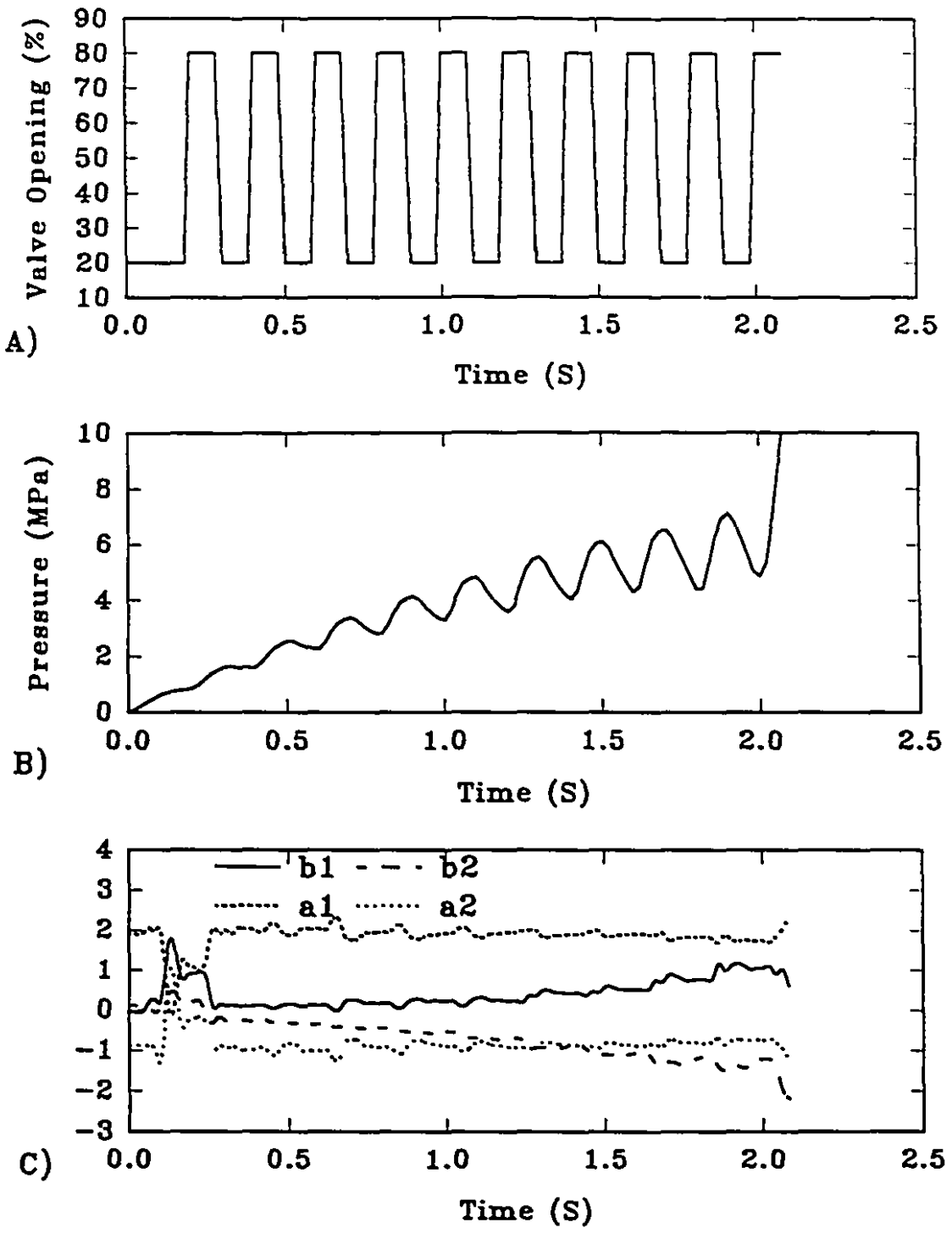

Figure 5.9 Servo-valve opening changes between 20 and 80 % (A), cavity pressure responses (B), and process model parameter variations (C)

process). Thus, the process zero is kept as part of the desired closed-loop performance. The dynamics of the closed-loop system can be conveniently expressed by poles. Second-order poles are specified as $z^2+p_1z+p_2=0$. The poles, p_1 and p_2, are obtained from the frequency, ω, and the damping factor, ξ, as:

$$p_1=-2\exp(-\xi\omega T)\cos(\omega T\sqrt{1-\xi^2}) \tag{5.24}$$

$$p_2=\exp(-2\xi\omega T) \tag{5.25}$$

A number of simulations were performed to determine the proper values of ω and ξ. The simulation results presented in Figures 5.10 and 5.11 were based on the averaged dynamics of the early filling phase. The parameters are listed in Table 5.1. For simplicity, the model for the simulation was assumed to be linear and time-invariant for the choices of ω and ξ. Figure 5.10A gives the closed-loop simulation responses to a constant ramp of 55.1 kPa (8 psi) per sample period (0.02 s) with ξ = 0.8 and different values of ω. Figure 5.10B gives the corresponding valve openings (the manipulated variable). Figure 5.10 indicates that a larger ω produces a closer tracking of the controlled variable to its set-point. However, the valve action also tends to be stronger. A compromise value of ω of 50 is chosen. Figure 5.11 gives the simulation results with different values of ξ and a constant value ω of 50. Again, Figure 5.11A shows the controlled variable responses, and Figure 5.11B gives the corresponding valve responses. Figure 5.11 indicates that a smaller value of ξ produces tighter tracking of the set-point profile and a larger valve opening variation. Again, a value of 0.8 for ξ provides a compromise between tracking ability and valve

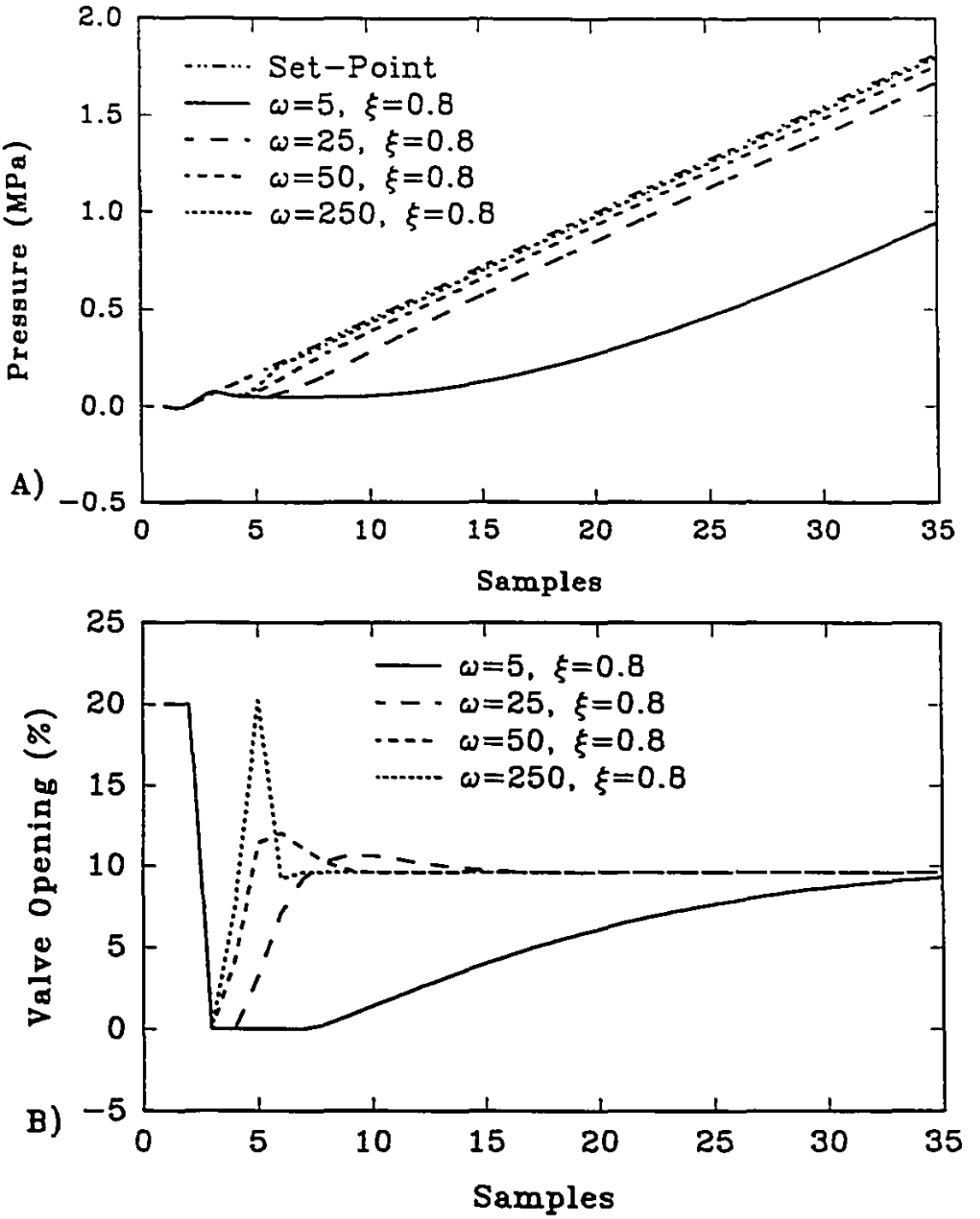

Figure 5.10 Simulated cavity pressure responses to different values of ω (A), and the corresponding servo-valve changes (B)

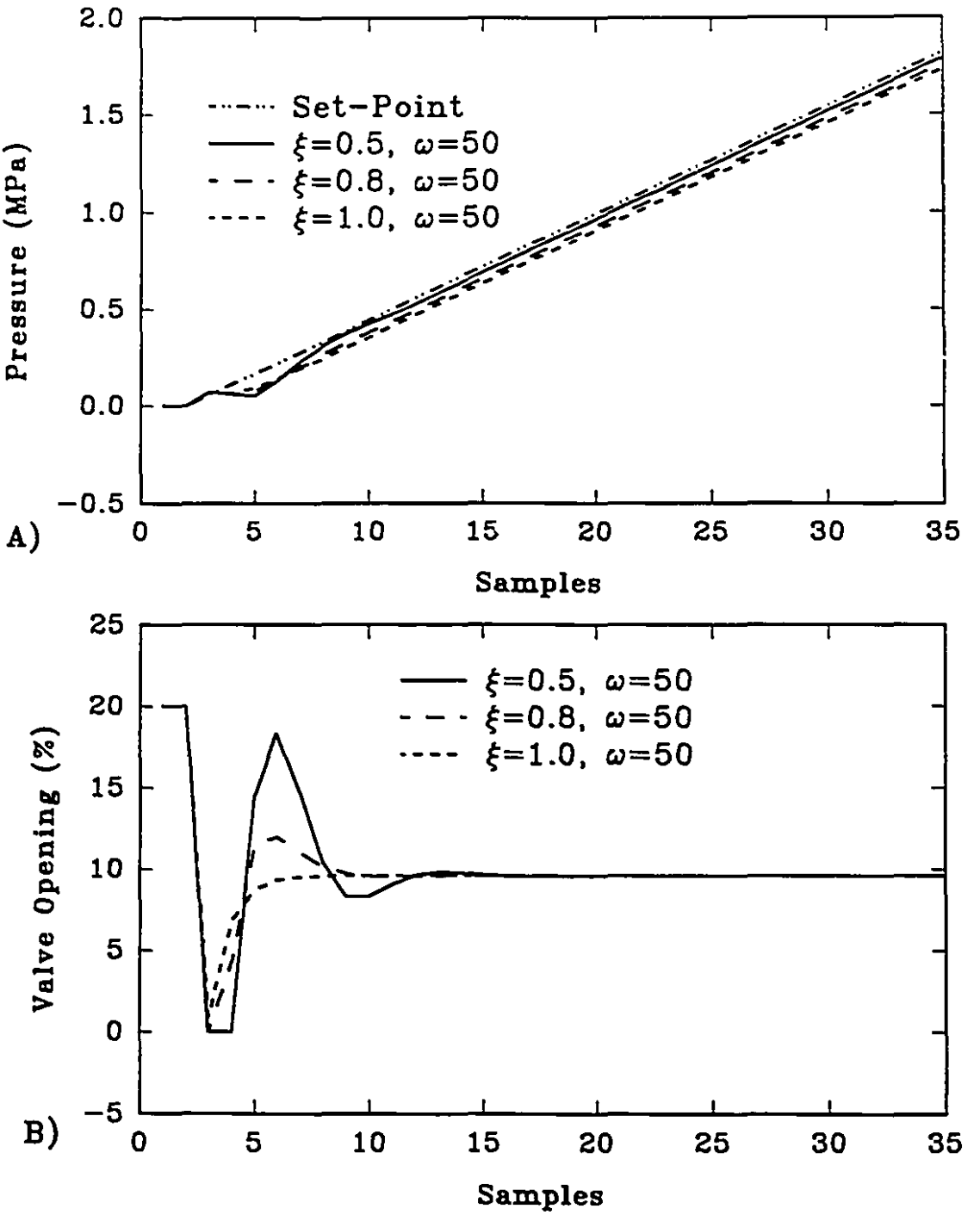

Figure 5.11 Simulated cavity pressure responses to different values of ξ (A), and the corresponding servo-valve changes (B)

Table 5.1 Process dynamics for determining the closed-loop STR poles

$y(k) = a_1y(k-1)+a_2y(k-2)+b_1u(k-1-nd)+b_2u(k-2-nd)$	
a_1	1.4
a_2	-0.4
b_1	0.8
b_2	-0.3
nd	1

action. The values of ω = 50, and ξ = 0.8 were used in the control experiments.

A delay term was added to ensure causality, and therefore $A_m = z(z^2 + p_1z + p_2)$. The closed-loop performance should have unity gain. The desired closed-loop control performance is:

$$H_m = \frac{B_m(z)}{A_m(z)} = \frac{\frac{1+p_1+p_2}{(b_1+b_2)}(b_1z+b_2)}{z(z^2+p_1z+p_2)} \tag{5.26}$$

The necessary controller terms R, T, and S, shown in Figure 4.4, were obtained by solving Equation (4.38). The method employed was to equate the coefficients of the right and left sides of the equation. The results are given by Equations (5.27) to (5.36).

$$R(z) = z^3+(r_1-1)z^2+(r_2-r_1)z-r_2 \tag{5.27}$$

$$S(z) = s_0 z^3 + s_1 z^2 + s_2 z + s_3 \tag{5.28}$$

$$T(z) = \frac{1 + p_1 + p_2}{b_1 + b_2} z^3 \tag{5.29}$$

where

$$r_1 = 1 - a_1 + p_1 \tag{5.30}$$

$$\begin{aligned} r_2 = {} & -b2[b_1^2(a_2 - a_2 a_1 + a_2 p_1) \\ & - b_2^2(a_1 p_1 - 1 - p_1 + a_2 - p_2 + a_1 - a_1^2) \\ & + b_1 b_2(a_2 p_1 - a_1 + a_1^2 - a_1 p_1 - a_2 a_1)]/c \end{aligned} \tag{5.31}$$

$$\begin{aligned} s_0 = {} & [b_1 b_2(a_1^3 + a_1 - a_1^2 + a_2^2 - a_1^2 p_1 - a_2 p_2 + a_1 p_2 - a_2 a_1^2 + a_1 p_1 - a_2 a_1 + a_2 a_1 p_1) \\ & b_1^2(a_2 a_1 - a_2 a_1^2 - a_2 p_1 - a_2 p_2 - a_2 + a_2^2 + a_2 a_1 p_1) \\ & - b_2^2(1 - a_1 p_2 + 2a_2 a_1 - a_2 p_1 + a_1 p_1 + a_1^2 p_1 + p_1 - a_2 + p_2 - a_1 + a_1^2 - a_1^3)]/c \end{aligned} \tag{5.32}$$

$$\begin{aligned} s_1 = {} & [b_1 b_2(a_1^3 - a_1^2 + a_2^2 - a_1^2 p_1 - a_2 p_2 - 2a_2 a_1^2 + 2a_2 a_1 p_1 + a_1 a_2^2 - a_2^2 p_1) \\ & + b_1^2(a_2 a_1 - a_2 a_1^2 + a_2 a_1 p_1 + a_1 a_2^2 - a_2^2 p_1) \\ & + b_2(a_1 p_2 - a_2 a_1 + a_1 p_1 - a_1^2 p_1 + a_1 - a_1^2 + a_1^3 + a_2^2 - a_2 p_2 - a_2 a_1^2 + a_2 a_1 p_1)]/c \end{aligned} \tag{5.33}$$

$$\begin{aligned} s_2 = {} & -a_2[b_1 b_2(a_2 p_1 - a_1 + a_1^2 - a_1 p_1 - a_2 a_1) \\ & + b_1^2(a_2 - a_2 a_1 + a_2 p_1) \\ & + b_2^2(1 - a_1 p_1 + p_1 - a_2 + p_2 - a_1 + a_1^2)]/c \end{aligned} \tag{5.34}$$

$$s_3 = 0 \tag{5.35}$$

$$c = (b_1+b_2)(a_1b_1b_2-a_2b_1^2-b_2^2) \tag{5.36}$$

5.5.3 Control Experiments

An experiment was carried out to test the designed self-tuning closed-loop control using a forgetting factor (λ) of 0.95, this value was chosen since $0.95 \leq \lambda \leq 0.99$ is commonly suggested in the literature. The experimental result is shown in Figure 5.12. In Figure 5.12A, the dot-dot-dash-line is the set-point of a constant ramp of 2.76 MPa/s (400 psi/s), and the solid line is the cavity pressure response. Figure 5.12B shows the corresponding servo-valve opening. The cavity pressure started to follow the set-point without much oscillation, then became oscillatory until about of 1.8 seconds after the start of injection. It then followed the set-point until the end of filling. The rapid pressure increase away from the set-point ramp at the time of 2.4 seconds indicates the beginning the packing. The servo-valve opening shows oscillatory behaviour similar to the cavity pressure. The oscillation indicates that a forgetting factor of 0.95 is much too slow to estimate the time-varying process dynamic model parameters properly. The less oscillatory behaviour at the beginning indicates that the initial model estimation is not far from the actual process model. However, with the continuation of filling, the actual process dynamics move away from the initial estimation at a speed with which the recursive identification cannot keep up using the forgetting factor of 0.95. The control responses become oscillatory

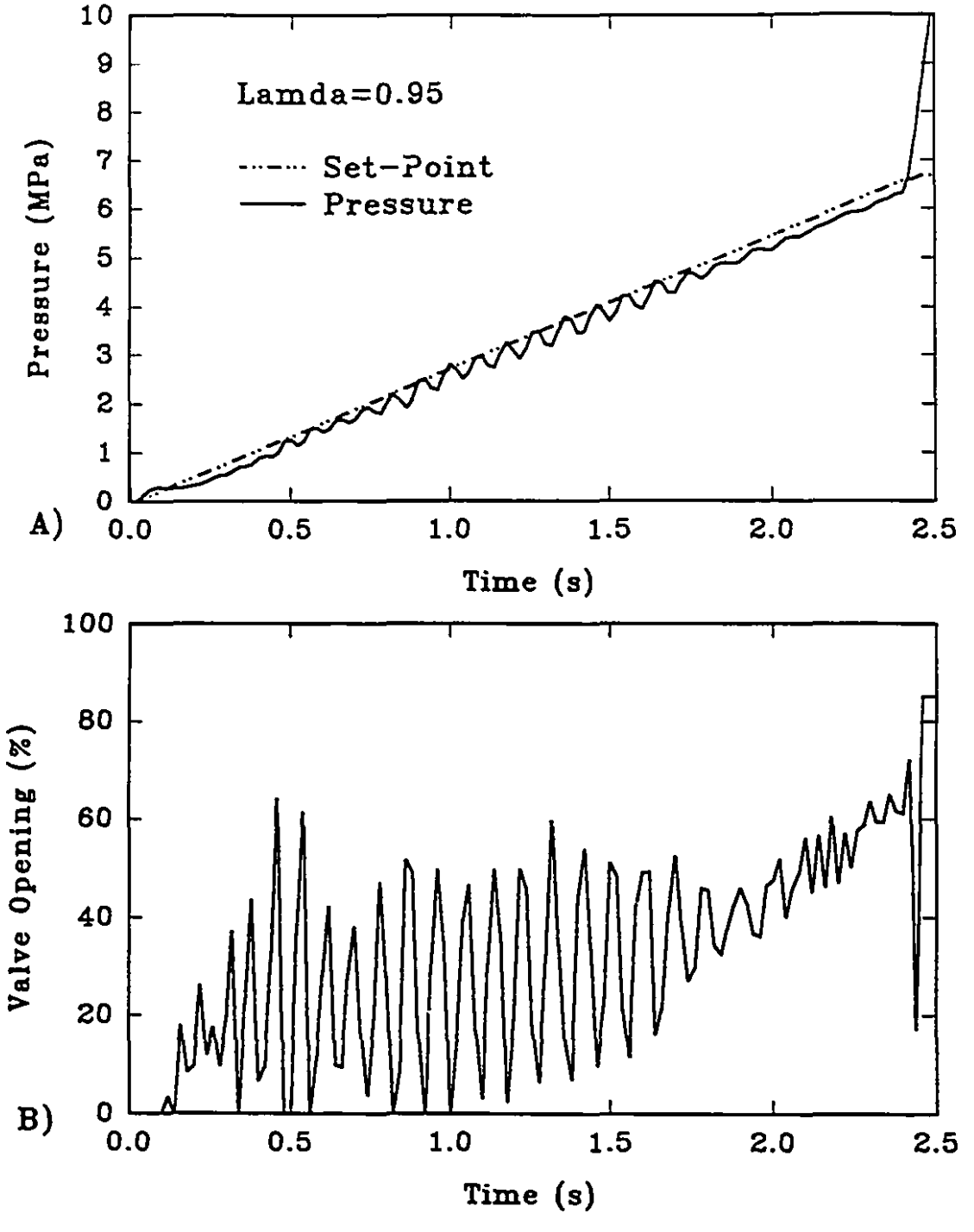

Figure 5.12 Experimental STR closed-loop of cavity pressure to follow a constant ramp set-point profile, forgetting factor of 0.95: cavity pressure responses (A), and the corresponding servo-valve changes (B)

as a result. Toward the end of filling, the estimated model reflects the actual process dynamic model to a certain degree, and consequently leads to less oscillatory control response.

Due to the time delay of the process itself and the relatively small ω, there is about a constant two samples lag in the control response, as indicated in Figure 5.12. In order to eliminate this lag, in the actual implementation of the controller, the commanding signal sent to the controller is shifted forward two steps.

To select a proper forgetting factor for the self-tuning control system, a number of experiments were carried out with different values of λ (λ = 0.95, 0.9, 0.8, 0.75), using the same set-point profile (a linearly increasing ramp of 2757 kPa/s (400 psi/s)). The responses of the controlled variable are shown in Figure 5.13. For the sake of clarity, the responses for λ = 0.95, 0.9 and 0.8 are shifted up 2068 kPa (300 psi), 1378 kPa (200 psi), and 689 kPa (100 psi), respectively. Strong oscillations occurred for a large part of early filling up to 1.2 seconds with λ=0.95, 0.9, and 0.8, because the injection process is rapidly time-varying. Thus, the estimation procedure is not quick enough to follow the changing process. As Figure 5.13 indicates, a forgetting factor of λ =0.75 is able to produce a smooth control. Common sense dictates that the forgetting factor should usually be small at the beginning of the experiment to help in obtaining reasonable model parameters within a short period of time. Once the proper model has been obtained, the forgetting factor can be increased slightly in order to increase the robustness of the recursive estimators in response to noises.

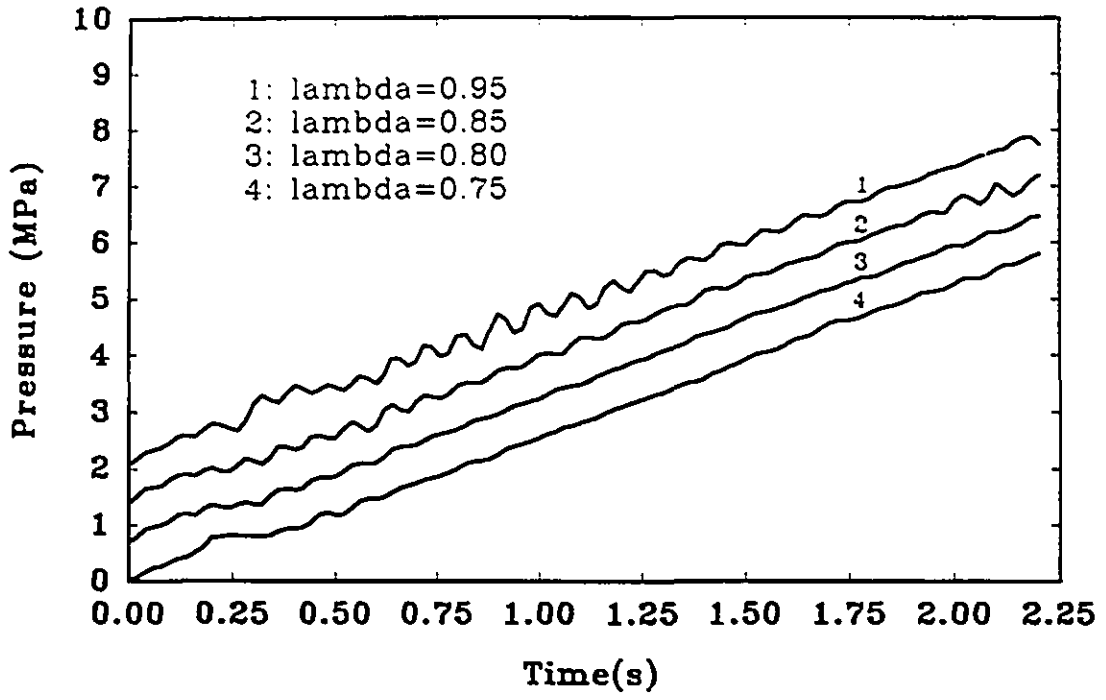

Figure 5.13 Experimental cavity pressure responses of the STR control to follow a constant ramp of 2.76 MPa/s (400psi/s), using different forgetting factors

On the basis of the above results, a self-tuning control system with a time-varying forgetting factor has been tested. The forgetting factor changes with time as follows:

$$\lambda = 0.98 - 0.23\exp(-t/0.06) \tag{5.37}$$

where t is the time in seconds. Clearly, the forgetting factor starts with the lower value of 0.75, and then it gradually increases to 0.98 after 120 samples (the sampling period is 0.02 seconds). Figure 5.14 shows how the forgetting factor varies with time.

Figure 5.15A gives the result of the self-tuning control response of the cavity pressure in tracking a three segment constant ramp set-point profile. The corresponding valve response is shown in Figure 5.15B. The controller starts with a small error, which is quickly eliminated with the improvement of the estimated model. However, with the continuous increase of the forgetting factor, the control system becomes slow in terms of its capability to track the time-varying process dynamics, and eventually, it becomes oscillatory.

In light of the results shown in Figures 5.13 and 5.15, a fixed value of the forgetting factor ($\lambda = 0.75$) was chosen to control the cavity pressure response for simplicity. More experiments were carried out to test the self-tuning control system.

Figure 5.16A shows the results for the case of $\lambda = 0.75$, where the solid line represents the set-point profile, while the short dashed line represents the cavity pressure measurement. It is obvious that the controlled variable followed the set-point (a constant ramp) closely with little oscillation. The rapid increase in cavity pressure near the end indicates the beginning of packing. Therefore, a value of λ of

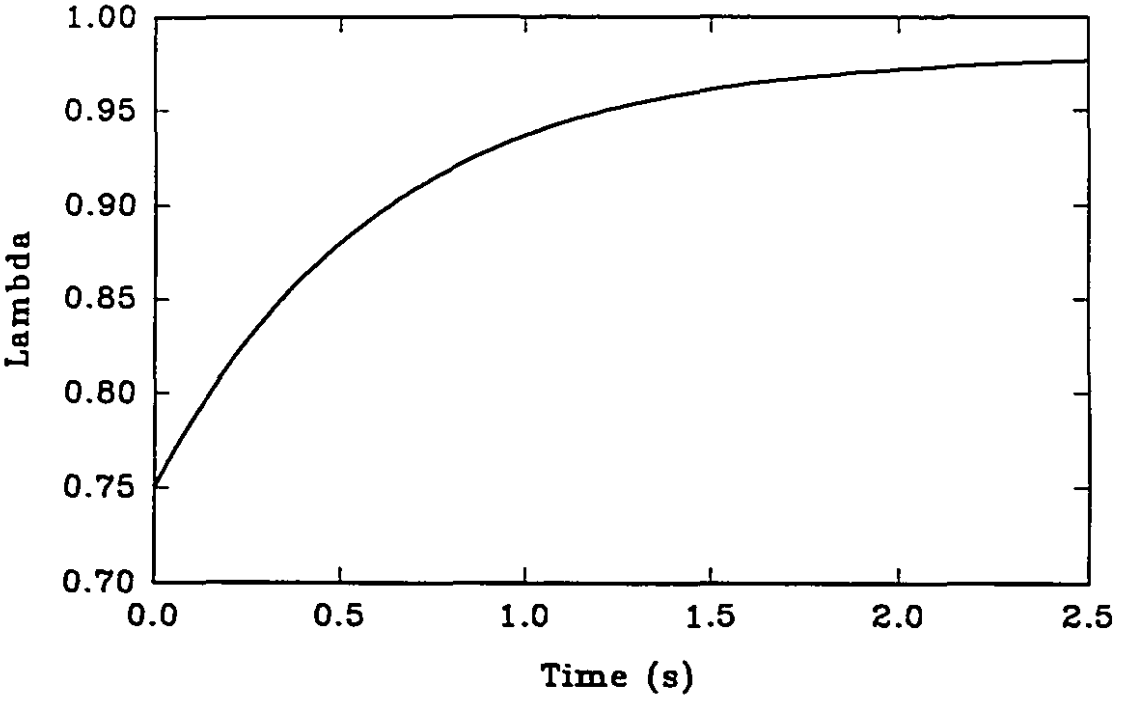

Figure 5.14 Time varying forgetting factor

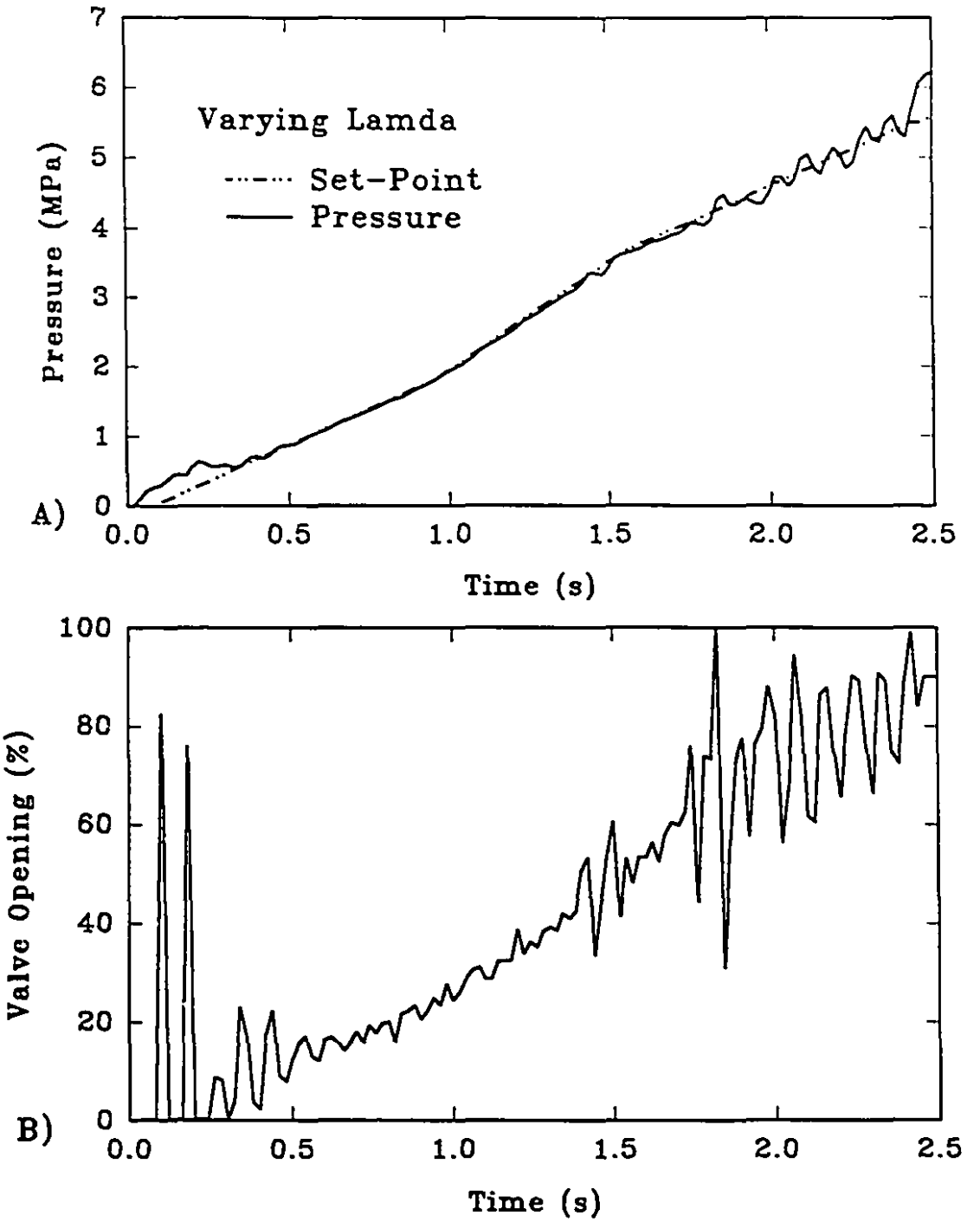

Figure 5.15 Experimental cavity pressure responses of the STR to a three segment ramp set-point profile using the time-varying forgetting as shown in Figure 5.14 (A), and the corresponding servo-valve changes (B)

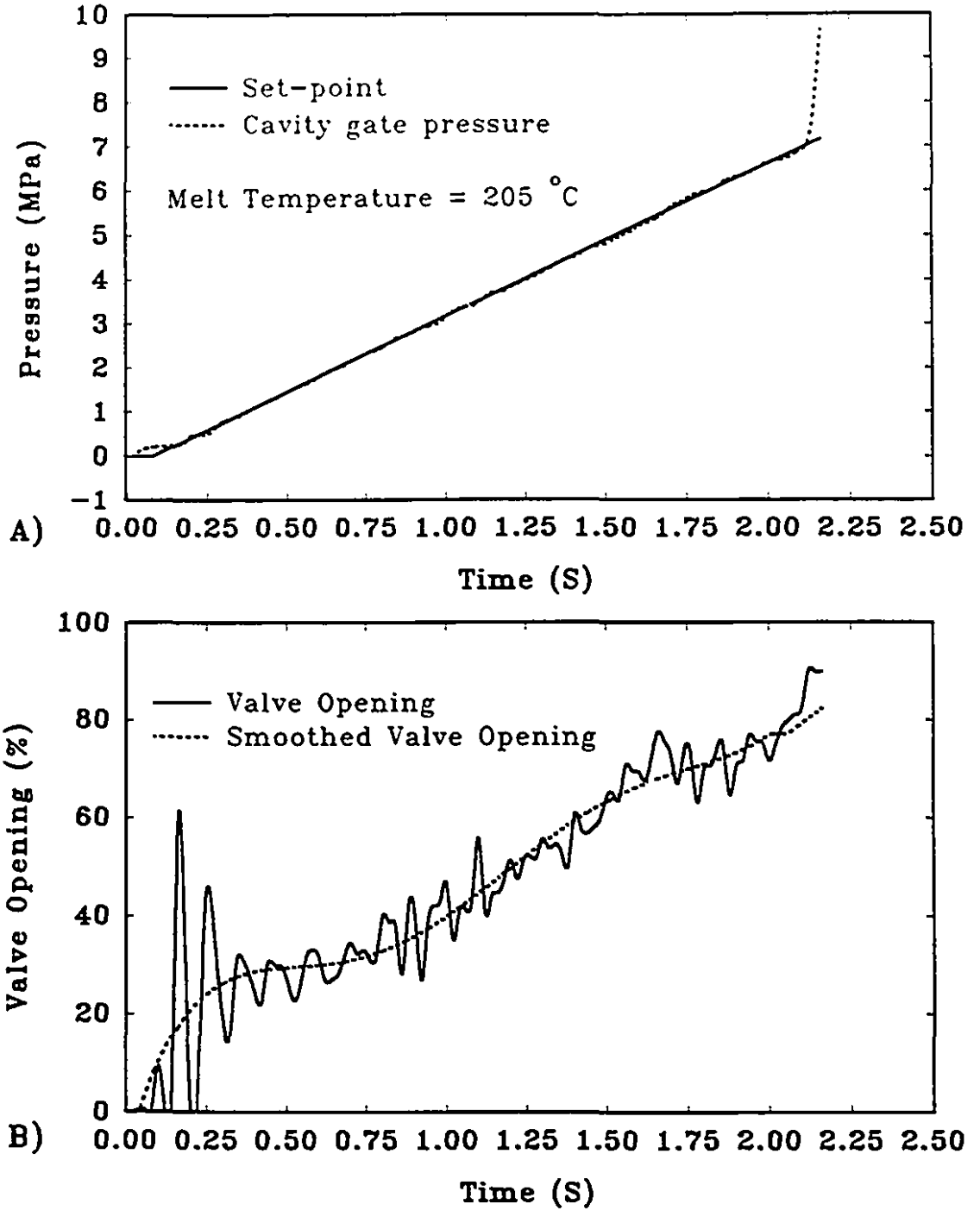

Figure 5.16 Experimental cavity pressure response of the STR control to a constant ramp set-point profile, using a forgetting factor of 0.75, and a melt temperature of 205 °C (A), and the corresponding servo-valve changes (B)

0.75 is close to that required. Figure 5.16B gives the supply servo-valve opening corresponding to the results of 5.16A. The solid line represents the actual valve opening, while the dashed line is filtered data using the data from the solid line. The purpose of presenting this dashed line here is to show the trend of the servo-valve opening. The relatively large variation of the servo-valve opening up to 0.25 seconds is due to initial start up of the control and to initial model mismatch. However, this large variation disappears quickly. The small oscillation of valve opening is due to measurement noises. The controlled cavity gate pressure is following a constant ramp; however, the trend of the servo-valve opening (the short-dashed-line) is not a constant ramp. This is a further indication of the non-linear and time-varying behaviour of the controlled process.

An experiment was conducted to test the regulating ability of the controller at a different melt temperature. Figure 5.17A gives the control responses with a melt temperature of 220 °C and can be compared with Figure 5.16A. In both cases, the cavity gate pressure follows the set-point profile closely, thus indicating that the self-tuning control can easily operate over a reasonable temperature range. Therefore, changes in the molding operating conditions do not require explicit controller changes.

Figure 5.18 shows the closed-loop responses of the cavity pressure for three different cycles using the self-tuning control method with the same set-point profile. The responses almost superimpose on each other. This clearly indicates that the self-tuning control system has very good repeatability.

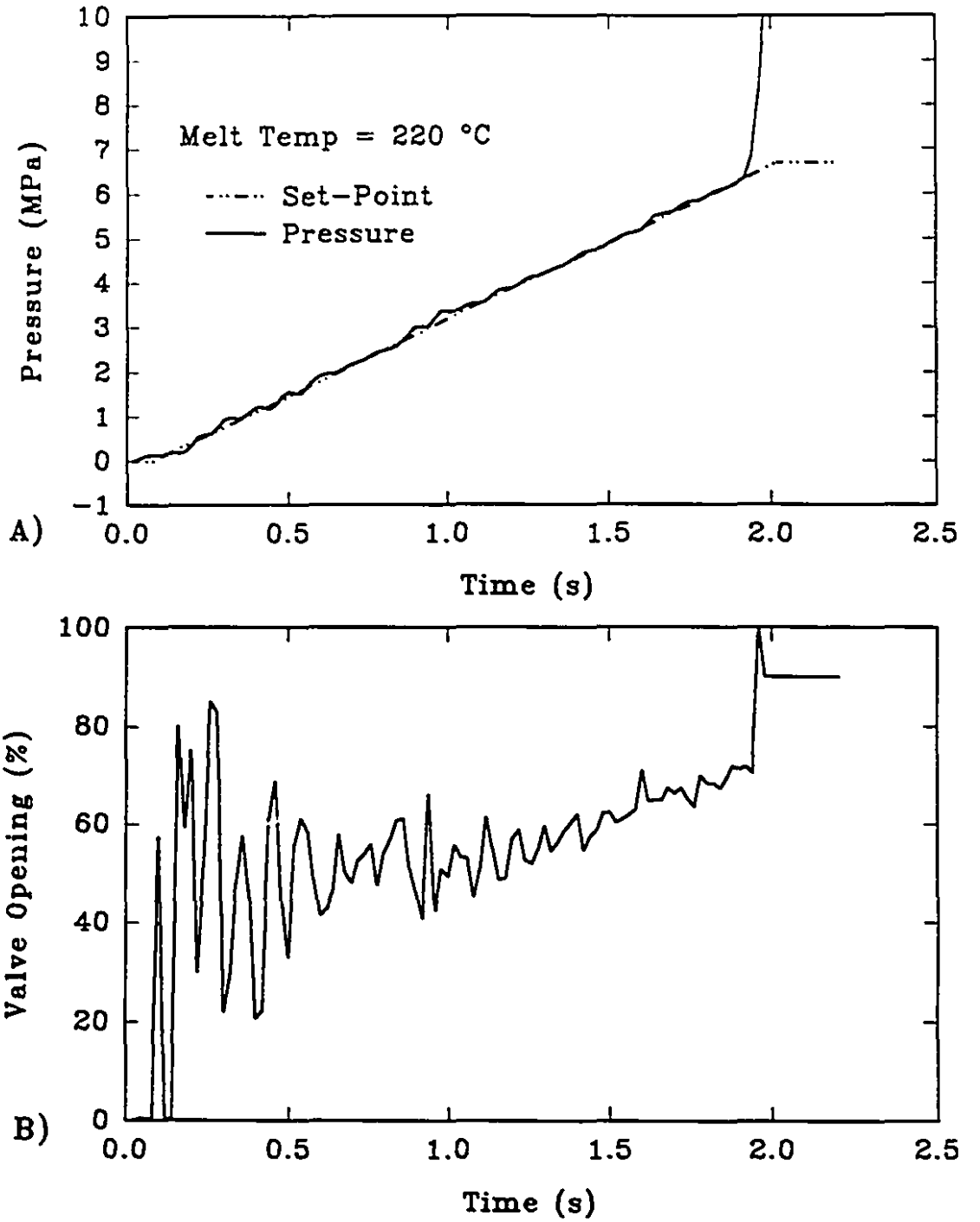

Figure 5.17 Experimental cavity pressure response of the STR control to a constant ramp set-point profile, using a forgetting factor of 0.75, and a melt temperature of 220 °C (A), and the corresponding servo-valve change (B)

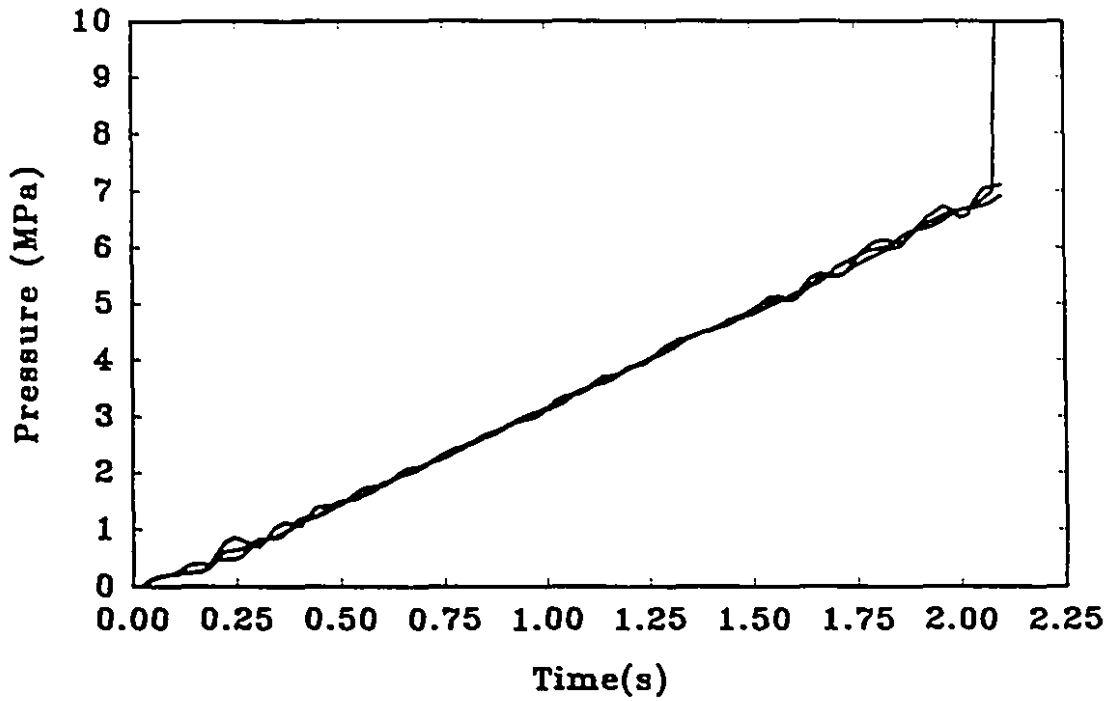

Figure 5.18 Cavity pressure responses of three different cycles with the STR control

One further experiment was carried out to test the tracking ability of the control system. Figure 5.19 shows the response of the cavity pressure to the set-point profile changes. The set-point, originally a ramp of 3.45 MPa/s (500 psi/s), becomes a 2.76 MPa/s (400 psi/s) ramp at a time shortly after t = 1s. This demonstrates that the controller can force the gate pressure to follow the set-point closely within the machine limitations. If, on the other hand, a ramp of 3.45 MPa/s (500 psi/s) were changed to one of 6.2 MPa/s (900 psi/s), this profile would not be followed, since there is insufficient hydraulic pressure available.

The above experiments indicate that the self-tuning controller can force the cavity pressure to follow any reasonable set-point profile. The reasonable profile is dependent on the machine and the cavity geometry. The profile can be determined by a few open-loop experiments. Figure 5.20 gives the open-loop cavity pressure responses to different constant servo-valve openings. It is obvious that different valve openings produce different profiles. The sudden pressure increases at about 1.25, 1.5 and 3.5 seconds indicate the beginning of the packing stage for each different opening. In Figure 5.20, the solid line gives the maximum rate of filling profile. Conversely, the dot-dashed line represents a filling profile with 12 % valve opening, where a short shot occurs. The dotted line represents a filling profile with 15 % opening which is just sufficient to prevent a short shot. Therefore, for this particular machine, cavity, and material, any filling profile between the solid line and the dotted line is a reasonable filling profile. However, the best filling profile depends on the cavity shape, the required production rate, and the desired molded part properties.

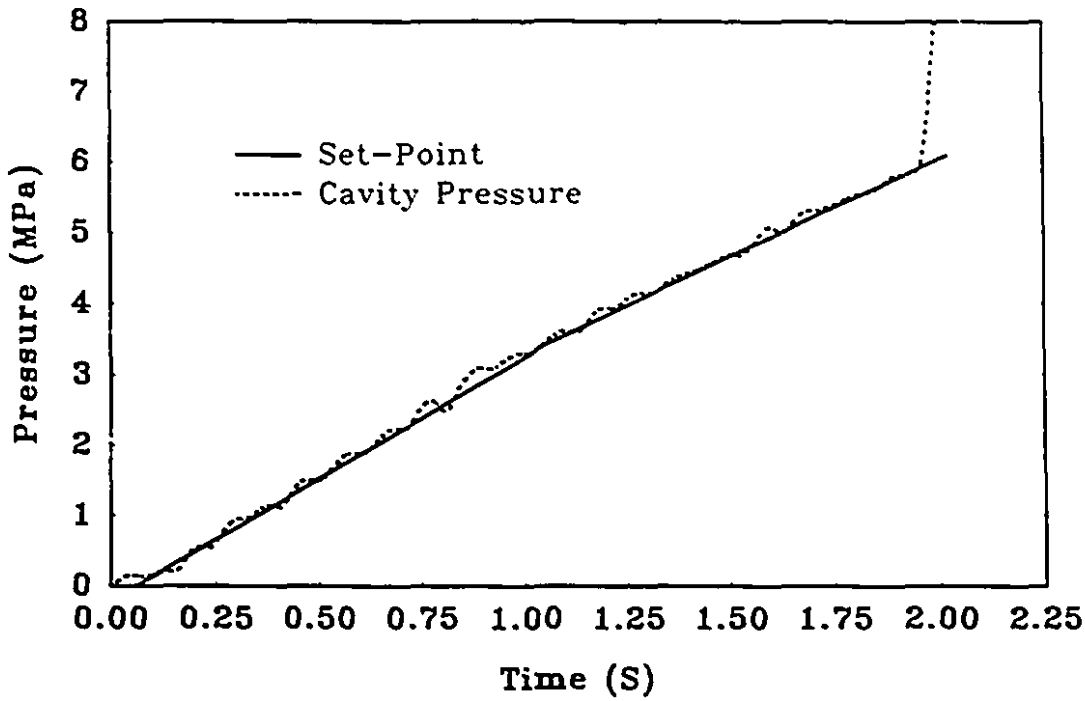

Figure 5.19 Cavity pressure STR control responses to a set-point profile change from a ramp of 3.45 MPa/s (500psi/s) to a ramp of 2.76 MPa/s (400psi/s)

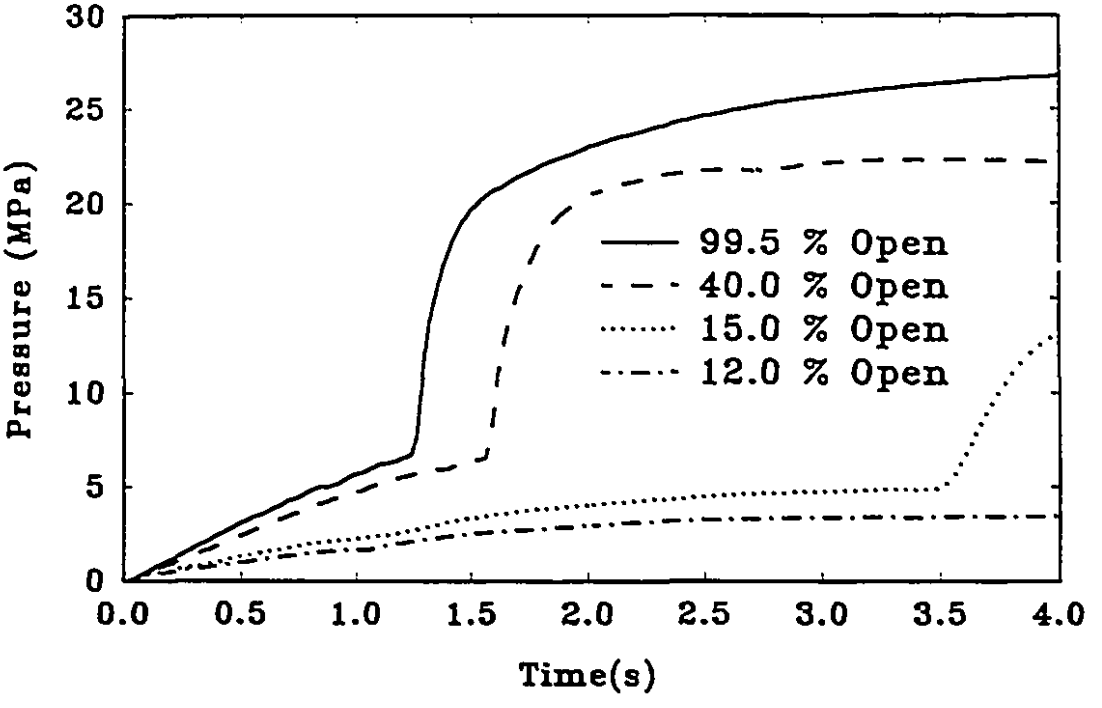

Figure 5.20 Open-loop responses of cavity pressure to different fixed servo-valve openings

It is important to point out that both the maximum and minimum filling profiles are also dependent on the resin and mold temperature.

The final experiment tested the adaptiveness of the controller. The simple fan-gate rectangular cavity was replaced with a three dimensional complex cavity as shown in Figure 5.21. The cavity has an insert, a variable cross-section and two step changes in thickness. The objective of the controller is to force the cavity pressure to follow a constant ramp set-point profile despite the complex geometry of the cavity. The variations in the cavity geometry imply that the pressure at the gate (cavity entrance) will vary considerably as the advancing melt encounters rapid changes in the cavity cross-sectional areas. The experiment, however, was carried out with no modification to the controller. Figure 5.22 shows the response of the controlled variable and indicates that it follows the set-point closely even though the cavity geometry changes considerably. The slightly larger deviation between 0.75s and 1.4 s is attributed to the effect of the insert, to the step change in thickness, and to the large change in width of the molded part in the middle cavity. The controlled variable follows the set-point profile very closely, in zones I and III, where the geometrical changes are not as great as in zone II. In spite of the large dimensional variability of the mold, the controller successfully tracks the very demanding set-point profile with an acceptable error. It would not be possible to achieve such results with a fixed gain controller. A more reasonable (i.e. harmonious with machine response and capabilities) set-point profile would make the deviation even smaller.

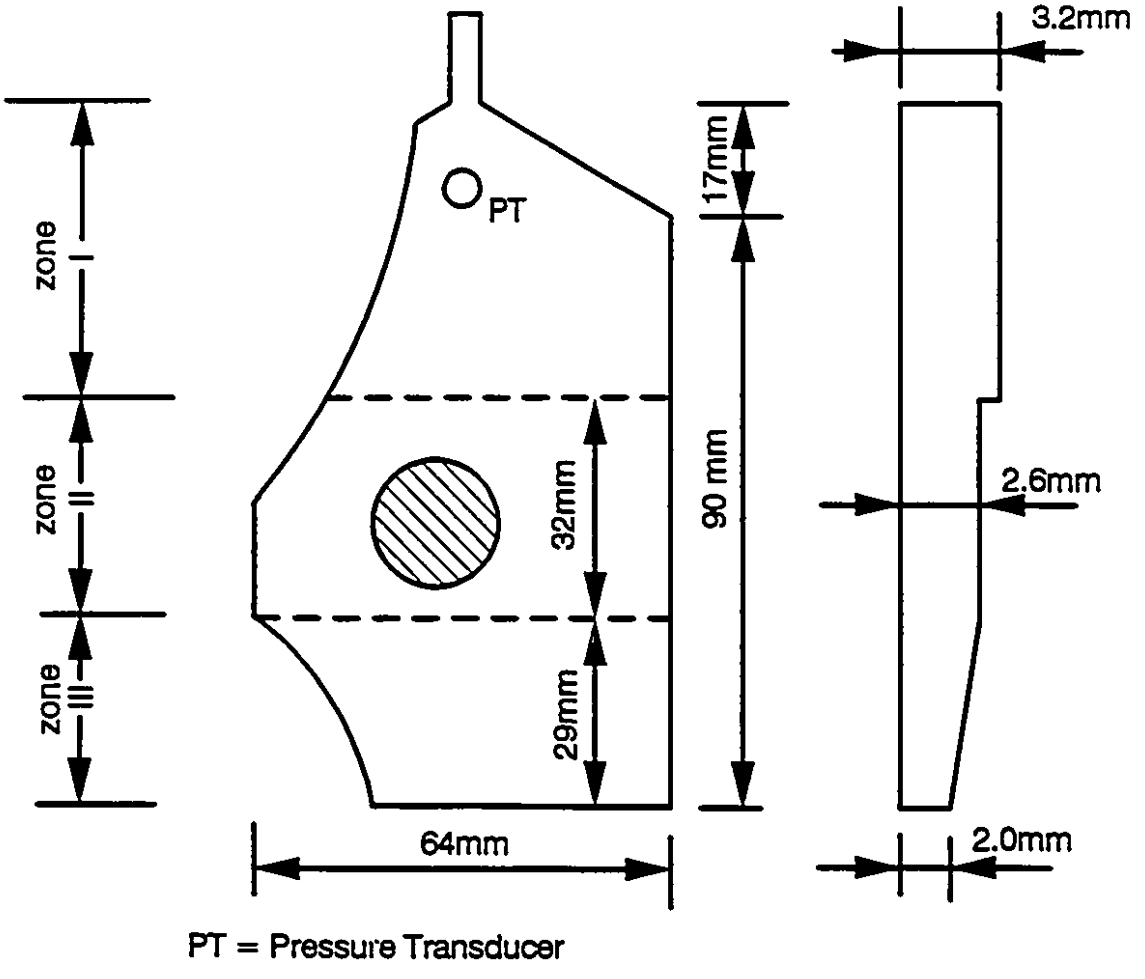

Figure 5.21 Schematic of the complex cavity and the location of pressure transducer

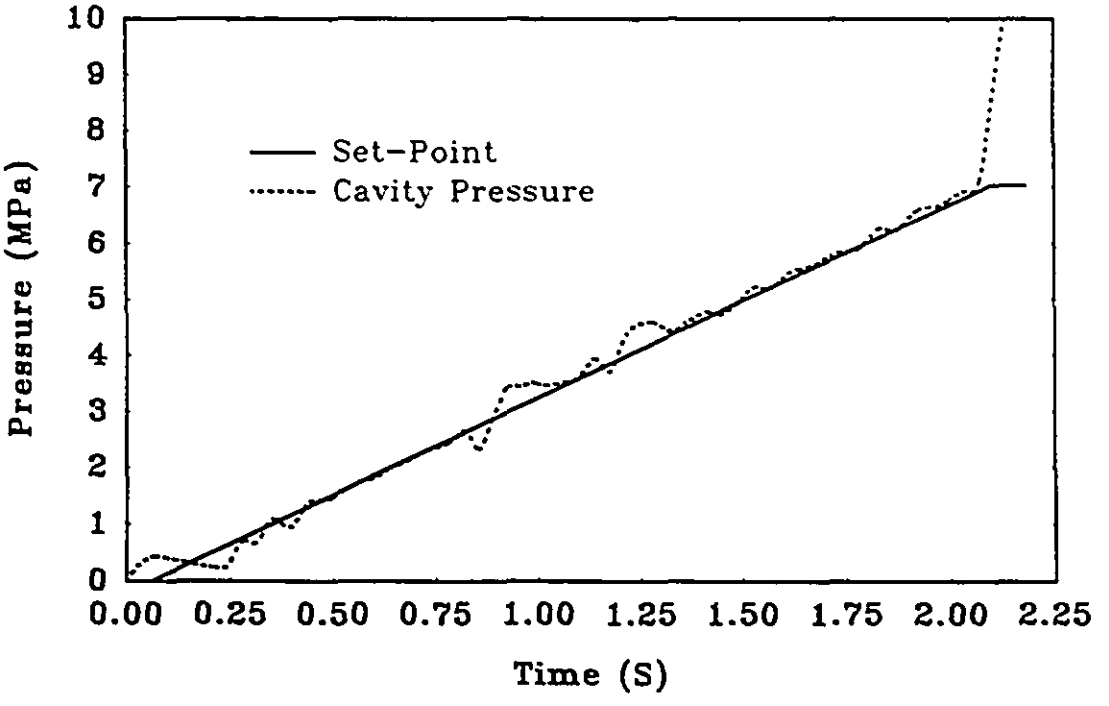

Figure 5.22 Cavity pressure in tracking a constant ramp set-point profile of 4.45 MPa/s (500psi/s), when the cavity has a complex geometry as shown in Figure 5.21

5.5.4 Summary

The nonlinear and time-varying nature of the cavity pressure in injection molding has been presented and modelled parametrically. A self-tuning controller has been designed, implemented and tested for a wide range of operating conditions. It was found that, because of the rapidly varying nature of the process dynamics, a low value of the forgetting factor ($\lambda = 0.75$) was required for the self-tuning regulator to function in an acceptable manner. This value of λ is considerably lower than those suggested previously for this class of controller.

The self-tuning controller, with $\lambda = 0.75$, has been demonstrated to possess good tracking and regulating abilities over a range of operating conditions, using different mold cavities, without further adjustment.

5.6 Detection of the Filling-to-Packing Transition

When the molten resin completely fills the cavity, the cavity and nozzle pressures increase suddenly, and the cavity pressure profile during the packing phase is different from the pressure profile during the filling phase. Therefore, it is necessary to shift from filling cavity pressure profile control to packing pressure profile control at this point. Researchers have pointed out that a correct detection of filling-to-packing transition is important to the proper control of cavity pressure during packing [1, 53].

The determination of the filling-to-packing transition can be based on one or more of the following criteria.

- Cavity filling time
- Screw displacement
- Screw velocity
- Cavity Pressure (P_c)
- Nozzle pressure (P_N)
- Nozzle pressure derivative (dP_N/dt)
- Cavity Pressure derivative (dP_c/dt)

The first three criteria are essentially based on the melt volume in the cavity. The following relations exist for these variables:

$$v_c = c\int_0^t V_s dt \tag{5.38}$$

$$X = \int_0^t V_s dt \tag{5.39}$$

where v_c is the melt accumulated in the cavity,

V_s is the screw velocity,

X is the screw displacement, and

c is the filling constant.

If the melt density is known, the exact screw velocity-time relationship is measured, and the volumetric changes caused by temperature and pressure variations are neglected, then it is possible to predict when the packing will start for a given cavity volume. However, these assumptions are usually not realistic. Therefore, cavity filling time is not a good criterion.

Based on Figure 5.5, it is obvious that cavity pressure, nozzle pressure, screw displacement and screw velocity all experience a dramatic change when packing starts. They all seem to be good candidates. However, from Figure 5.20, cavity pressure cannot be directly used for the detection of filling-to-packing transition, because different injection rates are associated with different cavity pressure values at the transition point. Neither can nozzle pressure and screw displacement be used as the transition point detection criteria, since different machine and cavity geometries have different values for the transition point. From Figures 5.5 and 5.20, the screw velocity, and cavity and nozzle pressure values change gradually during the filling stage, but start to increase dramatically at the beginning of packing. Figure 5.23 shows the derivatives of the nozzle and cavity pressures together with the screw

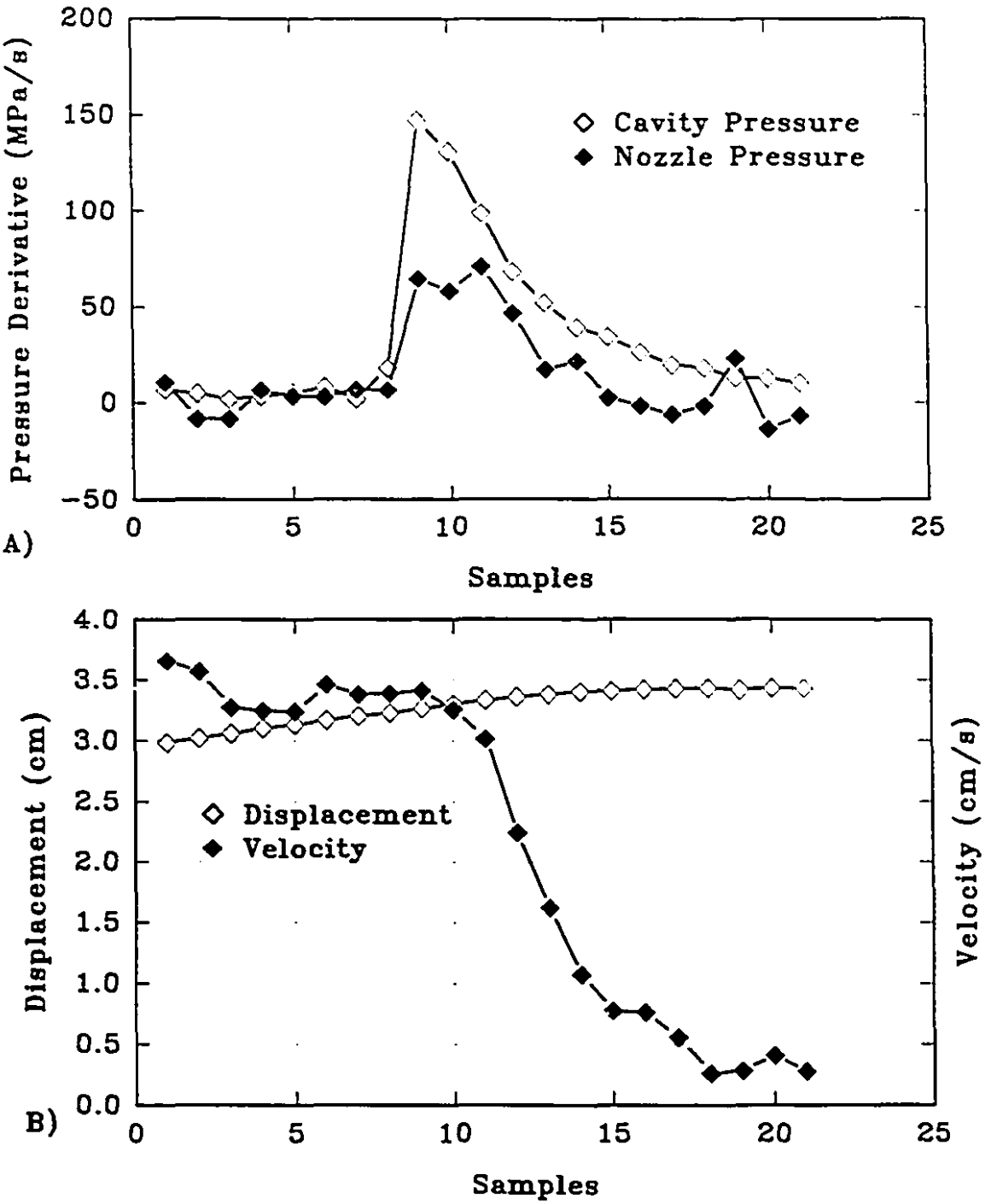

Figure 5.23 Cavity and nozzle pressure derivatives (A), screw and displacement (B) around the filling-to-packing transition, sampling period is 0.02s

displacement and velocity just before and during the transition. The screw velocity lags behind the pressure derivatives in indicating the transition point. This is possibly due to the screw inertia. Furthermore, use of the screw velocity as the detection measurement would require a velocity sensor. Therefore, the change in screw velocity is not a good candidate. The nozzle and cavity pressure derivatives, as shown in Figure 4.23A, both appear to be good candidates. The nozzle pressure derivative was not selected for the following reasons: (i) the signal amplitude and the signal-to-noise ratio of the cavity pressure derivative are greater than those of the nozzle pressure derivative, (ii) the use of the nozzle pressure derivative to detect the transition for cavity pressure control would require an additional pressure transducer. Therefore, the cavity pressure derivative was selected as the best candidate to detect the filling-to-packing transition, and was used for pressure control during packing in this research.

5.7 Cavity Pressure Dynamics and Control during Packing

5.7.1 Packing Profile

The packing pressure profiles in Figure 5.20 suggest that a sum of exponentials would be a good fit:

$$P_c = c_1(1-\exp(-T/\tau_1))+c_2(1-\exp(-T/\tau_2)) \tag{5.40}$$

where P_c is the cavity pressure,

T is the sampling time,

τ_1 and τ_2 are the time constants of the pressure, which indicate how fast the pressure rises, and

c_1 and c_2 are fitting coefficients.

Figure 5.24 shows a good agreement between the pressure with a constant servo-valve opening of 40 percent and the least squares fit to Equation (5.40). Both curves in the figure are normalized by subtracting the pressure at the end of filling. The coefficients of the fitted Equation (5.40) are given in Table 5.2.

From Table 5.2, it is obvious that the first term of Equation (5.40) dominates the packing process. For simplicity, the second term is suppressed and the packing pressure profile is selected to be of the following:

$$P_c = p_{FE}+(p_{PE}-p_{FE}) \cdot (1-\exp(-T/10)) \tag{5.41}$$

where p_{PE} and p_{FE} are the pressure values at the end of packing and filling, respectively, T is the number of samples after the packing starts, and 10 ($\approx$ 9.3) is the time constant of the packing pressure profile in the units of sampling period. The

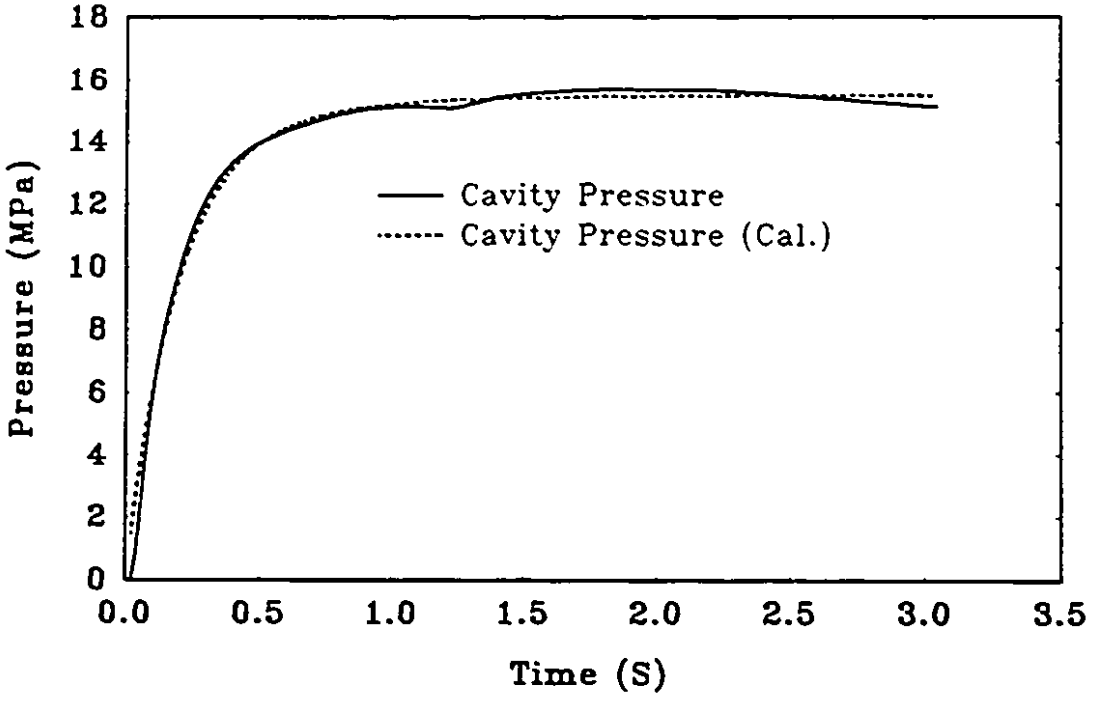

Figure 5.24 A comparison between measured and calculated cavity pressures based on Equation 5.40

Table 5.2 Parameters of the fitted packing pressure profile

Coefficients	Value
c_1	2044.8 (psi)
c_2	204.8 (psi)
τ_1	9.3 sampling periods (0.186 s)
τ_2	28.5 sampling periods (0.59 s)

pressure at the end of packing, p_{PE}, is independently specified. Equation (5.41) gives a reasonable packing pressure profile (close to the open-loop pressure profile). However, specification of a "good pressure profile" is dependent on the machine settings, cavity geometries, and material. Due to the time and space limitations of the thesis, it is beyond the scope of this investigation to provide a procedure for the identification of a "good pressure profile". The set-point pressure profiles employed here are considered to be reasonable profiles on the basis of experimental observations.

5.7.2 Packing Dynamics

Similar to the procedures employed in the filling dynamic investigation, a series of step changes of servo-valve opening was introduced, and the cavity pressure response was recorded. The valve opening changes and the pressure responses for both the filling and packing stages are shown in Figures 5.25A and 5.25B, respectively. With respect to machine operation, there is little difference between the

filling and packing stages, except that rate of the polymer entering the injection cavity is reduced as packing proceeds. Therefore, the same model structure as that employed for the filling stage is employed in the packing stage for simplicity. The recursive system identification method used for the filling stage is extended into the packing stage. The estimated model parameters with forgetting factor of 0.95 are presented in Figure 5.25C. The results between 0 and 2 seconds have been discussed in the filling stage section. The packing starts about two seconds after the start of filling. It is obvious that packing dynamics are different from those of the filling and change considerably in the first second.

In the filling stage, the forgetting factor of 0.75 was found to best estimate the dynamic model and to provide good control. Figure 5.26 gives the dynamic model estimated with a forgetting factor of 0.75 for both the filling and packing stages. The top graph gives the measured cavity pressure and the calculated pressure based on the estimated model. The bottom graph gives the corresponding model parameter changes. It is obvious that the estimated model parameters change considerably. This is because of the non-linearity of the process and because of the servo-valve opening changes between 20 and 80 percent (shown in Figure 5.25A). The trend of the model parameters are similar to Figure 5.25C, except that they change faster. This is expected because the forgetting factor is much smaller. The dynamic model parameters do not vary much after about one second from the start of packing. The quick variation is due to the non-linearity caused by servo-valve opening changes.

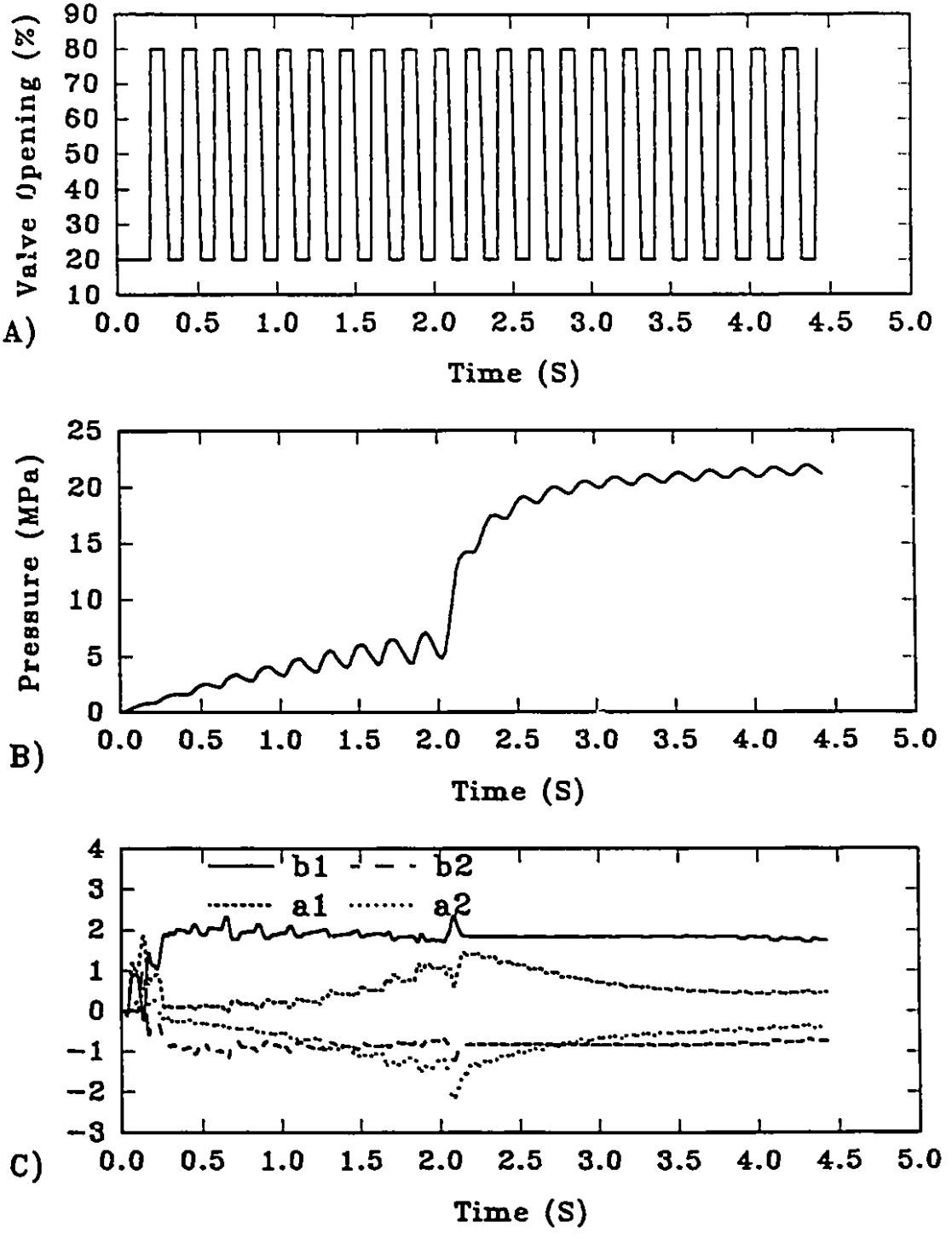

Figure 5.25 Servo-valve opening changes 20 to 80 % (A), the cavity pressure responses (B), and the estimated process model parameters with a forgetting factor of 0.95

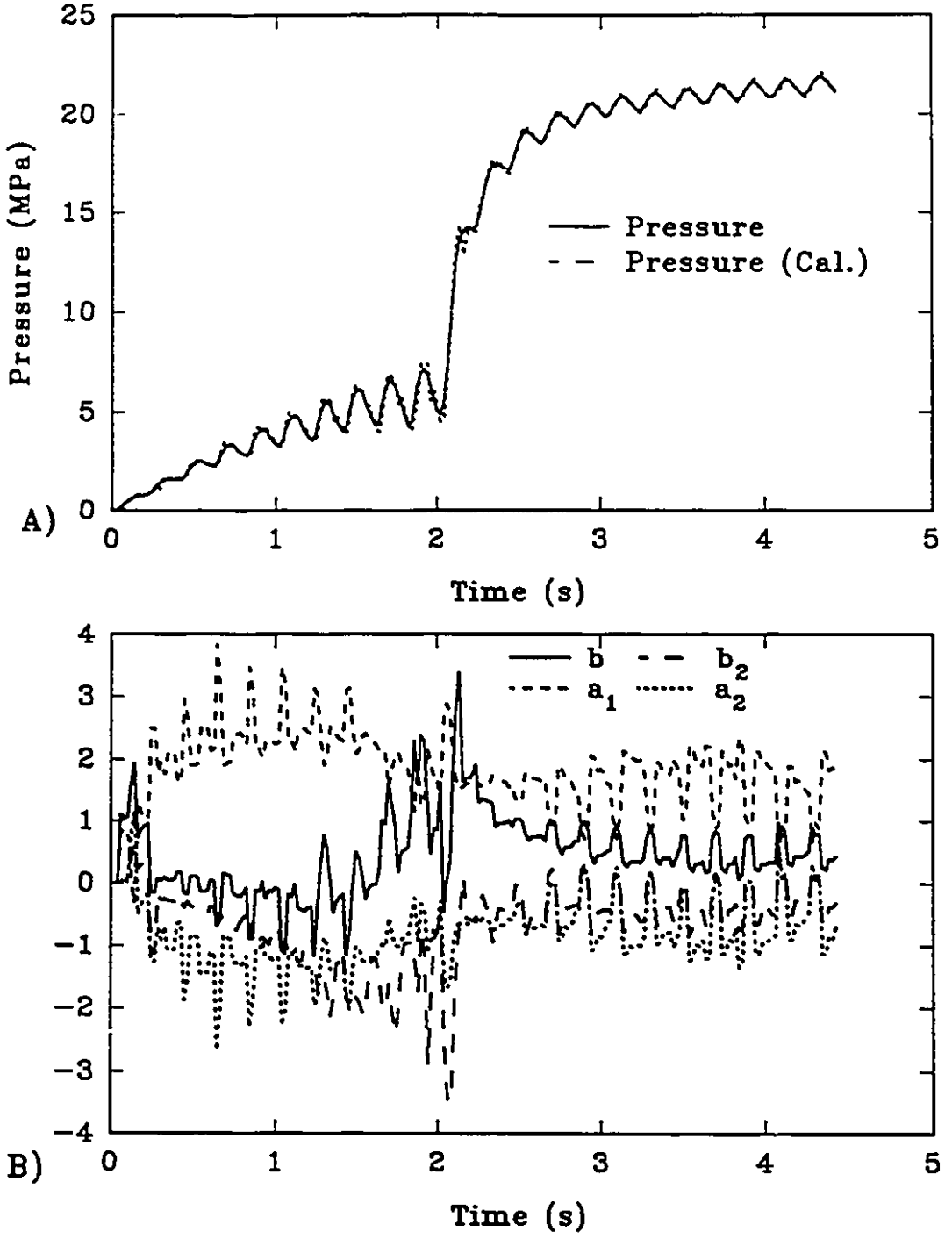

Figure 5.26 Cavity pressure and calculated value based on the estimated model (A), and the on-line estimated process model parameter changes (B) with a forgetting factor of 0.75

5.7.3 Packing Pressure Control

The self-tuning control for the filling stage is extended into the packing stage, except that the set-point profile is changed to Equation (5.41) from a constant ramp after the packing start is detected. The detection of filling-to-packing transition is based on the derivative value of the cavity pressure, a threshold of 8.61 MPa/s (1250 psi/s) of the cavity pressure derivative is used to trigger the switch to the packing profile. The p_{FE} of the packing profile equation is the cavity pressure measured at the moment when the packing start is detected. p_{PE} is set to 20.7 MPa (3000 psi). The forgetting factor of 0.75 found to be the best for the filling stage was also used for the entire packing stage.

Figure 5.27 gives the experimental closed-loop self-tuning control results. In the top graph, the dot-dot-dash line is the set-point profile, and the solid line is the cavity pressure response. The cavity pressure is very close to the set-point profile for both the filling and packing stages. The corresponding servo-valve opening is given in Figure 5.27B. The servo-valve opening for the filling stage has been discussed previously. The valve opening variation during packing is large possibly because the dynamic pressure information to the recursive identification and the process gain become relatively small after the process enters the packing stage. This problem can be remedied by either increasing the forgetting factor or using a filter to increase the signal to noise ratio.

A first order digital filter was added to the measured cavity pressure after the detection of the start of the packing stage. The filter is expressed as follows:

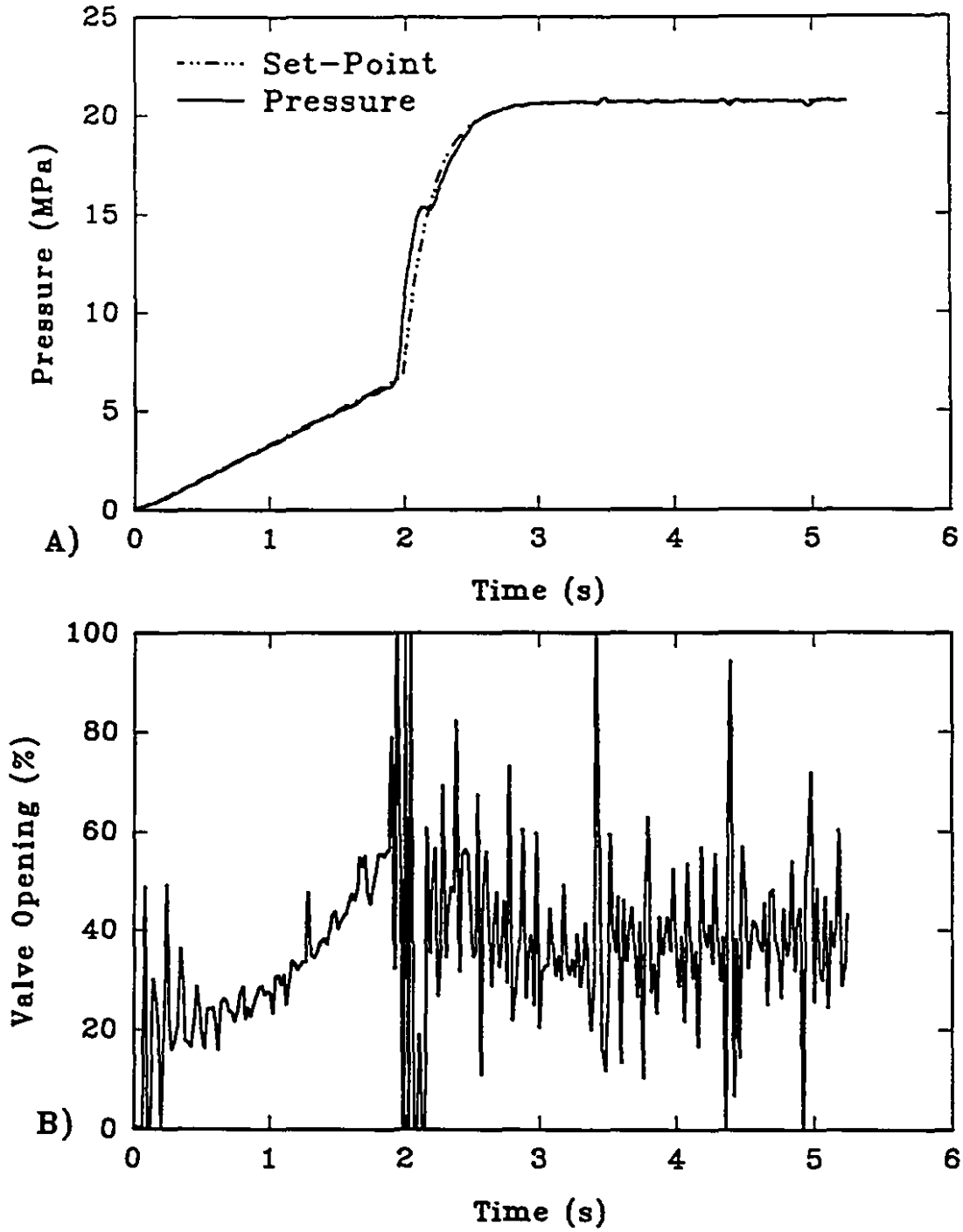

Figure 5.27 Experimental cavity pressure STR control with a forgetting factor of 0.75, pressure responses (A), and the corresponding servo-valve changes (B)

$$P_{cf}(n) = 0.4 \times P_{cf}(n-1) + 0.6 \times P_c(n) \qquad (5.42)$$

Where P_{cf} is the filtered cavity pressure measurement,

P_c is the cavity pressure measurement,

n is the nth sample.

A second experiment was carried out with the input filtered as in Equation (5.42), and with the same set-point profile and other conditions. The self-tuning closed-loop control results are shown in Figure 5.28. As previously, the set-point and the cavity pressure measurement are shown in Figure 5.28A. Figure 5.28B indicates the corresponding servo-valve opening. In comparison to Figure 5.27, the servo-valve opening variation becomes less frequent. However, it seems that the strength is about the same as the previous experiment during the packing stage.

As shown in Figures 5.25 and 5.26, the dynamic model parameters do not change much after one second following the start of packing. Therefore, to increase the robustness of the identification, a larger forgetting factor could be used one second after packing starts. Figure 5.29 shows how the forgetting factor changes during the filling and packing stages. Segment II lasts 45 samples (0.9 second) after packing starts. The forgetting factor (λ) for segments I and II is 0.75, and then it is changed to 0.975 for segment III. The dynamic model parameters for the last 10 samples in segment II are averaged as the initial condition for segment III. The implementation procedure of the self-tuning closed-loop control using the segmented forgetting factor and input filtering is illustrated in Figure 5.30.

Experiments (P1 - P5) were carried out to test the regulating and tracking

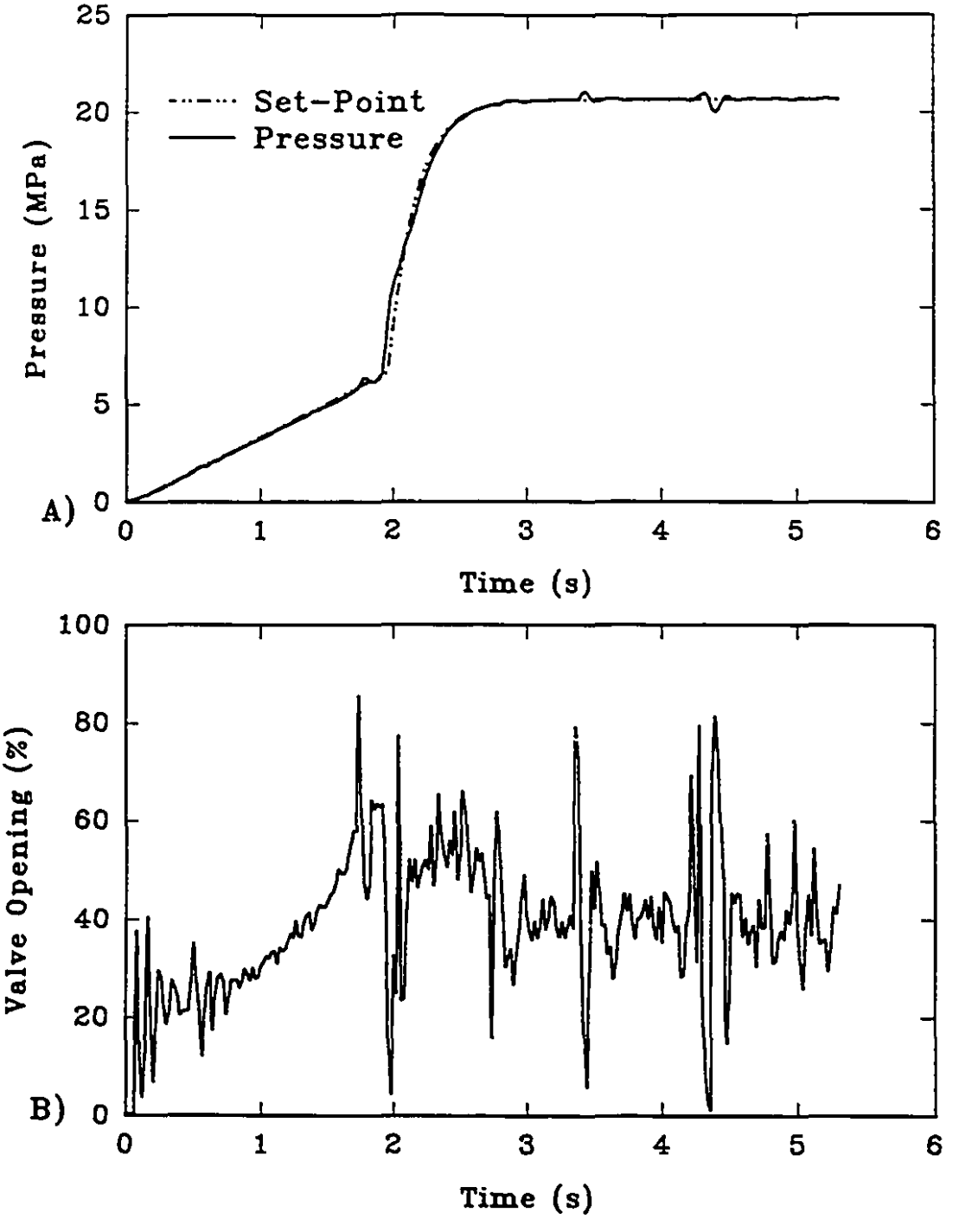

Figure 5.28 Experimental cavity pressure STR control with a forgetting factor of 0.75 and filtered input, cavity pressure response (A), and the corresponding servo-valve opening changes (B)

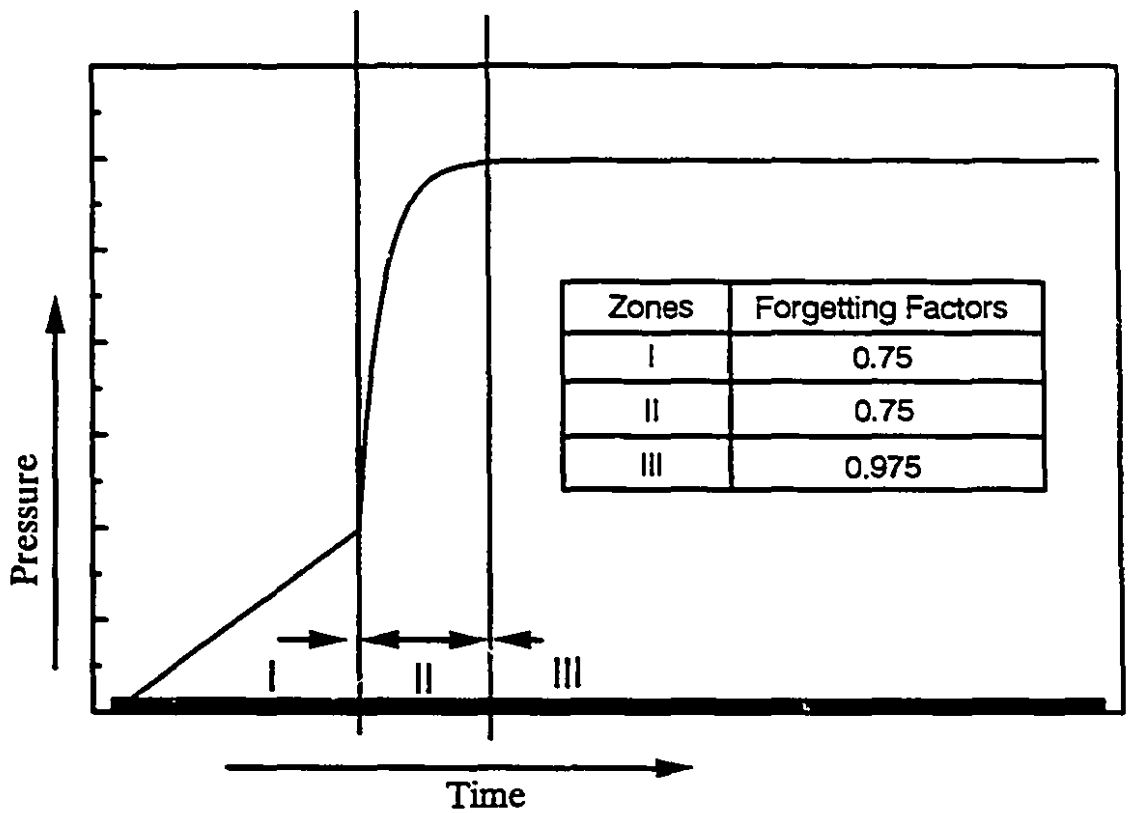

Figure 5.29 Cavity pressure and STR control forgetting factor zones

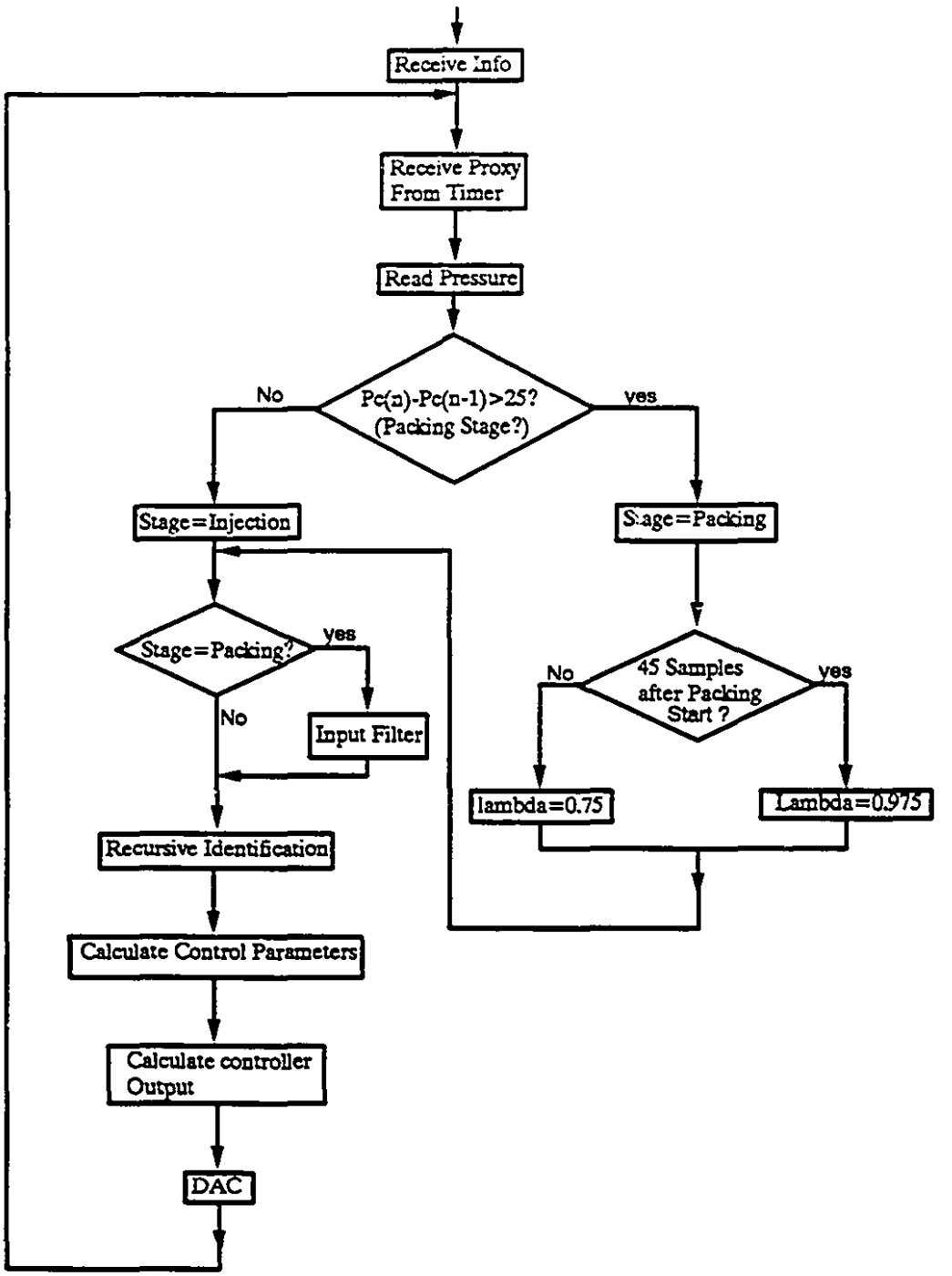

Figure 5.30 Cavity pressure STR control implementation for both filling and packing phases

capabilities of the controller. The self-tuning control system used the same forgetting factor and filter for these experiments. Changes in the melt temperatures, final packing pressure p_{PE} and the profile after about 1.5 seconds of packing were made. Table 5.3 gives the differences in the experimental conditions among experiments P1 - P5.

Experiment P1 was carried out with the forgetting factor changes as described above with all other conditions unchanged. Figure 5.31 gives the experimental results. The set-point and cavity pressure responses are represented with the dot-dot-dash line and solid line, respectively, in the top graph. The bottom graph gives the corresponding servo-valve opening. The cavity pressure follows the set-point, but the servo-valve opening change is considerably smaller compared with Figures 5.27 and 5.28.

Experiment (P2) was carried out with the same set-point profile as the previous experiment (P1), except that the melt temperature was changed to 205 °C. The results are shown in Figure 5.32. The cavity pressure follows the set-point profile closely, and the corresponding valve movement is also acceptable. This indicates that the controller performed well despite changes in the machine operating conditions.

Experiment P3 was carried out with the same conditions as in experiment P1, except that the final packing pressure was 19.0 MPa (2750 psi). The experimental results are shown in Figure 5.33. Again, the cavity pressure follows the set-point profile with very small error, and the corresponding valve opening change is also acceptable.

Table 5.3 Experimental conditions: P1 to P5

Experiment	Melt Temperature	Set-Point
P1	220°C	3000PSI
P2	205°C	3000PSI
P3	220°C	2750PSI
P4	220°C	Ramp change
P5	220°C	Step change

Experiment P4 was carried out with the same conditions as in experiment P1, except that the set-point was decreased at a rate of 1.72 MPa/s (250 psi/s) after the packing started about 1.5 seconds. The corresponding cavity pressure responses and valve-opening changes are both shown in the same Figure 5.34. Again, the controller produced excellent results.

Experiment P5 has in the set-point profile a step change. The corresponding cavity pressure and servo-valve opening are as shown in Figure 5.35. Once again, the self-tuning control system can follow the set-point without any problem.

5.7.3 Summary

In this section, the dynamics of the packing pressure in relation to the servo-valve opening was determined. Subsequently, the self-tuning control system for the filling stage was successfully extended into the packing stage.

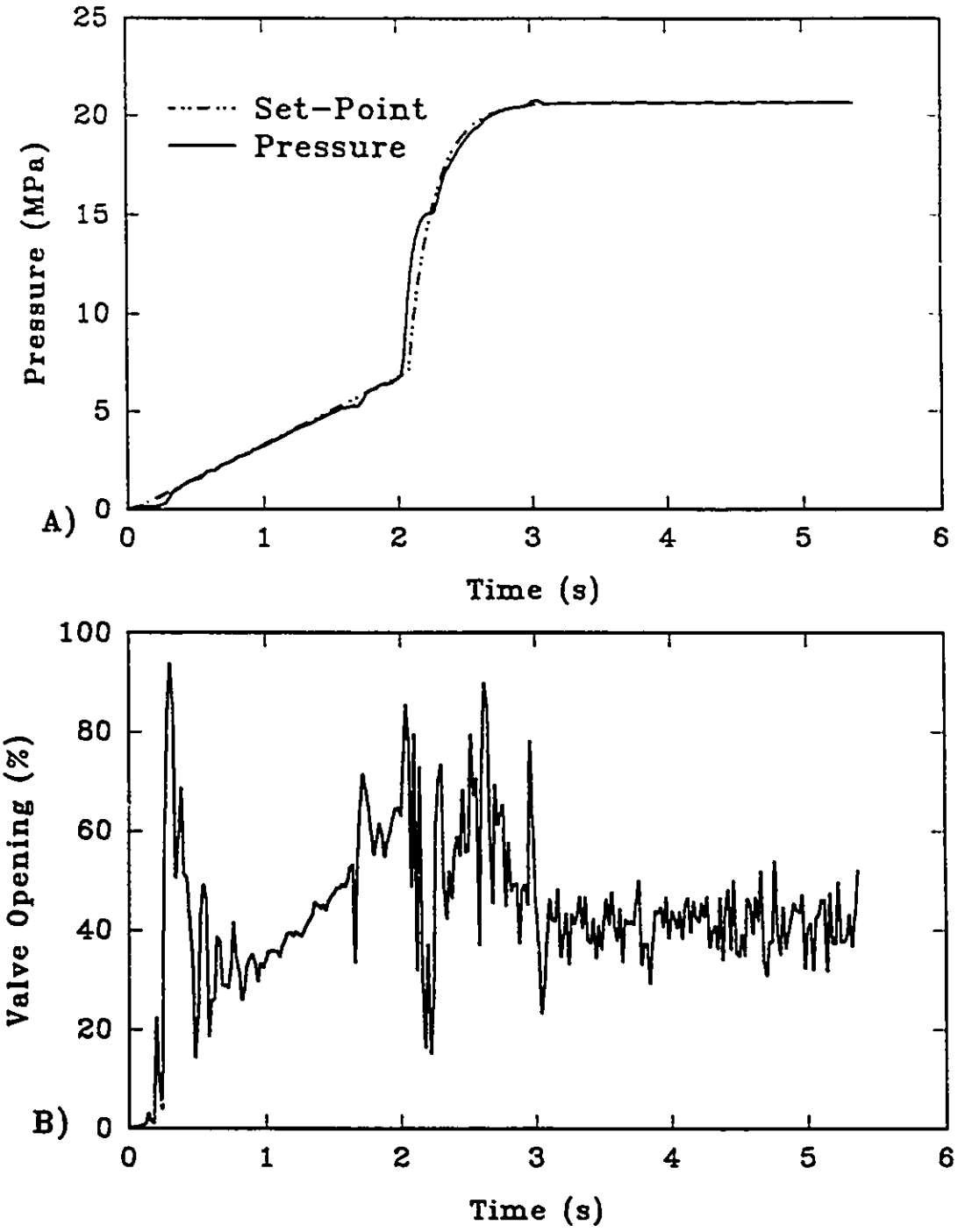

Figure 5.31 Cavity pressure STR control responses with a zoned forgetting factor (A), and the corresponding servo-valve changes (B)

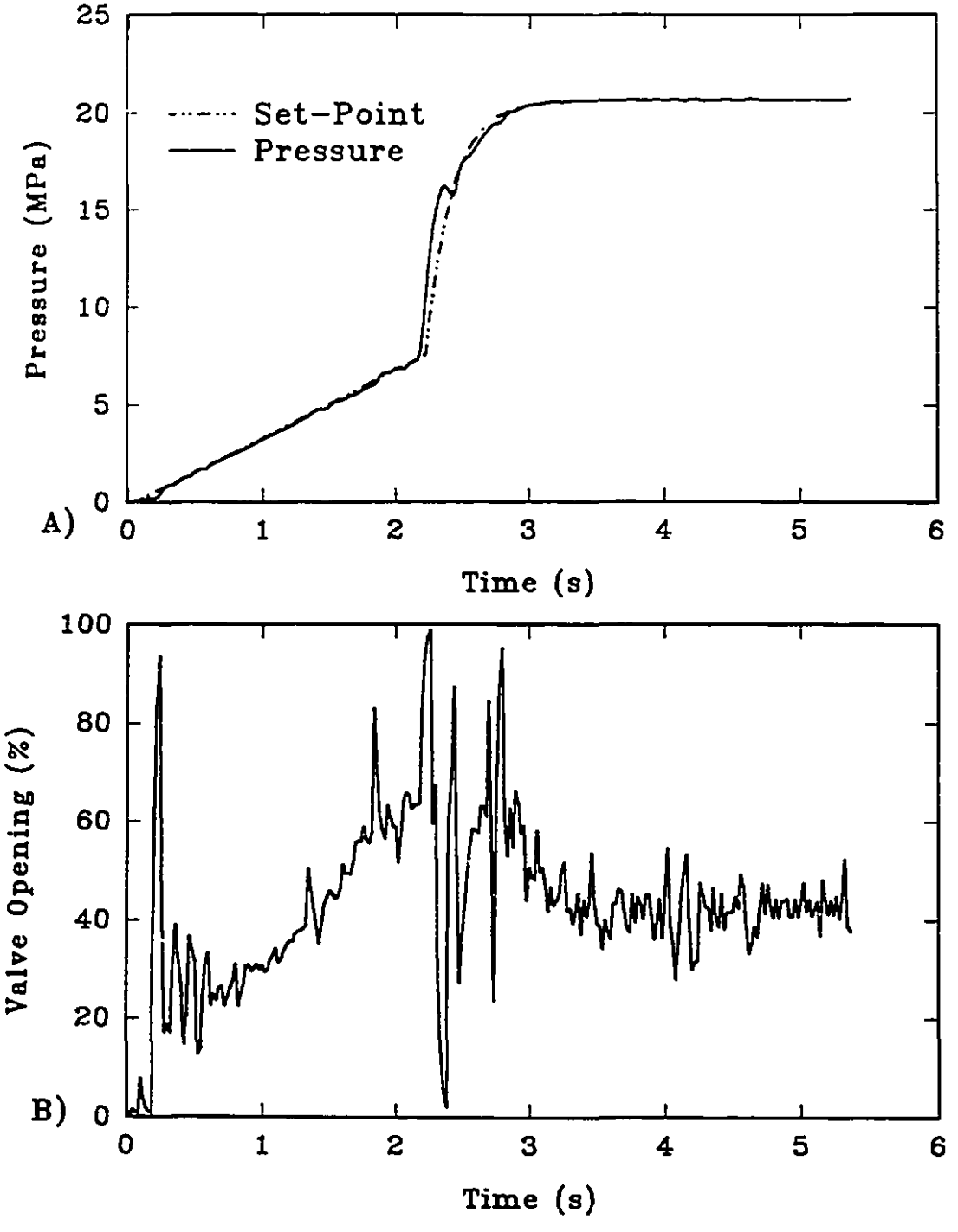

Figure 5.32 Cavity pressure STR control responses with conditions stated as P2 in Table 5.2 (A), and the corresponding servo-valve changes (B)

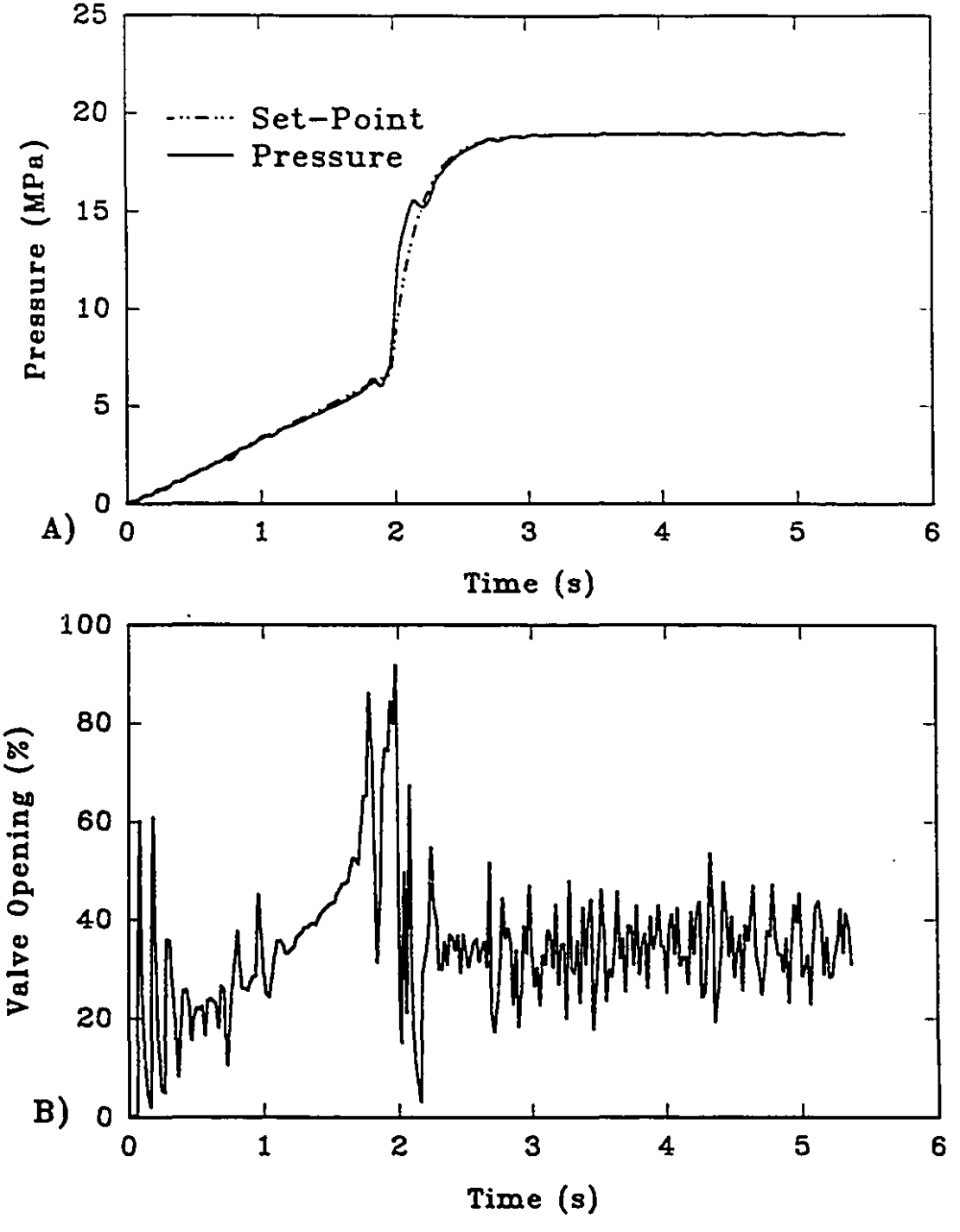

Figure 5.33 Cavity pressure STR control responses with conditions stated in P3 Table 5.2 (A), and the corresponding servo-valve openings (B)

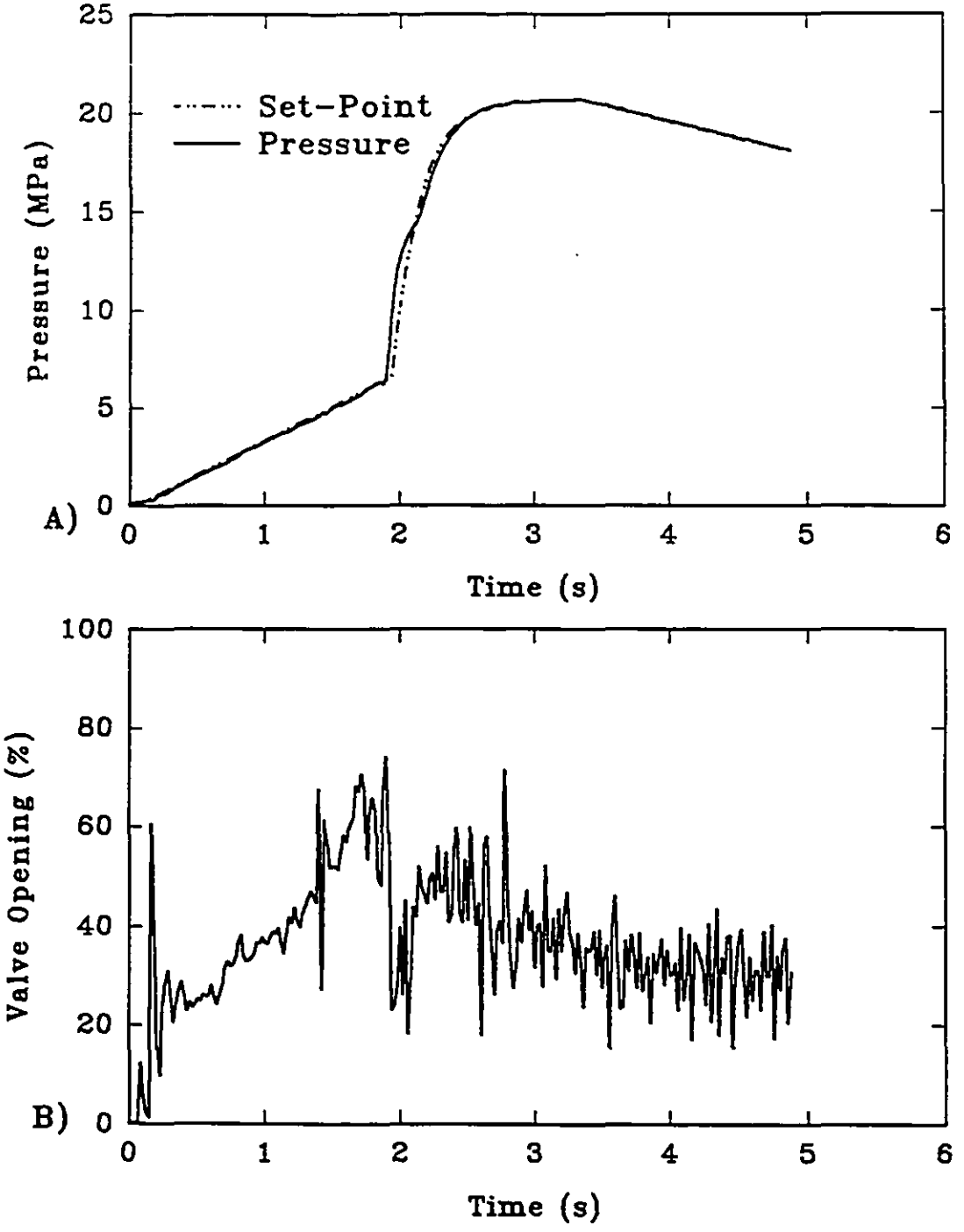

Figure 5.34 Cavity pressure STR control responses with the conditions stated as P4 in Table 5.2 (A), and the corresponding servo-valve opening changes (B)

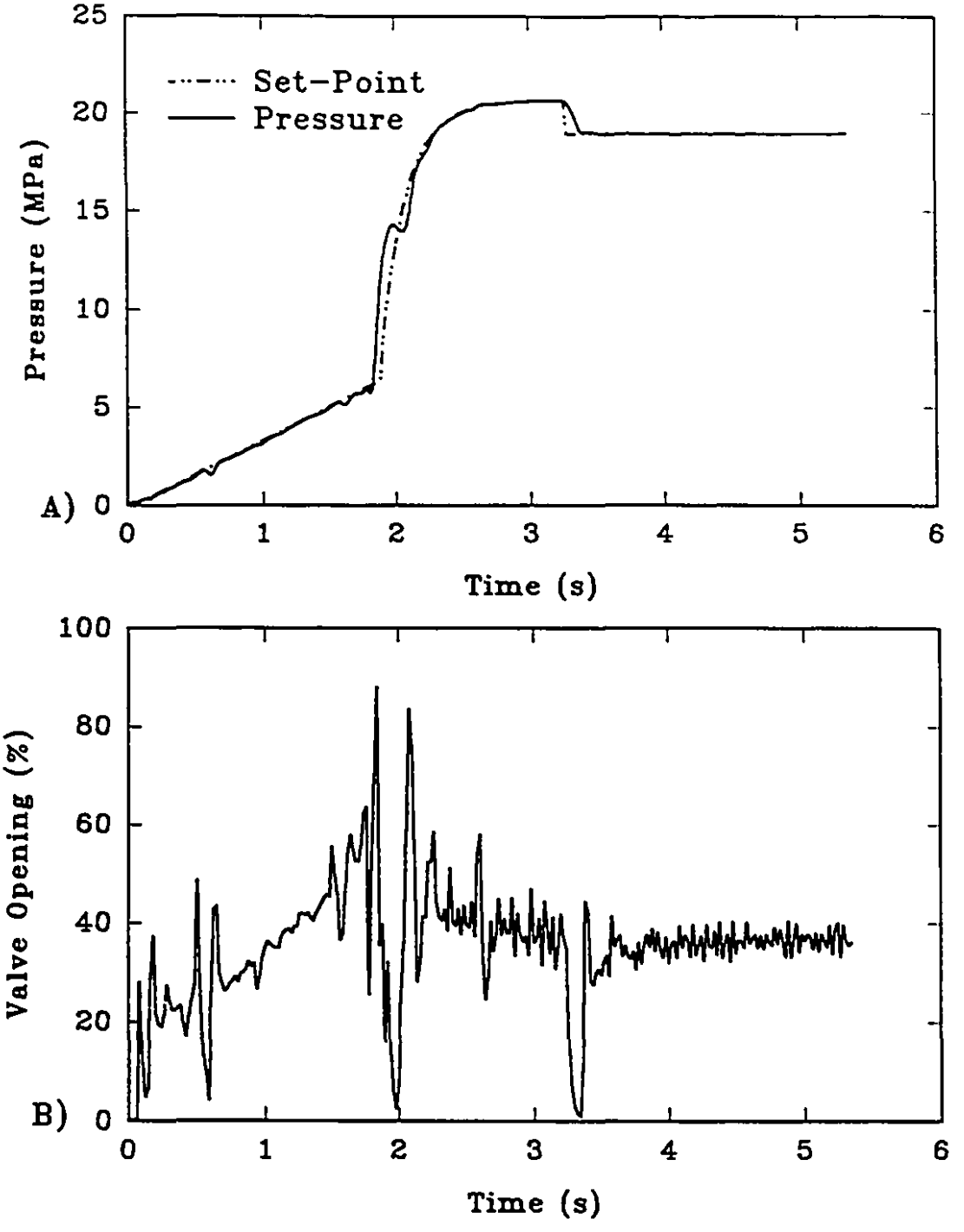

Figure 5.35 Cavity pressure STR control responses with the conditions stated as P5 in Table 5.2 (A), and the corresponding servo-valve changes (B)

5.8 Conclusions

The time varying model dynamics of cavity pressure were determined and analyzed for both the filling and packing phases. A self-tuning regulator control system was designed and tested for cavity pressure. The cavity pressure derivative was chosen to detect the filling-to-packing transition. The same control law was used to control pressure in both filling and packing phases.

Chapter 6

DYNAMICS AND CONTROL OF CAVITY PRESSURE DURING COOLING

6.1 Introduction

This chapter deals with the analysis of the process dynamics and control of cavity pressure during the cooling stage. Section 6.2 describes the cooling system, and studies the dynamics and control of mold coolant temperature. The dynamics and control of cavity pressure during the cooling stage are described in Section 6.3. Finally, a brief summary of this chapter is given in Section 6.4.

6.2 System Set-Up, Dynamics and Control for Cooling System

6.2.1 Cooling System

A mixing system was designed as shown in Figure 6.1 to control the mold coolant temperature and flowrate. There are three thermocouples (type E) installed in the cooling system to measure the cold water, hot water and mixed water temperatures. They are represented by the symbol TT in Figure 5.2. A paddle wheel flowmeter (SIGNET 3-8500) [115 - 116] was installed to measure the flowrate into the injection mold. Manual valves 1 and 2, installed in the hot and cold water sides, adjust the maximum flow rates. Manual valve 3 in the side branch is usually shut. It can be opened to provide cooling water to the injection mold, when the cooling system requires maintenance. There is a control valve installed on both the cold and the hot water supplies. These control valves (Fisher Control Valve Type 1 2-B-EQ. PCT) [114]) have equal percentage trim and are pneumatically operated. The control

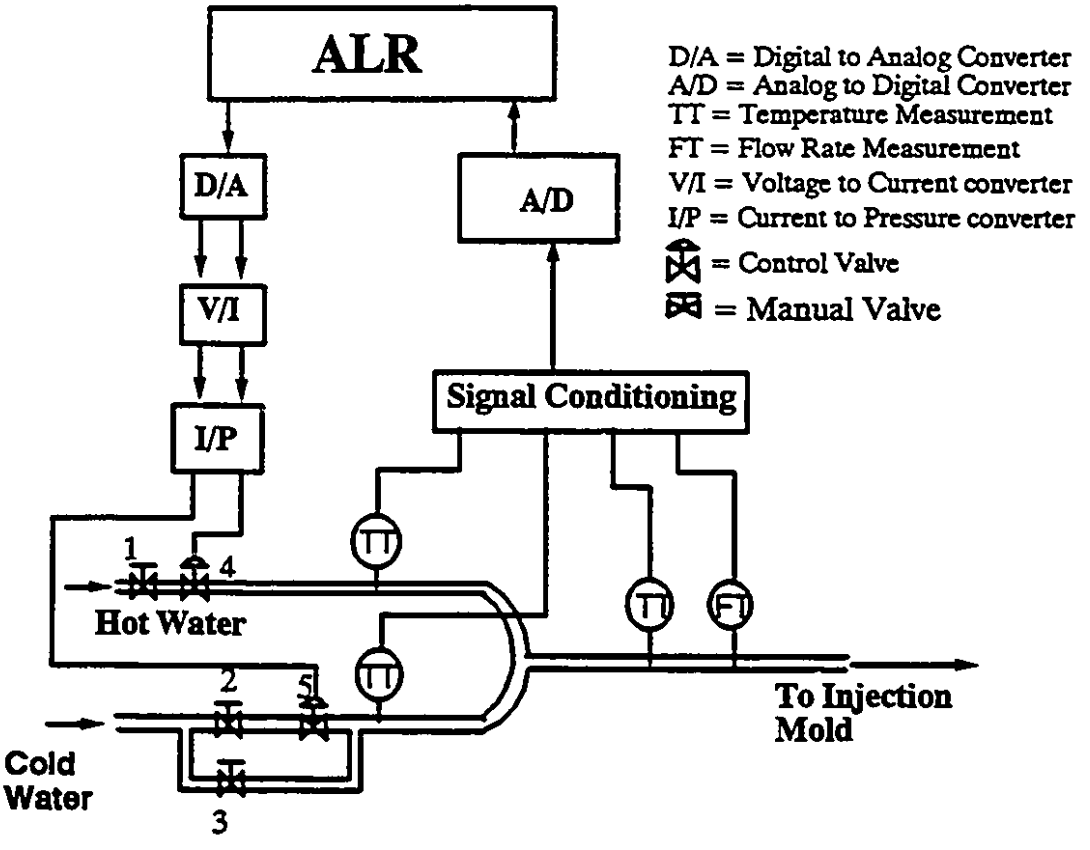

Figure 6.1 Schematic of the cooling system

signals from the computer are first converted to analog signals of 0-5 Vdc. The voltage signal is then converted to 4-20 mA current by a home-built voltage-to-current converter (V/I). A final conversion gives pneumatic pressures through the I/P converter supplied with the control valves. The electronic circuit of the V/I converter is given in Appendix F. As described in Chapter 3, the millivolt signals from the thermocouples are signal conditioned (i.e. cold junction compensated, linearized and amplified) before they are connected to the data acquisition board. The SIGNET flowmeter gives a current signal proportional to the flowrate, which is converted into a 0-5 Volts dc signal through a home-built current-to-voltage (I/V) converter. The I/V converter circuit is shown in Appendix G.

Based on results reported in reference [31] for turbulent flow, the coolant temperature has a much larger effect than coolant flow rate on the heat removal rate in injection molding. Therefore, coolant temperature was chosen as the manipulated variable to control cavity pressure during cooling.

The flow rates for both hot and cold water were set equal by adjusting the manual valves 1 and 2, and they were kept constant for all the experiments. The relationship between the two control valves is given as below:

$$CV_c = 100 - CV_h \tag{6.1}$$

where CV_c is the control valve opening (in percentage) in the cold water side, and CV_h is the control valve opening (in percentage) in the hot water side.

6.2.2 Dynamics of Coolant Temperature

An experiment was carried out to test the designed cooling water mixing system. Some step changes of the opening of the control valve (CV_h) in the hot water side were introduced. The cold, hot and mixed water temperatures, as well as the coolant flowrate, were recorded. The sampling rate for this experiment was 200 ms. The top graph of Figure 6.2 shows the step changes of the control valve (CV_h) opening. The bottom graph of the same figure shows the responses of the hot (T_h), cold (T_c) and mixed (T_m) water temperatures and total flowrate. The change in the flowrate is insignificant. Therefore, it is reasonable to assume that the flowrate is independent of the changes in control valve opening.

The response of the coolant temperature (i.e. the mixed water temperature) to the control valve opening approximates a first order system plus delay as shown in Figure 6.2. In Laplace transform, the model is

$$\frac{T_m(s)}{CV_h(s)} = \frac{k_p}{\tau s+1} e^{(-t_d s)} \qquad (6.2)$$

where k_p is the process gain, unit: °C/%

t_d is the process time delay, unit: seconds, and

τ is the process time constant, unit: seconds.

The process parameters for the last modelling experiment were obtained by the least squares fitting, and they are listed in Table 6.1.

The process gain (k_p) obtained in Table 6.1 depends on the hot and cold water temperatures. These temperatures depend on the supply conditions and are

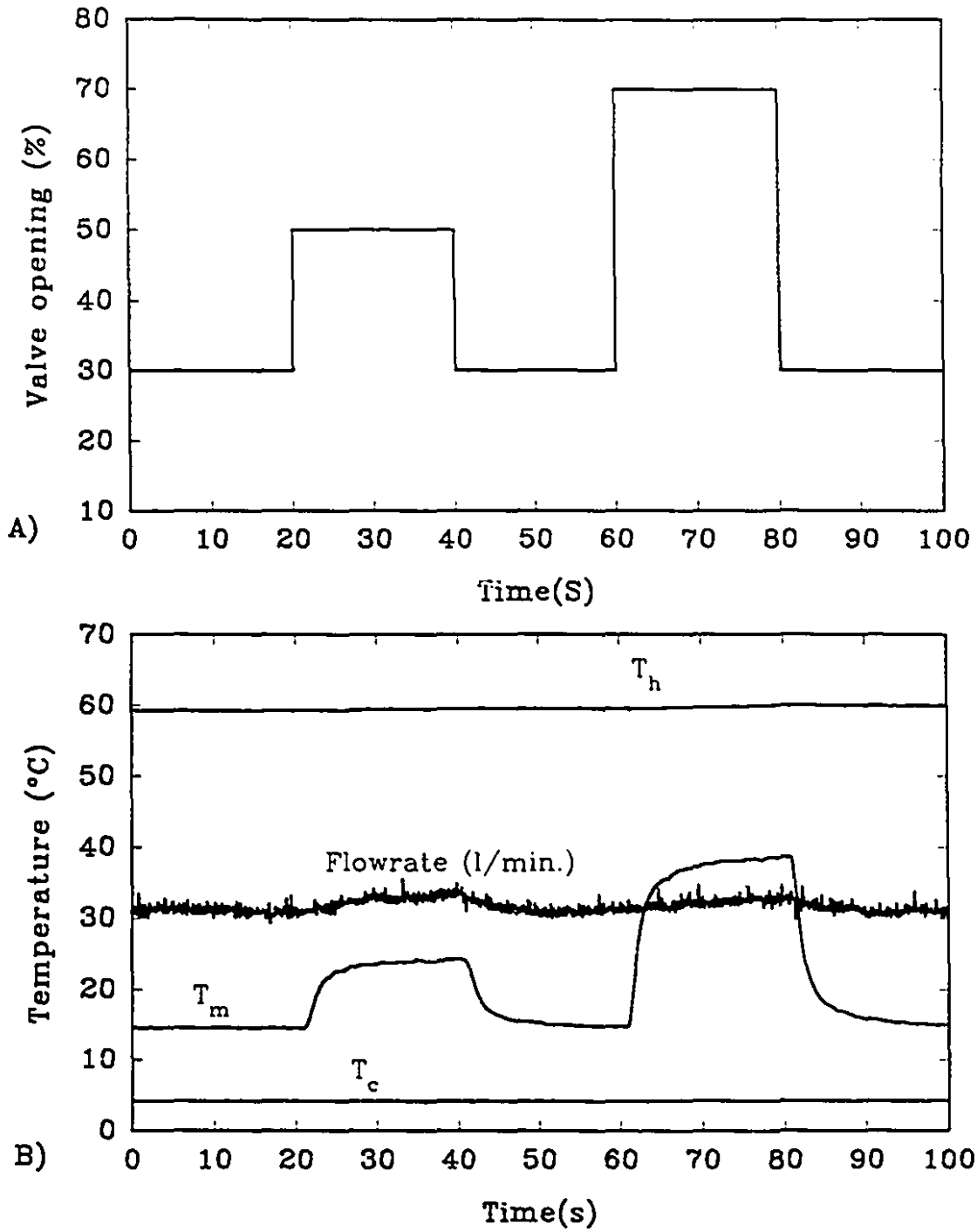

Figure 6.2 Control valve step changes (A) and the responses of the hot, cold, and mixed water temperatures and total flow rate (B)

Table 6.1 Process model for coolant temperature

Process Model Parameters		Step Tests			
		30 to 50 %	50 to 30 %	30 to 70 %	70 to 30%
k_p,	°C/s	0.466	0.460	0.571	0.572
τ,	s	1.568	1.634	1.376	1.361
t_d,	s	1.450	1.178	1.341	1.228

measured directly so that the mixed temperature can be non-dimensionalized as T_{mnd}:

$$T_{mnd} = \frac{T_m - T_c}{T_h - T_c} \tag{6.3}$$

Figure 6.3 gives the responses of T_{mnd} to the step changes shown in the top graph of the control valve opening. It is again obvious that the response can be modelled as a first order system plus delay:

$$G_{nd}(s) = \frac{T_{mnd}(s)}{CV_{h(s)}} = \frac{k_{pnd}}{\tau_{nd}s+1} e^{(-t_{dnd}s)} \tag{6.4}$$

where k_{pnd} is the process gain of T_{mnd} in relation to CV_h,

τ_{nd} is the process time constant, and

t_{dnd} is the process time delay.

The parameters for the above model are shown in Table 6.2. They vary slightly, showing some degree of non-linearity. This is attributed to the non-linearity

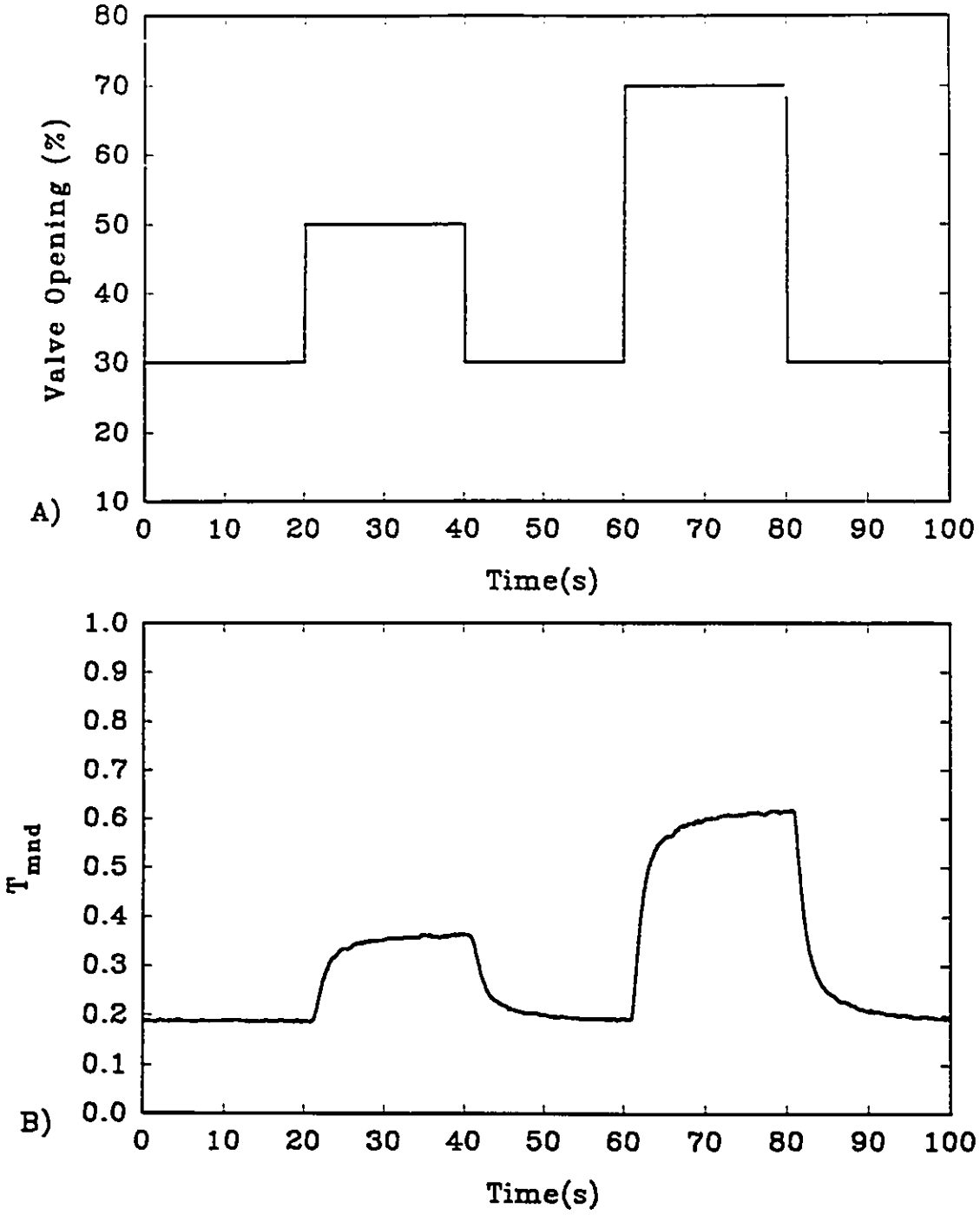

Figure 6.3 Control valve opening changes (A) and the responses of T_{mnd}

Table 6.2 Model parameters for T_{mnd}

Process Model Parameters	CV_h Step Changes				
	30 to 50 %	50 to 30 %	30 to 70 %	70 to 30 %	Averaged
k_{pnd} $[\%]^{-1}$	0.00848	0.00838	0.0102	0.0103	0.0093
τ_{nd} s	1.953	1.387	1.345	1.697	1.60
t_{dnd} s	1.203	1.384	1.295	0.908	1.20

and hysteresis of the valves in the cooling system. The averaged parameters are given in the same table and were used in the coolant temperature controller design.

6.2.3 Coolant Temperature Control

The Dahlin controller (Equation (4.24)), with the tuning parameter, $\mu = 1$ and a sampling rate of 0.2 seconds, was chosen to control the coolant temperature. The process gain K in Equation (4.24) is the actual process gain, $K = k_{pnd} \cdot (T_h - T_c)$. Therefore, the closed-loop control, in essence, is a gain scheduling system with respect to the varying temperatures T_c and T_h. An experiment, carried out to verify the controller effectiveness, started with a coolant temperature of about 15 °C. The set-point of the control system was initially 25°C for 8 seconds, then it jumped to 45 °C and stayed at that value for 8 seconds, then stepped down to 20 °C and remained there. The experimental results are shown in Figure 6.4. The top graph shows the set-

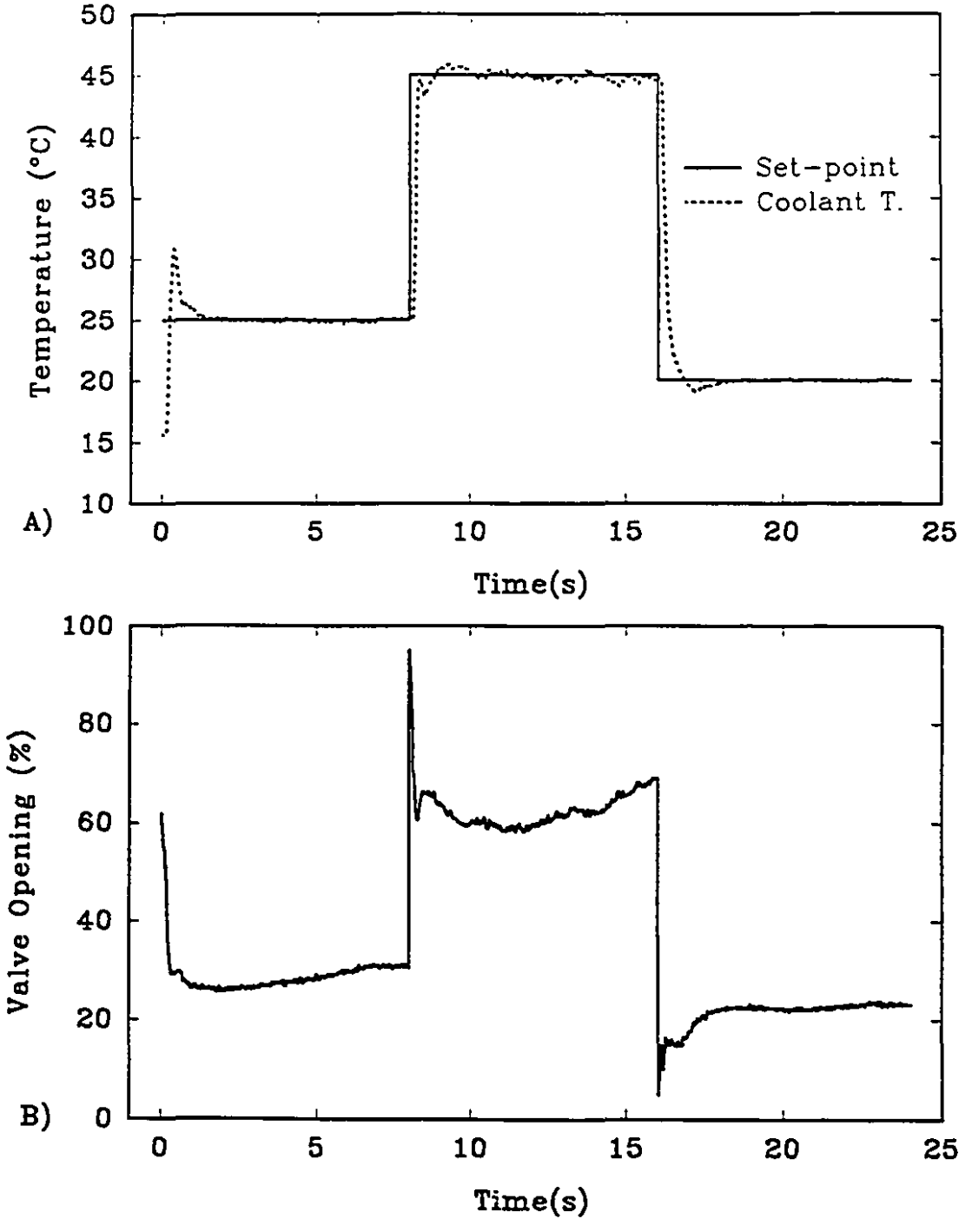

Figure 6.4 Closed-loop control of coolant temperature in tracking step changes of set-point (A) and the corresponding control valve opening changes (B)

point changes (solid line) and the coolant temperature responses (dashed line). It clearly shows that the coolant temperature closely follows the set-point profile. The coolant temperature reaches a new set-point within 2 seconds in the worst case. Figure 6.4B gives the corresponding control valve opening in percent on the hot water side. It is seen that with the coolant temperature at a fixed value, the valve opening tends to drift. This is due to the hot-cold water temperature difference drifting at the beginning of the experiment, when the water streams have been just turned on.

6.3 Dynamics and Control of Cavity Pressure during Cooling

6.3.1 Gate Sizing

The injection molding machine was originally equipped with a cylindrical gate of 6.35 mm (¼ inch) in diameter. Usually, the pressure supplied to the injection cylinder is removed by turning off the solenoid valve or servo-valves at the end of the packing stage. With this arrangement, an experiment was carried out in an attempt to obtain the cavity pressure cooling profile. The experimental results of both the cavity pressure and nozzle pressure are given in Figure 6.5A. Obviously, due to the unusually large gate, the melt is not completely frozen after a duration of 4 seconds packing. There are two problems associated with the results: (i) due to incomplete gate freezing, the cavity pressure does not have a cooling profile; (ii) the cavity pressure during cooling is greater than the nozzle pressure for a short time after packing, this causes an undesirable backflow of polymer from the cavity to the

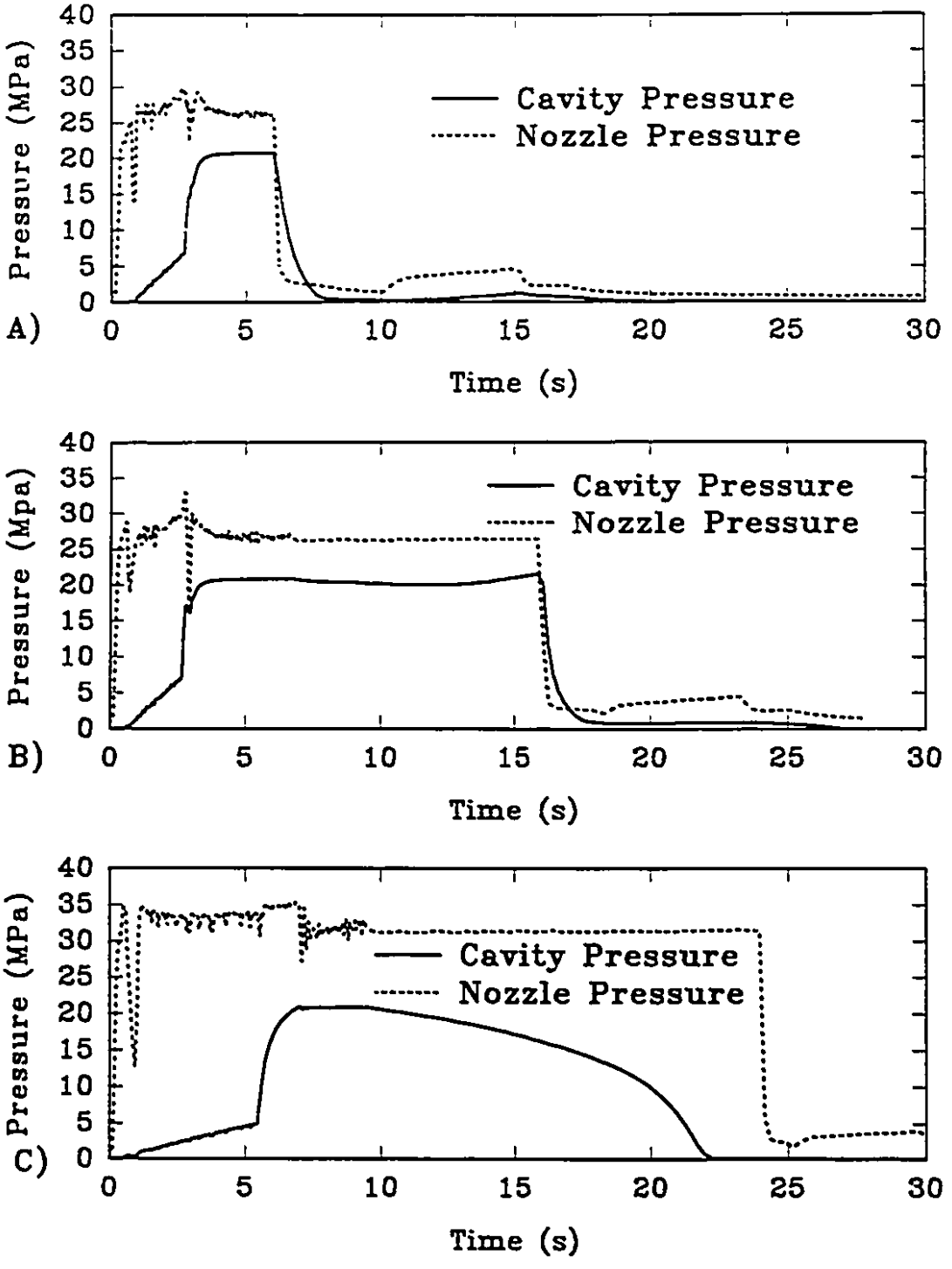

Figure 6.5 Nozzle and cavity pressures: cylindrical gate with four seconds of packing and holding (A); cylindrical gate with 17 seconds of packing and holding (B); new injection gate (C)

nozzle.

A longer packing and holding time was used in an attempt to eliminate the above problems. A second experiment was carried out with a packing and holding time of 17 seconds. The first four seconds of packing and holding were closed-loop controlled using the cavity pressure control technique described in Chapter 5. After that time, the servo-valve was kept at a fixed opening corresponding to the average value between the packing times of 3.8 to 4.0 seconds. The cavity pressure and nozzle pressure are presented in Figure 6.5B. The cavity pressure increases slightly for the late part of packing and holding. The same problems exist as with the previous experiment, suggesting that the gate was not frozen even with this long period of packing and holding.

Therefore, a smaller gate was determined to be necessary in order to eliminate the backflow problem. A round-cornered gate of 6.35 mm (¼ inch) in width, 1.6mm ($^1/_{16}$ inch) in thickness and 6.35mm (¼ inch) in length replaced the cylindrical gate. To eliminate the possible backflow, the servo-valve was kept at a fixed opening for 15 seconds after the end of four seconds closed-loop packing control. The experimental results are shown in Figure 6.5C. A cavity pressure filling profile was changed from a ramp of 2.76 MPa/s to a ramp of 1.72 MPa/s in response to the smaller gate. Figure 6.5C gives a reasonable cooling profile. The cavity pressure decreases with time after packing despite the existence of nozzle pressure. This new gate and servo-valve arrangement are used for all remaining experiments.

6.3.2 Experimental Conditions

The melt temperature was determined by setting the four barrel temperature set-points to 235, 215, 180, and 150 °C from the nozzle to the hopper, respectively. The sampling rate for pressure during the cooling stage was 50 ms. The total injection molding cycle was set to be 32 seconds. The filling pressure was controlled at a rate of 1.73 MPa/s (250 psi/s). The packing pressure was controlled at 20.7 MPa (3000 psi) for a duration of 4 seconds. The machine and material conditions were as stated in the previous chapter. These conditions were kept the same during all the following experiments, except when otherwise stated.

6.3.3 Definition of Representative Variables during Cooling

Once the injection gate is frozen, the cavity pressure can only be influenced by the coolant temperature or coolant flowrate. Due to the large thermal mass of the injection mold, it is not possible to manipulate the pressure during cooling within a cycle. However, it is possible to change it over successive cycles.

Figure 6.6 gives two experimental cavity pressure profiles with coolant temperatures of 45° and 15°C, respectively. The packing pressure for both experiments was 20.7 MPa (3000 psi). It is seen that the coolant temperature has a strong effect on the pressure profile during cooling. In both cases, the pressure starts to decrease slowly from the packing pressure. The rate of decrease becomes larger until it reaches zero.

Several quantitative descriptions of the cooling process are possible. The

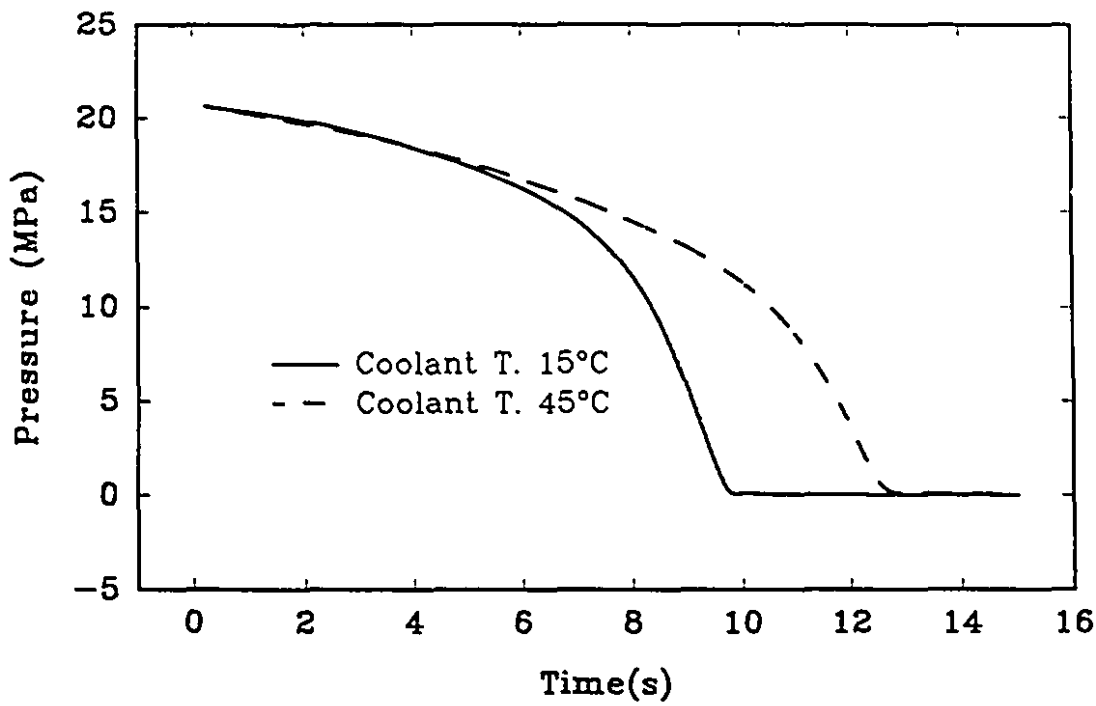

Figure 6.6 Cavity pressure profiles during the cooling stage with two different coolant temperatures

merits and disadvantages of these methods are discussed below.

6.3.3.1 Function Fitting

This describes the cooling pressure profile with a mathematical function (e.g. a polynomial or some form of exponential function). It gives an accurate description of the pressure profile during cooling, but the computation power needed to do this during every injection cycle is large. Therefore, this method was not chosen.

6.3.3.2 Pressure Cooling Time to Inflection (PCT_i)

This is defined as the time from the end of packing to the point where the pressure profile passes through the point of inflection. It can be determined from the maximum of the derivative of the pressure profile. The difficulty is that differentiation of a signal increases the noise-to-signal ratio, which makes the maximum difficult to determine.

6.3.3.3 Pressure Cooling Time (PCT_0)

PCT_0 is defined as the time from the end of packing to the time at which the pressure reaches a value which is (close to) zero. The PCT_0 is easy to measure, requires little computation time and indicates an "average" pressure loss rate. However, this variable only gives information about both ends of the pressure profile. The nature of the pressure profile between these two values is not taken into consideration.

6.3.3.4 Multiple Pressure Cooling Times (PCT_x), and Controlled Pressure Cooling Time (CPCT)

The pressure cooling time (PCT_x) is defined as the time from the end of packing to the time at which the pressure decreases to x percent of the pressure at the end of packing, p_{PE}.

To remedy the problem associated with PCT_0, multiple measurement of PCT_x is proposed. Instead of measuring the time from the end of packing to a near zero pressure, this method employs a vector of times from the end of packing to a vector of predetermined pressures. This method has all of the advantages of PCT_0. It also gives an approximate characterization of the pressure-time profile. However, multiple pressure cooling times give multiple (a vector of) times instead of a single scalar value. The vector size and the vector of predetermined pressure percentage values need to be determined. One practical simplification is to define a Controlled Pressure Cooling Time ($\Delta PCT_{67\text{-}33}$, or CPCT) which is the time required to progress from 2/3 (67%) of the packing pressure to 1/3 (33%) of the packing pressure. Figure 6.7 gives a graphical representation of the variables discussed.

An experiment was carried out to test the effectiveness of CPCT. Figure 6.8A gives the pressure profile during cooling for cycles 9, 11, and 13 with the same CPCT ($\Delta PCT_{67\text{-}33}$) value of 1.8 seconds. The pressure profiles for cycles 9, 11, and 13 are represented with the solid, long-dashed and short-dashed lines, respectively. All of these lines are almost superimposed on each other. Figure 6.8B gives the pressure differences between cycles 9 and 11, and cycles 11 and 13. It shows that the pressure

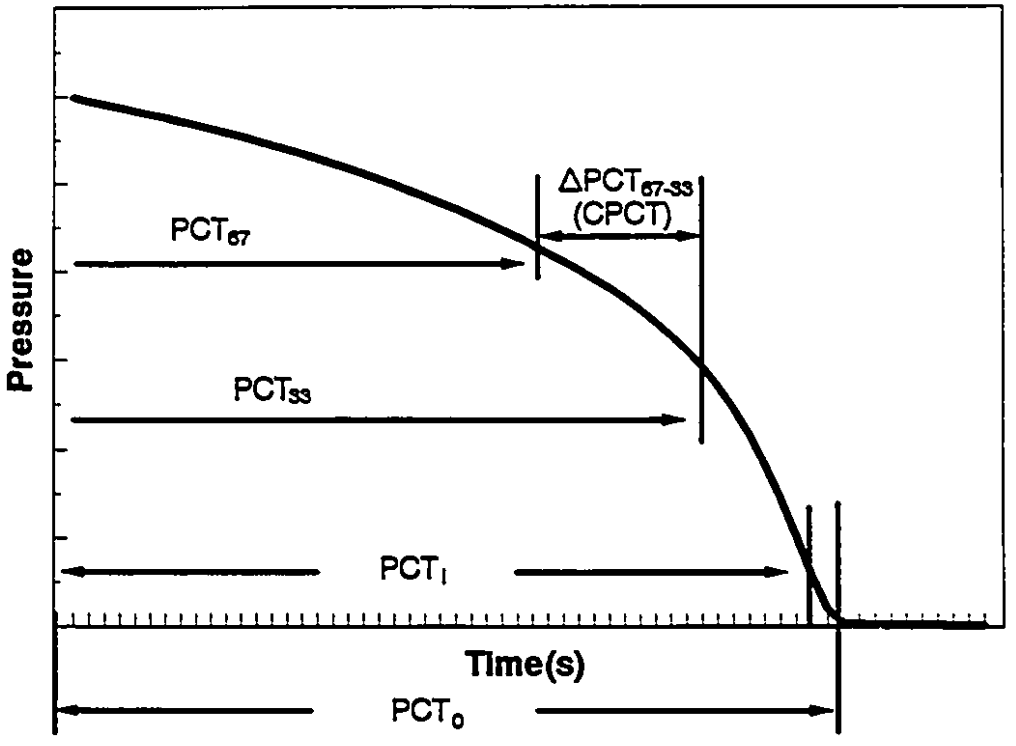

Figure 6.7 Graphical representation of the proposed CPCT, PCT_x, PCT_0, and PCT_i.

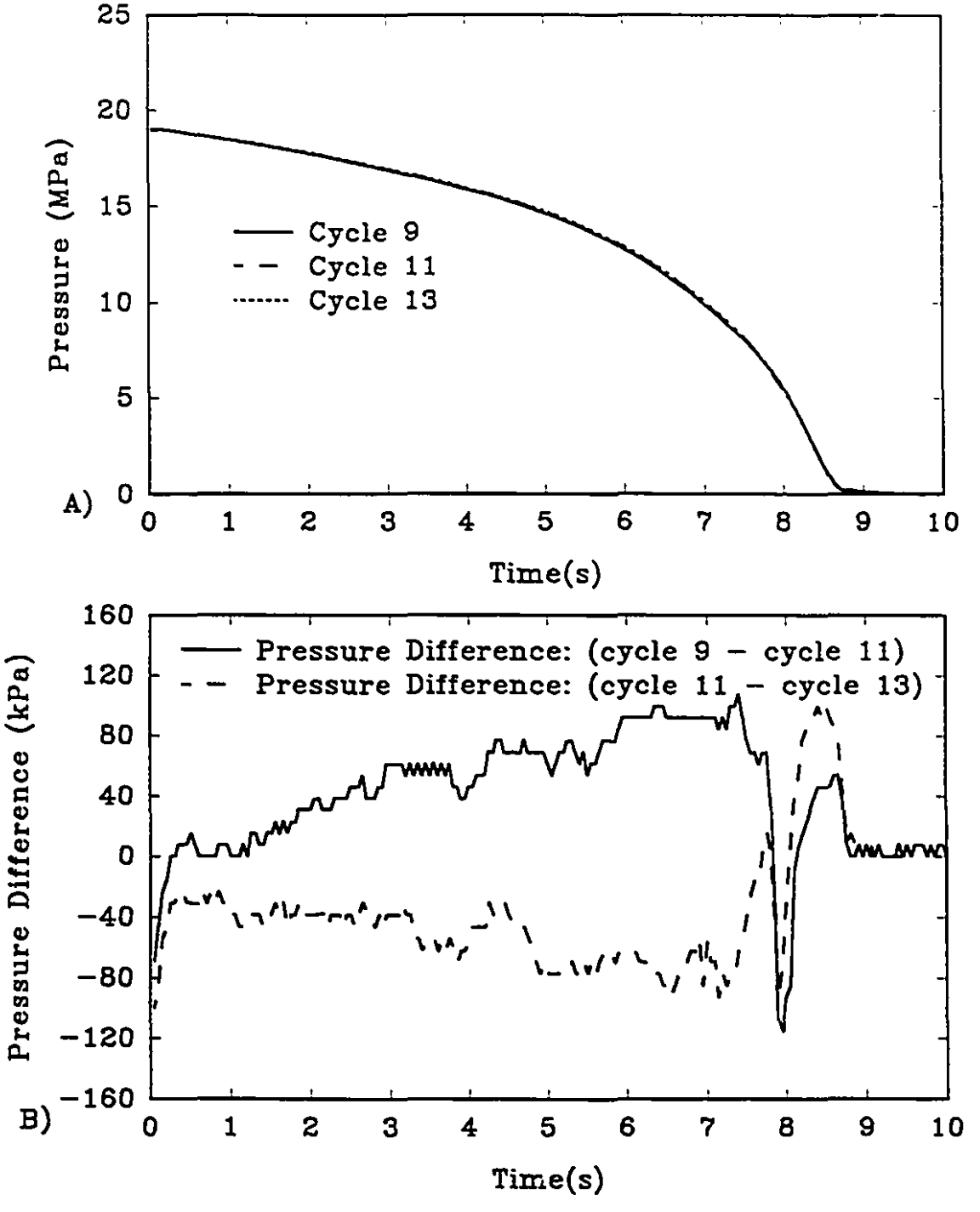

Figure 6.8 Pressure cooling profiles of different cycles with the same CPCT (A) and the pressure differences (B)

differences are very small. Figure 6.8 indicates that the same CPCT produces very similar pressure cooling profiles. Therefore, CPCT appears to be a suitable parameter to describe the pressure profile during cooling.

Different packing pressure, packing time and coolant temperature have a large effect on the controlled pressure cooling time (CPCT). The packing pressure and packing time are usually determined by the injection molded part geometry and quality requirements. They are normally not used to control the pressure cooling profile.

6.3.4 Dynamic Models Relating CPCT Response to Coolant Temperature

An open-loop experiment was conducted to test the dynamic model relating CPCT to the coolant temperature. The coolant temperature varies according to the top graph of Figure 6.9. The bottom graph gives the corresponding change in CPCT. The total cycle time for this experiment is 32 seconds. Since Figure 6.4 indicates that the coolant temperature can reach a new set-point within 2 seconds, the dynamics of the inner-loop (i.e. coolant temperature control loop) can be neglected.

The response of CPCT to a change in coolant temperature can be approximately modelled as a first order system. The small variation of CPCT is due to the measurement resolution and, possibly, incomplete gate freezing at the end of packing. The sampling rate for pressure measurement during cooling is 50 ms, which determines the resolution of PCT_x and CPCT ($\Delta PCT_{67\text{-}33}$).

Parametric models of first order with no delay, and with one molding cycle

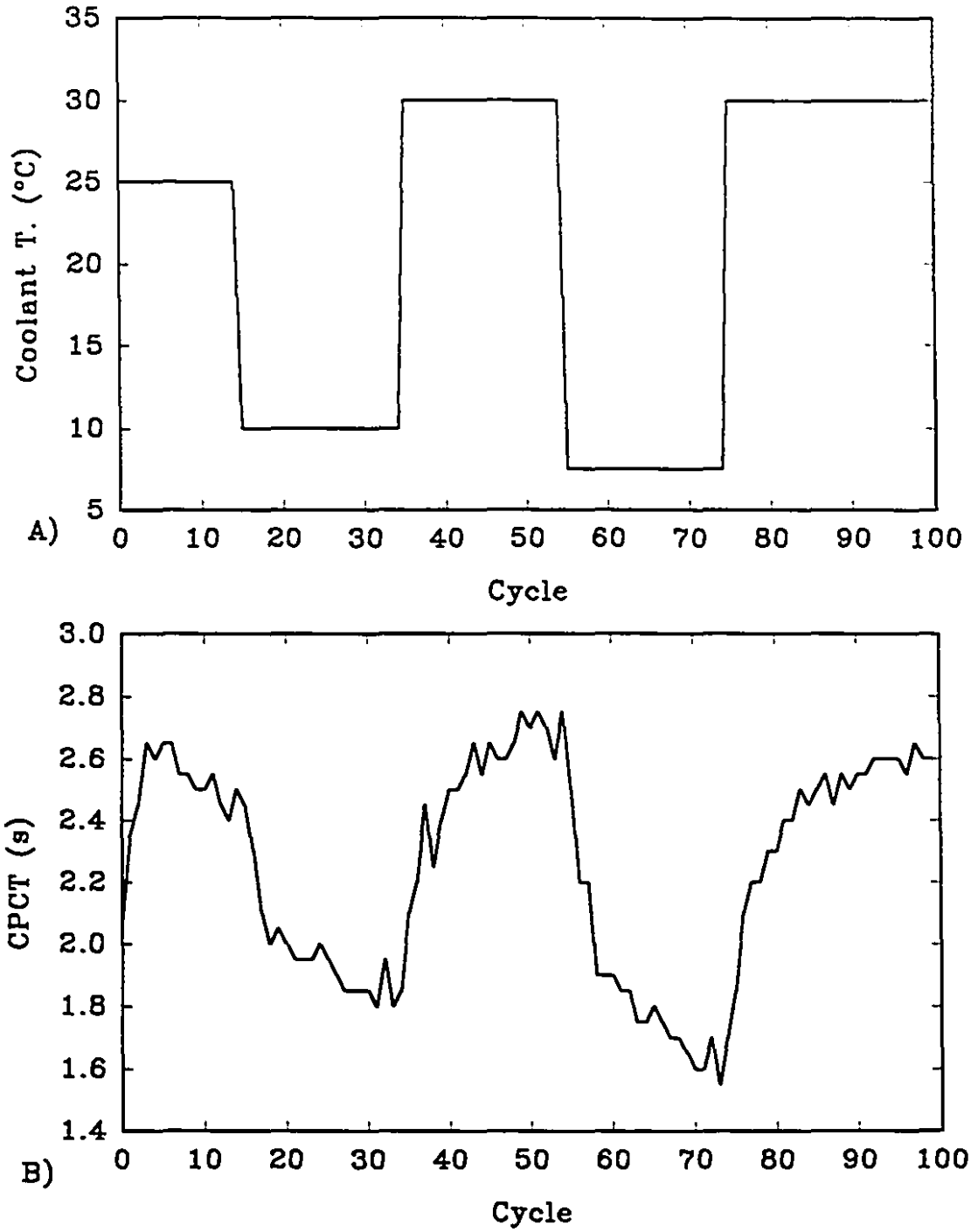

Figure 6.9 Coolant temperature changes (A) and responses of CPCT (B)

delay, are given in Table 6.3. Details of the methods used to estimate these parameters are given in references [83 - 85]. The final prediction error (FPE) is an indicator of the model accuracy. The smaller it is, the better the model. It indicates

Table 6.3 Dynamic model of CPCT

Temp. Changes	ARX	B		A		FPE
10->25°C	[110]	0.0145 0.0032		1 0	-0.6425 0.0863	0.00776
	[111]	0 0	0.0157 0.0046	1 0	-0.6074 0.1238	0.00947
25->10°C	[110]	0.0147 0.0028		1 0	-0.6248 0.0790	0.00365
	[111]	0 0	0.0183 0.0045	1 0	-0.5301 0.1244	0.00476
10->30°C	[110]	0.0130 0.0029		1 0	-0.6706 0.0839	0.00879
	[111]	0 0	0.0133 0.0045	1 0	-0.6606 0.1266	0.0117
30->7.5°C	[110]	0.0131 0.0022		1 0	-0.7041 0.0565	0.00684
	[111]	0 0	0.0157 0.0034	1 0	-0.6403 0.0863	0.00905
7.5->30°C	[110]	0.0102 0.0020		1 0	-0.7558 0.0557	0.00464
	[111]	0 0	0.0116 0.0029	1 0	-0.7189 0.0778	0.00562

that the first order with no delay model is a better representation of the system.

Based on FPE, the parametric model ARX[110] was therefore selected. The model parameters were then converted to the Laplace domain based on Equations (4.13), (4.14), and (4.15). The process gains and time constants are listed in Table 6.4.

6.3.5 Control of CPCT

6.3.5.1 Control Simulation of CPCT

As indicated in Chapter 4, Dahlin control and Internal Model Control designs are equivalent for a first order system. They both are quite robust to a certain degree of model to process mismatch. Therefore, the Dahlin control method was chosen. Simulations were carried out to determine the proper tuning parameter, μ, for the

Table 6.4 Process gain and time constant of CPCT

Case	k_p (s/°C)	τ_p (cycle)
10 to 25°C	0.041	2.80
25 to 10°C	0.040	3.88
10 to 30°C	0.040	3.04
30 to 7.5°C	0.044	3.38
30 to 30°C	0.041	3.56
Averaged	0.041	3.33

control system.

Figure 6.10 gives the simulation results in deviation variable form of the Dahlin controller responses to a step change in the set-point. The sampling period is one injection molding cycle. The dotted line is the set-point step change profile. The solid, long-dashed, and short-dashed lines are the responses of the controllers with $\mu = 1,2$ and 3, respectively. They indicate that the Dahlin controller can reach a new set-point without any problem. For smaller values of μ, the response becomes faster in following set-point changes. The bottom graph of Figure 6.10 gives the corresponding control variable (i.e. the coolant temperature) change. Again, the solid, long-dashed, and short-dashed lines are the coolant temperature changes (i.e. the controller output) for the cases when $\mu = 1,2$ and 3, respectively. Figure 6.10 shows that tight set-point tracking is due to the strong action in the coolant temperature changes. With this mixing system, a large temperature change is possible with the coolant temperature control system. Therefore, the tuning parameter μ was chosen to be 1.

Another simulation result is given in Figure 6.11 to show the robustness of the Dahlin controller. The solid line is the response of the CPCT to a set-point change with the estimated averaged dynamics. The long-dashed line is the CPCT response to the set-point change, with the process gain increased by 25%. The short-dashed line is the CPCT response with the process gain decreased by 25%. In all cases, the CPCT reaches the new set-point fairly quickly, without serious performance degradation. Figure 6.11B shows the corresponding coolant temperature changes.

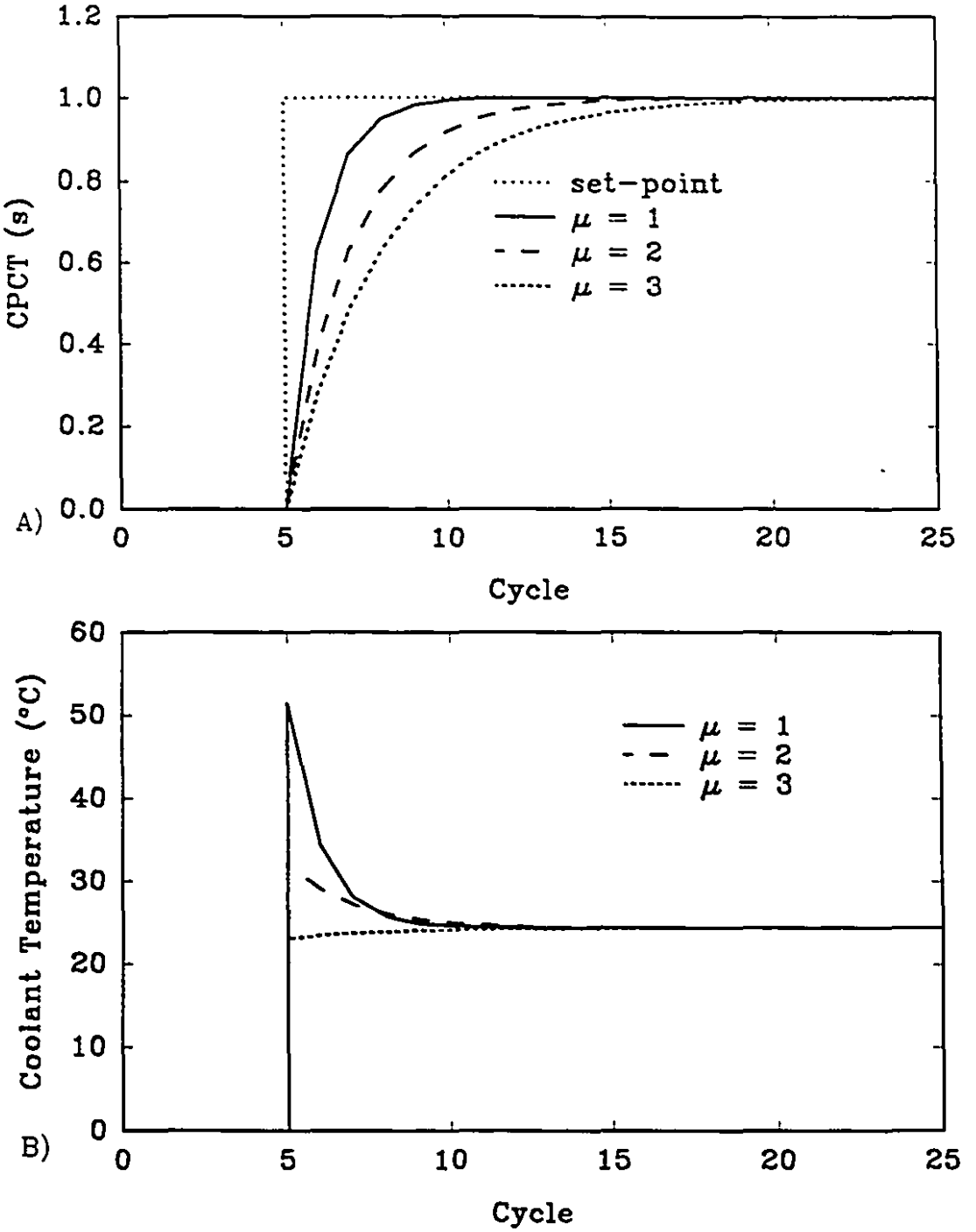

Figure 6.10 CPCT control simulation with different μ: the CPCT responses (A) and the corresponding coolant temperature changes (B)

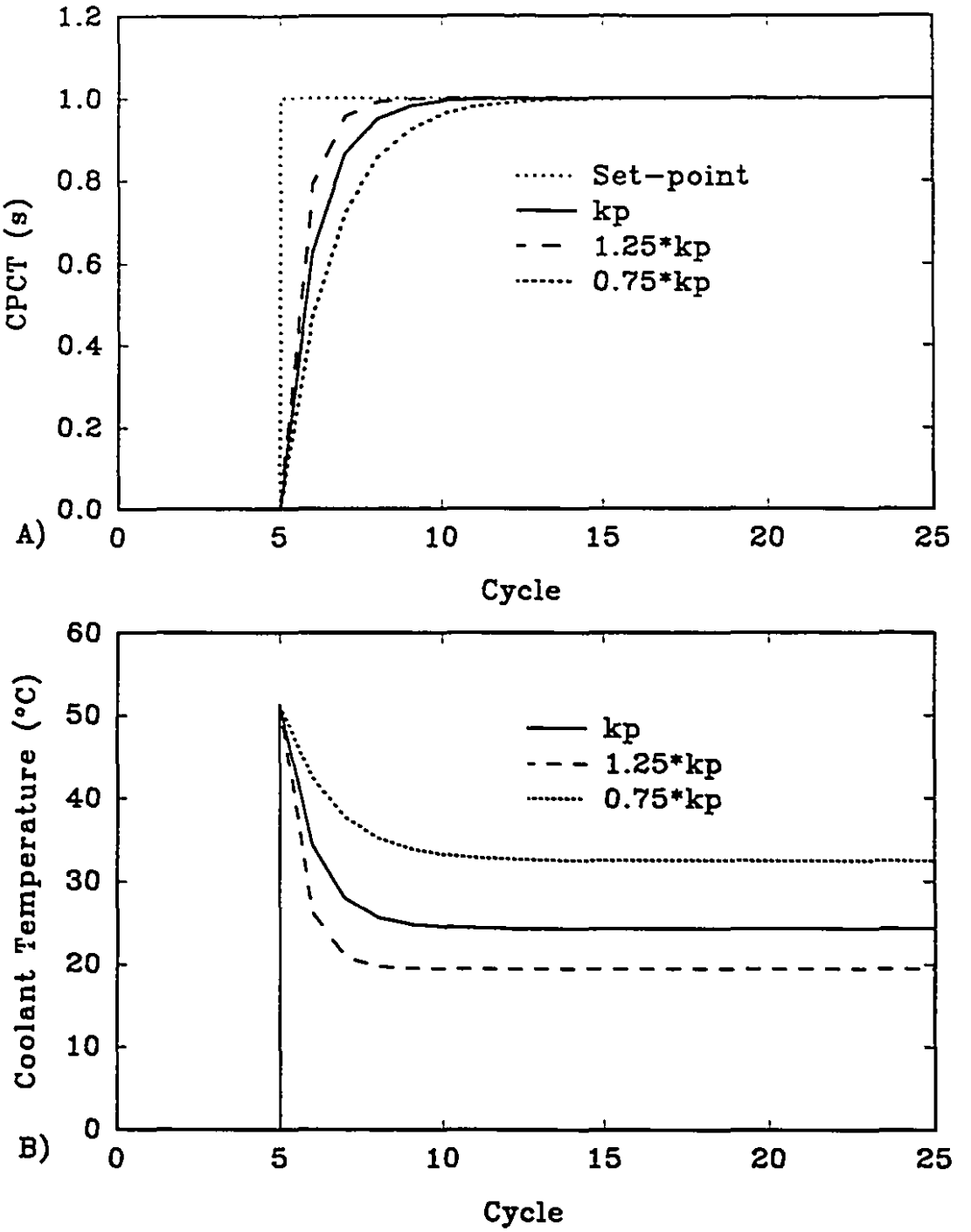

Figure 6.11 CPCT control simulation with different process gains: the CPCT responses (A) and the corresponding coolant temperature changes (B)

This figure indicates that the Dahlin controller can handle the process gain changes easily.

Figure 6.12 shows the robustness of the Dahlin controller to changes in the process time constant. The dotted line is the set-point profile. Again, the profile has a step change of 1 s. The solid line is the CPCT response of the closed-loop Dahlin control with the real process dynamics. The long-dashed line is the response with the process time constant increased by 25%, while the short-dashed line is the response with the process time constant decreased by 25%. The bottom graph shows the changes in the corresponding manipulated variable (i.e. the coolant temperature). In all three cases, the CPCT can reach the new set-point quickly.

In summary, the change of the process dynamics (i.e. process gain and time constant) only slightly degrades the control performance, without the risk of instability. Dahlin control with $\mu = 1$ gives good control performance. The control is also very robust to the changes in the process dynamics. Therefore, this controller was programmed and tested experimentally. The following section gives the experimental results.

6.3.5.2 Experimental Control of CPCT

A cascade control loop shown as in Figure 6.13 was implemented to test the control performance of CPCT experimentally. This control system has two control loops, i.e. the inner loop and outer loop. The inner loop is the closed-loop control of the coolant temperature. $G_{p2}(z)$ describes the dynamic model of the coolant

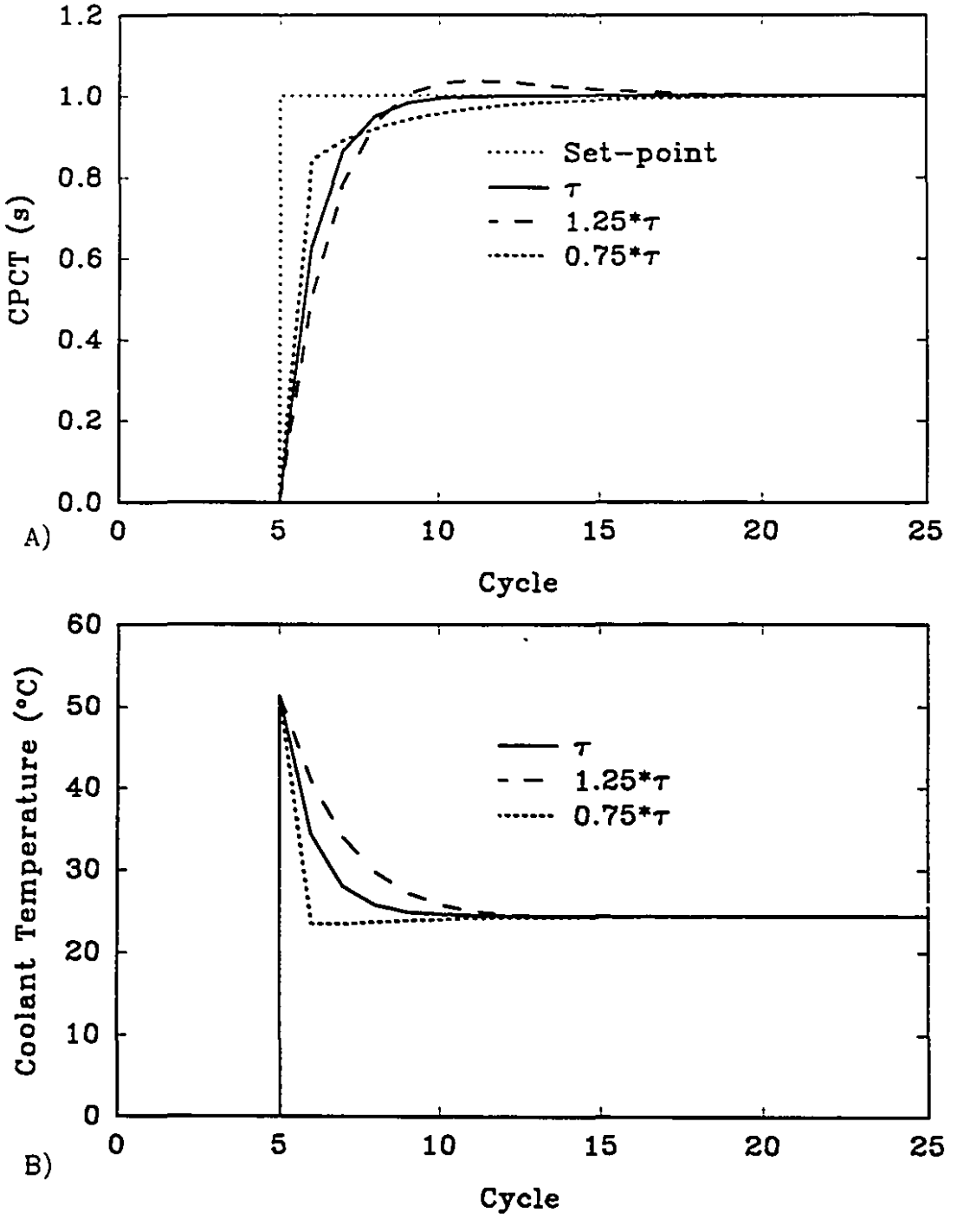

Figure 6.12 CPCT control simulation with different process time constants: the CPCT responses (A) and the corresponding coolant temperature responses (B)

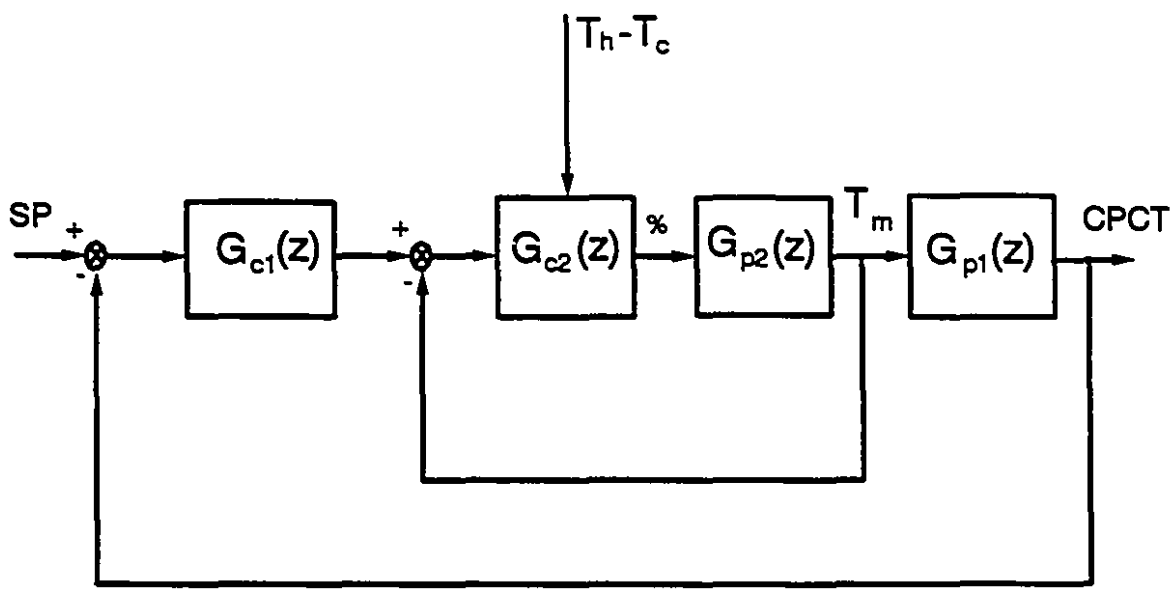

Figure 6.13 Block diagram of the cascade closed-loop control of CPCT

temperature relative to the percentage change in the opening of the control valve. $G_{c2}(z)$ is the Dahlin controller algorithm given in Section 6.3.3. As pointed out earlier, the inner loop actually is a gain scheduling control system. The controller parameter is automatically adjusted based on the value of the hot and cold water temperature difference. The outer loop is designed as outlined in the simulation section. $G_{p1}(z)$ describes the process dynamic model of the CPCT relative to the change in the coolant temperature. $G_{c1}(z)$ is the Dahlin controller as described in the previous section. The outer loop control is based on cycle-to-cycle operation. Therefore, the sampling period is the total injection cycle. The inner loop has a fixed sampling period of 200 ms.

The cascade control algorithm was programmed into the computer. The program functional structure is illustrated in Figure 6.14. Basically, the outer loop outputs a new control action every new injection cycle, while the inner loop updates its output every 200 ms, taking the output of the outer loop as its new set-point.

An experimental closed-loop control to track a changing set-point profile was carried out. The controller tuning parameter $\mu = 1$ (i.e. one injection cycle). The related injection molding conditions were as stated in the previous section. In this experiment, the CPCT set-point started at 2.5 seconds. At the 20th cycle, the set-point decreased at a rate of 50ms a cycle until the 34th cycle. Then, it stayed at 1.8 seconds until cycle 54. Subsequently, it stepped back to 2.5 seconds and stayed at this value until cycle 74. It then stepped again to 1.8 seconds and stayed at this value until the 94 th cycle, after which it increased at a rate of 50ms per cycle until it reached

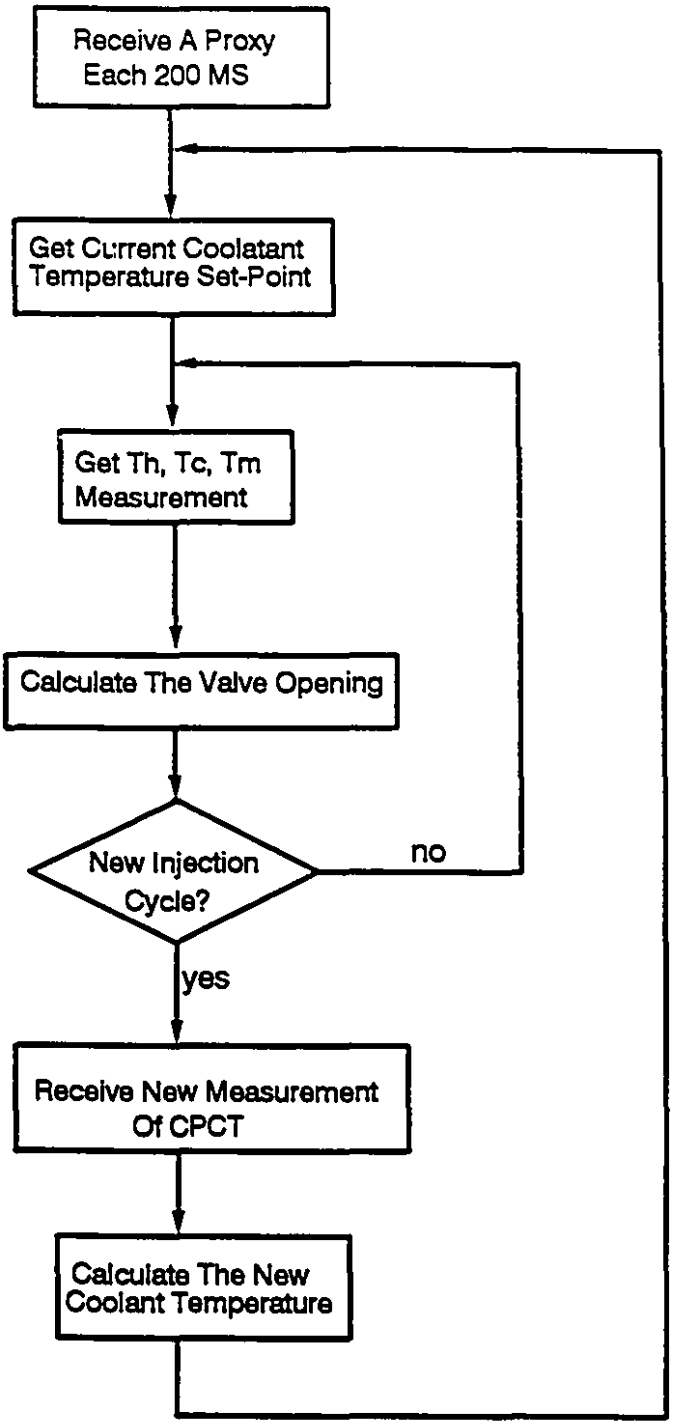

Figure 6.14 Cascade control implementation of CPCT

2.5 seconds, and remained at that value. The set-point is graphically represented as the solid line in the top graph of Figure 6.15. This set-point profile involves both step and ramp changes in both the up and down directions. The dashed line is the experimental response of the closed-loop control to the set-point changes. It is clear that CPCT follows the set-point closely. The bottom graph of Figure 6.15 shows the corresponding coolant temperature changes.

One more experiment was carried out to test the effectiveness of the control system in handling melt temperature changes. The melt temperature for this experiment was changed to 205°C from 235°C in the previous experiment. The set-point for this experiment was started at 2.5 seconds. It changed to 1.8 seconds at cycle 20. The solid and dashed lines in Figure 6.16 are the set-point and CPCT response, respectively. The corresponding coolant temperature changes are shown in the bottom graph of the same figure. CPCT is seen to follow the set-point closely, indicating that the control system can handle the melt temperature changes successfully.

The pressure cooling profiles of the last experiment of CPCT control are given in Figure 6.17. It shows the profiles of the cycles 15, 17, 19, 21, 23, and 25, just before, during, and after a step change of the CPCT set-point was introduced at cycle 20. The pressure cooling profiles of cycles 15, 17 and 19 superimpose, before the CPCT set-point change was introduced. The pressure cooling profiles of cycles 23 and 25 are also very similar after the set-point change of CPCT occurred. The pressure cooling profile of cycle 21 coincides with the transition of the controlled pressure

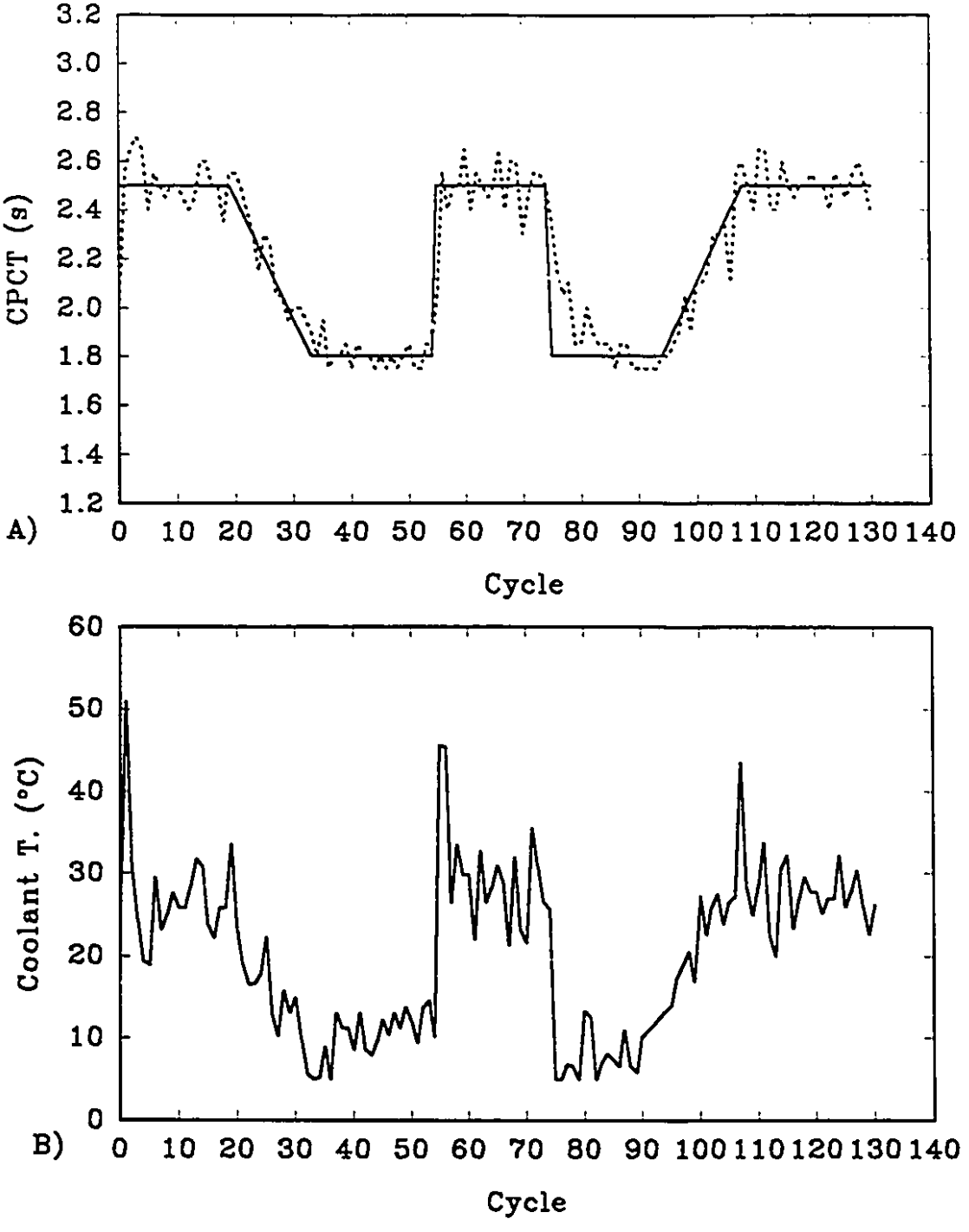

Figure 6.15 Experimental closed-loop control of CPCT with a melt temperature of 205 °C: the CPCT responses (A) and the corresponding coolant temperature changes (B)

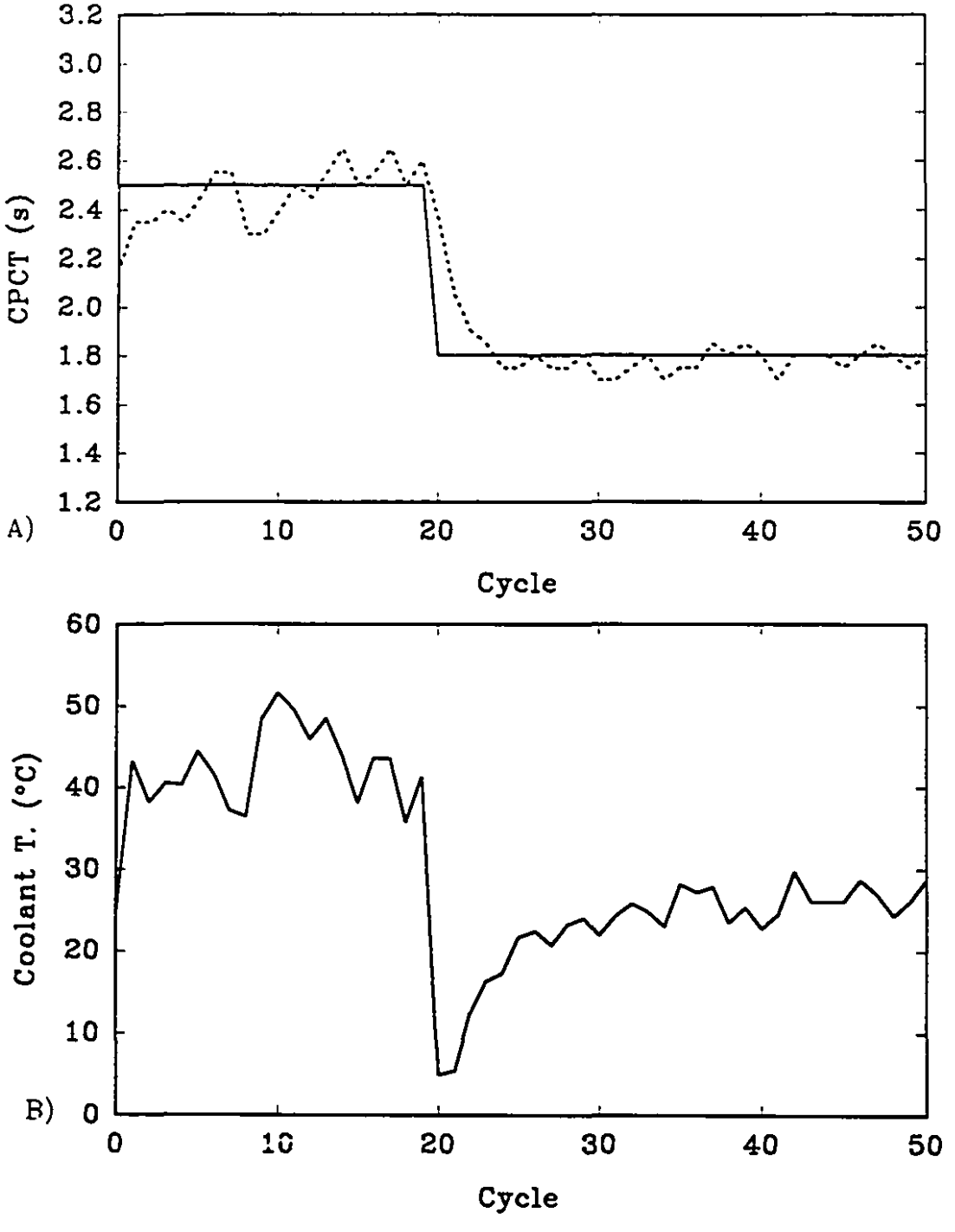

Figure 6.16 Experimental closed-loop control of CPCT with a melt temperature of 235 °C: the CPCT responses (A) and the corresponding coolant temperature changes (B)

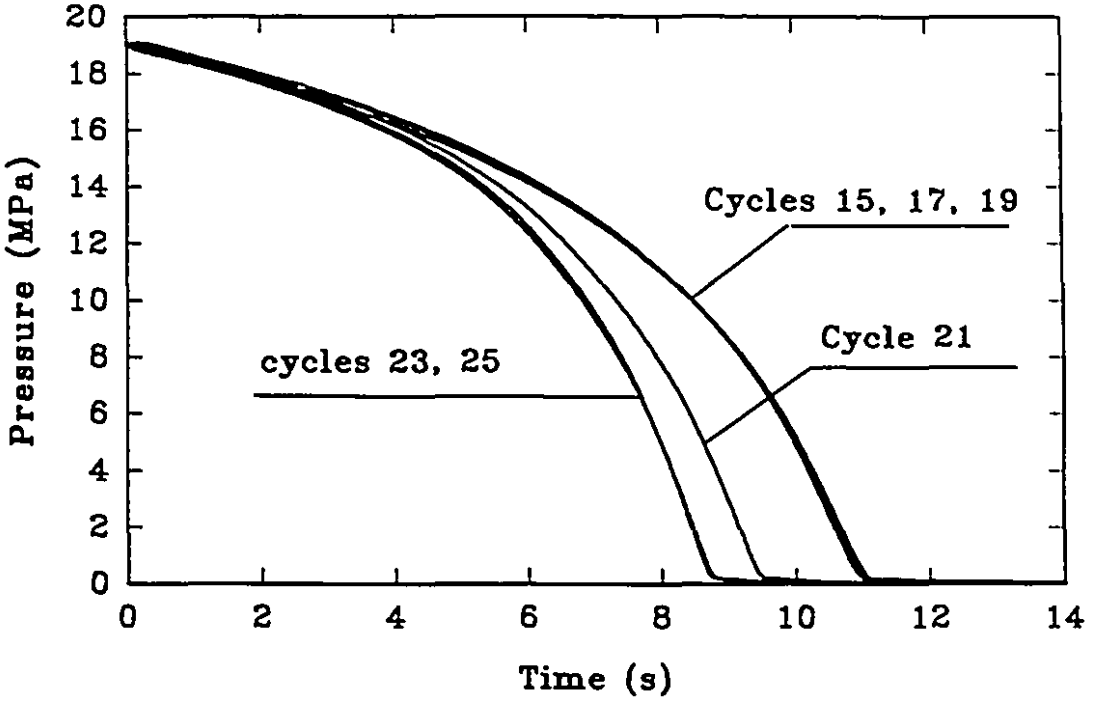

Figure 6.17 Pressure cooling profiles just before (cycles 15, 17, 19), during (cycle 21), and after (cycles 23, 25) a step change of CPCT set-point, the set-point step change occurred at cycle 20

cooling time (CPCT). It is clear, from Figures 6.16 and 6.17, that the control of CPCT is effective in controlling the pressure cooling profiles.

6.4. Summary

A coolant temperature control system has been successfully designed and implemented. Several alternative variables for pressure control during cooling have been proposed. The dynamics of one of these, CPCT, were investigated and modelled. A successful control system for CPCT was implemented and tested using coolant temperature as the manipulated variable.

Chapter 7

CONCLUSIONS AND RECOMMENDATIONS

7.1 Conclusions

The objectives of this research were to study the dynamics of cavity pressure over the complete injection molding cycle, to design and implement a cavity pressure control system for a wide range of conditions, and to design and implement a real-time computer control and data acquisition system for injection molding. These objectives have been realized successfully.

A real-time computer control and versatile data acquisition system with several user-selectable levels of operation has been developed. Closed-loop control of barrel temperatures, mold coolant temperature, cavity pressure, cyclic movement of the machine, and data acquisition have been carried out smoothly with one computer. The system is modular. The user can easily add, remove, modify or replace any task.

The cavity pressure variation during filling was analyzed. A first order system, in parallel with an integrating process, together in series with a delay, was found to be the best model in describing the cavity pressure dynamics. The time varying nature of the cavity pressure dynamic model was established and analyzed.

Cavity pressure dynamics during packing were analyzed, and the same dynamic model structure as during filling was found to be capable of describing the dynamics

during packing. The time varying behaviour was evaluated over the complete packing phase.

The detection of the filling-to-packing transition was studied, and the cavity pressure derivative was found to be the best criterion for this purpose.

Cavity pressure during filling was successfully controlled with the self-tuning control using pole-placement design. A forgetting factor of 0.75 was found to provide good control over different operating conditions and different cavities. This unusually low value of the forgetting factor was required by the rapid varying process. A complex geometry cavity was used to test the adaptiveness of the controller experimentally. Results superior to any reported in the literature on cavity pressure control have been obtained.

Cavity pressure control during packing was achieved using the same control technique as filling. Different cavity pressure profiles and melt temperatures were used to test the controller, and a step change in the forgetting factor from 0.75 to 0.975 after about one second from the start of packing produces small servo-valve variation and tight set-point profile tracking.

A new cooling system was designed. The dynamics of the mixed coolant temperature were studied, and a gain scheduling control of coolant temperature was implemented to adjust for cold and hot water temperature shifts automatically. Coolant temperature control was used as the inner loop of the cascade closed-loop control of cavity pressure during the cooling stage. Controlled pressure cooling time (CPCT), defined to be the time for cavity pressure to decrease from 2/3 to 1/3 of

the packing pressure during the cooling stage, was proposed as a viable variable for cavity pressure control during cooling. The CPCT dynamics in relation to coolant temperature were evaluated and a closed-loop control system was designed, implemented, and tested, with satisfactory results.

Figure 7.1 shows two cavity pressure profiles of different cycles over the complete cycle including the filling, packing, and cooling stages. The cavity pressure was controlled, using the self-tuning regulator (STR) discussed in Chapter 5 for the filling and packing stages, and using cycle-to-cycle based control of CPCT described in Chapter 6 for the cooling phase. The superposition of the pressure profiles of the two different cycles indicates good cavity pressure control over the complete injection molding cycle.

7.2 Claims for Original Work

This work has examined the dynamic modelling and control of pressure throughout the injection molding cycle. Previous work concerning part of the molding cycle has been extended significantly. Particular contributions may be stated as follows:

1) The present work is the first to present a time-varying dynamic model of cavity pressure for both filling and packing phases.

2) This work is the first application of self-tuning control to cavity pressure for both filling and packing phases with experimental verification. Controller robustness was examined experimentally using a complex geometry cavity

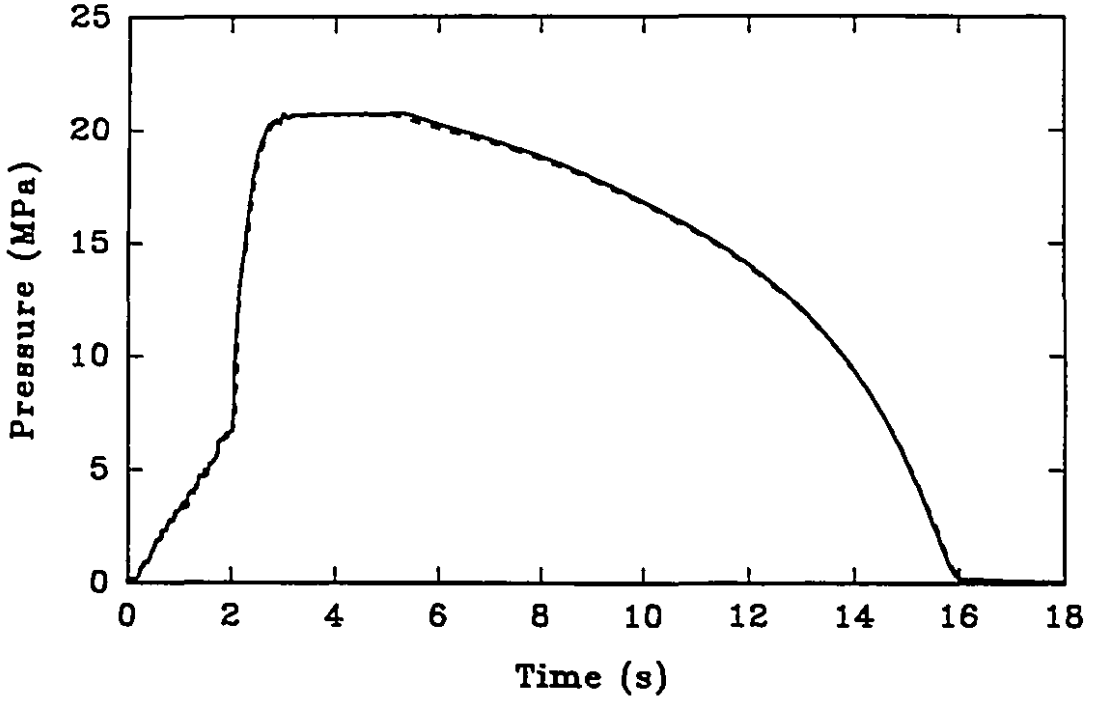

Figure 7.1 Cavity pressure profiles of two different cycles with self-tuning control for the filling and packing stages, and CPCT control for the cooling stage.

without re-tuning the controller. The same control law was applicable for both filling and packing.

3) This is the first study of the dynamics and the first work to achieve closed-loop control of cavity pressure during the cooling phase. Controlled pressure cooling time (CPCT) was proposed as the controlled variable for the cooling phase. The dynamics and control of CPCT were investigated experimentally.

4) This work is the first to examine control of cavity pressure throughout a complete injection molding cycle, including filling, packing and cooling.

7.3 Recommendations

It is recommended to implement a graphics user interface to the computer control package to follow the trend in the computer and control industries. Such an interface would greatly enhance the user-friendliness of the software package.

Experience regarding the injection molding machine operation and material data should be incorporated into the control system to improve system intelligence.

With good and reliable control of cavity pressure, melt temperature, and mold temperature, and with a stable computer control system, the time is ripe to investigate the relationship between material properties such as part weight or residual stresses with the set-points of these variables. An understanding of this relationship will allow the implementation of closed-loop control of some important product properties.

REFERENCE

1 Abu Fara, D., Ph.D. Thesis, McGill University, Montreal, Canada (1989)

2 Criens, R.M., Händler, M., and Moslé, H.G., "Influence of Injection Moulding Conditions on the Strength of Thermoplastics", Kunststoffe, **8**, 74 (1985)

3 Chiu, C.P. and Hsieh, M.C., "The Correlation Between the Residual stresses of ABS Terpolymers and Injection Molding Conditions", Journal of Engineering Material and Technology, **109**, 171 (1987)

4 Fritch, L.W., "Velocity-Pressure Transfer and Packing: Use Them to Optimize Part Properties", SPE Annual Technical Conference Paper, P. 218 (1987)

5 Chao, O.Y., and Maul, G.P., "Optimal Injection Velocity Profiling", Int. J. Prod. Res., **27**, 1917 (1989)

6 Cox, H.W. and Mentzer, C.C., "Injection Molding: The Effect of Fill Time on Properties", Poly. Eng. Sci., **26**, 488 (1986)

7 Greener, J., "Pressure-Induced Densification in Injection Molding", Poly. Eng. Sci., **26**, 534 (1986)

8 Thomas, R., and McCaffery, N., "The Prediction of Real Product Shrinkages, Calculated from a Simulation of the Injection Molding Processes", SPE Annual Technical Conference Paper, **35**, 371 (1989)

9 Mathew, B.A., Nunn, R.E, and Orroth, S.A., "Effects of Injection Molding Parameters on the Percentage of Crystallinity and Physical Properties of Crystallizing Polyethylene Terephthalate (CPET)", SPE Annual Technical Conference Paper, **35**, 333 (1989)

10 Patel, U.G, and Nunn, R.E., "Effect of Processing Conditions on Injection Molded Poly(phenylene sulfide)", SPE Annual Technical Conference Paper, **36**, 292 (1990)

11 Boldizar, A., Kubát, J., and Rigdahl, M., "Influence of Mold Filling Rate and Gate Geometry on the Modulus of High Pressure Injection-Molded Polyethylene", Journal of Applied Polymer Science, **39**, 63 (1990)

12 Nelissen,L., Nies, E., and Lemstra, P.J., "Influence of Pressure on the Phase behaviour of Polymer Blends: Polystyrene/Poly(2,6-dimethyl-1,4-phenylene ether)", Polymer Communications, **31**, 122 (1990)

13 Pierick, D., Noller, R., "The Effect of Processing Conditions on Shrinkage", SPE Annual Technical Conference Paper, 37, 252 (1991)

14 Hastenberg, C.H.V., Wildervanck, P.C., Leenen, A.J.H., and Schennink, C.G.J., "The Measurement of Thermal Stress Distributions Along the Flow Path in Injection-Molded Flat Plates", Poly. Eng. Sci., 32, 506 (1992)

15 Matsupka, T., Takabatake, J., Koiwai, A., Inoue, Y., Yamamoto, S., "Integrated Simulation to Predict Warpage of Injection Molded Parts", Poly. Eng. Sci., 31, 1043 (1991)

16 Maul, G.P., Glozer, G.R., and Engelfried, U., "An Investigation of Injection Pressure Prediction in Simulation Packages", Int. Prod. Res., 29, 1811 (1991)

17 Singh, K.J., "Complete Mold Filling Analysis of Thermoplastics with a Single Computer Run", SPE Annual Technical Conference Paper, 30, 783 (1984)

18 Kamal, M.R., Chu, E., and Lafleur, P.G., "Computer Simulation of Injection Molding Filling for Viscoelastic Melts with Fountain Flow", SPE Annual Technical Conference Paper, 31, 818 (1985)

19 Wang, V.W., Hieber, C.A., and Wang, K.K., Mold-Filling-Simulation in Injection Molding of Three-Dimensional Thin Parts", SPE Annual Technical Conference Paper, 32, 97 (1986)

20 Gogos, C.G., Huang, C.F. and Schmidt, L.R., "The Process of Cavity Filling Including the Fountain Flow in Injection Molding", Poly. Eng. Sci., 26, 1457 (1986)

21 Goyal, S.K., Chu, E., and Kamal, M.R., "Non-isothermal Radial Filling of Center-Gated Disc Cavities with Viscoelastic Polymer Melts", Journal of Non-Newtonian Fluid Mechanics, 28, 373 (1988)

22 Huilier, D., Lenfant, C., Terrisse, J., and Deterre, R., "Modelling the Packing Stage in Injection Molding of Thermoplastics", Poly. Eng. Sci., 28, 1637 (1988)

23 Nguyen, K.T., and Kamal, M.R., "Two-Dimensional Packing Analysis of a Viscoelastic Melt", SPE Annual Technical Conference Paper, P.247 (1991)

24 Titomanlio, G., and Piccarolo, S., "On the Packing-Holding Flow in the Injection Molding of Thermoplastic Polymers", Journal of Applied Polymer Science, 35, 1483 (1986)

25 Turng, L.S., Wang, V.W., and Wang, K.K., "Numerical Simulation of the

Coinjection Molding Process", Journal of Engineering Materials and Technology, Transactions of ASME, 115, 48 (1993)

26 Papathanasiou, T.D., and Kamal, M.R., "Filling of a Complex-Shaped Mold with a Viscoelastic Polymer. Part I: The Mathematic Model", Poly. Eng. Sci., 33, 400 (1993)

27 Kamal, M.R., and Papathanasiou, T.D., "Filling of a Complex-Shaped Mold With a viscoelastic Polymer. Part II: Comparison with Experimental Data", Poly. Eng. Sci., 33, 410 (1993)

28 Chu, E., Kamal, M.R., and Goyal, S.K., "A Computer Simulation of the Injection Molding Process Including Filling, Packing and Solidification", SPE Annual Technical Conference Paper, 37, 344 (1991)

29 Chiang, H.H., Hieber, C.A., and Wang, K.K., "A Unified Simulation of the Filling and Postfilling Stages in Injection Molding. Part I: Formulation". Poly. Eng. Sci., 31, 116 (1991)

30 Chiang, H.H., Hieber, C.A., and Wang, K.K., "A Unified Simulation of the Filling and Postfilling Stages in Injection Molding. Part II: Experimental Verification". Poly. Eng. Sci., 31, 125 (1991)

31 Gao, F, M.Eng. Thesis, McGill University, Montreal, Canada (1989)

32 Patterson, W.I, Kamal, M.R., and Gao. F., "Mold Temperature Measurement and Control", SPE Annual Technical Conference Paper, 36, 227 (1990)

33 Gao, F., Patterson, W.I., and Kamal, M.R., "Dynamics and Control of Surface and Mold Temperatures in Injection Molding", Intern. Polymer Processing, 8, 147 (1993)

34 Rinderle, J.R., United States Patent, No. 4387762 (1983)

35 Kim, B.H., and Suh, N.P., "Low Thermal Inertia Moulding (LTIM)", Poly. Plas. Technol. Eng. 25, 73 (1986)

36 Kim, B.H., and Wadhwa, R.R., "A New Approach to Low Thermal Inertia Molding", Poly. Plast. Technol. Eng. 26, 1 (1987)

37 Kim, B.H., and Suh, N.P., "A Study of Isothermal Simple Flow Followed by Nonisothermal Stress Relaxation in a Low Thermal Inertia Molding", Poly. Plast. Technol. Eng. 26, 23 (1987)

38 Gomes, V.G., M.Eng. Thesis, McGill University, Montreal, Canada (1985)

39 Patterson, W.I., Kamal, M.R., and Gomes, V.G., "Dynamic Modelling and Control of Melt Temperature in Injection Molding", SPE Annual Technical Conference Paper, 31, 754 (1985)

40 Kamal, M.R., Patterson, W.I., and Gomes, V.G., "An Injection Molding Study. Part. I: Melt and Barrel Temperature Dynamics", Poly. Eng. Sci., 26, 854 (1986)

41 Gomes, V.G., Patterson, W.I., and Kamal, M.R., "An Injection Molding Study. Part II: Evaluation of Alternative Control Strategies for Melt Temperature", Poly. Eng. Sci., 26, 867 (1986)

42 Ruscitti, G., M.Eng. Thesis, McGill University, Montreal, Canada (1993)

43 Kamal, M.R., Patterson, W. I., and Abu Fara, D., "A Study of Injection Molding Dynamics", SPE Annual Technical Conference Paper, 29, 658 (1983)

44 Kamal, M.R., Patterson, W.I., Abu Fara, D., and Haber, A., "A Study in Injection Molding Dynamics", Poly. Eng. Sci., 24, 686 (1984)

45 Kamal, M.R., Patterson, W.I., Conley, N., Abu Fara, D., and Lohfink, G., " Dynamics and Control Pressure in the Thermoplastics Injection Molding", SPE Annual Technical Conference Paper, 32, 189 (1936)

46 Kamal, M.R., Patterson, W.I., Conley, and Abu Fara, D. "Dynamics and Control of Pressure in the Injection Molding of Thermoplastics", Poly. Eng. Sci., 27, 1403 (1987)

47 Chiu, C., Wei, J., and Shih M., "Adaptive Model Following Control of the Mold Filling Process in an Injection Molding Machine", Poly. Eng. Sci., 31, 1123 (1991)

48 Costin, M.H., Okonski, D.A., Ulicny, J.G., "Control of an Injection Molding Machine: Adaptive regulation during Filling", Proceeding of the American Control Conference, 33. 711 (1987)

49 Agrawal, A.R., Pandelidis, I.O, and Pecht, M., "Injection-Molding Process Control - A Review", Poly. Eng. Sci., 27, 1345 (1987)

50 Srinivasan, K., Srinivasan, T., and Maul, G.P., "Improvements in Closed Loop Control of Thermoplastic Injection Molding Processes", SPE Annual Technical Conference Paper, 37, 343 (1991)

51 Hara, S.J., Yamamoto, Y., Omata, T., and Nakano, M., "Repetitive Control System: A New Type Servo System for Periodic Exogenous Signals", IEEE Transactions on Automatic Control, 33, 659 (1988)

52 Srinivasan, K., and Srinivasan, T., "Learning Control of Melt Pressure in Injection Molding Process", ASME, Winter Annual Meeting (1991)

53 Malloy, R.A., Chen, S.J., and Orroth, S.A., "A Study of Injection to Holding Pressure Switch-Over Techniques Based on Time, Position or Pressure", SPE Annual Technical Conference Paper, 33, 225 (1987)

54 Haber, A., and Kamal, M.R., "The Dynamics of Peak Cavity Pressure in Injection Molding', SPE Annual Technical Conference Paper, 32, 107 (1986)

55 Haber, A., and Kamal, M.R., "The Dynamics of Peak Cavity Pressure in Injection Molding", Poly. Eng. Sci., 27, 1411 (1987)

56 Abu Fara, D., Kamal, M.R., and Patterson, W.I., "Comprehensive Strategies for Sequential Closed-Loop Pressure Control Throughout the Injection Molding Cycle", SPE Annual Technical Conference Paper, 36, 239 (1990)

57 Abu Fara, D., Patterson. W.I., and Kamal, M.R., "Cavity Pressure Control in Injection Molding during Filling, Packing, and Holding", SPE Annual Technical Conference Paper, 33, 221 (1987)

58 Smud, S.M., Harper D.O., and Leffew, K.W., "Advanced Process Control for Injection Molding", Poly. Eng. Sci., 31, 1081 (1991)

59 Abu Fara, D., M.Eng. Thesis, McGill University, Montreal, Canada (1984)

60 Wang, K.K., Shen, S.F., Cohen, C., Hieber, C.A., and Isayev, A.I., Progress Report #10, Cornell University (1984)

61 Pandelidis I.O, and Agrawal, A.R., "Self-Tuning Control of Ram Velocity in Injection Molding", SPE Annual Technical Conference Paper, 33, 235 (1987)

62 Pandelidis, I.O, and Agrawal, A.R., "Optimal Anticipatory Control of Ram Velocity in Injection Molding:, Poly. Eng. Sci., 28, 147 (1988)

63 Unebehauen, H., and Göhring, "Tests for Determining Model Order in Parameter Estimation", Automatica, 10, 233 (1974)

64 Gustavsson, I., "Comparison of Different Method for Identification of Industrial Processes", Automatica, 8, 127 (1972)

65 Aström, K.J., "Theory and Application of Adaptive control - A Survey", Automatica, **10**, 471 (1982)

66 Isermann, R., "Practical Aspects of Process Identification", Automatica, **16**, 575 (1980)

67 Seborg, D.E., Edgar, T.F., and Shah, S.L., "Adaptive Control Strategies for Process Control: A Survey", AIChE Journal, **32**, 881 (1986)

68 Chien, I., Seborg, D.E., and Mellichamp, D.A., "Self-Tuning Control with Decoupling", AIChE Journal, **33**, 1079 (1987)

69 Ferretti, G., Maffezzoni, C., and Scattolini, R., "Recursive Estimation of time Delay in Sampled System", Automatica, **27**, 653 (1991)

70 Neta, G.W., Kaufman, H., and Steinvorth, R., "Comparison and Extension of a Direct Model Reference Adaptive control Procedure", Int. J. Control, **55**, 945 (1992)

71 Niederlinski, A., and Moscinski, J., "Towards a Bench-Mark Standard for Stochastic Adaptive Control", Int. J. Control, **55**, 1009 (1991)

72 Saelid, S., "A Truly Distributed Process Control System with On-Line Configuration and Expansion Capabilities", Modelling, Identification and Control, **8**, 201 (1987)

73 Parkum, J.E., Poulsen, N.K., and Holst, J., "Recursive Forgetting Algorithms", Int. J. Control, **55**, 109 (1991)

74 Allidina, A.Y., and Yin, H., "Explicit Pole-Assignment Self-Tuning Algorithms", Int. J. Control, **42**, 1113 (1985)

75 Wellstead, P.E., Edmunds, J.M., and Prager, D., "Self-Tuning Pole/Zero Assignment Regulators", Int. J. Control, **30**, 1 (1979)

76 Belanger, P.R., Rochon, L., Dumont, G.A., and Gendron, S.,"Self-Tuning Control of Chip Level in a Kamyr Digester", AIChE Journal, **32**, 65 (1986)

77 Daraijer, W., Steinbuch, M., and Bosgra, O.H., "Adaptive Control of the Radial Servo System of a Compact Disc Player", Automatica, **28**, 455 (1992)

78 McDermott, P.E., Mellichamp, D.A., "Pole-Placement Self-Tuning Control of a Fixed-Bed Autothermal reactor", AIChE Journal, **32** (1986)

79 Tan, P.C., Berger, C.S., Dabke, K.P., and Mein, R.G., "Recursive Identification and Adaptive Prediction of Waste Water Flow", Automatica, 27, 761 (1991)

80 Billiman, L., and Bergmann, H., "Adaptive Control of Temperatures of Plastics processing Machines", Kunststoffe German Plastics 81, 5 (1991)

81 Jang, Y.J., and Wu, W.T., "Adaptive Pressure Control for Melt Spinning Processes", Poly. Eng. Sci., 31, 1108 (1991)

82 Elicabe, C.E., and Meira, G.R., "Model Reference Adaptive Control of A Continuous Polymerization Reactor under Periodic Operation", Poly. Eng. Sci., 29, 374 (1989)

83 Anonymous, PC-MATLAB User's Guide, The Math Works Inc., MA, USA (1990)

84 Ljung, L., System Identification Toolbox, User's Guide, The Math Works Inc., MA (1991)

85 Ljung, L., System Identification: The Theory For the User, Prentice-Hall, Inc, Englewood Cliffs, NJ (1987)

86 Ljung, L., and Söderström, T., Theory and Practice of Recursive Identification, The MIT Press, Cambridge, MA (1983)

87 Wellstead, P.E., and Zarrop, M.B., Self-Tuning Systems: Control and Signal Processing, John Wiley & Sons, NY (1991)

88 Isermann, R., Digital Control Systems, Volume 1 & 2, 2nd Ed., Springer-Verlag, Berlin (1989)

89 Söderström, T., and Stoica, P., System Identification, Prentice Hall, New York (1989)

90 Landau, I.D., System Identification and Control Design, Prentice Hall, Englewood Cliffs, N.J. (1990)

91 Aström K.J., and Wittenmark, B., Computer Controlled System: Theory and Design, 2nd Ed., Prentice Hall, Englewood Cliffs, N.J. (1990)

92 Davies, W.D.T., System Identification for Self-Adaptive Control, John Wiley and Sons, Ltd. NY (1970)

93 Stephanopoulos, G., Chemical Process Control: An Introduction to Theory and Practice, Prentice-Hall, Inc., Englewood cliffs, NJ (1984)

94 Seborg, D.E., Edgar, T.F., and Mellichamp, D.A., Process Dynamics and Control, John Wiley & Sons, NY (1989)

95 Grace, A., Laub, A.J., Little, J., and Thompson, C., Control System Toolbox: User's Guide, the Math Works, Inc., MA (1990)

96 User's Manual, RTI220, Analog Devices

97 User's Guide, STB-HL02 High-level Voltage Panel, Analog Devices

98 User's Manual, RTI217, Analog Devices

99 Instruction Manual #5070, Infrared Thermal Monitor, Model LTD, Vanzetti Systems, Stoughton, MA, USA

100 Installation and Instruction Manual, MTS TemposonicsTH Linear Displacement Transducer System with Analog Output, MTS Systems Corporation, Machine Controls Division, Eden Prairie, MN (1989)

101 CMOS/NMOS Special Functions Data, Motorola, Inc., Austin, TX (1991)

102 Peripherals, Intel Literature, Mt. Prospect, IL., USA (1990)

103 Leibson, S., The Handbook of Microcomputer Interfacing, Tab Brooks Inc, Blue Ridge Summit, PA (1983)

104 Linear Products Data Book, Analog Devices, Norwood, MA., USA

105 Didsbury, K., Leroux, P.N. and Ostrander, J.M., QNX - System Architecture, QNX Software Systems Ltd, Kanata, Ontario, Canada (1991)

106 Didsbury, K., Leroux, P.N., and Ostrander, J.M., QNX - User's Guide, QNX Software Systems Ltd, Kanata, Ontario, Canada (1991)

107 Didsbury, K., Leroux, P.N., and Ostrander, J.M., QNX - Utilities Reference, QNX Software Systems Ltd, Kanata, Ontario, Canada (1991)

108 Anonymous, QNX - VEDITTH Text Editor, QNX Software Systems Ltd, Kanata, Ontario, Canada (1991)

109 Crigger, F.W., Schueler, J.B., Welch, J.W., Bazinet, L., Bell, G., Boyd, A.,

Dodge, D., Flowers, W., Hildebrand, D., and McPolin, S., WATCOM C Library Reference for QNX, WATCOM Publications Limited, Waterloo, Ontario, Canada (1991)

110 McDowell, S.G., WATCOM C Language Reference, WATCOM Publications Limited, Waterloo, Ontario, Canada (1991)

111 Coschi, G., Schueler, J.B., and Scian, A.F., WATCOM C Optimizing Compiler and Tools User's Guide for QNX, WATCOM Publications Limited, Waterloo, Ontario, Canada (1991)

112 Schueler, J.B., WATCOM VIDEO User's Guide, 3rd Edition, WATCOM Publications Limited, Waterloo, Ontario, Canada (1991)

113 Coschi,G., WATCOM linker User's Guide, 3rd Edition, WATCOM Publications Limited, Waterloo, Ontario, Canada (1991)

114 Instruction Manual Type 546 and 5466 Electro-Pneumatic Transducers, Fisher Controls, Inc. (1977)

115 Instruction manual, CompackTH 8500 Flow Transmitter, SIGNET Industrial, El Monte, CA, USA

116 Instruction Manual, MK 588, Digital Flowmeter, SIGNET Scientific, EL Monte, CA., USA

117 Fusser, H., M.Eng. Thesis, McGill University, Montreal, Canada (1992)

118 Spencer, R.S., and Gilmore, G.D., "Some Flow Phenomena in the Injection Molding of Polystyrene", J. Colloid Sci., **6**, 118, 1951

119 Cross, M.M., "Rheology of Non-Newtonian Fluids: A New Flow Equation for Pseudoplastic Systems", J. Colloid Sci, **20**, 417 (1965)

120 Williams, M.L., Landel, R.F., and Ferry, J.D., "The Temperature Dependence of Relaxation Mechanisms in Amorphous Polymers and Other Glass-forming Liquids", J. Am. Chem. Soc., 77, 3701 (1955)

121 Tait, P.G., Physics and Chemistry of the Voyage of H.M.S. Challenger, Vol. II, Part IV., Scientific Papers LXI, Vol. II, 1 (1888)

122 Isermann, R., Lachmann, R.H., Matko, D., Adaptive Control Systems, Prentice Hall International (UK) Ltd (1992)

Appendix A

Voltage to Current Converter for McGill Injection Molding Machine Servo-valves

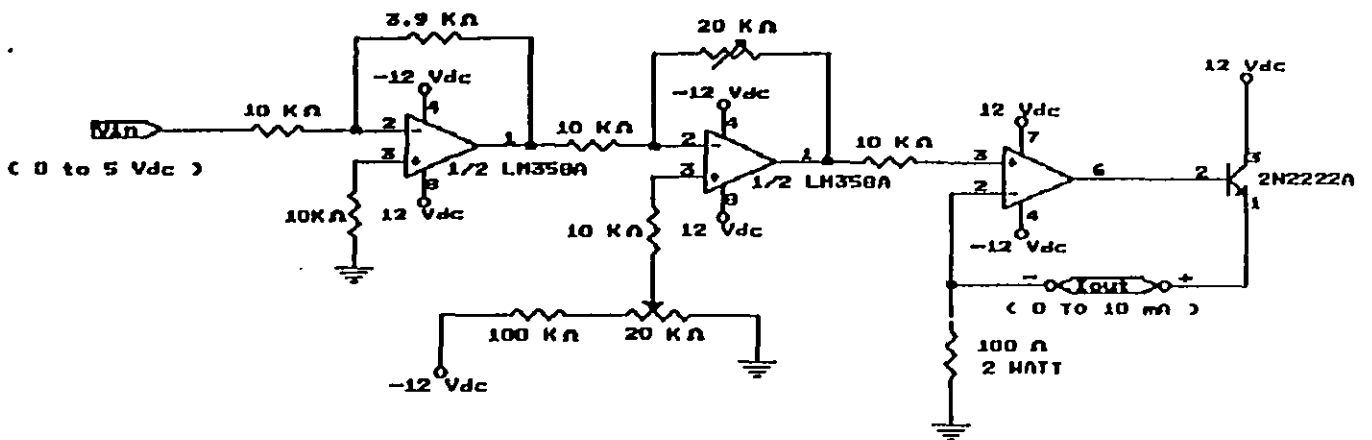

INJECTION MOLDING MACHINE		
Title: SERVO VALVE VOLTAGE TO CURRENT CONVERTER		
Size: A	Document Number: VTOICONV	REV
Date: September 7, 1993	Sheet 1 of 1	

Appendix B

De-bouncing Circuit for Limit Switches

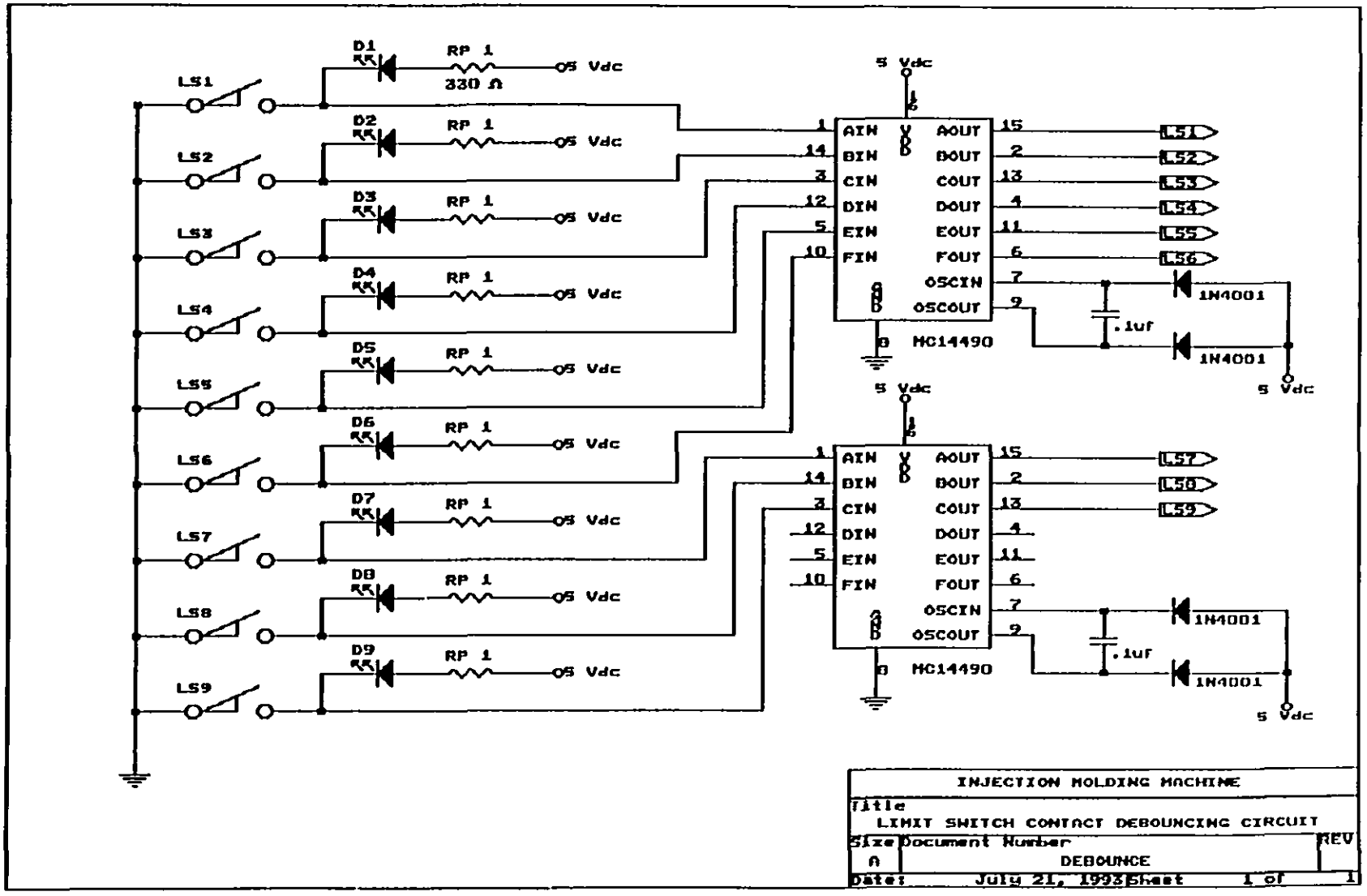
D1
RP 1
330 Ω
5 Vdc
LS1
D2
LS2
D3
LS3
D4
LS4
D5
LS5
D6
LS6
D7
LS7
D8
LS8
D9
LS9
AIN
BIN
CIN
DIN
EIN
FIN
AOUT
BOUT
COUT
DOUT
EOUT
FOUT
OSCIN
OSCOUT
MC14490
.1uf
1N4001
LS1
LS2
LS3
LS4
LS5
LS6
LS7
LS8
LS9
INJECTION MOLDING MACHINE
title
LIMIT SWITCH CONTACT DEBOUNCING CIRCUIT
Size
A
Document Number
DEBOUNCE
REV
Date: July 21, 1993
Sheet 1 of 1

Appendix C

Heater Control Circuit

The heater control circuit is shown on the next page. The heart of the heater control system is a programable interval timer (PIT) chip 82C54 from Intel [102, 103]. The system has four 82C54s with 12 programable timer outputs. Only four of these are used for heater control purposes, the rest are provided for future expansion. PIT has six modes of operations, mode one (hardware retriggerable one-shot) of operation is employed for this use. Detailed information on the operation and programming of this chip can be found in Intel literature [102].

Ports 1 and 2 of RTI-217 digital I/O board were configured as outputs for the PIT data and control signals, respectively. Bit 0 and 1 of port 2 are connected to A0 and A1 of 84C54s to select the mode of operation; bits 2 and 3 are used as the chip selector signal to the input of 74LS135; bits 4 and 5 are used for RD and WR lines of PIT 84C54 to select the read and write operation of the chip respectively. Bits 6 and 7 are not connected. Bits 0 to 7 of port 1 of RTI217 are connected to the data input line 0 to 7 of the PIT 84C54s. The input clock frequency to the PIT is 491400 Hz. Gate 0 of each PIT receives a pulse signal to restart counting every 1/120 second. The output 0 of each PIT is connected to the heaters through an opto-isolator (MOC320) and a triac (MAC3020-25).

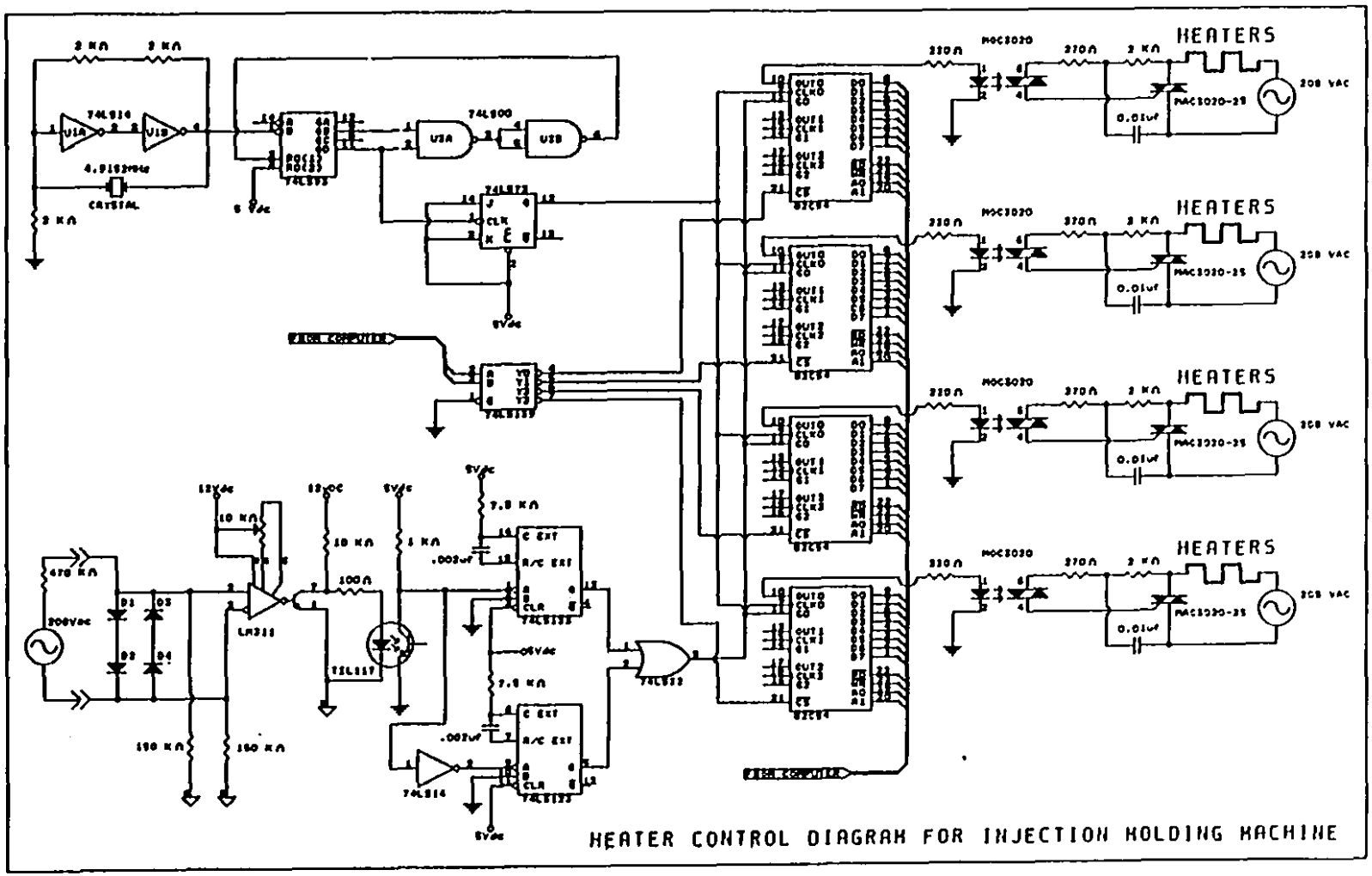
HEATERS
HEATERS
HEATERS
HEATERS
HEATER CONTROL DIAGRAM FOR INJECTION HOLDING MACHINE

Appendix D

Thermocouple Amplification, Linearization and Cold Junction Compensation Circuit

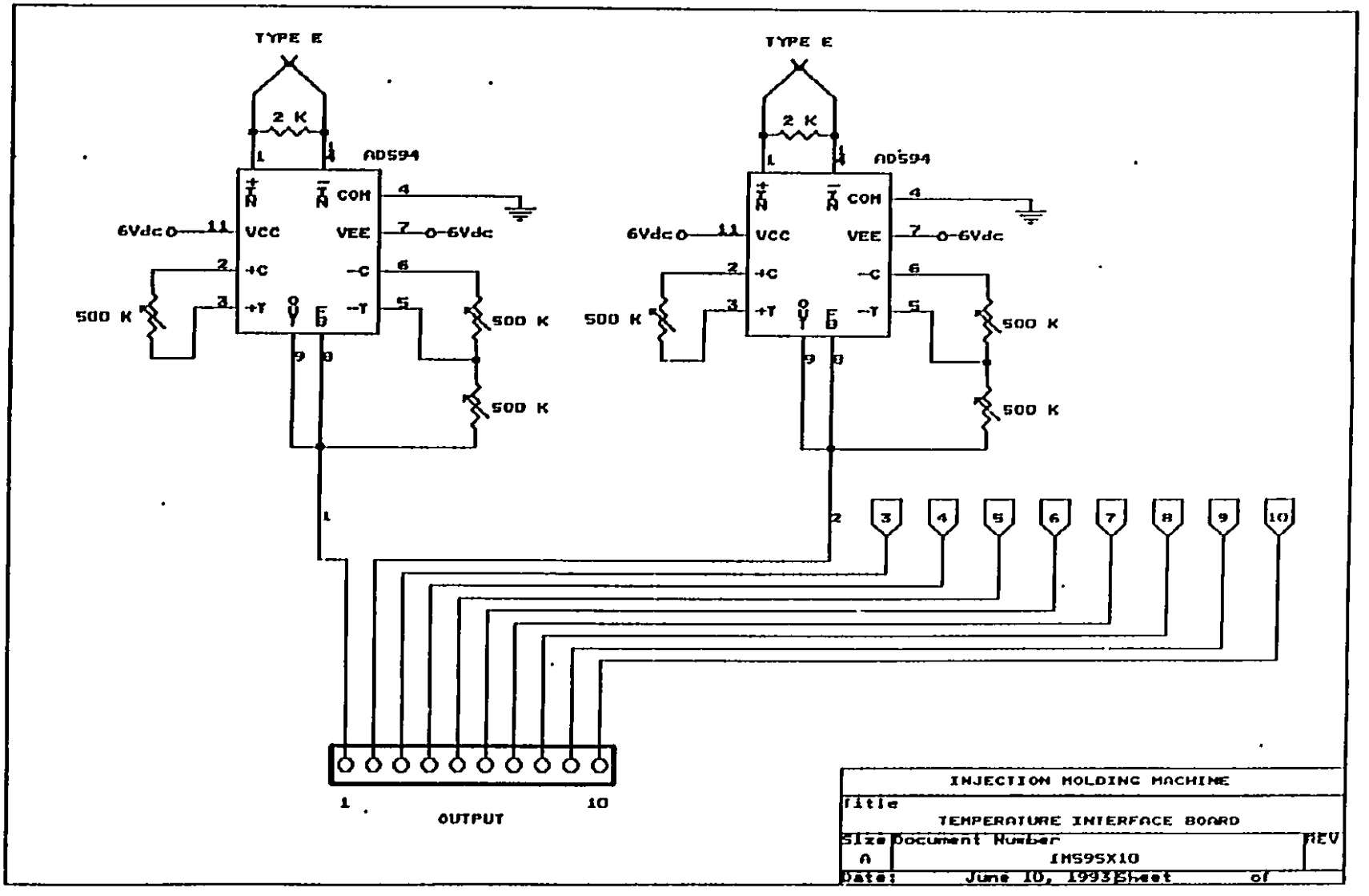
TYPE E
2 K
AD594
+IN
-IN
COM
VCC
VEE
+C
-C
+T
-T
6Vdc
0-6Vdc
500 K
500 K
500 K
TYPE E
2 K
AD594
6Vdc
0-6Vdc
500 K
500 K
500 K
1
2
3
4
5
6
7
8
9
10
1
10
OUTPUT
INJECTION MOLDING MACHINE
Title
TEMPERATURE INTERFACE BOARD
Size
A
Document Number
IMS95X10
REV
Date: June 10, 1993 Sheet of

Appendix E

Pressure Transducer Amplification Circuit

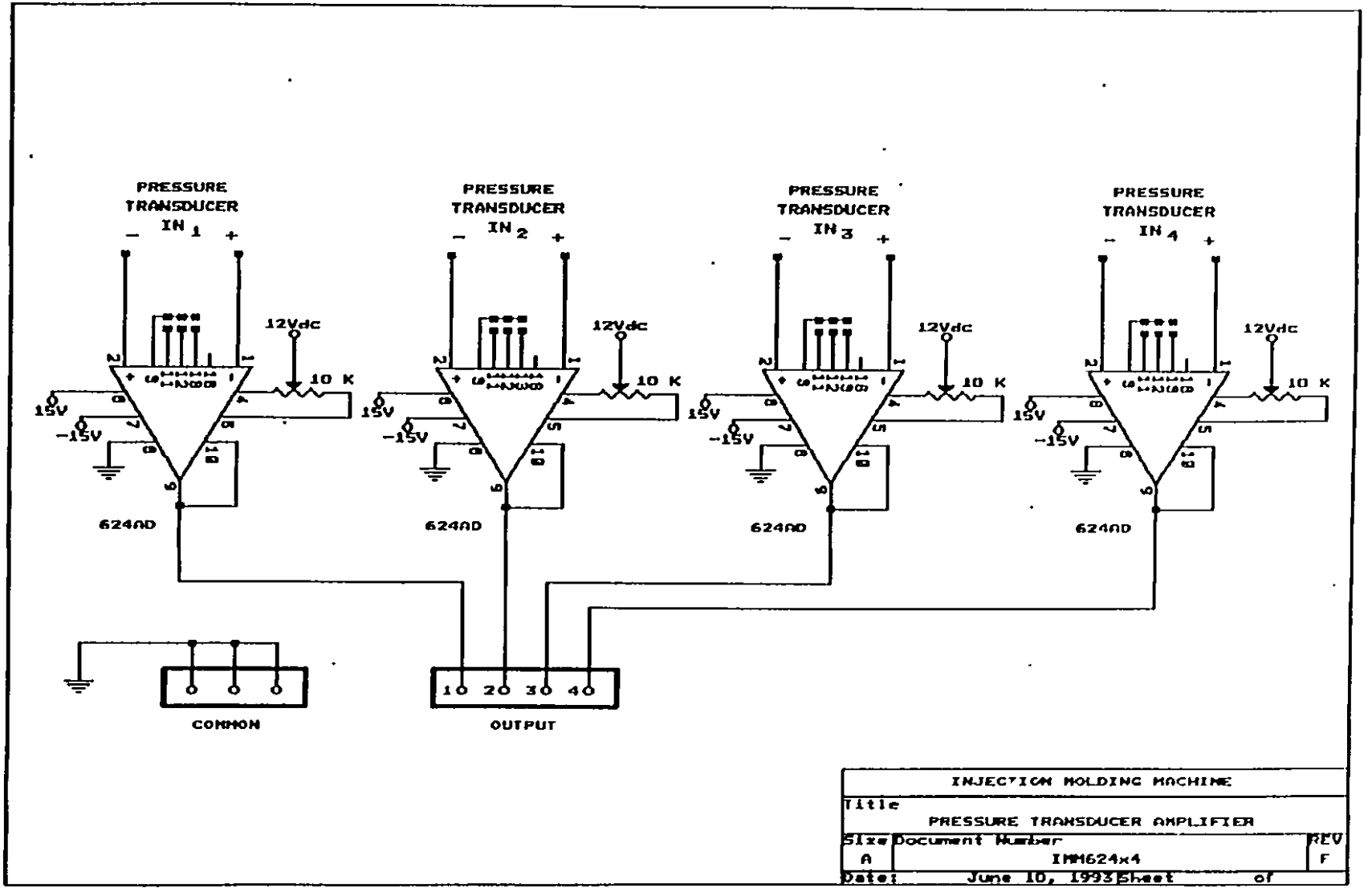
PRESSURE TRANSDUCER IN 1
PRESSURE TRANSDUCER IN 2
PRESSURE TRANSDUCER IN 3
PRESSURE TRANSDUCER IN 4
12Vdc
10 K
15V
-15V
6240D
COMMON
OUTPUT
1 2 3 4
INJECTION MOLDING MACHINE
Title
PRESSURE TRANSDUCER AMPLIFIER
Size
A
Document Number
IMM624x4
REV
F
Date: June 10, 1993
Sheet of

Appendix F

Voltage-to-Current Converter Circuit for the Control Valves

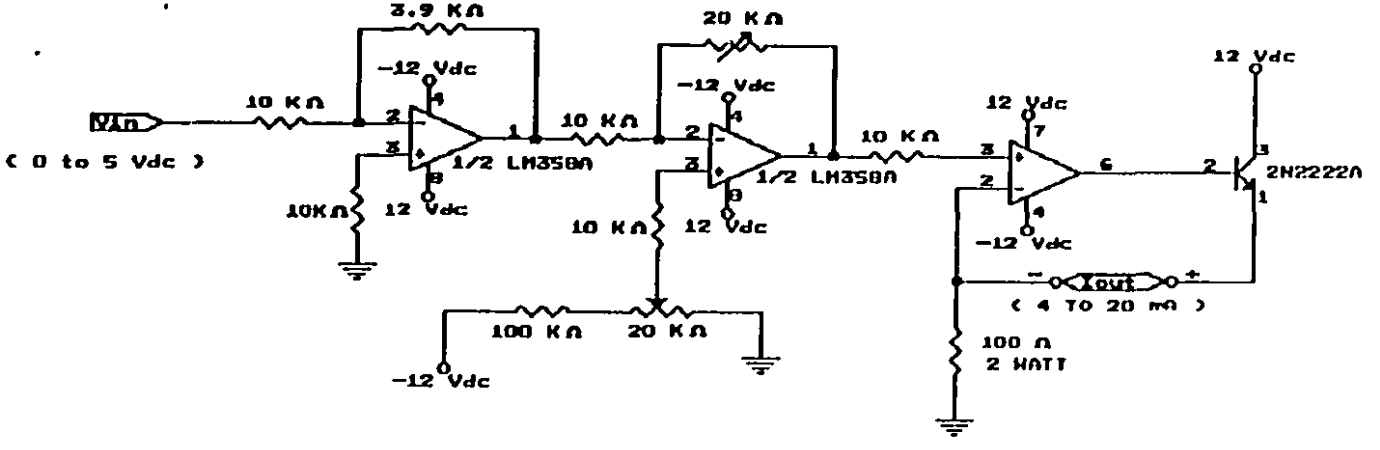

INJECTION MOLDING MACHINE		
Title: CONTROL VALVE VOLTAGE TO CURRENT CONVERTER		
Size: A	Document Number: VTOICONV	REV
Date: September 7, 1993	Sheet 1 of 1	

Appendix G

Current-to-Voltage Converter for the Flowmeter.

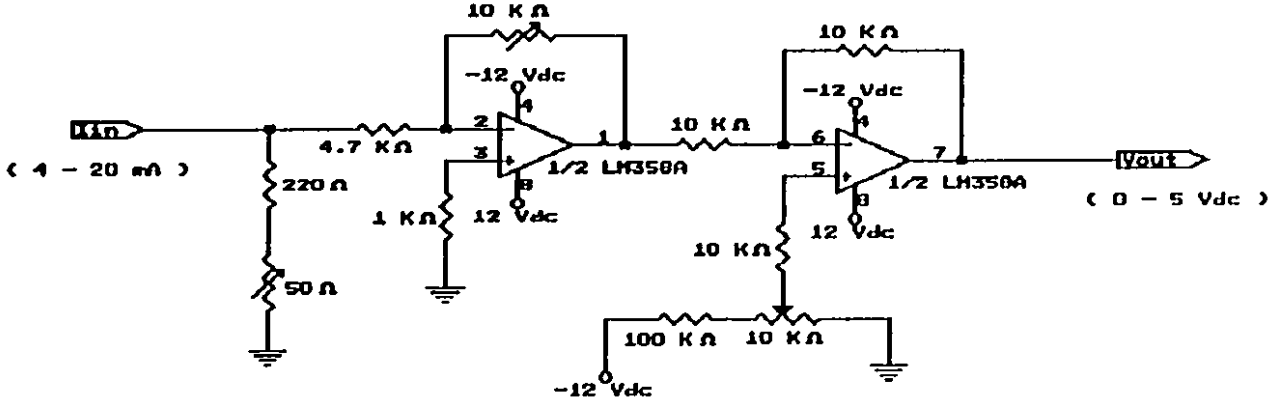

INJECTION MOLDING MACHINE		
Title: CURRENT TO VOLTAGE CONVERTER WITH OFFSET		
Size: A	Document Number: ITOVCONV	REV
Date: July 21, 1993	Sheet 1 of 1	